Spring 2015

Barrier-mediated pulsatile release

Swapnilkumar J. Gandhi
University of Iowa

BARRIER-MEDIATED PULSATILE RELEASE

by

Swapnilkumar J Gandhi

A thesis submitted in partial fulfillment
of the requirements for the Doctor of
Philosophy degree in Chemical and Biochemical Engineering
in the Graduate College of
The University of Iowa

May 2015

Thesis Supervisor: Assistant Professor Eric E. Nuxoll

Graduate College
The University of Iowa
Iowa City, Iowa

CERTIFICATE OF APPROVAL

PH.D. THESIS

This is to certify that the Ph.D. thesis of

Swapnilkumar J Gandhi

has been approved by the Examining Committee
for the thesis requirement for the Doctor of Philosophy
degree in Chemical and Biochemical Engineering at the May 2015 graduation.

Thesis Committee: _____
Eric E. Nuxoll, Thesis Supervisor

_____
C. Allan Guymon

_____
David G. Rethwisch

_____
Julie L. P. Jessop

_____
Douglas R. Flanagan

To my loving wife and wonderful parents.

ACKNOWLEDGMENTS

First and foremost I would like to thank my research advisor Dr. Eric Nuxoll for his support, brilliant advice, professionalism and endless patience. He has been a great mentor throughout my doctoral studies at the University of Iowa since I became his first graduate student. Besides overall research skills, I learned much more including how to address a problem in a practical way, determine priorities and most importantly how to express and defend ideas.

I am also very grateful to my committee members, Dr. C. Allan Guymon, Dr. David Rethwisch, Dr. Julie Jessop and Dr. Douglas Flanagan for their guidance and support. Each member contributed their unique perspective culminating to make me a better researcher. From start to finish their timely reviews and valuable suggestions were instrumental to my success.

I thank the Department of Chemical and Biochemical Engineering for providing the resources required for successful completion. I am very thankful to both Dr. Charles Stanier and Dr. David Murhammer for their counselling during the unforeseen challenge that was my visa renewal process. I want to thank Linda Wheatley, Natalie Potter, Katie Schnedler, Wendy Meyers and Jacquie Albrecht for their help and assistance. A special thanks goes to Glenn Johnson for providing access to the High Performance Computing system (Helium Cluster) at University of Iowa.

I have had the privilege to work with very talented undergrad students Matthew Gosse and Derek Baerenwald, who directly contributed to this project. I am also grateful to Yasuhiro Nishii, a visiting scholar from Japan, for his partial contributions to this work and continued work forward with this project. Guiding and mentoring these bright individuals was an exciting opportunity and also a great experience for me. Others who have helped me along the way include my fellow research group members Ann O'Toole, Joel Coffel, Erica Bader and Bryce Hundley.

I am incredibly grateful to my parents who have always supported me. I have been blessed to be born in a loving family that has fully encouraged and enabled me to achieve my dreams. Finally, no words can express my thankfulness to Khushbu, my wife, who always stood by me throughout this journey. Without her encouragement and motivation I would not have pursued the education to the length I have.

ABSTRACT

Solutes are often most efficiently deployed in discrete pulses, for example in the delivery of herbicides or drugs. Manual application of each pulse can be labor-intensive, automated application of each pulse can be capital intensive, and both are often costly and impractical. Barrier-Mediated Pulsatile Release (BMPR) systems offer a materials-based alternative for automated pulsatile drug delivery, without pumps, power supplies, or complex circuitry. While earlier materials-based approaches such as delayed-release microcapsules are limited to two or three pulses due to the independent nature of each pulse's timing control, BMPR systems link the timing of each pulse to the previous pulse. Each dose of drug is sequestered in its own stimuli-sensitive depot, releasing only upon contact with the stimulant. These depots are stacked with sacrificial barriers in between, each of which block the stimulant for a predetermined time. For instance, layers of soluble drug may be separated by degradable polymer layers. Water, as the stimulant, will erode the polymer layer over a fixed period of time, followed by quick dissolution and release of the underlying drug and the start of degradation for the next polymer layer. This example, however, is quickly limited by irregular polymer erosion, a single stimulant (water), and difficulty in scaling delay times.

The research work presented in this thesis reports the development of a generalized BMPR system which overcomes those limitations. Model drugs (methylene blue and methyl orange) were immobilized in a pH-sensitive polymer [poly(methyl methacrylate-co-dimethylaminoethyl methacrylate)] which released only at low pH. Zinc oxide (ZnO) nanoparticles immobilized in a pH-insensitive matrix [poly(vinyl alcohol)] served as the barrier layer. The time required for acid to penetrate the barrier layer scaled with the ZnO concentration and with the square of the polymer thickness, allowing wide scaling of the delay time with only minor changes to the barrier layer. Harnessing the swelling pressure of the acid-sensitive hydrogel, each barrier/depot bilayer can delaminate upon solute release, directly exposing the next bilayer to the stimulant source.

This system has demonstrated tuned release using a citric acid stimulant to produce up to ten pulses of model drug (methylene blue) over various preset timescales. This system has also demonstrated the alternate release of multiple solutes (methylene blue and methyl orange) at regular time intervals up to five pulses from a single BMPR device. For non-delaminating BMPR systems, spent bilayers impede stimulant diffusion to the inner layers and solute diffusion from the inner layers, increasing the delay time and the pulse width. To predict these changes, a computational model was constructed in FORTRAN. This model was extensively explored over a wide range of parameter space to understand the release behavior of various kinds of non-delaminating BMPR systems. The computer model also validates the performances of experimental delaminating BMPR system. This model can be used to guide the physical modeling of BMPR systems. The model also allows to incorporate variety of stimulants other than just acid. BMPR technology introduces efforts to further generalize the delivery strategy by incorporating glucose as a stimulant.

TABLE OF CONTENTS

LIST OF TABLES

Table

LIST OF FIGURES

Figure

CHAPTER 1 INTRODUCTION

Over the past three decades, numerous approaches of administering therapeutic drugs have been developed for designing controlled release systems. The market value for advanced drug delivery systems has been estimated to be $175.6 billion by the year 2016, an increase of $44 billion over the 2010 estimate.[1] The primary goal of drug delivery is to release the right amount of solute at the right time at the target site without losing drug stability. Many researchers have made enormous efforts to develop materials that release solutes over a prolonged period of time. Some examples of continuous release of drugs include Implanon[2] (a multi-layer birth control implant), daily transdermal patches for nicotine delivery (smoking cessation)[3], monthly depot injection of paliperidone palmitate (schizophrenia)[4] and daily oral tablets of nifedipine (angina and hypertension)[5]. However, many solutes such as biocides, master hormones, opiates and vaccines are best released in pulses rather than delivering them at a constant rate.

1.1 Pulsatile Release

1.1.1 Importance of Pulsatile Release

Pulsed release is defined as quick and temporary release of specific molecules within a defined time frame after a preprogrammed lag time. A pharmacokinetic curve (Figure 1.1) explains the typical behavior of pulsed release compared with bolus and extended release. Bolus release (thin line) is rapid and sometimes disadvantageous especially for the drugs with toxic side effects. When the peak of the bolus is too high it can cause toxicity to the patient and if the solute concentration drops rapidly then it might not stay in a therapeutic window for the extended period of time necessary for the drug to

be effective. Solutes can be delivered at a constant steady rate (dotted line) to keep the

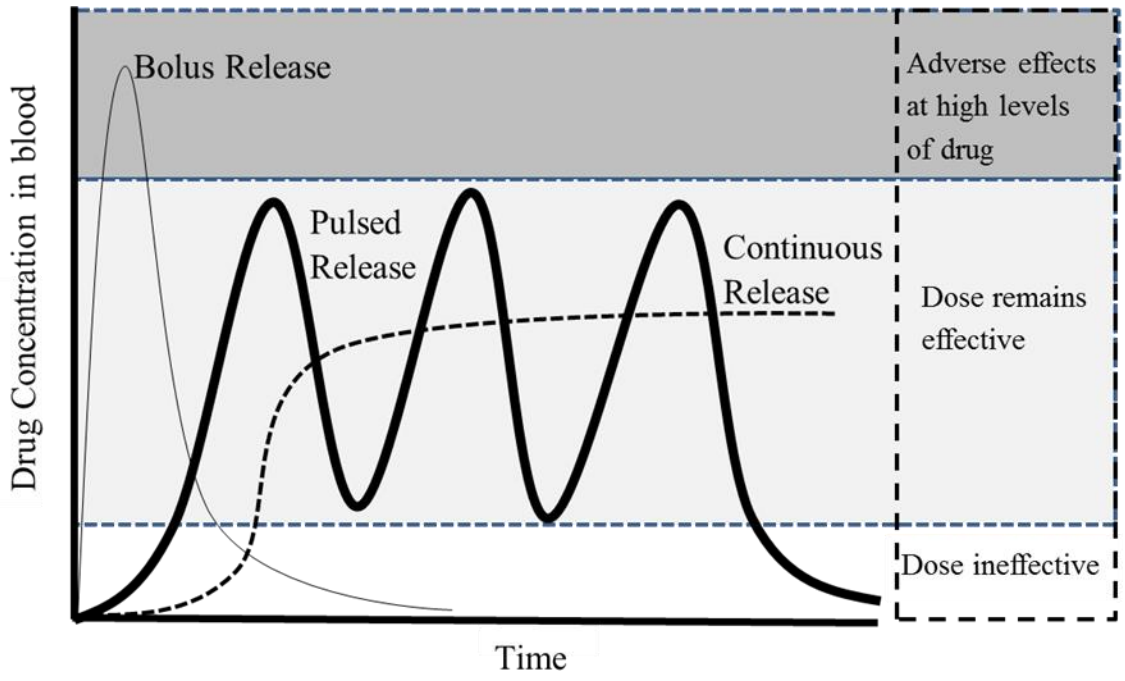

Figure 1.1 Modes of drug delivery: bolus release, continuous release, and pulsatile release[1]

concentration in desired window, but it is most efficient in some cases if the pulses of drugs are released (thick line) at regular time intervals based on a warning sign or indications.

Deploying solutes in concentrated pulses is more effective than slow, steady release for applications which require the specific amount of dosage to be delivered within a defined time frame. The primary advantage of a pulsed release system is to reduce the consumption of solute lowering the chemical cost and provide better efficacy when released at targeted sites in the correct amounts at correct timings. Timed release of biocides on ship hulls or herbicide on crop fields is often required to mitigate biofilms on hulls or kill specific unwanted targets leaving the desired crop unharmed.

Pulsatile release systems are beneficial for treating diseases that show predictable cyclic rhythms. Such systems can deliver the correct amount of solute at the correct site with a predetermined release delay between pulses for maximum therapeutic effect against disease. Circadian rhythms often require pulsatile release of various hormones depending upon sleep-wake cycles, body temperature and other biological activities. Regular peaks and troughs of physiological variables are observed during these circadian rhythms. If released continuously, such hormones can produce not only hormonal imbalance that could drop down the regulation of hormone receptors on the target cells but can also cause undesired side effects. For instance, parathyroid hormone (PTH) is most effective when released in pulsatile manner which not only provides stimulated bone growth (as in case of daily boluses) but it also prevents bone resorption (compared to delivery at a constant rate over a long period of time).[6,7] Many other biological functions in the body are regulated by temporal and pulsatile release of signaling molecules such as insulin[8], pituitary hormones[9], thyroid stimulating hormone (TSH)[10], follicle stimulating hormone (FSH)[9,11], gastrointestinal hormones[11], luteinizing hormone (LH)[11], luteinizing hormone releasing hormone (LHRH)[11], estrogen[9] and progesterone[9]. For the treatment of such site specific areas, pulsatile delivery is beneficial: for drugs that produce biological tolerances, for drugs that experience first pass metabolism, for adapting to circadian rhythms and also for protecting the drug before its action at particular site.

Many opiates such as morphine, codeine, thebain and heroin are used in various medicinal purposes as a pain reducer.[12] These opiates attach to opioid receptors in the body and often produce dependence, tolerance and addiction. It is important that such

opiates be delivered in a controlled way to create or to avoid tolerance depending upon the requirement, maintaining their effectiveness at desired concentration level.

Treatment of common infectious diseases (such as influenza, rabies and tuberculosis) and many allergies often requires a regular dosage of vaccines[13,14] and allergens[15] in specific quantities at periodic times to have desired biological response. Releasing small amounts in pulses also reduces the dose frequency and ultimately reduces side effects.

In all of the above mentioned instances, which operate in different surroundings on a wide range of timescales, it is beneficial to have discrete pulses of solute rather than sustained release.

1.1.2 Strategies for Pulsed Release Systems

The simplest way to achieve pulsed release is obtained by manually spraying, spreading, swallowing or injecting the solute at the target site. These manual ways generally rely on user intervention and sometimes become impractical. Automation of pulsed release is not only desired but it is also important and necessary especially when these manual ways are impractical. Medications (pills, injections) are difficult to administer during sleep. In addition, people (especially the geriatric population) who need the most medications often dislike or sometimes forget such manual ways of administering them due to mental or physical discomfort. The other method for releasing drug in pulses is to pump the drug out of a reservoir, which also has a possible disadvantage of pump failure and disastrous consequences of reservoir rupture if implanted in body. External reservoirs require transcutaneous catheters for prolonged

periods of time. Controlled-release microchips consisting of an array of micro-reservoirs of solutes have a good control on pulsatile release and mitigate the risk of reservoir failure[1,16,17]. Each reservoir is sealed by thin membrane of conductive materials (such as gold) which can be dissolved later when applied to certain electromotive force; more recently, they have used electrical current to simply burn the gold off like a fuse, in order to provide solute release from that reservoir. However, this technique is also expensive and complicated. Unlike these expensive and impractical methods, material based release systems are becoming more attractive for designing controlled release devices. The predominant method for material based release systems is to encapsulate the solutes in shells that are destroyed one by one after defined time periods either by degradation[18], dissolution[8] or breaking apart because of osmotic pressure[19] inside the shell. By varying the degradation times of each shell, multiple pulses of solutes can be achieved. However, the self-regulating nature of individual encapsulated particles restricts the number of pulses that can be delivered. As one particle set has no information about the former pulses, small timing errors can produce long delays interspersed by overlapping pulses. Since the lag time of the last pulse becomes orders of magnitude longer than that of first pulse, the rupture time of the shell needs to be tunable over a vast range, making significant timing errors more likely. Therefore, such strategies have not been tested for more than three pulses.

1.2 Material-based Release Systems Based on Degradation and Dissolution

Time-controlled pulsed release systems have been designed using degradable polymers such as poly(lactic acid) (PLA), poly(lactic-co-glycoclic acid) (PLGA) and polyanhydride, in which solutes were encapsulated in the non-degraded polymer matrix,

and as the stimulant (for instance, water) diffuses into the polymer matrix, polymer degrades and releases the solute. The pulse timing of such systems depends on the type of degradation (surface or bulk), the rate of degradation and the rate of diffusion of stimulant in the polymer matrix. Combinations of polymers, one degrading faster than the other in a single device, can provide multiple pulses on various timescales.[20]

1.2.1 Bulk Eroding Systems

In bulk eroding systems, degradation occurs throughout the polymer because of the faster diffusion of the stimulant (water) than the degradation of the material itself. The degraded products are small enough to be solubilized making the polymer more porous and hydrated. Because the rate of ingression of water is more rapid than the rate of polymer degradation, the encapsulated solute gets dissolved and releases from the degraded matrix.

Dissolution of a gelatin based ethyl cellulose capsule is a simple example of a degradable single pulsed release device based on bulk erosion.[21] The degradable capsule of ethyl cellulose was prepared by coating a parent mold of gelatin, which was later coated with ethyl cellulose with various thicknesses. Upon dissolving gelatin in water, the coating of ethyl cellulose provided a large number of mechanically produced micropores that allowed the diffusion of water in the capsule. A model drug, fluorescein, was preloaded in a drug reservoir made of swellable hydroxypropylcellulose inside these capsules. As water penetrated through micropores of the ethyl cellulose capsule, it allowed the hydroxypropylcellulose to hydrate and swell due to increased osmotic pressure, and burst release of the model drug was observed. Poly(lactic acid) (PLA) is another material that has shown bulk erosion when exposed to aqueous conditions. The

degradation rate of PLA can be varied by copolymerizing PLA with glycolic acid. PLA along with poly(glycolic acid) (PGA) and poly(lactic-co-glycolic acid) (PLGA) are widely studied aliphatic polyesters used for designing degradable pulsed delivery systems based on bulk erosion.[20] For an example, a single pulse of HIV-1 vaccine was released after a lag time of couple of weeks from PLGA microspheres of various compositions. Continuous release of antigen was observed for an almost 4 week time period after a lag of more than few weeks.[22] In another study, pulsed release of follicle stimulating hormone (FSH) in female rabbits was achieved using PLA/PLGA capsule.[23] Rapid diffusion of water inside the shell was caused by bulk erosion of the PLGA matrix resulting in burst release of encapsulated solutes. However variation in thickness of PLGA membrane did not affect the lag time due to significantly faster bulk erosion. PLGA microspheres have also been widely used for controlled release of DNA and insulin in last two decades.[24-26]

Besides having their own advantages of using bulk-eroding polymers, they also have limitations such as high initial burst release, drug instability, premature and sometimes incomplete release profiles. Various individual attempts have been tried to overcome these individual limitations over the years, however, it becomes important to design a system which can overcome all of these challenges.

1.2.2 Surface Eroding Systems

Surface eroding systems have become more desirable for controlled delivery applications in recent years. In such systems, the solute loaded reservoirs are protected with soluble or erodible polymer which gradually degrade/dissolve over time. For certain polymeric devices, it is often desirable that the system experience only surface

degradation as it provides better stability of the drug and also avoids the uncontrollable release of the drug due to minimal water interaction with solute before the release occurs.

Ideal surface erosion can provide nearly zero order release profiles[27]. Hydrolysis of surface eroding polymers (SEP) happens faster than the diffusion of water into polymer matrices which results in more rapid mass loss of eroding polymer from the surface than from the bulk. This provides controllable release profiles without losing the stability of drugs. This nature of SEP have attracted recent development in pulsed delivery by combining multi-laminated systems consisting of drug loaded depots altered with surface erodible isolation layers or barriers.

Polyanhydrides are most suitable materials that show surface erosion and have been studied extensively over the last few decades.[20,28-30] Polyanhydride degradation mainly occurs through chain scission at the polymer matrix surface and the mass is translocated from the periphery of the matrix to the inside of the matrix upon degradation.[31] Desired degradation time can be achieved by modifying the structure of polyanhydrides. Various polyanhydrides such as aliphatic, aromatic, and a combination of aromatic and aliphatic have been synthesized to vary the degradation time for drug delivery systems.[30,32]

Polyanhydrides have been widely used in designing implantable chips for drug delivery in the brain. In late 80s, it was reported that polyanhydrides are safe implantable material for treating brain cancer.[28] Nitrosourea a therapeutic drug for brain cancer has a half-life time of 12 to 15 min and causes severe toxicity if administered intravenously. Instead, polyanhydride disks containing nitrosourea were implanted locally in the brain. These disks protected the drug from getting released at once. As the polymer started

eroding, the drug was delivered locally at a controlled rate due to gradual and relatively slow degradation of the polymer matrix, maintaining its efficacy throughout the life time of the polymer (in this case, almost a month) and patient lifetime was increased. This release was a sustained release over long period of time. In recent years, there has been a lot of modification and development in polyanhydride to provide robust implantable device with efficient drug release profiles. Gliadel® and Septacin™ are the traditional examples of clinical drug delivery systems using modified polyanhydrides.[33] Gliadel wafers are comprised of 1,3-bis-(p-carboxyphenoxy) propane-co-sebacic acid [P(CPP/SA)(20/80)] which contains carmustine for treating cancer. Septacin™ consists of a poly(erucic acid dimer-cebacic acid) [p(EAD/SA)] (50/50) matrix in which gentamicin is delivered for the treatment of osteomyelitis.

In short, in most of above mentioned material-based systems (both surface eroding and bulk eroding systems), the solute was released after fixed period of time either by dissolution, degradation or rupture by osmotic pressure. While it is possible to produce multiple pulses using such mechanism by protecting the solute in number of shells with variable expiration time, the independent nature of each set of shells filled with solute limits the number of pulses that can be delivered. As one set of shells has no information about the previous pulses, small timing error can result in long delays which may cause overlapping pulses. Since the pulse time required for the last pulse is orders of magnitude higher than the first pulse, the rupture time of the shell must be adjustable over a large range, making such timing errors more likely. Due to such erroneous mechanism, most of material-based systems described above were not established beyond two to three pulses.

1.3 Barrier-Mediated Pulsed Release (BMPR): Concept

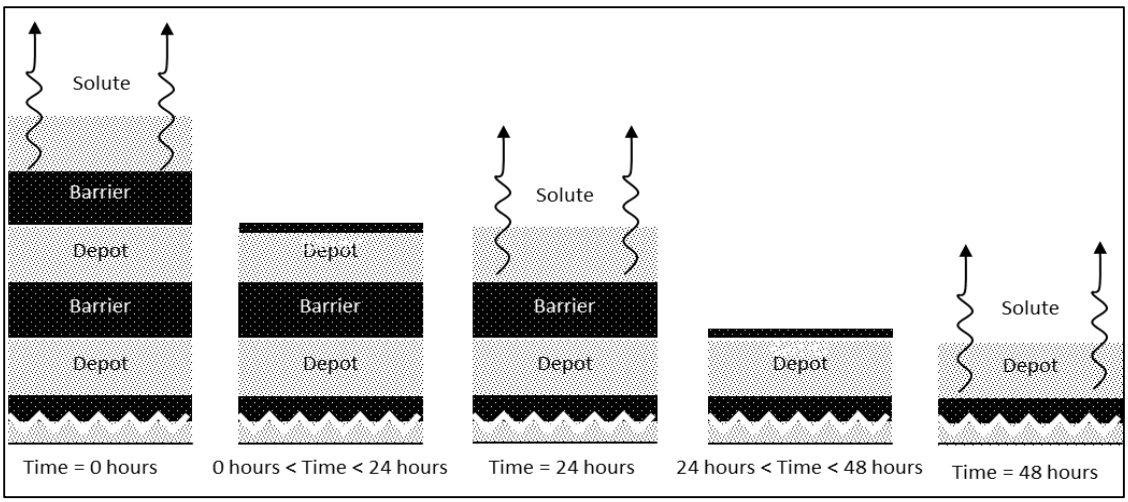

Figure 1.2 Schematic representation of pulsatile release from surface erodible polymer stack. Sequential release of solute occurs when each barrier gets eroded over time when exposed to water as stimulant.

By coupling the release of one pulse to the release of previous one, the shortcomings mentioned in the previous section can be diminished. This is the principle for Barrier-Mediated Pulse Release (BMPR) technology. Sacrificial barriers can be placed in between depots of solutes to provide barrier-mediated pulsed release systems. These barriers protect the stimulant for a specific time period before it reaches the depot layer. Once the barrier is completely exhausted, stimulant hits the depot layer and triggers release of solute and starts penetrating into the barrier layer underneath for the next pulse. BMPR provides a separate pulse of solute from each depot layer, with timing controlled by intermediate barrier layers. Thus, a BMPR system with no power source, moving parts or fixed reservoir has the advantages of a convenient implant at lower cost, a potential for custom or mass manufacture, and comparatively lower risk of device failure for therapeutic delivery.

BMPR strategy relies on linking the release of sequential pulses for predefined time intervals using barriers. The preloaded solute from the thin layers of depot matrix is released from each layer one after the other when subjected to a specific stimulant. The barriers are alternately layered between each depot layer to protect the depot from the stimulant for a fixed period of time. When the stack of layers is exposed to a stimulant, the stimulant will take a specific period of time to travel through first barrier before triggering solute from the underneath depot. In a similar way, stimulant can diffuse through the second barrier, again for a fixed period of time before causing the release from the next depot layer. This process continues until the stimulant diffuses through all the depots in the stack. Figure 1.2 describes the simplest case of BMPR using layered polymers to provide multiple pulses from a single release system. Each surface eroding polymer (SEP) layer protects its underlying solute depot from water for some fixed period of time until it gets eroded completely. Sides of the stack are sealed and the underlying solute depot is exposed to the stimulant (water). The solute from the depot is released as the water triggers the depots by dissolution mechanism and thus exposes the next barrier to the water and the process repeats.

1.4 BMPR: Existing Work

Over two decades ago, the concept of BMPR was introduced[34] in alternating layered system of drug-containing polymeric layers and drug-free polymeric layers; with the entire system coated with the third polymer (almost insoluble to water) in the perpendicular direction of the layered polymers. This system provided only two or three distinct pulses over a two days of time span. Using surface eroding polymers such as polyanhydrides, this concept was further applied in 2000.[35,36] The polyanhydrides were incorporated as barriers to water, and as the polymer eroded the water starts dissolving the underlying drug depots, as depicted in Figure 1.3. Recently, a pair of groups studied[6,37] polyanhydride barrier systems to explain osteogenesis with various growth

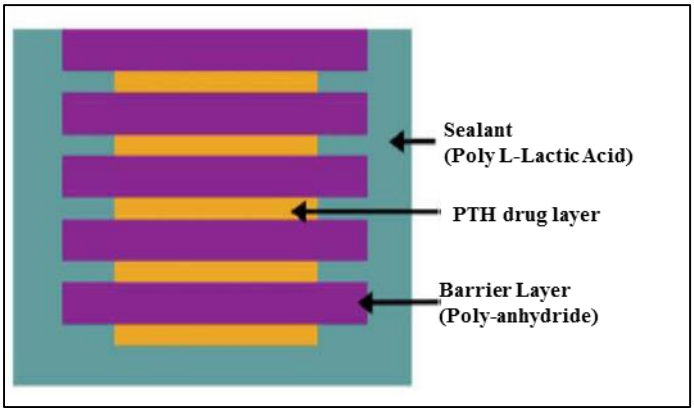

Figure 1.3 Cross section view of the implantable drug device based on polyanhydride BMPR system.[6]

factors, demonstrating in vivo efficacy and sequential delivery of multiple drugs[38]. As shown in Figure 1.3, the system[6] was made by alternating polyanhydride barrier layers and parathyroid hormone loaded depots using biodegradable poly L-lactic acid (PLLA) as a sealant. As indicated in Figure 1.4, multiple pulses of protein were achieved using this implantable device. The time between the pulses varied directly with the thickness of

the barrier layers. The pulse time in each case was on the order of one day and no attempt was made to deliver more than five pulses using this system.

Although such BMPR system can produce sharp and reliably-timed pulses, this straightforward case requires degradation and dissolution of the layers tuned with release of the solute. The stimulant must trigger degradation and dissolution to allow the release of solute. Such systems limit the number and type of stimulants and assures the

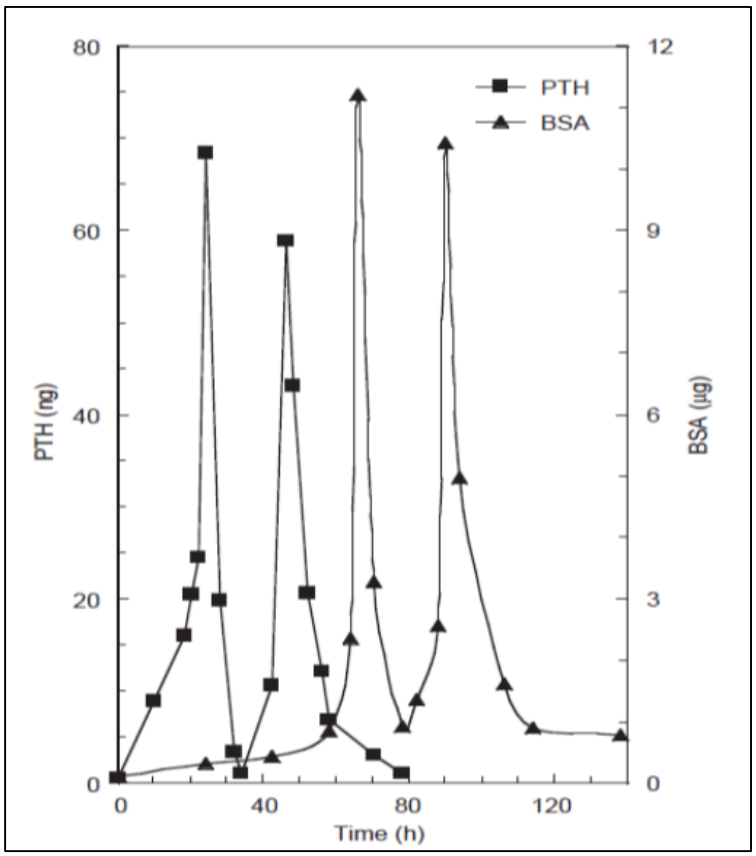

Figure 1.4 Pulsatile release of PTH and BSA from polyanhydride BMPR system[6]

associated release of layer matrix byproducts. The other very important limitation of this system is that the time required for stimulant to diffuse through the isolation layers (also called as penetration time) varies linearly with the thickness of layer, which means penetration times of one hour and one month would require barriers of different thickness

of three orders of magnitude, which is geometrically impractical to design, and most importantly pulse timings would be unpredictable, as the surface vs bulk erosion characteristics of these polymers are likely to be relative to the layer thickness[39]. It was also reported that there was an incomplete release in certain pulses when compared to the amount that was incorporated in respective drug layers.

1.5 BMPR: A Generalized Approach

The degradation/dissolution mechanism for providing pulsed release both limits the the variety of stimulants and requires a large variation in barrier properties to provide a wide range of pulses with precise control. On the other hand, stimuli sensitive hydrogels are very reliable materials for depot layers which can be triggered to release the solute without dissolution or degradation. A large variety of stimuli-sensitive comonomers can be incorporated into the hydrogel matrix based on requirement. Acrylate and acrylamide based hydrogels (such as poly(methyl methacrylate) p(MMA) and poly(N-isopropylacrylamide)(p-NIPAm)) hydrogels can be tuned to make them sensitive to a variety of stimulants such as pH[40], temperature[41], pressure[42], light[43], electromagnetic fields[44] and specific antigens[45]. Thus, decoupling the release mechanism from degradation/dissolution not only allows a wide range of stimulant choices but also provides a safer solute release without any associated release of matrix degradation products. pH-sensitive hydrogels are well established materials for designing controlled release systems. An acid or base prompts the previously hydrophobic polymer to swell with water, increasing the hydrogel's permeability allowing the dissolution and diffusion of solute particles from the gel.

Having flexibility on the choice of stimulant, a reliable barrier must be constructed which can block the stimulant for a specific time period, and then, it can allow rapid stimulant penetration and solute release. One strategy uses a highly permeable matrix containing sacrificial scavenger that consumes the stimulant until they are exhausted; and so provide varying breakthrough times which varies with both thickness of the barrier layer and the amount of scavenger in the layer. Unlike surface erodible polymers where the breakthrough time is linearly proportional to thickness, it is now proportional to the square of the thickness, which allows a much wider range of breakthrough times within given geometric constraints.[46,47] The breakthrough time can be tuned precisely without changing the thickness at all, but rather by varying the scavenger concentration within the barrier matrix, or by changing its location within the matrix. The effects of varying layer thickness and scavenger concentration are multiplicative and can allow precise control over a wide range of breakthrough times. Decoupling the depot layers separately from the barriers allows the solute release without any simultaneous release of matrix degradation products.

1.6 BMPR: Current System

Earlier BMPR systems described in Section 1.3 and 1.4 provide sharp multiple pulses of solute based on a degradation/dissolution mechanism which effectively limits the choice of stimulant to water. The primary objective of the research described in this thesis is to open the BMPR delivery technique to a wide range of applications by creating a generalized BMPR system whose mechanism of release (hydration and swelling of the depot layer) is responsive to a variety of stimulants which can be blocked by reactive barriers already filled with scavenging additives.

Objective 1: Develop an Experimental Delaminating BMPR System

The first objective of the research was to develop an experimental BMPR system with non-degrading matrix layers which delaminate upon solute release. An experimental BMPR model was created using multiple layers of acid sensitive poly(methyl methacrylate-co-dimethylamino ethyl methacrylate) p(MMA/DMA) depots pre-loaded with model drugs (methylene blue or methyl orange) which were alternately protected by poly(vinyl alcohol) barriers already immobilized with ZnO nanoparticles. This BMPR model relies on acid as the specific stimulant which was provided by citrate buffer of pH 3. ZnO-laden PVA barriers blocked the acid stimulant for a preprogrammed time period before triggering the depot matrix. Release of solute occurred due to triggered hydration and swelling of the p(MMA/DMA) depot layer. The developed pressure of the swelling caused the depot layer to delaminate from the device. Each depot layer delaminated from the device and released its solute. This system provided sharp and timely controlled multiple pulses of both single and multiple solutes on various timescales. Chapter 2 of this thesis describes the delaminating BMPR system in detail. It includes the synthesis and characterization of p(MMA/DMA) depot layers, solute incorporation in depots and swelling and release behaviors of solute loaded p(MMA/DMA) depots. It also includes the synthesis and characterization of ZnO-laden PVA barriers. It also discusses the permeability of each mobile species (acid, solutes) through both depot and barriers separately. Chapter 2 further includes the design of BMPR devices and release studies of various delaminating BMPR systems which show the effect of thickness, effect of scavenger loading, effect of scavenger location with a variety of pulse periodicities over a

wide range of time scale. These BMPR systems also depict the release of multiple solutes from a single device, and also demonstrate a 10-pulse device.

Objective 2: Develop an Experimental Non-Delaminating BMPR System

The second objective was to create an experimental BMPR system with non-degrading matrix layers which do not delaminate upon solute release. A non-delaminating BMPR system was developed using the same polymeric layers of p(MMA/DMA) depots filled with model drug (methylene blue/methyl orange) protected by ZnO-filled PVA barriers that were used for the delaminating BMPR systems. However, in this approach the swelling of the depot matrix was restricted both chemically and mechanically to a single direction. Swelling of the depot was restricted chemically by incorporating more crosslinks into the depot matrix, while we also mechanically restricted any possible delamination by mechanically clamping a metal mesh to the top of the stack and a slidable PTFE plug to the bottom held in place by the flexible rubber cement. Chapter 4 of this thesis describes the details of non-delaminating BMPR systems, which includes anisotropic swelling and release studies of p(MMA/DMA) polymers, design of non-delaminating BMPR device and corresponding release studies.

Such non-delaminating BMPR systems are helpful for applications where dispelling spent layer pieces is undesirable. However, due to anisotropic swelling of the depot layer and the accumulated mass transfer resistance from spent layers above the underlying layers of the device, this system does have some limitations compared to that of delaminating BMPR system. As the layer matrix is not removed from the device in non-delaminating BMPR devices, the mathematical complexity of the system increases dramatically. Once the scavenger from the barrier layers gets depleted completely and the

layer has finished serving its purpose, the layer matrix still remains. Similarly, after the release from the swollen depot layer, the spent depot matrix still remains. These spent layers provide additional mass transfer resistance to both stimulant diffusing in and solute diffusing out. Increased diffusional resistance from each spent layer adds complexity in the release profiles and the system itself. This could cause the solute not to release in discrete pulses, but rather releasing in pseudo-Gaussian peaks, which get wider with the additional resistance of each spent layer. In this case, the operative time of each barrier becomes a function of its position in the layered stack. On simplification of the system, assuming no external mass transfer resistance, immediate penetration of stimulant, prompt stimulant scavenging, and rapid depot layer response without any volume change (no swelling), the system can be demonstrated by a set of partial differential equations, one for each mobile species in each layer. Even in the perfect system of layers with no intra layer variation in thickness, scavenger or solute concentration, or permeability, more complications are likely to occur such as depot layer response kinetics and moving layer boundaries due to obvious swelling of depot layers. Hence, prediction of the release behavior in such system requires significant computation, as described in the next objective.

Objective 3: Develop a Computational Model for BMPR Systems

The third and final objective was to develop a computational model for both delaminating and non-delaminating BMPR systems. The predictions of solute release for the BMPR system for delaminating BMPR system were calculated using Fickian diffusion equations and instantaneous hydrogel swelling, with supplementary details as required based on outcomes from the experimental system. The first part of Chapter 3

describes the analytical predictions of the barriers and depots that were used for delaminating BMPR devices described in Chapter 2. However, as there is no analytical solution for the physical models of BMPR devices (non-delaminating BMPR in particularly), a FORTRAN-based 1-D computational model was developed for both BMPR systems. Chapter 3 also describes the details on how the model was constructed for the delaminating BMPR system, the assumptions made, how the model was tested for its accuracy and stability limits and how it was validated against experimental resutls. This model was successfully validated using the experimental BMPR systems described in Chapter 2.

The FORTRAN-based computational model also serves as a guide to calculate the performance of the physical model, especially for the non-delaminating BMPR system where it becomes much more difficult to predict the performances analytically. The computational model was further expanded to predict the performances of non-delaminating BMPR systems. The model was studied extensively on a wide range of physical parameters that produced a variety of release profiles for a given 5-pulse non-delaminating BMPR system. Chapter 5 describes this investigation of the model on various parameter space and their effects on release behavior of non-delaminating BMPR systems.

Finally, Chapter 6 summarizes the BMPR research and provides future insight for using enzymatically derived organic acids as an alternate choice of stimulant, for instance, gluconic acid that can be derived from glucose (blood sugar).

CHAPTER 2 DELAMINATING BMPR SYSTEM

The primary aim of the proposed research is to create a BMPR system in which the solute release occurs due to triggered hydration and swelling of the depot layers, and this swelling pressure allows the spent layers of both depot and barriers to delaminate from the device. This phenomenon is schematically described in Figure 2.1. The device consists of barriers and depot layers that are alternately stacked together. Hydrophilic solute particles are immobilized in hydrophobic matrices of depot layer. Solute

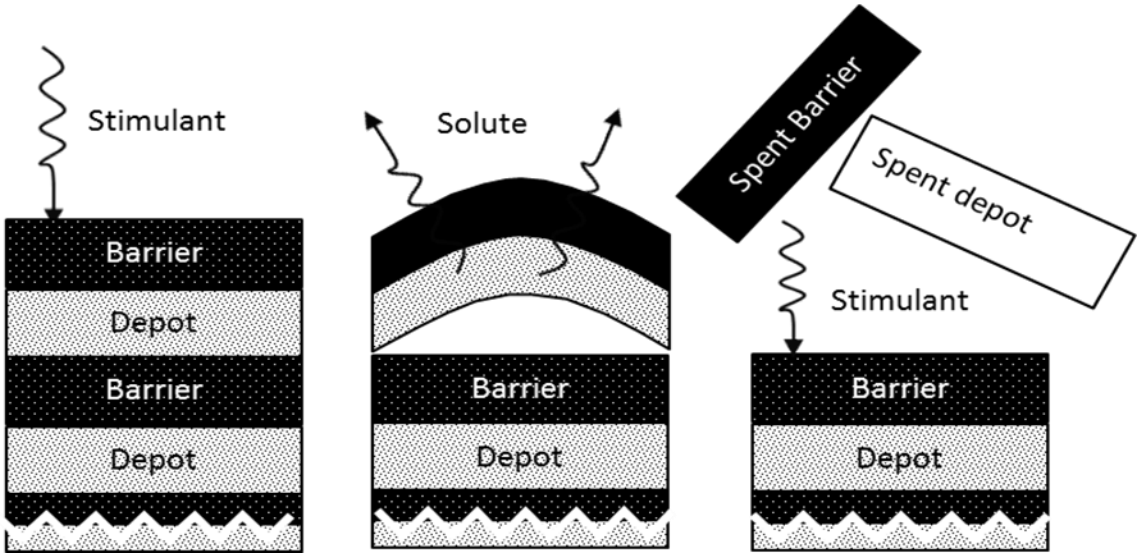

Figure 2.1 Schematic of delaminating BMPR system; release of solute occurs due to triggered hydration of depot layers which also allows the delamination of spent layers from the device.

permeability largely depends on hydration and swelling of the depot layer. Stimulant (acid) triggers the matrix of the depot layer making it hydrophilic and allowing them to swell with water. This water dissolves the pre-loaded solid solute particles and assists the diffusion of solute from the layer matrix. The function of barriers is to provide a resistance to stimulant for a specific time period before it can reach the depot layer. As shown in Figure 2.1, the first depot layer is allowed to swell isotropically. Upon swelling

this depot layer bows up and pops out from the stack as it is only bonded to its perimeter. The next barrier layer protects the underlying depot for a specific period of time before initiating the progressive swelling and delamination of that depot, and the process repeats.

For the above generalized system, depots were constructed using pH-sensitive methacrylate hydrogels that are glassy polymer at and above pH 7 but they swell significantly with water (almost 5 times their dry weight) at pH 3. Reactive barriers of poly(vinyl alcohol) (PVA) immobilized with Zinc Oxide (ZnO) nanoparticles (sacrificial scavenger) were used to protect the acid sensitive depots from the acid stimulant for predefined time intervals. We constructed the BMPR system by placing alternating layers of acid sensitive depots and scavenger-filled barriers together. Pulse timing of this BMPR system primarily depends on the scavenger concentration and the thickness of the barriers.

2.1 Materials

Methyl methacrylate (MMA), 2-dimethyl aminoethyl methacrylate (DMA), and divinyl benzene (DVB) were obtained from Aldrich (Milwaukee, WI). Polymerization inhibitors in these monomers were removed by adsorption on alumina (80-200 mesh size) (Fisher Scientific, Pittsburgh, PA), the monomers were then refrigerated until use. 2-2' Azobisisobutyronitrile (AIBN), zinc oxide (ZnO), citric acid and sodium hydroxide (NaOH) pellets were obtained from Sigma-Aldrich and used as received. Monobasic potassium phosphate (KH_2PO_4) and sodium chloride (NaCl) were obtained from Research Products International Corp. (Mt. Prospects, IL) and used as received. Poly (vinyl alcohol) (PVA, 99% hydrolyzed, MW ~ 133,000) was obtained from Polysciences

(Warrington, PA) and used as received. Methylene blue (MB) was obtained from Sigma Aldrich. Methyl orange (MO) was obtained from Alfa Aesar (Wardhill, MA). Both dyes were ground with a mortar and pestle and then screened using a gold tone mesh filter (Cusinart, Model GTF-B, 100 mesh size) before use.

2.2 Depot Films

2.2.1 Construction of Solute-free Depot Layers

Poly (methyl methacrylate) [p(MMA)] is a well-studied polymer and has the advantage of its superior mechanical properties.[40,48] When combined with a basic comonomer, p(MMA) has a strong sensitivity to acidic stimuli. Various basic comonomers have been studied that may enhance acid sensitivity in the p(MMA) matrix

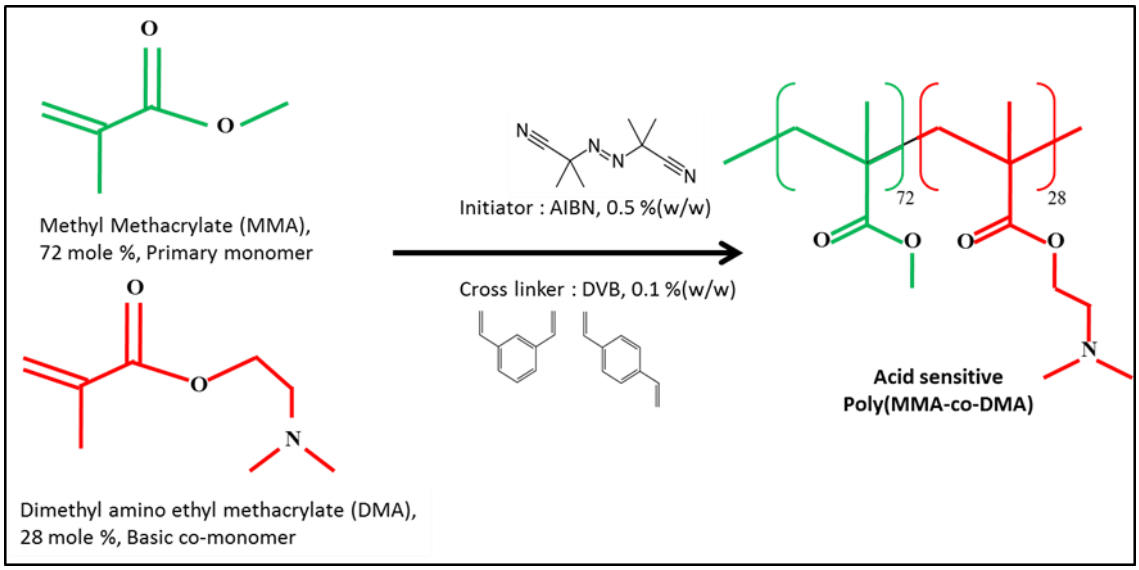

Figure 2.2 Polymerization reaction of p(MMA-co-DMA)

but dimethylaminoethyl methacrylate (DMA) has the strongest observed effect.[40] p(MMA) itself is a glassy hydrophobic polymer. In earlier published work, it was shown that by incorporating DMA in the p(MMA) matrix (for example, a 70/30 (mole ratio) of MMA/DMA), the polymer remains in it glassy hydrophobic state at neutral pH and

becomes strongly hydrophilic in acidic conditions (pH 6 and below). [45,49-51] For the proposed BMPR system, depot layers of poly(methyl methacylate-co-dimethyl amino ethyl methacrylate (p(MMA/DMA)) were constructed using stimuli-sensitive copolymer of methyl methacrylate (MMA) and DMA in 72/28 monomer mole ratio, respectively. The polymerization of p(MMA/DMA) is initiated by 0.5% (w/w) azobisisobutyronitrile (AIBN) and crosslinked with 0.1 % (w/w) divinyl benzene (DVB). The reaction mechanism is shown in Figure 2.2.

Solute-free p(MMA/DMA) samples were synthesized by adding 3.909 mL of DMA to 6.315 mL of MMA, 10.5 µL of DVB crosslinker, and 48.03 mg 2-2' AIBN initiator in a 20 mL vial. The solution was then poured between two silanized glass plates (20 cm × 20 cm) with PTFE spacers of various thicknesses ranging from 50 to 400 µm. A solution of 2% (w/w) dichlorodimethylsilane (DCDMS) in toluene was used to silanize the glass plates. The plates were then mounted vertically in a vacuum oven and complete polymerization was carried out at 60°C in an inert atmosphere of nitrogen (1 atm) for 18

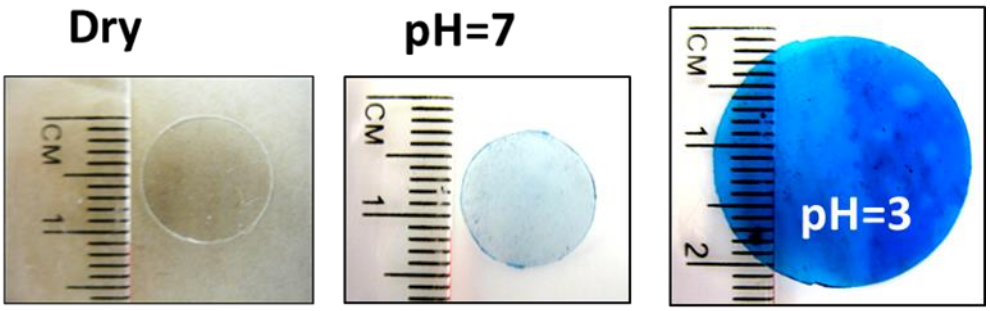

Figure 2.3 Circular disk of p(MMA/DMA) hydrogel in dry condition (left), at pH 7 (center), at pH 3 (right); blue dye was added in pH 7 and pH 3 buffers to contrast the pictures.

hours. Polymerized films were later peeled off of the glass plates and cut in to circular disks of 10 to 15 mm in diameter (Figure 2.3) using a metal cork bore. These disks were

further subjected to various pH environments to study their swelling behavior. As depicted in Figure 2.3, a dry p(MMA/DMA) disk (left) remained in its glassy hydrophobic state at neutral pH (center) with almost no swelling, but when immersed in pH 3 citrate buffer, it swelled with water by almost 5 times of its dry weight. Swelling behavior of these p(MMA/DMA) hydrogels at various pHs is further discussed later.

2.2.2 Construction of Solute-loaded Depot Layers

Methylene blue (MW 320 g/mole) and methyl orange (MW 327 g/mole) were used as two primary solutes for this study. Both small molecule organic dyes are hydrophilic, highly soluble in water and insoluble in organic liquids including MMA and DMA. The absorption spectra [λ_{max} of 664 nm (methylene blue), 461 nm (methyl orange

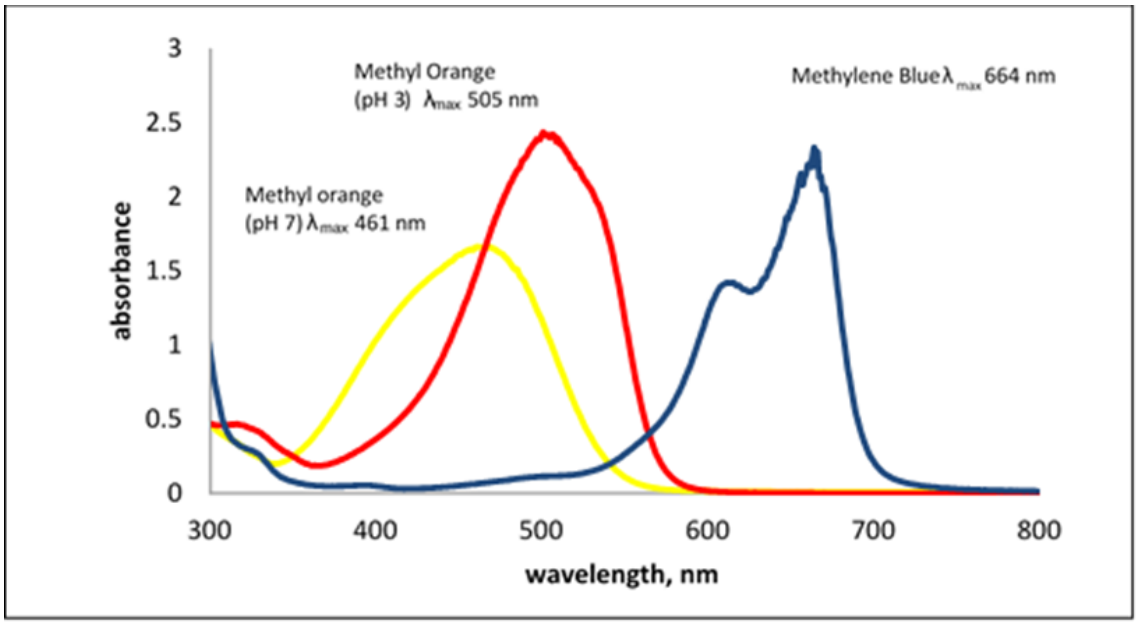

Figure 2.4 Absorption spectra of methylene blue and methyl orange; methylene blue concentration was 15 mg/L in water and methyl orange concentration was 25 mg/L for both pH 3 (citrate buffer) and pH 7 (phosphate buffer) for these spectra.

at pH 7) and 505 nm (methyl orange at pH 3)] for these two dyes are non-overlapping and in the visible range, as shown in Figure 2.4. The fine particles of these dyes can be

immobilized into the hydrophobic matrices of depot layer made of p(MMA/DMA) at substantial (at least 10 % wt) concentration and remain undissolved while the hydrogel is in the dry glassy state. As soon as the hydrogel is protonated by acid, it swells with water and the preloaded dye particles dissolve quickly. The release of each solute was independently monitored using a Cary 50 UV/Vis spectrophotometer.

The pre-screened dye particles were mixed into the monomer solution and polymerized as explained in section 2.2.1. However, it was observed in initial trials that particles started to settle during the transition phase from liquid monomer to polymer. This caused all of the dye particles to segregate to one side of the polymer sheet and it also created surface patterning on the polymer. As the liquid monomer started to polymerize, the volume of the material decreased and the polymer sheet started to shrink away from the spaced glass plate. This caused the polymerized sheet to stick smoothly on only one side of the glass plate leaving the other side with surface patterning with settled dye particles on it. This suggested that the presence of dye particles might have favored detachment during the transition phase of polymerization leaving the particles settled on that side. It was also observed that methylene blue loaded p(MMA/DMA) films were found to be more rubbery and weak than that of solute-free p(MMA/DMA) films which suggests that the presence of methylene blue particles inhibited the rate and degree of polymerization.[52]

For homogeneous distribution of dye particles in depot layers and to avoid surface patterning in the films, the polymerization procedure was slightly altered. After mixing the reactants in a 20 ml vial, the solution was pre-polymerized at 80°C hot plate temperature (70°C solution temperature) at 1200 rpm to increase the viscosity to

approximately 65 cP. Thickening of the solution was measured by visual observation of the vortex in the vial. Upon disappearance of the vortex, the viscous solution was immediately quenched at room temperature. The required amount of pre-screened dye particles (methylene blue or methyl orange) was added to this viscous monomer solution and homogeneously distributed using an ultrasonic homogenizer (Cole-Parmer CPX750, with 3.2 mm microtip, 1 min at 300 W, 20 kHz). This prepolymerized homogeneous, dye loaded, viscous suspension was then poured on a silanized glass plate and immediately covered with another silanized glass plate with 100-300 µm Teflon spacer between. The plates were mounted vertically in a vacuum oven where complete polymerization was conducted at 60°C in 18 hours. It was observed that the resulting films had relatively homogeneous distribution of dye particles throughout the film without any surface patterning. These films were also found to be glassy and robust in nature, which confirmed that immersing dye particles (especially methylene blue) after thickening the monomer solution minimized the possibility of their inhibiting the rate and degree of polymerization. The p(MMA/DMA) depots were successfully immobilized with up to 10% solute loading (w/w). Both solute-free and solute loaded p(MMA/DMA) films of uniform thicknesses between 50 to 350 µm were prepared. Circular disks of these depot films were then studied for swelling and release analysis at pH 7 and pH 3. However, solute loading was consistently maintained at 5 % (w/w) for the swelling and release studies of dye-loaded depot films.

2.2.3 Depot Layer Characterization

As described in section 2.2.1, p(MMA/DMA) depots were constructed by polymerizing methyl methacrylate (MMA) with basic commoner dimethyl aminoethyl

methacrylate (DMA) in 72/28 (MMA/DMA) molar ratio, which makes the depot acid-sensitive. The pK_a of DMA is 8.4.[53] To confirm the DMA content in p(MMA/DMA), circular disks of the depots (triplicates with an average weight of 40 mg, average thickness of 346 µm and average diameter of 12 mm) were equilibrated in 150 mM saline solution (~300 times sample weight) set to pH 2 via HCl addition. As the acid protonated the amine groups of DMA inside the hydrogel, the pH of the solution rose from 2.0 to 2.76 (± 0.06 on n=3). This indicates the actual molar ratio of MMA:DMA to be 75:25 in the depot, suggesting a slightly lower conversion of DMA than MMA.

2.2.3.1 pH Dependent Swelling Behavior

Weak acid buffers have a sharp effect on the swelling rate of polybasic methacrylate based hydrogels. The swelling rate of the gel is mediated primarily by the effect of pH on the concentration of the conjugate acid form of the buffer, rather than a direct effect of pH on the gel.[50] Swelling of the gel also depends on the molar concentration of the buffer solution even at lower pH.[40,49,50] For this study, citric acid was chosen as a stimulant and used in the form of citrate buffer (pH 3, 4, 5 and 6) with an ionic strength of 0.1 M and a buffer concentration of 0.01 M. We also used 0.01 M phosphate buffer (pH 7, and 8) with an ionic strength of 0.1 for the swelling studies. The p(MMA/DMA) hydrogels are hydrophobic at pH 7 and above and adsorb almost negligible amounts of water.

Swelling studies of 75/25 p(MMA/DMA) were conducted in various pH environments as shown in Figure 2.5, where 12 mm-wide, 223 µm (± 1.7% RSD, for n=27) thick circular disks were immersed in citrate (pH 3, 4, 5, 6) or phosphate (pH 7, 8) buffer and periodically reweighed. Each trial was done in triplicate. There was no

significant swelling at pH 7 or 8, as the pK_a of p(DMA) ranges from 7.4 to 7.8.[53] At low pH, as the acid diffuses into the hydrogel it triggers swelling and the hydrogel absorbs a significant amount of water. A dramatic change in swelling was observed near pH 3 where the hydrogel (240 µm thick, 14 mm wide) absorbs to five grams of water per gram of dry gel within two to three hours. This swelling behavior is very important feature of

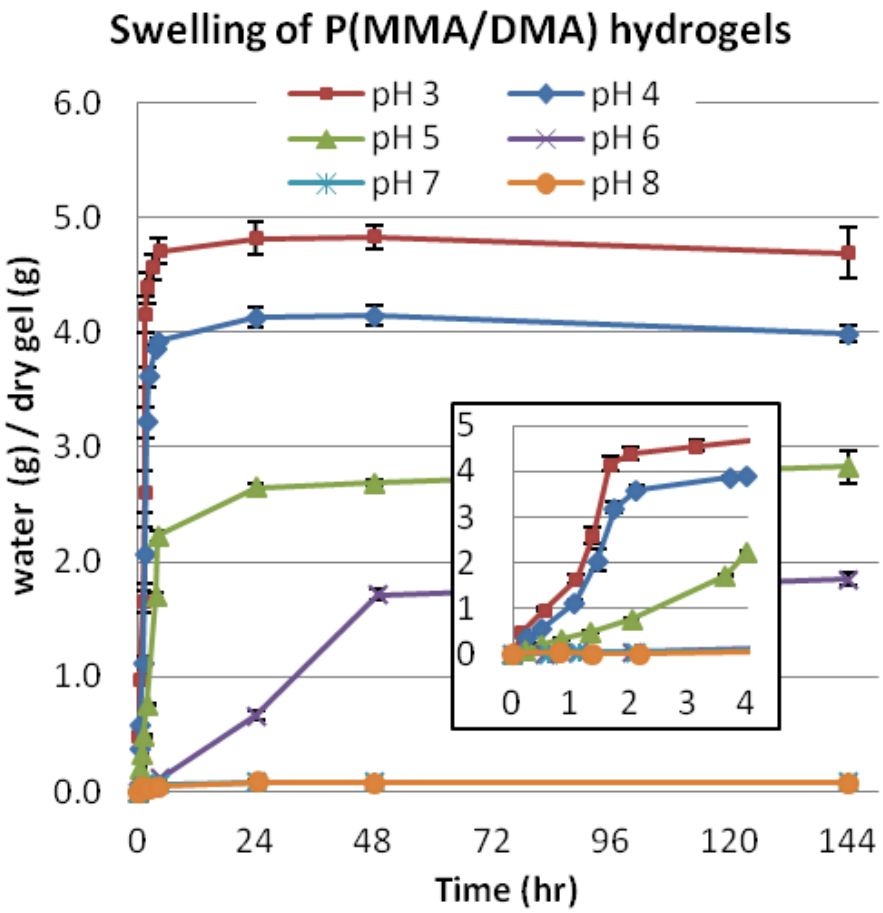

Figure 2.5 Swelling behavior of p(MMA/DMA) hydrogels at various pH

the p(MMA/DMA) hydrogel. As p(MMA/DMA) is a hydrophobic copolymer, one can preload hydrophilic solutes as insoluble (and therefore immobile) particles. The dramatic swelling at acidic pH provides a significant change in solute release profiles which will be further discussed later. When the hydrogel absorbs a significant amount of water, the

solute particles dissolve and diffuse out of the layer. As shown in Figure 2.5, for each case below pH 6, both swelling rate and equilibrium swelling ratio varied strongly with pH, which reconfirms the previously published swelling studies of p(MMA/DMA) hydrogels.[40,49] The S-shape curve (shown more clearly in the inset of Figure 2.5) of the swelling profiles implies that the swelling is transport limited. The swelling front moves inward in a single direction from each face of the disk towards the center and moves gradually at a slower rate as the diffusional distance for the stimulant increases. When these fronts meet in the center of the layer, there is no possible further swelling in the longitudinal direction, and the hydrogel swells promptly in the lateral direction.

2.2.3.2 Release Trials with Solute-loaded Depots

The next set of swelling trials were done with the depots loaded with 5% (w/w) solute (methylene blue or methyl orange) where the release of the solute was

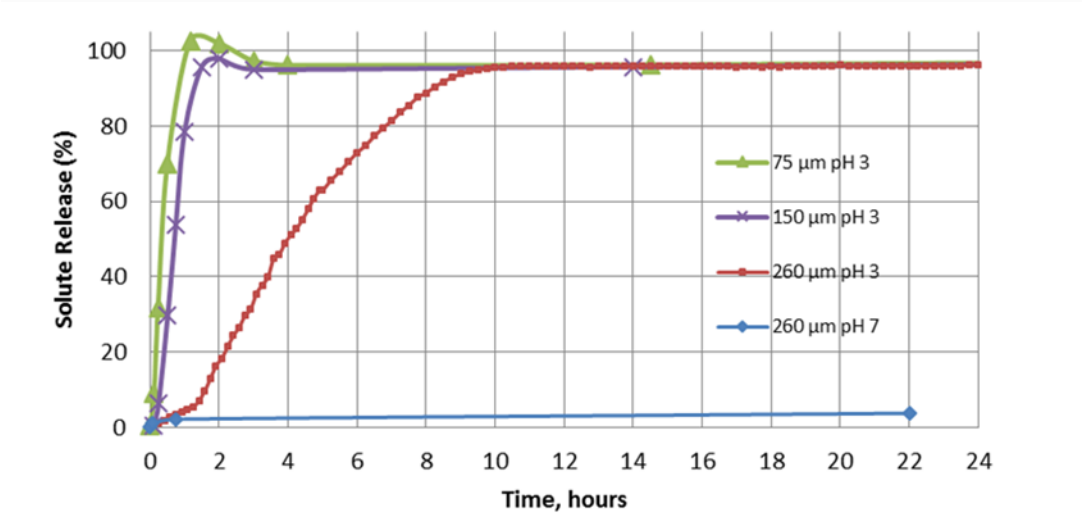

Figure 2.6 Methylene blue release from p(MMA/DMA) hydrogels, no significant release at pH 7 (< 4%), Dye gets released completely at pH 3.

simultaneously monitored using a UV/Vis spectrophotometer. The methylene blue spectrum is well known and is independent of pH. The methyl orange spectrum changes with pH, but is non-overlapping with methylene blue. Swelling and release trials of these

solute loaded depots were conducted for films that varied in thickness from 75 to 350 µm at pH 3 and pH 7. Figure 2.6 depicts the release of methylene blue from the p(MMA/DMA) hydrogels at various thicknesses and pHs. Due to hydrophobicity of the p(MMA/DMA) hydrogel at pH 7 the hydrogel remained in its glassy shrunken state and did not absorb water into the gel matrix. As a result of which, only ~4 % of loaded solute was released from the 260 µm p(MMA/DMA) hydrogel at pH 7. This small amount of release occurred instantly because the dye was directly exposed to the buffer solution around the perimeter of the disk where it was cut. Figure 2.6 also depicts methylene blue release that occurred at pH 3, where nearly all of the solute was released. Solute from thinner films (75 µm and 150 µm) was released during the first hour of exposure. Equilibrium swelling ratios of these hydrogels were ca. 7 g water/g dry gel, which were roughly 30% higher than that of solute-free depots depicted earlier in Figure 2.5, which indicates that presence of methylene blue affects the degree of polymerization.

Similar trials were also conducted with 5% (w/w) methyl orange loaded p(MMA/DMA) depots. Figure 2.7 (left) shows the swelling behavior of 5% (w/w) methyl orange loaded p(MMA/DMA) hydrogels at pH 7 and pH 3 for thicknesses of 190 µm and 312 µm. Equilibrium swelling of these hydrogels was 6 to 7 g of water/g polymer at pH 3, which was similar to that of methylene blue loaded hydrogels. Figure 2.7 (right) shows the release profiles of 190 µm and 348 µm thick 5% (w/w) methyl orange loaded p(MMA/DMA) hydrogels. The release rate of methyl orange was faster from the 190 µm films than that of the 348 µm films. It took ca. 10 and 24 hours to release 70 % of the loaded dye for 190 and 348 µm films respectively. It was possible to release essentially all of the dye from swollen hydrogels by replacing the pH 3 buffers periodically. The

release rate increased each time when the gels were placed in fresh buffer. However,

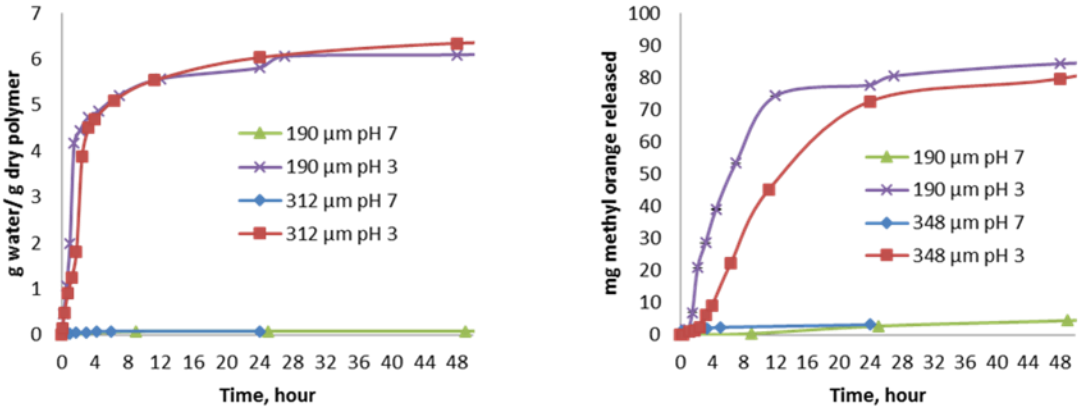

Figure 2.7 Swelling and release profiles of methyl orange loaded p(MMA/DMA) hydrogels; significant release occurs at pH 3 as the hydrogel swell, release rate also corresponds to swelling rate at pH 3, very low release (< 5 %) observed at pH 7, which mostly occurred from the periphery of the gel where it was cut.

release rates of methyl orange were slower than the release rates of methylene blue. Methylene blue is a positively charged molecule (Figure 2.8, left) and releases faster from the protonated depot matrix of a swollen hydrogel whereas methyl orange is a negatively charged molecule (Figure 2.8 right) and releases at comparatively slower rate

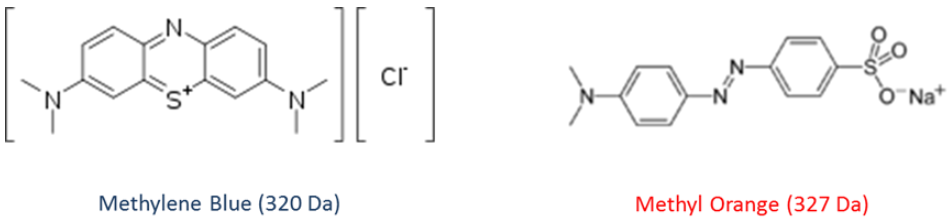

Figure 2.8 Structure of methylene blue and methyl orange; positively charged methylene blue releases faster and negatively charged methyl orange releases at slower rate from protonated swollen p(MMA/DMA) hydrogel.

from the protonated hydrogel. Thus, the hydrophobic nature of p(MMA/DMA) and it being glassy at pH 7 allows it to release negligible amounts of dye, while at pH 3 it swells dramatically and releases the solute completely. This behavior of p(MMA/DMA)

is a key feature for the proposed BMPR system and serves as an ON-OFF mechanism. When the hydrogel is in its shrunken state at neutral pH, the release of BMPR system can be considered on the "off state" with a negligible release rate. When the hydrogel is swollen in an acidic environment, dissolves the solute which diffuses away from the gel, it is considered in the "on state". The "on state" mechanism relies on different states of the hydrogel. It starts when the stimulant (acid) diffuses to the gel to trigger the swelling followed by complete swelling of gel. Once the gel is swells with sufficient amount of water it dissolves the solute and then diffuses out from the swollen hydrogel.

2.2.3.3 Thickness Dependence

Swelling trials of solute-free depots were conducted on hydrogels of a various thicknesses. Circular p(MMA/DMA) disks (12 mm wide) with different thicknesses

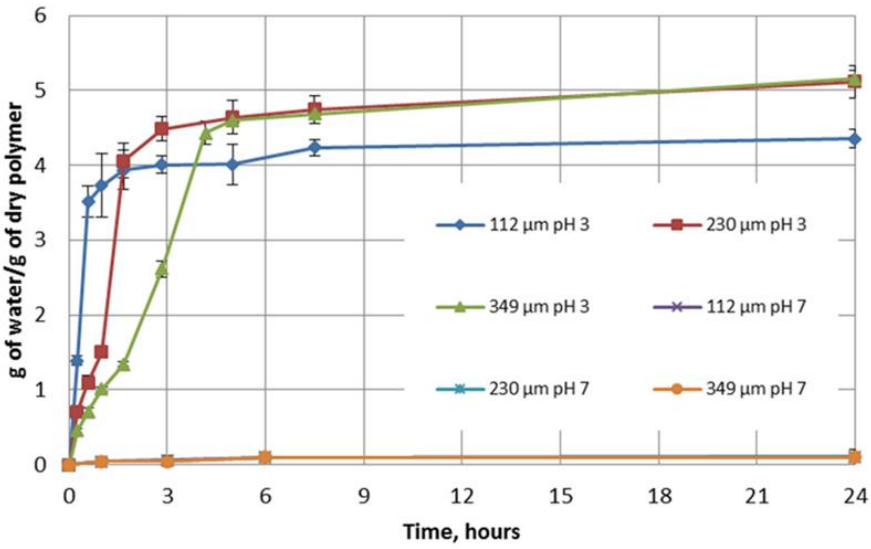

Figure 2.9 Effect of thickness on swelling of p(MMA/DMA) hydrogels

(range 100-350 µm) were immersed in pH 7 (0.01 M phosphate buffer, ionic strength 0.1) and then in pH 3 (0.01 M Citrate buffer, ionic strength 0.1). Each trial was done in triplicate. Figure 2.9 shows the effect of thickness on swelling of p(MMA/DMA)

hydrogel at pH 3 and 7. There was no significant swelling of the hydrogel at pH 7 as discussed earlier. At pH 3, significant swelling was observed in each case. The swelling curves for each thickness (112, 230 and 349 μm disks) indicate that thinner hydrogels swelled more rapidly than thicker ones. The sigmoidal shape of the swelling curves shown in Figure 2.9 for 230 μm and 349 μm films reconfirms that the swelling is transport limited which is also visible in the pH dependent swelling behavior of p(MMA/DMA) as described earlier (Figure 2.5). However, the thinnest film (120 μm) does not follow the sigmoidal shape as there is no inflection point and also does not show second order dependence on thickness. This indicates that the swelling rate of the thinnest film is not transport limited and swells very rapidly in less than an hour. Swelling times of less than an hour for such thin films (100 to 150 μm) becomes very important in determining swelling rate, at it directly affects the release rate if the depots were filled with solute. Figure 2.6 also showed this effect where the release rate of methylene blue was not transport limited with the thinner depots (both 75 μm and 150 μm) in the earlier described release study of 5% methylene blue loaded p(MMA/DMA) films where all the dye was released in less than an hour at pH 3.

2.2.3.4 Effect of Buffer Strength on Swelling

While Figure 2.5 and Figure 2.6 showed that the swelling of p(MMA/DMA) hydrogels is pH dependent and diffusion limited, previous studies have indicated that this is not due to higher H^+ concentrations providing faster transport.[50] While higher H^+ concentration leads to more protonation of the amine groups in the hydrogel matrix and hence a larger equilibrium swelling ratio, the swelling rate is also dependent on buffer concentration (*i.e.* concentration of the neutral acid and its conjugate base) along with its

pH dependence. This is shown in Figure 2.10, which indicates that the rate limiting stimulant species is not H_3O^+, but rather neutral citric acid, whose concentration changes

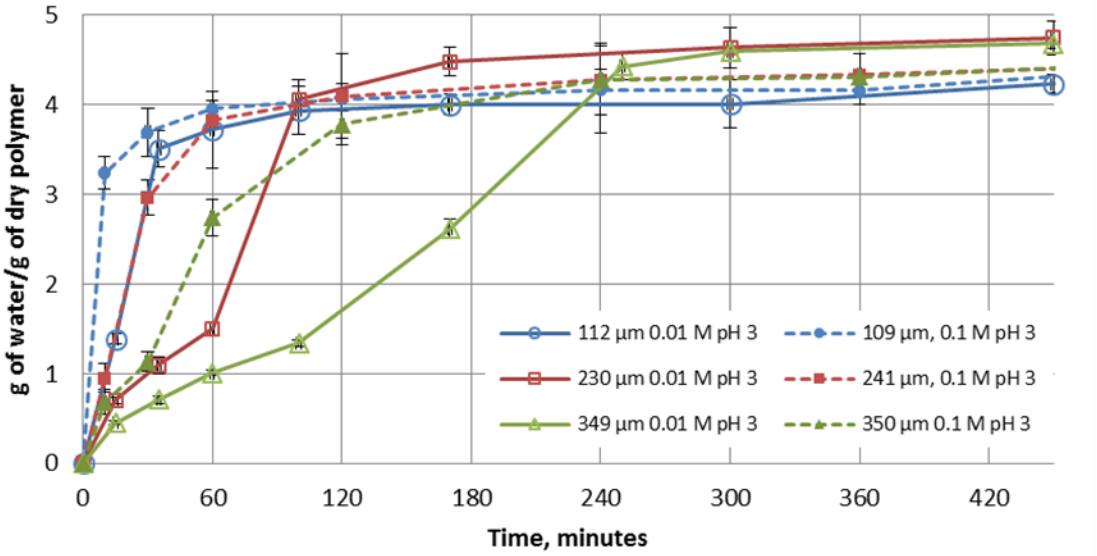

Figure 2.10 Effect of buffer strength and thickness on swelling of p(MMA/DMA) hydrogel; at any thickness, depot films swell considerably faster in more concentrated buffer at the same pH, showing the importance of the neutral weak acid in these systems.

with both buffer concentration and pH. Neutral citric acid was not the dominant diffusing species when films were subjected to 0.01 M pH 3 citrate buffer; the fluxes of neutral and dissociated acid in the p(MMA/DMA) matrix should be roughly the same. However, when the buffer concentration was increased to 0.1 M from 0.01 M, the swelling rate increased dramatically even though with the same ratio of dissociated acid to undissociated acid (*i.e.* pH 3). Hydronium ions do not easily diffuse in the hydrophobic glassy polymer. The swelling rate in 0.01 M citrate buffer was significantly slower than in 0.1 M citrate buffer, which is depicted in Figure 2.10 with dashed lines vs solid lines of the same color and marker shape. It was also observed that swelling rate is several orders of magnitude slower in non-buffered straight HCl solution of pH 3. This also explains the similarity in the swelling behavior of p(MMA/DMA) in pH 3 and pH 4 in Figure 2.5 where the swelling rates are faster compared to those at pH 5 and 6. In the former case,

undissociated citric acid concentrations are high and similar, while the concentration of citric acid drops 10-fold for each pH shift of 1 unit (*i.e.* pH 4 to pH 5, and pH 5 to pH 6). This explanation becomes very important for using the proposed BMPR system as an implantable drug delivery system, as gluconic acid (another weak acid similar to citric acid) can be considered as a likely stimulant for such a system. Gluconic acid can be obtained enzymatically from blood sugar.

2.2.3.5 Transport of Acid through p(MMA/DMA) Membranes

The transport studies of acid through a p(MMA/DMA) membrane was conducted in a diaphragm cell as shown in Figure 2.11, along with a titrator (Metrohm Titrando 842, Herisau, Switzerland). Calculating the permeability of acid through the p(MMA/DMA)

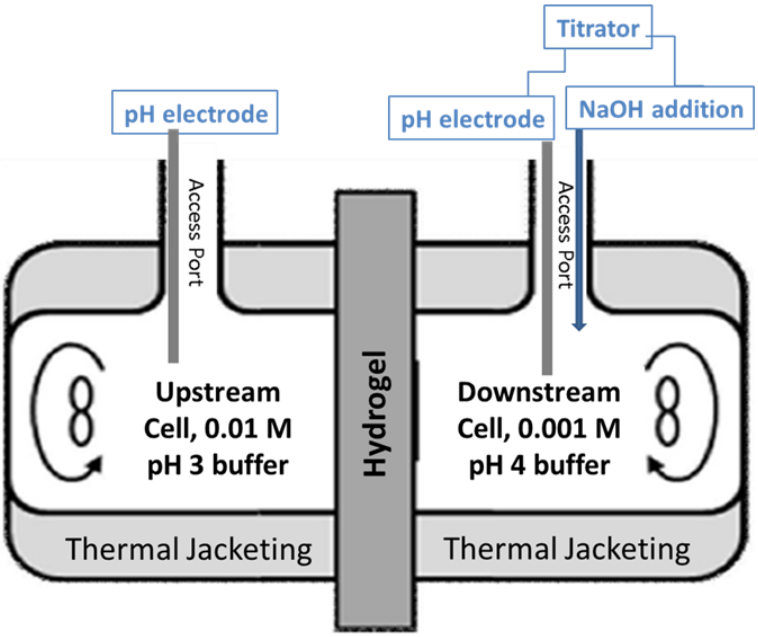

Figure 2.11 Schematic of diaphragm cell used to calculate transport of acid through p(MMA/DMA) hydrogel

membrane accurately was challenging because the transport properties of pH sensitive p(MMA/DMA) films are dependent on acid concentration. Prior to testing, the p(MMA/DMA) films were soaked in pH 4 citrate buffer (buffer strength 0.001 M) for 3

days. The pre-swollen hydrogel was then sandwiched between two diaphragm cells (22 mL volume). The upstream solution was spiked with pH 3 citrate buffer (0.01 M). The titrator maintained the downstream pH at 4.0 (initial buffer strength 0.001 M) while recording the rate of sodium hydroxide addition required to maintain this pH across from an upstream citrate buffer (initial buffer strength 0.01 M) at pH 3. The rate of NaOH addition to maintain the steady pH of 4 at downstream indicated the rate of total acid transport across the film. Sodium was the buffer counter ion. An ionic strength of 0.1 was maintained throughout the cell by adding 95-99 mM NaCl solution. The steady state permeability of acid across the p(MMA/DMA) film was determined to be 5.1×10^{-5} cm^2/s. Since this value is a composite from the flux of two separate species, it may be more useful to consider the equivalent overall acid flux across a 100 μm film which is 5.5×10^{-9} mol /(cm^2 s). This value will be compared below against the overall acid flux across 100 μm of water.

Neutral citric acid has a diffusion coefficient in water of approximately 6.6×10^{-6} cm^2/s [54], comparable to sodium citrate [55](Na^+ being the most concentrated cation in the buffer) but about 4.8 times slower than the 3.2×10^{-5} cm^2/s diffusion coefficient of H_3O^+ coupled with chloride[56] (Cl^- being the fastest and most concentrated anion in the buffer). Though neutral citric acid diffuses 4.8 times slower, its concentration in 0.01 M pH 3 buffer (5.8×10^{-3} M) is 5.8 times higher than that of dissociated protons, so the flux of neutral citric acid into the depot is only (5.8/4.8=) 1.2 times greater than that of dissociated protons. In the diaphragm cell experiments, the depot membrane separates 0.01 M pH 3 upstream buffer solution and a 0.001 M pH 4 downstream buffer solution. As both acid species diffused to the downstream side, all of the dissociated acid and 90%

of the neutral acid (becoming dissociated due to the 1-point pH shift) were neutralized by constant titration with NaOH to maintain a downstream pH of 4. As discussed earlier, the rate of NaOH addition indicated an overall acid flux of 5.5×10^{-9} mol/(cm^2 s) per 100 µm of film thickness. A 100 µm thick film of stagnant water under the same conditions should have an overall acid flux of 6.6×10^{-9} mol/(cm^2 s). The acid permeability of the film is 80% that in water, and the film, spanning pH's from 3 to 4, is approximately 80% water, suggesting that the acid has no significant interaction with the swollen hydrogel network and that its partition coefficient in the hydrogel is essentially the hydrogel's water volume fraction.

2.2.3.6 Transport Properties of Solutes through p(MMA/DMA) Hydrogel

The transport properties of p(MMA/DMA) hydrogels were determined using a diaphragm cell. In short, the hydrogel was placed between two well stirred 22 mL glass

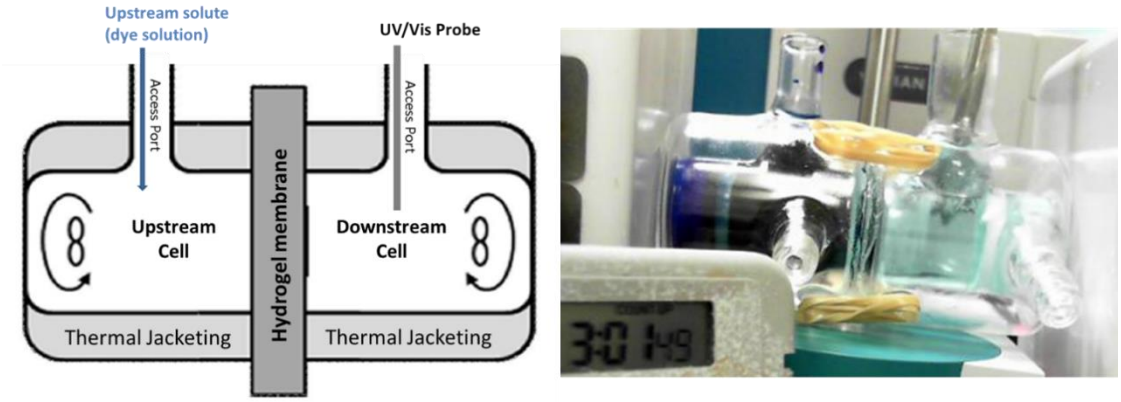

Figure 2.12 Schematic of diaphragm cell (left) used for characterizing transport studies of solute through p(MMA/DMA) hydrogel membrane, actual diaphragm cell (right).

cells as shown in Figure 2.12. The upstream cell contained a concentrated solute solution of dye (methylene blue or methyl orange) and downstream cell solute concentration was monitored using an immersed fiber optic probe coupled to a UV/Vis spectrophotometer

in real time at 664 nm to calculate the permeability of the solute through the membrane. For these dye permeability trials, p(MMA/DMA) depots were soaked in 0.01 M buffer of pH 3 or pH 7 for 1-3 days before being used in the diaphragm cell.

At pH 3, both solutes diffused through the swollen matrix of the p(MMA/DMA) depot and showed steady-state permeability through the film. Permeability of methyl orange and methylene blue through p(MMA/DMA) was determined to be 3.4×10^{-7} cm^2/s (± 7.9%) and 3.0×10^{-7} cm^2/s (± 16%), respectively. Using the lag times for these trials, the diffusion coefficient of methylene blue in the depot film was calculated to be 7.1×10^{-7} cm^2/s, yielding a partition coefficient of 0.43. It was reconfirmed when the depot films were equilibrated in a pH 3 buffer of a known methylene blue concentration (7.27 mg/L), and then the solute was desorbed out in fresh buffer for the quantification. This yielded a partition coefficient of 0.48. Diffusion coefficient of methylene blue in water is $\sim7\times10^{-6}$ cm^2/s [57], which indicates that, unlike acid, methylene blue avoids entering the depot and diffuses more slowly in the gel than it does in water. This is because of the larger particle size of methylene blue (MW 320 g/mole), its planar configuration, and also its positive charge. In the case of negatively charged methyl orange, the depot behaves as an ion exchange resin and the difference between partitioning and adsorption becomes unclear. However, the low permeability of methyl orange (3.0×10^{-7} cm^2/s) in the depot (half that of methylene blue) suggests that it also diffuses more slowly in the gel than it does in water. The size of methyl orange (MW 327 g/mole) and its planar configuration are comparable to that of methylene blue's. At pH 7, none of the solutes (either methylene blue or methyl orange) diffused through p(MMA/DMA) hydrogel and the permeability of these solute through the film was found negligible.

2.2.4 Comparison of Swelling vs. Release Times

Despite the slower mass-transport coefficients, the release rate of the solute from the depot appears to be consistent with the swelling rate, as shown in Figure 2.13 which shows both the swelling and drug release rate vs. time for depots of different thickness. The equilibrium swelling ratios of methylene blue loaded depots were clearly greater than those observed in solute-free depots (Figure 2.5) due to possible inhibition in

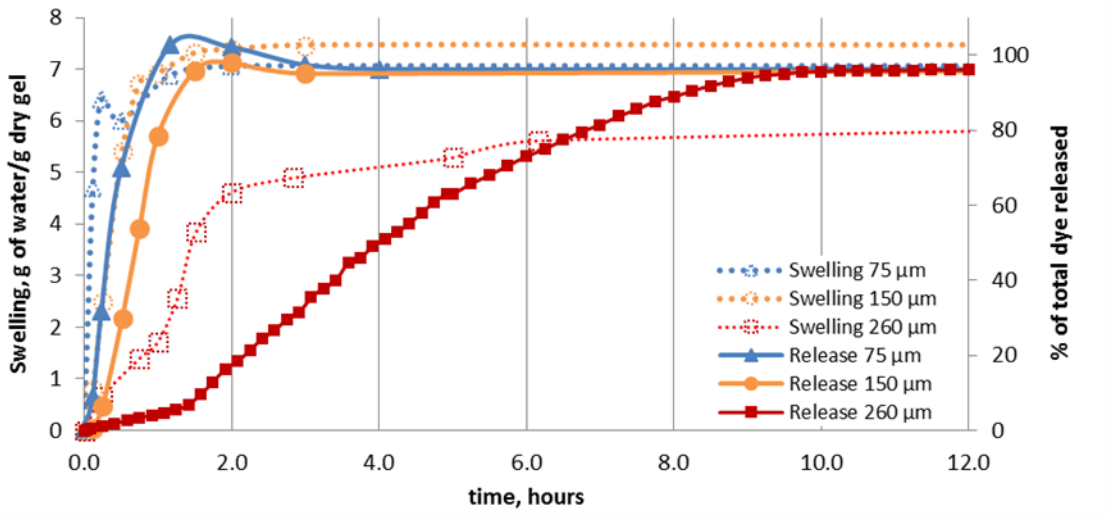

Figure 2.13 Comparison of swelling and solute release rates in p(MMA/DMA) hydrogels; No swelling and negligible release of methylene blue at pH 7. At pH 3 the characteristic swelling and release times can be estimated analytically.

polymerization by methylene blue particles. However, as indicated in Figure 2.13, the time required for the hydrogel to release its loaded drug is approximately twice the time required for swelling regardless of film thickness, which reconfirms that solute release is transport limited. Based on this transport limited release and swelling, characteristic swelling time (t_{swell}) and release time (t_{rel}) can be determined using Equations 2.1 and 2.2, where C_{stim} and C_{sat} are the external acid concentration and the solute saturation concentration, respectively, while C_{scav} and C_{solid} are the concentration of the acid-scavenging amine groups and solid solute in the depot, respectively. DH is the

permeability of the indicated species in the depot, and l is the film half-thickness in the swollen state.

$$t_{swell} = \frac{C_{scav}}{C_{stim}} \frac{l^2}{2\,DH_{stim}} \tag{2.1}$$

$$t_{rel} = \frac{C_{solid}}{C_{sat}} \frac{l^2}{2\,DH_{solute}} \tag{2.2}$$

Based on effective molar ratio of MMA/DMA [75/25 (by mole)] in the depot, the concentration of amine groups in dry shrunken polymer was calculated to be 2.33 M. The effective methylene blue concentration in 5%(w/w) loaded p(MMA/DMA) was found to be 0.145 M. Saturation concentration of methylene blue in the earlier described trial was 5.9 mM. From the sigmoidal curves of p(MMA/DMA) swelling (Figure 2.5 and Figure 2.9), it was observed that these hydrogels swell by almost a factor of two in a single direction before swelling laterally, which was verified by covalently bonding p(MMA/DMA) samples to a glass substrate to permanently restrict the swelling in one direction. Thus, doubling the half-thickness of each depot shown in Figure 2.13, l becomes dry thicknesses shown in figure legend. The amine concentration and solid drug concentration for those membranes now become to 1.17 M and 0.073 M, respectively. Using these values along with permeabilities calculated in diaphragm cell trials, the characteristic swelling time for a 75, 150 and 260 µm thick depot are 0.17, 0.66 and 1.99 hours, respectively. This matches well with the swelling data in Figure 2.13. The characteristic release times are also comparable to be 0.28, 1.14 and 3.41 hours, respectively. It is important to note that release starts well before the swelling is complete but cannot end until after swelling is complete. However, it is important to note these

times because they impact the overall release profiles which are now dependent on both swelling and drug diffusion process. Both characteristic swelling and release times suggest that both rate processes affect the final release profile from a given release trial from the depot. The overall release rate and shape of drug containing p(MMA/DMA) depot can vary with change in any of the parameters shown in Equation 2.1 and 2.2, which will affect the overall speed of the "on-state" BMPR mechanism.

2.3 Barrier Films

2.3.1 Barrier Layer Fabrication

Polyvinyl alcohol (PVA) is a commonly used inert and water soluble polymer.

Figure 2.14 ZnO nanopowder.

When cross-linked and immersed into water, it forms a water-swollen hydrogel which is highly permeable[46,47]. By incorporating zinc oxide (ZnO) nanoparticles in PVA film, it becomes an effective acid barrier[47]. ZnO is a white nanopowder (Figure 2.14) which is

nearly insoluble in water. Upon reacting with most acids, ZnO forms a soluble inert zinc salt. Thus, it works as a sacrificial scavenger for specific acid stimulants for a certain time period until it is completely consumed by the stimulant. The nanostructure of these

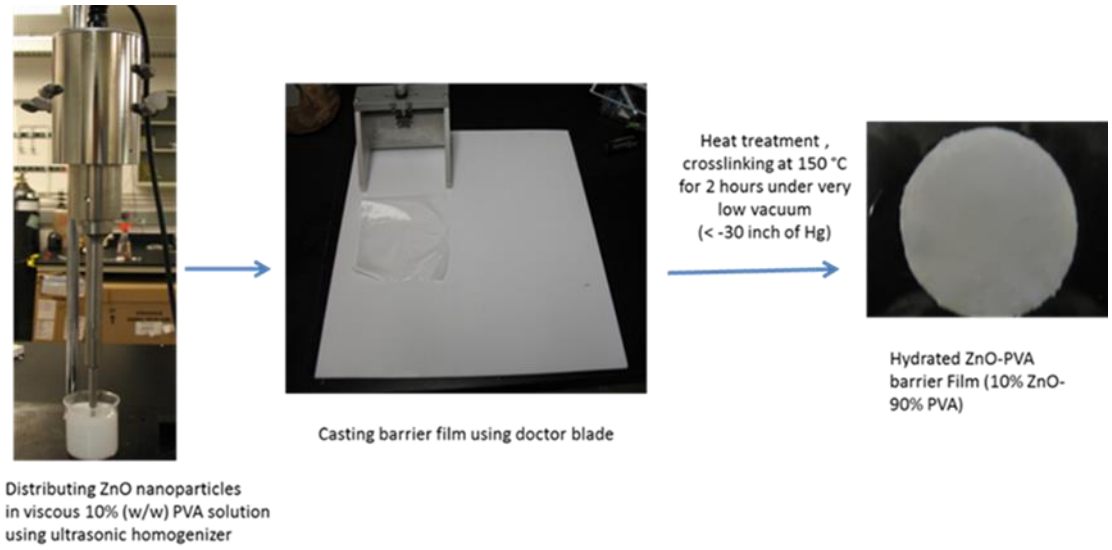

Figure 2.15 Fabrication of zinc oxide loaded barrier film.

ZnO particles aids in distributing them in the PVA matrix and simultaneously increases their reactivity to stimulant because of the large surface area of the particles.

The barrier films in the proposed study were prepared using PVA (MW 133,000) as described in an earlier published procedure[46]. A 10 wt % PVA solution was prepared by adding 15 g PVA to 135 g of water at 90°C with continuous stirring for 1-2 hrs. ZnO powder was added to water to make a slurry and sonicated using an ultrasonic homogenizer for 1 min at 300 W power. The ZnO slurry was then added to the 10 wt% PVA solution. The weight % of ZnO in PVA was varied from 10%, 20%, 30%, 40%, 60% to 80% by solid weight. The prepared ZnO loaded PVA solution was degassed under vacuum for 5-10 minutes to remove bubbles. The solution was cast on a PTFE block using a doctor blade with variable casting thickness from 0.5-2.5 mm. The films

were dried overnight and cross-linked for 2 hours at 150°C under vacuum (< -30 inch of Hg). The resulting films were strong, slightly yellowish in color and approximately 50 to 250 µm thick. These films were then hydrated in deionized water for at least 24 hours before using them for either diaphragm cell studies or in construction of BMPR device. Small dry pieces of these films were sampled for SEM characterization. Barrier films of different purported ZnO content (10% to 80% by weight) were equilibrated with HCl to confirm their ZnO content. Upon titration, it was always found to be within 0.3 % of the purported values.

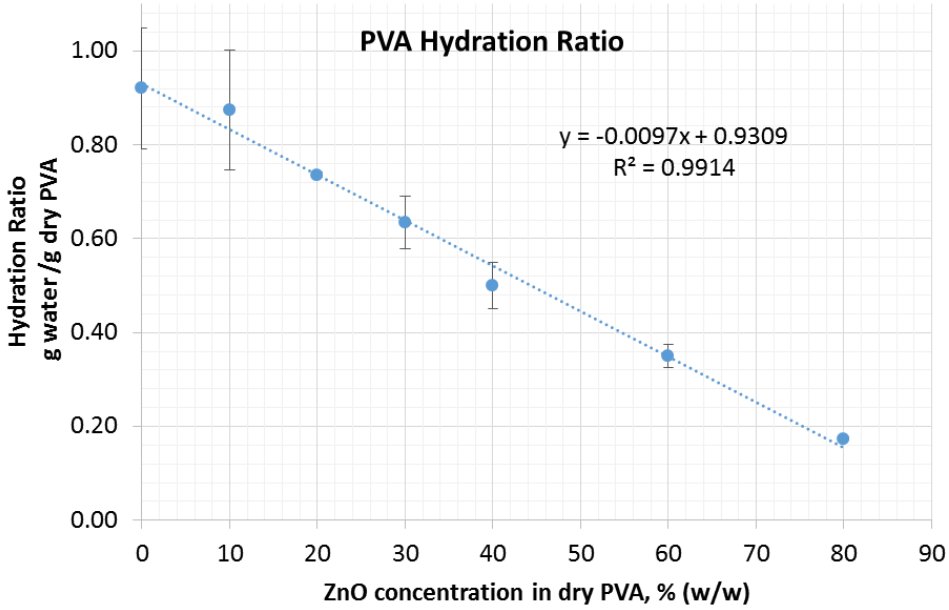

Figure 2.16 Hydration ratio changes with zinc oxide loading in barrier films.

Various PVA films with different ZnO loading (10% to 80 % by weight) were tested for hydration studies with the thickness ranging from 39 to 167 µm. Figure 2.16 depicts the hydration ratio of these films. When immersed in deionized water for at least 24 hours, PVA barrier films swelled with water. The hydrated films were rubbery but robust in nature. However, the hydration ratio in these cross-linked PVA barriers varied

with the ZnO loading. PVA films containing no ZnO absorbed 0.93 g of water / g of dry PVA. With increased ZnO loading in PVA, the hydration ratio gradually decreased, indicating no contribution in swelling by the ZnO particles.

2.3.2 SEM Characterization of PVA Barrier Films

ZnO loaded PVA barrier films were cut into small pieces and freeze fractured in liquid nitrogen. The fractured portions were mounted vertically on an aluminum stub using silver chloride (AgCl) paint to support the film. The resulting exposed film cross sections were then subjected to micro-imaging using a scanning electron microscope Hitachi S-4800.

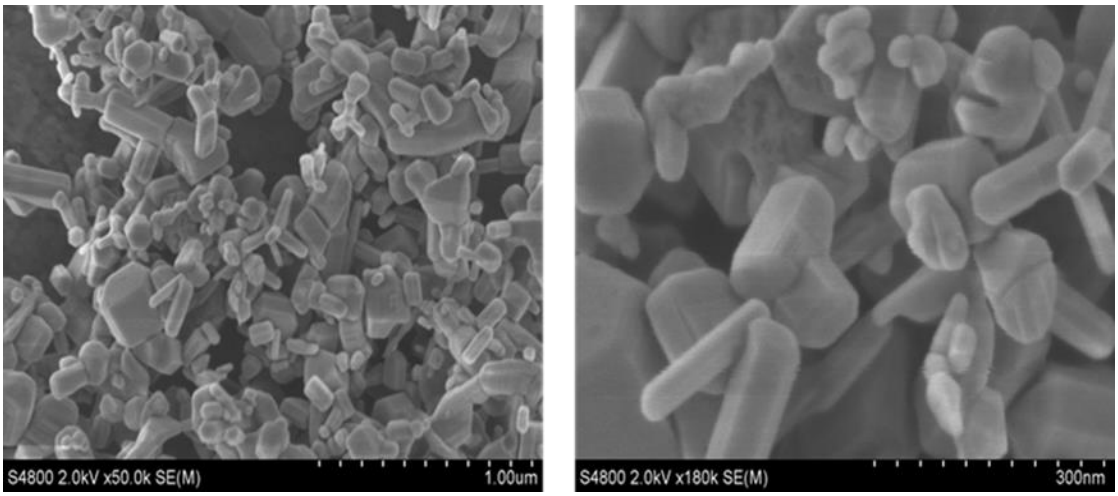

Figure 2.17 SEM images of ZnO nanopowder with a particle size less than 300 nm.

Figure 2.17 shows the nanostructure of bare ZnO particles that were dispersed in methanol, coated on an aluminum stub and dried under vacuum. These particles have a size of approximately 100-300 nm. These particles when dispersed in PVA films tend to distribute homogeneously. Figure 2.18 (A) shows the SEM image of the cross section of the PVA film without any zinc oxide. Figure 2.18 (B) shows the SEM image of PVA film

which has 10 wt% ZnO loaded in it. This indicates that the presence of ZnO particles in the films clearly differs from the one that does not contain any ZnO. This phenomenon is even better illustrated in Figure 2.18 (C) where a ZnO free layer was cast on top of a ZnO

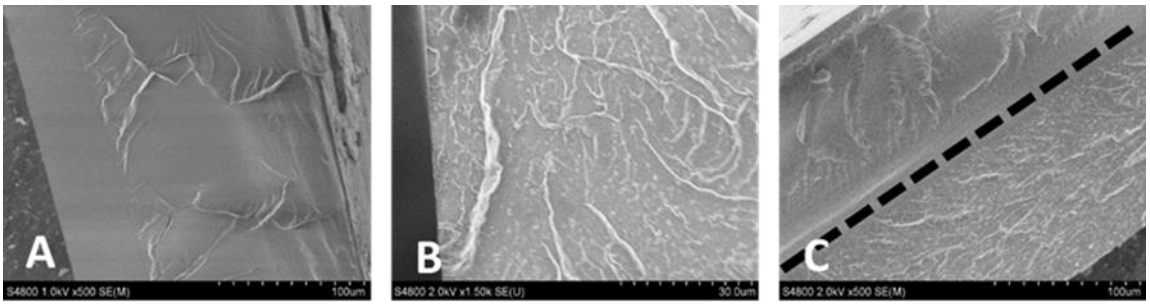

Figure 2.18 SEM image of barrier films; ZnO-free PVA film (A), ZnO-rich PVA film with 10% ZnO (w/w) (B), Dashed line separates top ZnO free PVA layer from the bottom ZnO rich PVA layer (C) The fracture-lines are just topographical ridges on the surface of cross-section where the film was freeze fractured.

rich layer prior to cross linking. In this SEM image of the cross section of a double layered PVA film, the dashed line separates the ZnO free top layer from the ZnO rich bottom layer which had 10% ZnO (w/w) loading.

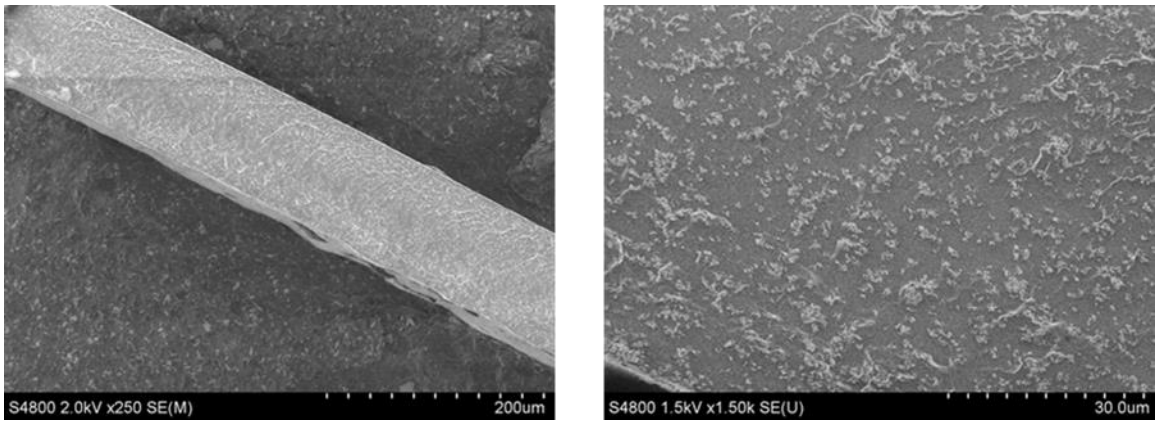

Figure 2.19 SEM images of 20% ZnO (w/w) loaded PVA film.

Figure 2.19 shows the SEM images of cross-sections of 20% (w/w) loaded PVA films. It indicates that the particles were still homogeneously distributed within the film containing 20% ZnO (w/w) loading without any agglomeration or settling. While SEM

images indicate qualitatively the homogenous dispersion of the acid scavenger, slight asymmetry in the ZnO distribution due to settling cannot be easily observed visually. Such asymmetry will alter the lag time of acid across the film, however, with faster acid breakthrough occurring if the scavenger has settled toward the upstream face of the membrane.[47] Diaphragm cell experiments with barrier samples from the same film oriented in opposite directions confirmed negligible ZnO settling at concentrations up to 40% (w/w).

2.3.3 Characterization of Barriers using Diaphragm Cell Trials

The ZnO loaded PVA barrier films are expected to selectively block the stimulant (acid) for a specific period of time (which is termed as lag time), and once the loaded ZnO has been consumed by the stimulant, the spent layers provide a transport resistance

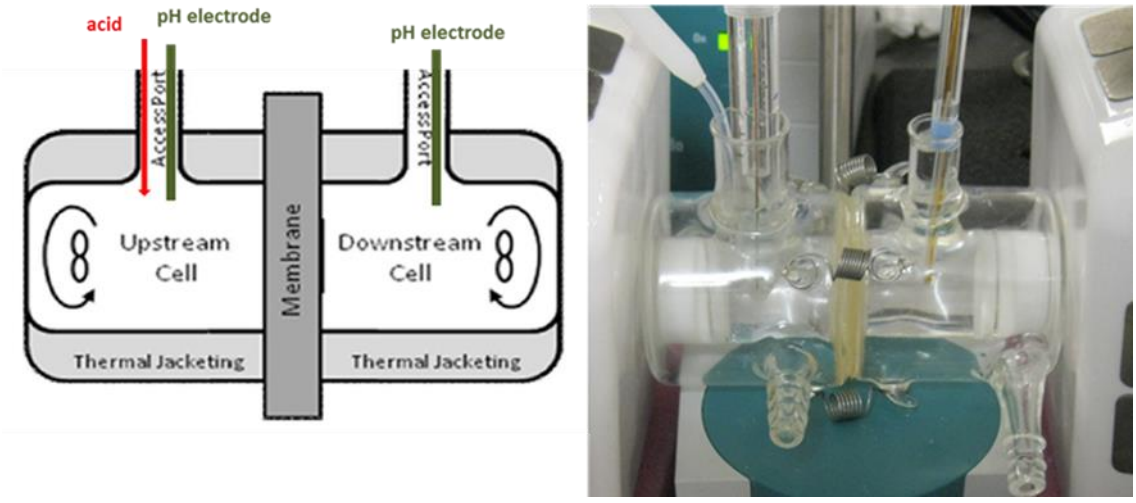

Figure 2.20 Diaphragm cell assembly for characterization of barrier films.

to incoming stimulant and outgoing solute in the device. The transport resistance varies linearly with the barrier layer's thickness, whereas the lag time varies with the square of the barrier layer's thickness, so a large change in lag time can be attained with only a small change in transport resistance. In addition, lag time also varies linearly with the

loading of ZnO in the barrier layer, which is important as it allows the lag time to be varied without changing the barrier matrix.

Hydrated PVA barriers films were separately characterized in a diaphragm cell as shown schematically in Figure 2.20 to determine the lag time and permeability of acid through the barriers. Each barrier film was mounted between the two compartments of a glass diaphragm cell. The upstream cell was filled with 22 mL of 0.01 M pH 3 citrate buffer (ionic strength 0.1 M) and the downstream cell was filled with 22 mL of acid-free 100 mM NaCl solution. Solution in each compartment was stirred continuously at 1200 rpm. Various PVA films ranging in thickness from 72 to 520 (multilayer) μm with initial ZnO content ranging from 0 to 60% (w/w) were characterized using this diaphragm cell. Select ZnO-laden films were soaked in deionized water for at least 72 hours after testing, then retested to observe their lag time and acid permeability without ZnO. Due to the high ZnO content of some barrier films, the upstream cell was titrated with 0.1 M HCl as needed to maintain pH at 3 using an automatic titrator (Metrohm Titrando 842, Herisau, Switzerland).

Theoretically, the lag time (t_L) for a stimulant to diffuse through a barrier filled with scavenger can be calculated using the formula described in earlier published work of reactive barrier films,[46,47,58]

$$t_L = \frac{\ell^2}{6D}\left(1 + \frac{6C_{Scav}\,Z_m}{\nu H C_{Stim}}\right) \tag{2.3}$$

where C_{Scav} is the initial concentration of scavenger (ZnO) in the membrane, C_{Stim} is stimulant concentration in solution upstream of the membrane, ℓ is the barrier thickness and ν is the stoichiometric coefficient for reaction (HCl + ½ ZnO → ½ $ZnCl_2$ + ½ H_2O)

which is ½ for this case. The location of the center of mass of the scavenger is termed as Z_m which is 0.5 for the films with homogeneously distributed ZnO. Equation 2.3 indicates that the lag time varies with both the concentration of scavenger and with the square of the thickness.

Figure 2.21 shows the breakthrough curves of various films with thickness ranging from 72 to 224 µm with a variety of ZnO content ranging from 0 to 30 %. Short lag times on the order of minutes were observed when the barrier film (118 µm, ZnO-free PVA) did not contain any scavenger. Upon increasing the ZnO content to 10% by weight, the lag time was increased to 1.64 hours for the barrier film with a thickness of 94 µm.

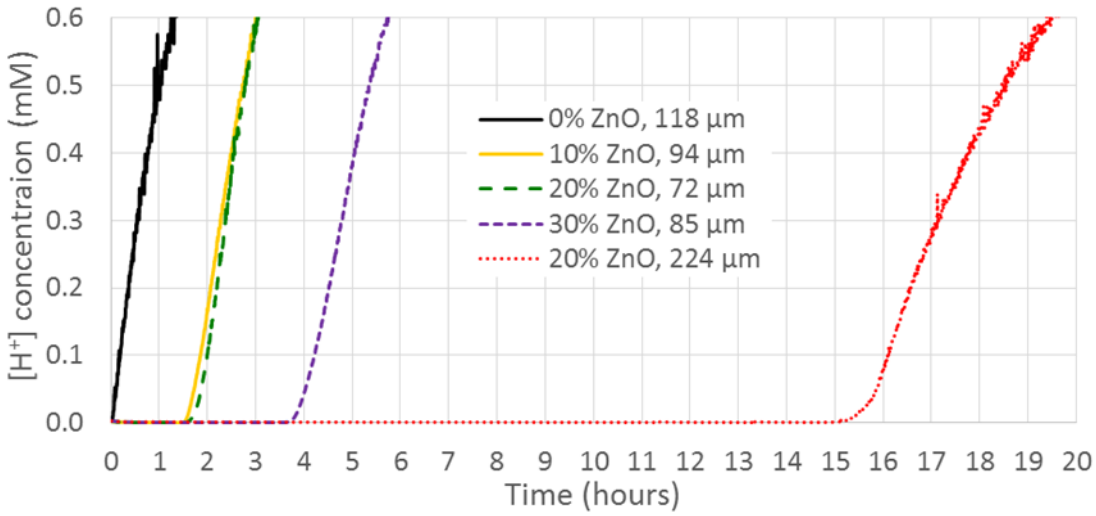

Figure 2.21 Breakthrough curves for acid diffusion across the PVA barrier films with various thicknesses and ZnO content

According to Equation 2.3, the lag time for the 20% and 30% ZnO films should be increased by a factor of the ratio of ZnO fractions times the square of the ratio of film thicknesses, *i.e.* to 1.92 and 3.99 hours, respectively. Experimentally, it was observed that the lag times for these films were 1.86 and 3.97 hours respectively. As shown in Figure 2.21, when a thick film of 224 µm was used by stacking three identical 20% ZnO loaded

barriers films together, the lag time was increased to 15.63 hours. This lag time is within 7% of anticipated lag time of 16.74 hours. However, it is important to note that only protons (H^+) are blocked by the scavenger (ZnO), while other species (including the acid's conjugate base) pass through the membranes without interacting with ZnO. If the buffer was changed out at 15 hours, then this effect is seen in Figure 2.21, where increased lag times provides a buildup of citrate concentration downstream, decreasing the downstream dissociation of neutral citric acid after the lag time and so reducing the slope of the breakthrough curve (apparent acid flux) through the film. For the multilayer film of 224 μm thickness with 20% ZnO content, the buffer was replaced at 11, 13 and 15 hours to make sure that there is enough citrate gradient after the breakthrough. As a result, the acid flux of the 3-layer laminate was reduced by a factor of 3 as compared to that of single layer, despite an order of magnitude increase in lag time.

Despite the lag time being increased by an order of magnitude, the permeability of acid through the barriers remained unchanged. A series of similar trials were conducted with variety of ZnO-free PVA films with thickness ranging from 72 to 520 μm to determine the permeability of acid through PVA membranes. Permeability data for these trials are shown in APPPENDIX A. These trials indicated an acid permeability across the barrier membranes of 1.47 (±0.1) × 10^{-5} cm^2/s (for n =3, trials 9 to 11 in APPENDIX A). As PVA has little pH sensitivity, acid flux in these trials was measured directly from pH shift in the unbuffered downstream cell, spanning a pH range where the flux of neutral acid species contributes as little as (~12%) to the measured shift. This was confirmed by trials using unbuffered citric acid operated in a lower pH range where even less of the neutral acid flux would dissociate downstream (trials 1 to 8 in APPENDIX A). Under

these conditions, observed permeability was 1.38 (±0.2) × 10^{-5} cm^2/s (for n=8, trial 1 to 8 in APPENDIX A), which was only 9% lower. The importance of this result is to show that despite being able to completely block the stimulant for a long, prescribed period of time; the barrier has a very large stimulant permeability, comparable to pure water. Swelling studies showed that the barrier membranes (excluding the scavenger) contain 55% water by volume. The acid permeability data listed above is 46% of the acid permeability through pure water. This indicates that, like the depot membrane, acid permeates the barrier membrane nearly as rapidly as it would through pure water without getting affected by the surrounding polymer network.

Permeability of methylene blue and methyl orange through PVA barrier films were also determined using similar diaphragm trials using ZnO-free PVA films with the thickness ranging from 92 to 373 µm. The scavenger-free PVA films of known thicknesses were placed in between two diaphragm cells. The upstream cell was filled with 22 mL of known solution of dye (400 mg/L for methylene blue and 62.5 mg/L for methyl orange) in 0.01 M pH 3 citrate buffer. The downstream cell was filled with 22 mL of fresh 0.01 M pH 3 citrate buffer and monitored for concentration change of dye using UV-vis spectrophotometer. We observed an average permeability of methylene blue to be 3.57×10^{-7} cm^2/s with a relative standard deviation of 18.3% through various PVA films of different thicknesses. This result was only 10% of its permeability through a comparable amount of pure water. Permeability of methyl orange through 88 micron scavenger-free PVA film was found to be 1.8×10^{-8} cm^2/s.

2.4 BMPR Device Fabrication

Solute (dye) loaded p(MMA/DMA) depot layers and ZnO-rich barriers are stacked together in an alternating arrangement. As discussed earlier, swelling of the depot matrix is transport limited and swelling rate varies with the square of layer thickness. As a result, thin layers were desirable for providing sharp pulses. However, very thin layers (< 50μm) can have a larger relative variation in thickness, which could sometime result in experimental error in the system for accurate predictions of pulse times. Thickness of the

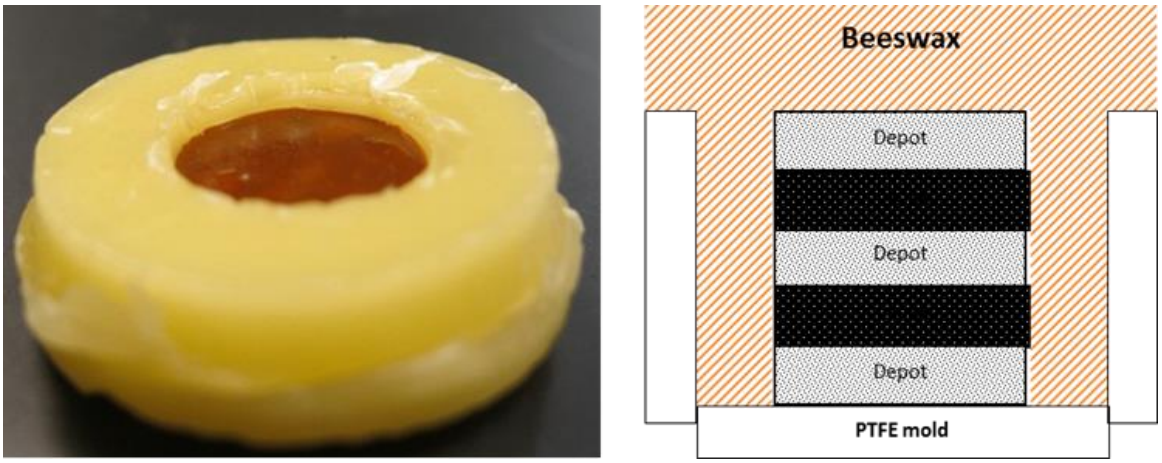

Figure 2.22 BMPR device fabrication; schematic of device assembly (right), beeswax was used to seal the BMPR stack (left); device is not drawn to scale, aspect ratio of actual stack resembles a dime.

depot layer is also limited by the amount and size of the solute particles, which means that depot layer thickness should not be less than the particle size of the loaded drug to make sure the drug particles remain inside the depot matrix and any possible burst release of drugs from the surface of the dry depot is avoided when the depot is in shrunken state. It was also important that depots should come off from the device on their own when they swell for the proposed delaminating BMPR system. Considering all of these factors in mind, aspect ratio of each layer in the stack was kept on the order of 100, using 1 to 2 cm wide circular discs with a varying thickness of 100-200 μm. Depot layers consisted of up to 5% solute by weight. ZnO nanoparticles loading in barrier matrix varied from 10 to 40

% by dry weight of the membrane. It was necessary to seal the edges of the membrane stack to prevent any seepage of stimulant into the edges of the layers yet the layers must be able to delaminate from the stack upon swelling when triggered with acid. While stacking the multiple layers of hydrated barriers and dry depots together alternatively, it was important that the barriers should remain hydrated keeping their dimensions in hydrated state. To keep the stack intact, beeswax (melting point 80°C) was used for sealing the BMPR stack. Beeswax had a comparatively better adhesion with dry hydrophobic depot layers than the hydrated barriers. When the layers (both barriers and depots) were stacked together and sealed with melted beeswax followed by instant freezing, the beeswax held the entire stack together. As a common protocol for BMPR device design, the disks of dry PMMA/DMA depot film 15 mm wide were stacked alternately with 16 mm wide disks of hydrated PVA barrier film atop a 0.5 mm thick, 16 mm wide PTFE plug. The plug was placed within a circular PTFE mold 6.7 mm thick. The beeswax was melted in a beaker on a hot plate (135°C) and then poured in the PTFE mold where the BMPR stack had already been placed. The stack was then promptly put in to a freezer (-20°C) for 15 min to solidify the wax which held the BMPR stack in place. The PTFE mold was removed later and the stack was inverted and further used for release trials. Schematic of the device assembly is shown in Figure 2.22Figure 2.22. During swelling trials when this beeswax-sealed device was kept in acidic buffer environment, the depot layer swelled laterally, and the beeswax prevented the lateral swelling which caused the hydrogel to bow up and the gel popped out and moved away from the device, exposing the underlying barrier to the external stimulant. Various release trials were conducted using this laminate pulsatile release device.

2.5 BMPR Release Trials

The release trials were conducted by placing the BMPR device in to first pH 7 phosphate buffer to confirm that there was no release during its "off-state", followed by transferring the device in pH 3 citrate buffer. Each device was taped to a glass platform and immersed in at least 300 mL of 0.01 M pH 7 phosphate buffer with an ionic strength of 0.1 M. After confirming no release at pH 7, the device was then transferred into > 500 mL of 0.01 M citrate buffer of pH 3 (ionic strength 0.1 M). All these trials were carried out in crystallizing dish (size: 12 to 24 cm wide, 6 to 12 cm tall, depending upon the volume of buffer) with continuous stirring. pH of both the buffers were monitored by pH meter (Orion 3-star). The solute (dye) release was monitored with a Cary 50 UV/Vis spectrophotometer in real time continuously using a fiber optic probe immersed in the solution. Various pulsed release trials were conducted by varying thicknesses of barriers, thicknesses of depot, amount of scavenger (ZnO) in barriers, position of ZnO in barriers and type of solutes that provided various pulsed release profiles on a wide range of timescales. No significant release was observed at pH 7, while at pH 3 each depot layer swelled after periodic intervals, got delaminated from the device and released its payload. Each device along with its delaminated layers were transferred to fresh buffer solution to retain the solute sink conditions and avoid solute saturation. Details of each BMPR trials are explained below.

2.5.1 5-Pulse BMPR Devices: Effect of Thickness

As shown in Figure 2.23, two 5-pulse BMPR devices were fabricated in which depots of methylene blue (5% w/w) loaded p(MMA/DMA) were protected with 30% ZnO (w/w) loaded PVA barriers. All depots and hydrated barriers in both devices were of identical diameters (15 mm) as they were cut using the same cork bore (size-8). Barriers

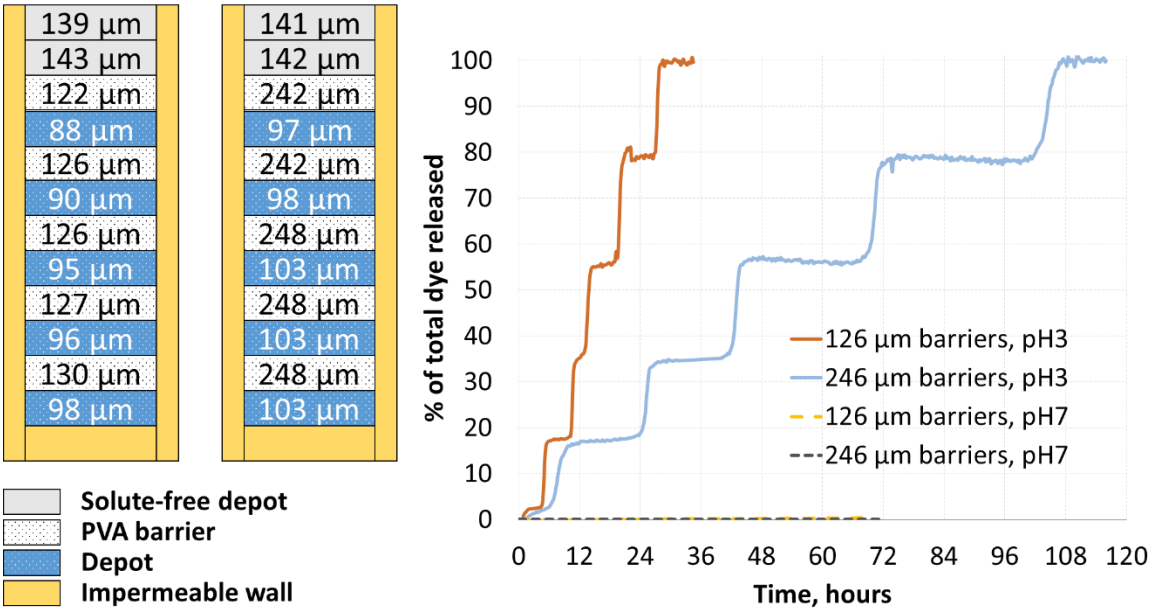

Figure 2.23 Configuration and release profiles of 5-pulse BMPR devices; (left) configuration of two BMPR devices. Devices are not drawn to scale, actual devices look like a dime. (right) solute release profiles at pH 7 (no significant release) and pH 3 (regular sharp pulsed release).

and depots used in the first device had an average thickness 94 and 126 µm, respectively. The second device shown in Figure 2.23 had nearly identical depots with an average thickness of 100 µm, but the thicknesses of the barriers were almost doubled with an average thickness of 246 µm. Dye-free depots were placed at the top in each device to avoid any possible pre-delamination of hydrated PVA barrier at the surface of the device because of loose bonding of hydrated PVA with beeswax. Both devices were first immersed in 200 mL of pH 7 phosphate buffer for 68 & 72 hours, respectively, and then

transferred to 1 liter of pH-3 citrate buffer for release studies. Neither device showed any significant release during three days of immersion in pH 7 buffer. At pH-3, the protons gradually penetrated through all the layers, consumed ZnO in barriers and triggered swelling of depot that released the solute. This resulted in sequential delamination of each depot from the device producing a sharp pulse of methylene blue at regular time intervals. It was observed that each pulse from the device was released in a rapid sharp manner within an hour of release time, agreeing with Equation 2.2. However, the lag times between the pulses were consistently $2/3^{rd}$ of the predicted lag time based on Equation 2.3. The pictures of the devices (recorded every 15 minutes), indicated that the ZnO scavenger at the outer edge of every barrier layer was consumed completely before the scavenger in the center portion of the barrier. Regardless of the contact issues in these two devices, the control over the pulse periodicity by changing the barrier thickness was preserved. The time interval between pulses was increased by a factor of four when barrier thickness was doubled, as depicted in Figure 2.23 (right). Thus, distinctive pulse time can be achieved not only by incorporating ZnO in PVA barriers (as shown in first device) but these pulse times can also be increased significantly by a comparatively small increase in thickness (as shown in second device).

2.5.2 3-Pulse BMPR Release: Effect of Scavenger's Location

The lag time of the barriers can also be tweaked by changing the location of the scavenger within the barrier. As shown in Equation 3, the lag of the barrier varies linearly with the scavenger's center of mass. The effect of scavenger is doubled when it is sequestered entirely at the downstream interface, while it is zero when all scavenger is at the upstream interface and immediately consumed. To check these effects, bi-layered

PVA barriers were fabricated by casting ZnO-rich PVA films on top of ZnO-free PVA films. ZnO-rich PVA barriers contained 40% (w/w) ZnO, while ZnO-free PVA films did not contain any amount of scavenger. SEM image of the dry film (cut from the same bilayer) is shown in Figure 2.24 which indicates that almost 42% of bilayer contains

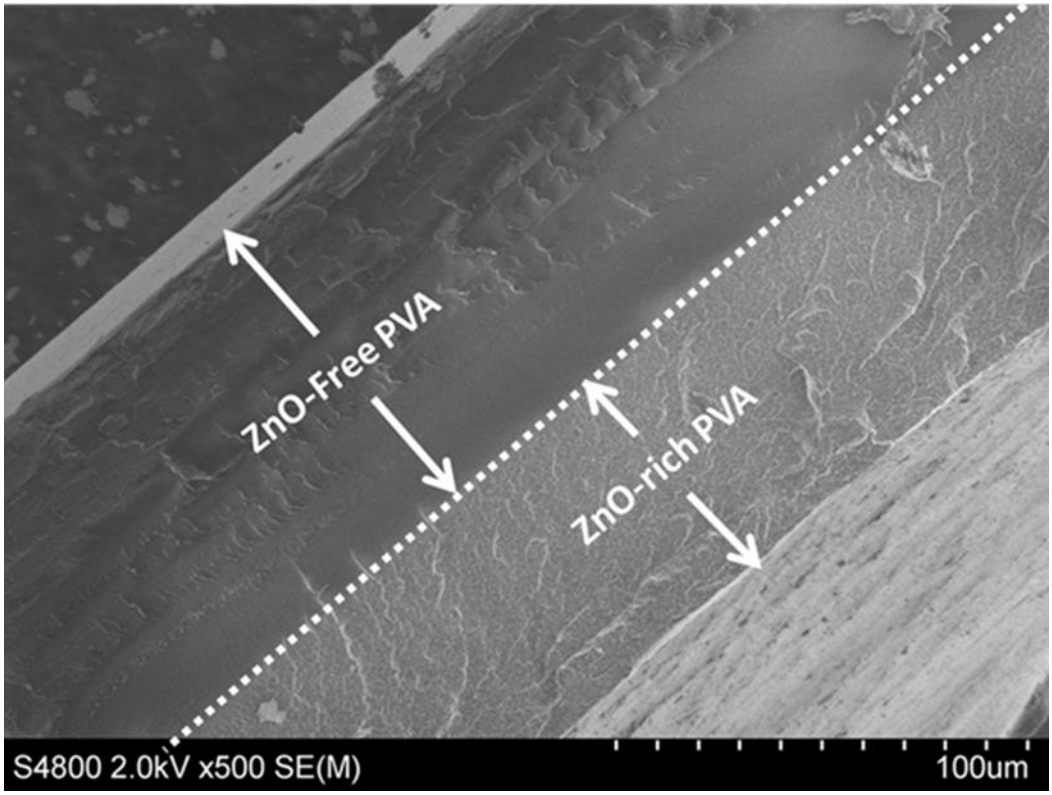

Figure 2.24 SEM image of bi-layered PVA film; dotted line separates ZnO-rich region (40% w/w) and ZnO-free region in the bilayer PVA barrier.

homogeneously distributed ZnO in the scavenger-rich portion of the barrier and the remaining 58% of the film was scavenger-free. These barriers were used to fabricate two different BMPR devices as shown in Figure 2.25 (left). The depot films in both the devices were 15 mm diameter, whereas the barriers were 16 mm diameter, 1 mm wider to mitigate the contact issues discussed previously. A dye-free depot was also placed at the

top of the device to avoid any prior delamination due to poor contact of hydrated barrier to beeswax. All the films in both devices were nearly identical, but the orientation of barriers in the second device was reversed compared to the first one.

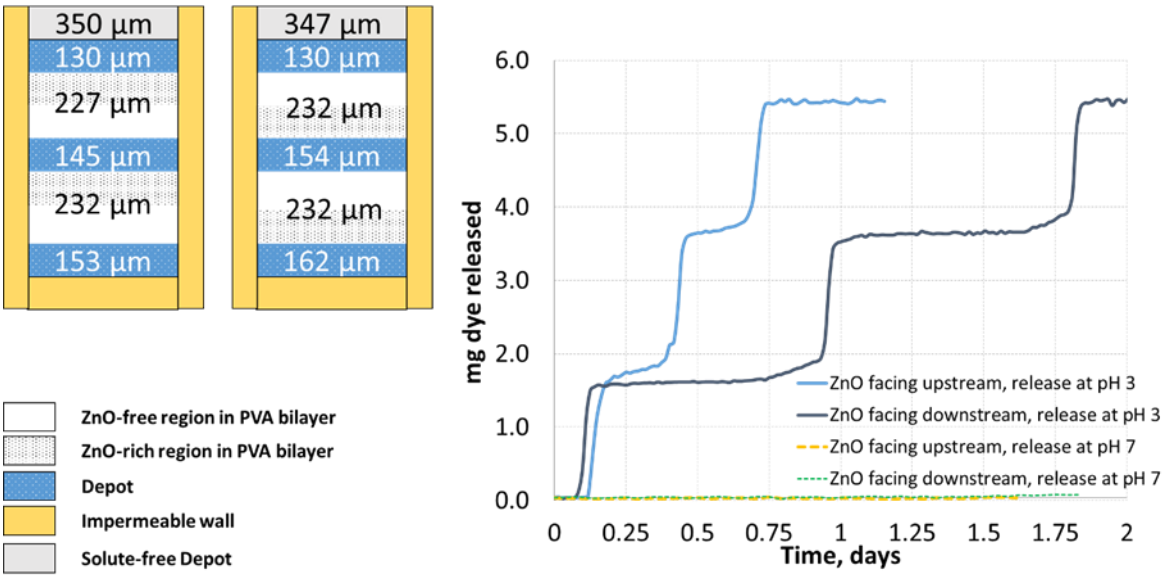

Figure 2.25 3-pulse BMPR device showing the effect of position of the scavenger. (left) configuration of two BMPR devices made from the identical film, but the orientation of the film was reversed. (right) Corresponding release profiles of these two BMPR devices at pH 7 and pH 3. Lag times can be tuned by controlling the location of the scavenger in barrier.

Figure 2.25 (right) shows the release profiles of these two trials which clearly depict the effect of location of ZnO. When subjected to pH 7, none of the devices showed significant release as expected. Upon immersing in to pH 3 buffer, pulse times observed in case of the device where ZnO is facing upstream are significantly shorter than the other device where ZnO is facing downstream in the barrier. When ZnO in PVA was facing upstream (in case of 1st device), the lag times of 2nd and 3rd pulse are 5.4 and 5.6 hours, respectively. These lag times were increased by a factor of four when ZnO in PVA was facing downstream (in case of 2nd device). The lag times of 2nd and 3rd pulse were 20.2 and 20.7 hours, respectively. The lag times in both cases follow the Equation 3

within 3%. The change in lag time in these two scenarios is due to effect of position of ZnO in the barrier. When the ZnO is facing upstream, the acid consumes ZnO as it penetrates through the layer. When ZnO is facing downstream, the acid has to travel the extra distance of the ZnO-free region to consume every molecule of the ZnO in the ZnO-rich region. In the first case, the ZnO-rich phase of the PVA barrier (almost 42 % of total barrier thickness) was facing upstream. Relative center of mass of ZnO of this bilayer was located at almost 21% of total thickness from top. So the lag time provided by this bi-layered PVA barrier should be 42% of that of a homogenously distributed PVA barrier with same amount of ZnO. In the second case, the ZnO-rich phase of the PVA barrier was facing downstream. Each molecule of acid had to travel an extra distance of ZnO-free PVA (almost 60% of total bilayer thickness) before consuming ZnO in ZnO-rich phase of the bilayer. Relative center of mass of ZnO this bilayer was located at 79% of total thickness of bilayer. So the lag time provided by this bi-layered PVA barrier should be 1.58 times higher than that of homogenously distributed PVA barrier with same amount of ZnO loading. For instance, if the ZnO was homogeneously distributed in this bilayer PVA film with same amount of ZnO, the film would have provided a lag time of 13.2 hours based on Equation 2.3. During the 1st trial, 232 µm bi-layered barrier film with ZnO-rich phase facing upstream, provided a lag time of 5.6 hours which is almost 42% of that of a homogeneously distributed film (13.2 hours). During 2nd trial, 232 µm identical bi-layered barrier film with ZnO-rich facing downstream, provided a lag time of 20.2 hours which is 1.58 times higher than that a homogeneously distributed film (13.2 hours).

2.5.3 Multiple Solute Release from a Single BMPR

BMPR technology has an advantage of delivering multiple solutes from a single system. Figure 2.26 (left) shows the schematic of 5-pulse BMPR device in which depots of methylene blue and methyl orange were alternately placed. The first, third and fifth depot layers were loaded with methylene blue. The second and fourth depot layers were loaded with methyl orange. Solute loading in each depot was 5% (w/w). Each depot was

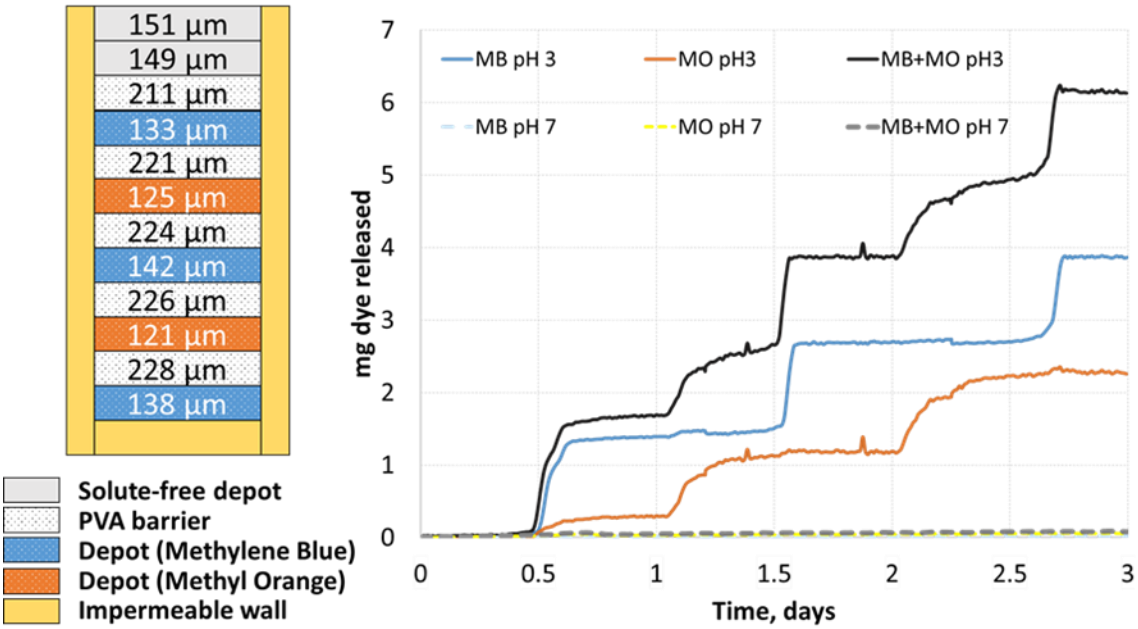

Figure 2.26 Multiple solute release from a single 5-pulse BMPR device; alternate pulses of methylene blue and methyl orange were released; each solute was released once per day, offset by 12 hours from each other.

protected by 20% ZnO loaded (w/w) PVA barrier. All the barrier layers were 16 mm in diameter, while all the depots were 15 mm in diameter. The thickness of each layer is shown in Figure 2.26 (left). This device was first immersed in 200 mL of 0.01 M pH 7 phosphate buffer (0.1 M ionic strength) for 3 days and then transferred to 1 liter of 0.01 M citrate buffer (0.1 M ionic strength). As shown in Figure 2.26 (right), there was no significant release at PH 7. As the device was subjected to pH-3, gradually each layer got

delaminated from the device and provided alternate pulse of methylene blue and methyl orange. Each solute was released once per day, offset by 12 hours from each other. The lag times between pulses provided by the corresponding barriers were almost 7% faster than analytically predicted based on Equation 2.3. The shape of the release profiles of methylene blue and methyl orange are different due to the nature of the solute. It is important to realize that methyl orange is negatively charged, and it binds reversibly with the positively charged depot membrane. As a result, methyl orange was released slowly as it dissociated from the gel into the buffer at much lower concentration. Methylene blue on the other hand, is positively charged, and released much faster, providing sharp pulses. However, due to sufficient lag time provided by the corresponding barrier films in this trial, it was possible to achieve distinct pulses of methyl orange even with its slow release behavior. This was possible not only due to presence of sufficient ZnO in barrier but also a significant ratio of barrier to depot thicknesses. Average thickness ratio (barrier thickness / depot thickness) in this trial was 1.6 and 1.8 in case of methylene blue and methyl orange respectively.

Figure 2.27 (left) shows the schematic of similar 5-pulse BMPR device in which 5-depots were interspersed by ZnO loaded PVA barriers with a lowered thickness ratio of barrier to depot. Average ratio of thicknesses (barrier/depot) in this trial was kept to 1 for methyl orange and 0.96 for methylene blue. Each layer in the stack was approximately 200 μm thick and 15 mm wide. Each of the depot layer contained 5 % solute (dye) by weight. The first, third and fifth depot layer contained methyl orange, and the second and fourth layer contained methylene blue as solute. Scavenger content was also reduced in the PVA barriers for this trial to 10% ZnO (w/w). This stack was directly immersed in

300 ml of pH 3, 0.01 M citrate buffer (0.1 M ionic strength). Solute release was continuously monitored using real time spectrophotometer. The release profile of the

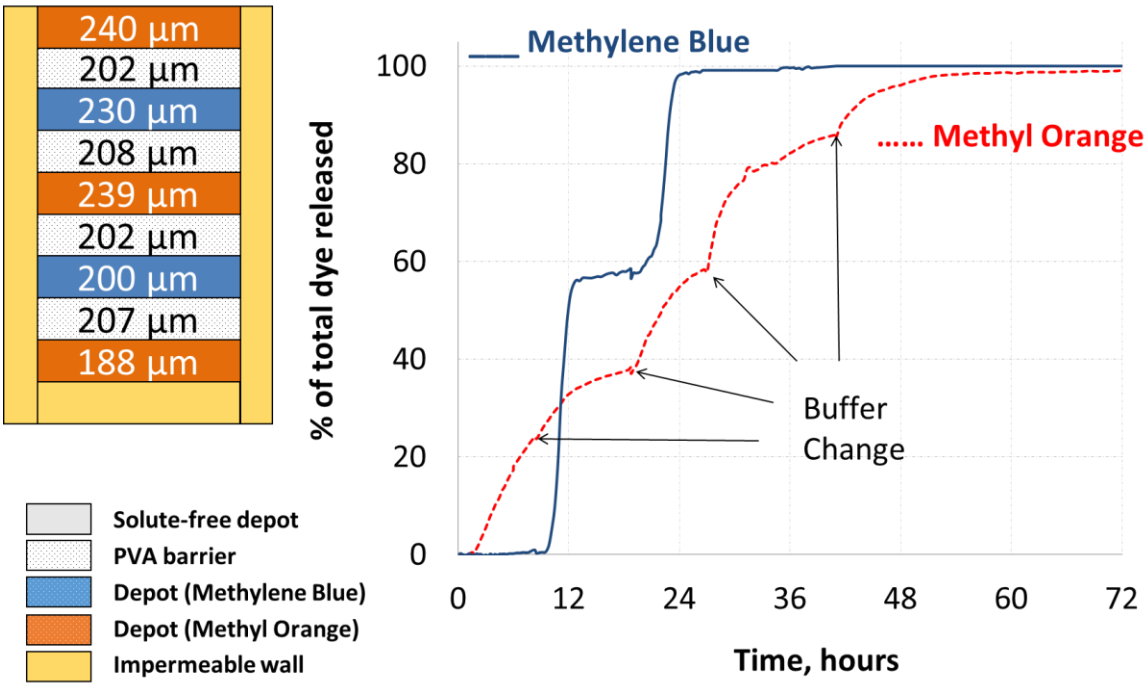

Figure 2.27 Multiple solute release with two distinct release profiles from a single BMPR device. 1st, 3rd and 5th depot contained 5 % methyl orange, 2nd and 4th depot contained 5 % methylene blue by weight; buffer solution was replaced at 8.5, 19, 27 and 41 hours, methylene blue was released in two distinct pulses, while methyl orange was released continuously.

solutes has been demonstrated in Figure 2.27 (right).

As described earlier, methyl orange is negatively charged and releases at slower rate from protonated hydrogel. It was also important to note that the thickness ratio (barrier/depot) in this trial was set close to 1 by increasing the depot thickness. Due to binding of methyl orange with protonated hydrogel, the rate of release of methyl orange was even slower from these thicker hydrogel which only changed when the surrounding buffer solution was replaced. This resulted in steady release of methyl orange throughout the experiment regardless of sequential delamination of each pulse. However, methylene blue got

released in two distinct pulses due to its faster release behavior due to its positive charge and lower partition coefficient. Thus, two distinct release profiles of multiple solutes (sustained release of methyl orange and pulsed release of methylene blue) were achieved from a single BMPR device.

2.5.4 10-pulse BMPR System

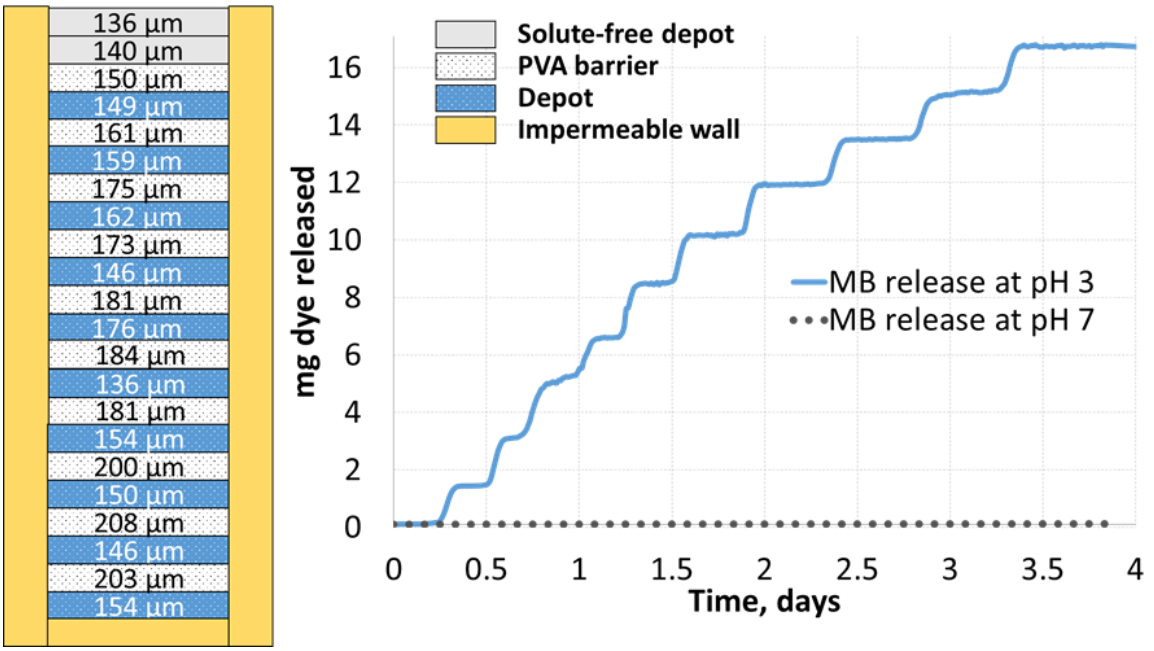

Figure 2.28 BMPR system can produce up to 10 distinct pulses from single device. Configuration of a 10-pulse device (left); device is not drawn to scale, overall height of the device was 4 mm and width was 2 cm, solute release profiles (right) for the device at pH 7 and pH 3.

Theoretically, there is no limit on how many pulses can be delivered from a single BMPR system. As shown in Figure 2.28, ten equal doses of methylene blue were delivered using 10-pulse BMPR device. Ten depots of 5% (w/w) methylene blue loaded p(MMA/DMA) were protected by PVA barriers that were loaded with 20% (w/w) ZnO. Thicknesses of all the depots and barriers are shown in Figure 2.28. The widths of all the barrier layers were 16 mm. All the depots were 15 mm wide. The depots were cut using a

brass cork bore (size-8) and the hydrated barriers were cut with a stainless steel cork bore (machine-shopped). This 10-pulse device was only 4 cm tall and 2 cm wide. This device was first immersed in 200 ml of pH-7 phosphate buffer for 4 days and then later transferred to 1 liter of citrate buffer (pH-3). The release profile for this 10-pulse device is shown in release profile (Figure 2.28 (right)). At pH 7, no release was observed. At pH 3, acid penetrated gradually through all the layers, consumed the scavenger in the barrier and triggered the swelling of depots to provide sequential delamination and release of the methylene blue. Each pulse provided the same pulse height indicating the complete release of solute that was loaded in each pulse. However, it is noticeable that as the number of layers increases in the device, the chances for the contact problems between hydrated barriers and sidewall of wax increases. This is visible in pulses 3-6 delaminating 30% earlier than predicted. The remaining pulses, and the last ones in particular, occurred within few percent of their analytically predicted lag times.

2.5.5 BMPR Device with Dual Release Profiles

A 4-pulse delaminating BMPR device is shown in Figure 2.29 (left) in which four depots (average thickness 147 µm) of methylene blue (5% loading (w/w)) were protected alternatively by comparatively thinner PVA barriers (average thickness 106 µm) with increased loading of ZnO (30% w/w). The release profile of this trial is shown in Figure 2.29 (right), which shows that for each pulse there is a sufficient lag time after which there is a slow release for short duration which is followed by a sharp pulse. Increased loading of ZnO (30% w/w) in relatively thinner barriers (average thickness 106 µm) provided sufficient lag time of 4 to 5 hours. The barriers were slightly thinner than the depots, making an average thickness ratio (barriers/depot) of 0.7. Due to relatively

thinner barriers with their diameter a little wider than depots, it was observed that the barriers remained in place in the device for some time period until the hydrogel

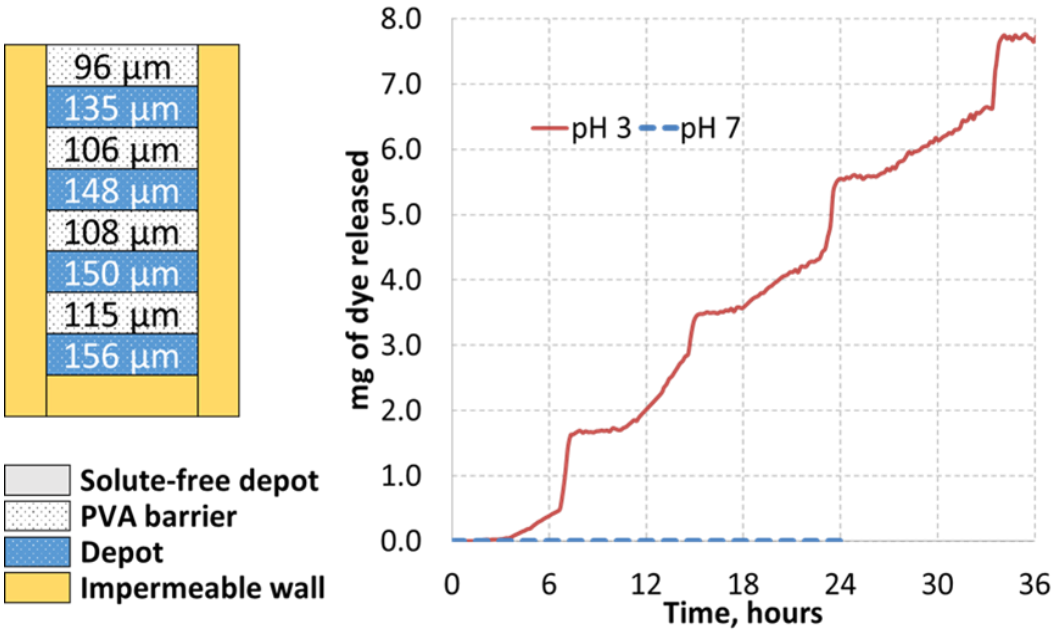

Figure 2.29 BMPR device releasing four pulses of methylene blue with combination of sustained and pulsatile release profiles; each pulse showed initial slow release followed by sharp pulses upon delamination.

effectively started swelling in lateral direction. In the previous devices, pulses appeared to occur almost immediately after barrier lag time without any significant delay for swelling the entire depot. In this device, however, the layers did not delaminate until the depot was fully swollen, which takes hours when the acid is coming from only one side, through spend barriers. However, during this anisotropic swelling of each hydrogel, the dye started to get released through each spent barrier before delamination occurred, which resulted in initial slow release during each pulse before delamination. Lateral swelling of hydrogel provided enough pressure to delaminate both spent barrier and hydrogel itself from the device. Upon delamination, sharp release of methylene blue was

observed for each pulse. As shown in Figure 2.29 for this 4-pulse BMPR trial, initial slow release during each pulse indicated that it was possible to release the solute without delaminating the layers at all if the swelling can be restricted in only one direction. This was encouraging to design a non-delaminating BMPR device for applications in which scattered or delaminated layers are not desirable. Strategies for designing an experimental non-delaminating BMPR system are discussed in Chapter 4, in which a 2-pulse non-delaminating BMPR device was successfully constructed. However, a BMPR system with multiple layers held in place creates a significant increase in mass transfer resistance for stimulant to diffuse in and solute to diffuse out through the spent layers. It also requires relatively long times to conduct the experiments for studying the release behaviors of multilayered non-delaminating BMPR devices. To predict the performance of such multilayered system analytically is challenging. A FORTRAN-based numerical model was constructed which predicts the performances of both delaminating and non-delaminating BMPR systems. This model is validated against the performance of delaminating BMPR systems as discussed in Chapter 3. The model compares the results of 2-pulse non-delaminating BMPR system which is discussed in Chapter 4. The model is further expanded to investigate 5-pulse non-delaminating BMPR systems in Chapter 5, where the key parameters are correlated to the resulting release profiles.

2.6 Conclusions

While current methods of pulsatile delivery needs labor-intensive manual applications of individual dose, or costly complex devices, BMPR technology offers an elegant material-based alternative for pulsatile delivery using stimuli-sensitive depots protected by reactive barriers. pH-sensitive depots of p(MMA/DMA) loaded with model

drugs (methylene blue or methyl orange) were synthesized. These hydrogels demonstrated the complete immobilization of the drug at pH 7. In acidic environment, depots swelled significantly and completely released the model drugs. Experiments on swelling and solute release kinetics showed that both processes are usually transport limited. Characteristic swelling and characteristic release times of these depots were comparable, which can also be analytically predicted and manipulated. To protect the acid stimulant for these depots, ZnO-loaded barrier films were synthesized and demonstrated. The lag time of the barrier is proportional to the square of the thickness of the barrier and varies linearly with the amount of scavenger loading. The lag time also depends on the location of the scavenger in the barrier in a precisely quantifiable fashion. Characteristics of both depots and barriers were independently investigated. Diffusion and partition coefficients were experimentally determined for weak acid stimulant and model drugs in both depot and barrier membranes. Acid appears to have little interaction with polymer, diffusing through absorbed water as through bulk water. Model drug diffusion is hindered by polymer network; however, the drug diffuses out as the hydrogel swells and is completely released at equilibrium.

Various multi-pulse delaminating BMPR devices were designed by integrating depots and barriers together using beeswax. No solute was released at pH 7, but sharp pulses of drug were observed from the device at regular time intervals at pH 3. These BMPR devices were demonstrated for variety of pulse periodicity where pulse times varied with the square of the thicknesses and also with the location of the scavenger in the barriers. Sequential release of multiple solutes was achieved from a single device. The number of pulses assimilated in to a single device is limited only by the art of

making them. Up to ten distinct pulses were demonstrated at regular time intervals from a single delaminating BMPR device.

These results demonstrate several advantages to this approach of pulsatile delivery compared to earlier approaches using polymer degradation which relied upon a linear dependence on erosion time and faced limitations due to difficulty in maintaining perfect surface erosion across a wide range of thicknesses. Here, the BMPR approach has been decoupled from polymer degradation and instead linked to sacrificial scavenging of the external stimulant. Now BMPR systems allow the delay time between pulses to be scaled across orders of magnitude with only minor changes in barrier properties (such as thickness, scavenger loading and scavenger location) and open the BMPR approach to variety of stimulants. There are no electronic or mechanical components, nor power supply or circuitry, greatly reducing the cost and possible failure modes of the device. This is the first time that non-degrading BMPR device has ever been constructed and its performance is clean enough to be modeled analytically, which is described in next chapter.

CHAPTER 3
ANALYTICAL PREDICTIONS & NUMERICAL MODELING

As discussed in Chapter 2, delaminating BMPR devices provided various shapes of pulsed release profiles. The pulse timings of these devices can also be predicted analytically by calculating independent lag times provided by the barriers, along with the release times provided by solute-laden depots. Although these analytical predictions of lag times and release times were discussed briefly based on Equation 2.1 and 2.2 in Chapter 2, a detailed comparison of analytical vs experimental pulse timings are discussed here in Chapter 3, Section 3.1. However, these analytical predictions were calculated based on Fick's second law of diffusion and simplified instantaneous hydrogel swelling with supplementary details required based on the outcomes of the experimental system. There are several different parameters in the design of BMPR system that can be manipulated to control these release profiles. With a relatively large number of parameters with various combinations, it is challenging to predict the performances of the BMPR systems analytically (especially for non-delaminating system in particular) and so these systems demand a computational model. For instance, it is extremely difficult to analytically predict the shape of the release profile, particularly in more complicated systems like in Figure 2.29. It is also extremely difficult to predict anything in non-delaminating systems with multiple layers fused together where increased mass transfer resistance also make analytical predictions intractable. Without a computational model, it is almost impossible to determine how many discrete pulses can be achieved for a given non-delaminating system. Current non-delaminating systems are also difficult to get clean experimental data from, so having a delaminating system model which has been

validated against its analytical calculations and experiments as a starting point for the non-delaminating system is valuable. It is also straightforward to add more complications like changing boundary conditions or variable diffusion coefficients with the use of computational model. The FORTRAN based numerical model was constructed for delaminating BMPR system, which is discussed in Section 3.2 of this Chapter, and later developed for non-delaminating BMPR system. This model was first validated against performance of delaminating BMPR systems. The computational model was then explicitly expanded for non-delaminating BMPR systems. Thorough investigation of the non-delaminating BMPR system on a wide range of parameter space is discussed in Chapter 5. The computational model also compares the 2-pulse experimental non-delaminating BMPR system which is discussed in Chapter 4.

3.1 Analytical Calculations

3.1.1 Barriers

The lag time of a barrier film can be calculated analytically in various ways. If a stimulant-free barrier is exposed to a stimulant on one side at time t=0, but remains stimulant-free on the other side, then the total amount of stimulant which has crossed the membrane Q_t at time t is given by Eq. 3.1,

$$Q_t = \frac{DH\,C_{up}}{\ell}(t - t_L) \tag{3.1}$$

where, $t_L = \frac{\ell^2}{6D}$ (for barriers with no fillers) (3.1a)

In above equations, t_L is the lag time, D is the diffusion coefficient, H is the partition coefficient, C_{up} is the upstream stimulant concentration and ℓ is the thickness of the barrier. In case of homogeneous barrier that does not contain any fillers, then this lag

time, can be correlated with the thickness of the barrier ℓ and the diffusion coefficient (D) as shown in Eq. 3.1a. This relationship was first introduced by Daynes[59] and also in work of Barrer [60].

However, Equation 3.1a needs to be modified when the barrier is filled with reactive materials or fillers. In the work of Higuchi,[61] it was suggested that for barriers containing fillers, the lag time would be significantly larger than that obtained for a homogeneous barrier due to the presence of filler and its activity with the stimulant. This was described by equation Eq. 3.2, in which V_C and V_f are the volume fractions of the continuous and filler phase respectively, and K is the distribution coefficient of the stimulant between the two phases.

$$t_L = \frac{\ell^2}{6D}\left(V_C + KV_f\right) \tag{3.2}$$

Higuchi[61] also stated that when the thermodynamic activity of the stimulant in equilibrium with the filled material is negligible until the critical amount of stimulant has been consumed, the lag time for such strongly adsorptive fillers containing barriers can be expressed by Eq. 3.3, where C_f is the concentration of filler, k is the maximum adsorptive capacity of the filler and C_0 is the initial concentration of the stimulant at the surface of the barrier.

$$t_L = \frac{\ell^2}{4D}\left(1 + \frac{2C_f k}{C_0}\right) \tag{3.3}$$

Barrier calculations in BMPR systems presented in Chapter 2 were based on the diffusion of stimulant (acid) and mobile solute (dye) through ZnO loaded PVA layers. Permeability of stimulant and solute through the barriers were calculated as one diffusion

and partition coefficient per species. Barrier membrane calculations were performed using barrier equations derived by Cussler *et al*.[47] Lag time across sacrificial scavenger laden barrier can be predicted using following equation.

$$t_L = \frac{\ell^2}{6D}\left(1 + \frac{3C_{So}}{\nu H C_{Ao}}\right) \tag{3.4}$$

where D is the diffusion coefficient of the stimulant being scavenged, H is the acid's partition coefficient in the membrane, C_{Ao} is the stimulant concentration in solution upstream of the membrane and C_{So} is initial concentration of scavenger (ZnO) in the membrane, ℓ is the barrier thickness & ν is the stoichiometric coefficient for reaction, which is ½ for this case. (HCl + ½ ZnO → ½ $ZnCl_2$ + ½ H_2O). Eq. 3.4 can be obtained using three independent derivations[46,58,61] in which C_{Ao}, ℓ, D and H parameters were assumed to be constant and ZnO was considered homogenously distributed within the film. These assumptions can be typically considered valid for the delaminating system described in Chapter 2, hence delay time of each barrier can be calculated using Eq. 3.4, which is the same as to Eq. 2.2 in Chapter 2 for homogeneous barriers with Z_m = 0.5.

When ZnO-free PVA barrier is hydrated with water, it holds almost 1 g water/g of dry barrier. With increase in ZnO loading this hydration ratio reduces as shown in Figure 2.16 as the solid ZnO takes no water itself. Using this hydration ratio, the partition coefficient (H) of acid through PVA barrier was calculated based on the volume fraction of water held by PVA matrix. The water in the barrier was assumed to be thermodynamically similar to external water. This assumption is supported by the acid permeability studies discussed in Section 2.3. So, the partition coefficient of acid in

hydrated PVA can be expressed as the volume fraction of water in PVA matrix as shown in Eq. 3.5, which takes the volume of ZnO in account, too.

$$H_{acid} = \frac{volume\ of\ water\ in\ swollen\ barrier\ membrane}{volume\ of\ dry\ PVA} \tag{3.5}$$

Figure 3.1 shows the partition coefficients of acid in PVA films with different ZnO loading, which ranges from 0.545 for ZnO-free PVA film to 0.657 for 80% (w/w) ZnO rich PVA film. An average partition coefficient of acid (H_3O^+) in PVA barriers was

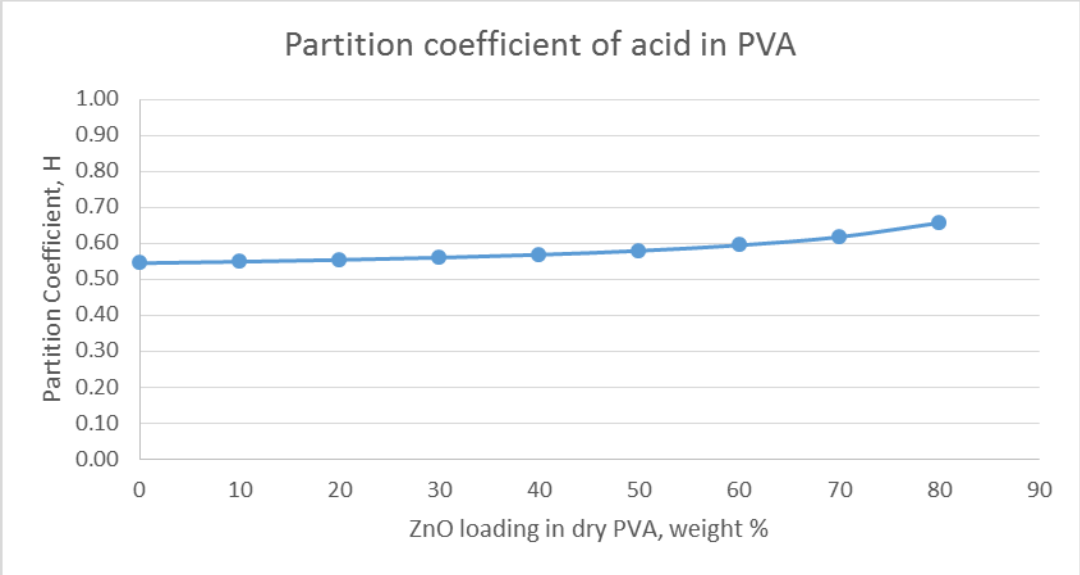

Figure 3.1 Partition coefficient of acid in PVA barriers with various ZnO loading based on volume fraction of water in PVA matrix.

0.58. Using this partition coefficient data with an average permeability (DH) of 1.47×10^{-5} cm^2/s (as already described in Chapter 2), the lag time for various barriers used in delaminating BMPR trial was analytically predicted using Eq. 3.4. For bilayer barriers with different ZnO loading, lag time was predicted based on Eq. 2.2, with their corresponding value of center of location of mass (Z_m).

3.1.2 Depots

Depot layer calculations are more complicated than the barrier-calculations and require more simplistic assumptions in determining release times. Release time of a solute from the depot is dependent on a) how long it takes for acid to diffuse in the depot to trigger the swelling, b) how long it takes to completely swell the depot, c) how long it takes for the solute to get dissolved in swollen hydrogel and d) how long it takes for the solute to come out from the depot. While swelling and dissolution both appear to happen rapidly, the two transport processes (acid diffusing in, and solute diffusing out from depot) appear to both occur on similar timescales. As these four phenomena occur in series, but overlap, the analytical prediction becomes more complicated than that of barrier calculations. A few assumptions were made to describe these phenomena to calculate characteristic swelling time and characteristic release time of the p(MMA/DMA) depots.

i) Depots were assumed to be of only two states, either shrunken or swollen, with no intermediate swelling states in only the anisotropic direction. Each state of the depot was assigned its own diffusion and partition coefficients for both stimulant and dissolved solute and a layer thickness. When the depot changes from a shrunken to a swollen state, it would instantly occupy the parameters of its swollen state. Solid solute inside the depot matrix was considered to be totally inert in the shrunken state, while in the swollen state it would instantly get dissolved to its saturation concentration and diffuse away from the matrix with its swollen-state diffusion and partition coefficients.

ii) Swelling of the depot layer is instantaneous in response to stimulant. Upon arrival at the shrunken portion of the depot, stimulant is instantly consumed by DMA groups. pK_a of citric acid is 3.13,[62] and pK_a of DMA is approximately 8.4.[53] Upon exposing p(MMA/DMA) to pH 3 citrate buffer, acid instantly diffuses in the matrix consuming amine groups and protonates the hydrogel. For p(MMA/DMA) with 75/25 mole ratio, the concentration of amine groups in shrunken polymer was measured to be 2.33 M. Once all the scavenging DMA- groups at that location have been reacted with stimulant, the depot at that location swells with water instantaneously, despite the fact that stimulant concentration for that point is still computed as zero, since all the stimulant arriving at that point was assumed to be consumed.

iii) Dissolution of solute occurs instantaneously as soon as the stimulant triggers the depot matrix to swell with water. The amount of water occupied by a swollen depot determines the swelling factor. Model drugs (methylene blue and methyl orange) are completely insoluble in the depot matrix in shrunken state. Upon swelling, they dissolve instantaneously in water, up to their saturation concentration, and eventually get completely dissolved in the swollen matrix of depot and diffuse out of the matrix based on their diffusion and partition coefficients in water.

iv) Concentrations of solute (either solid or dissolved) are sufficiently low that they do not alter the properties of the depot layer matrices. For instance, the volume occupied by solid in a shrunken depot is small enough compared to the overall volume of the depot matrix and does not affect the depot properties. Solute

loading in physical model never exceeded more than 5% of the depot weight. The same assumption is made for barrier scavenger, that ZnO disappearance does not significantly change barrier diffusion coefficient. For instance, ZnO loading in PVA barrier with 40% by weight is equivalent to that of less than 10% by volume.

Based on the above assumptions, characteristic swelling time of the depot and release time of the solute from corresponding depots can be calculated from following equations which are the same as Equation 2.1 and 2.2.

$$t_{swell} = \frac{C_{scav}}{C_{stim}} \frac{l^2}{2\,DH_{stim}} \tag{2.1}$$

$$t_{rel} = \frac{C_{solid}}{C_{sat}} \frac{l^2}{2\,DH_{solute}} \tag{2.2}$$

All the relevant parameters used in these equations are already calculated and described in Section 2.2.3 and 2.2.4.

3.1.3 Analytical Predictions of Delaminating BMPR Systems

Using Eq. 3.4, lag times of various barriers used in delaminating BMPR trials (described in Chapter 2), are analytically calculated and compared with experimental lag times, which is depicted in Table 3.1 to 3.7. In most of these trials, the analytical lag times provided by the barriers compare well with the experimental lag time, except in the cases where there were some delamination issues because of the design flaws, already explained in Chapter 2. Characteristic swelling and release times of the depots used in the delaminating BMPR trials are also analytically calculated using Equations 2.1 and 2.2, which are also depicted in Tables 3.1 to 3.7, along with the lag times provided by barriers.

Table 3.1 Analytical prediction of 5-pulse BMPR device (thin barriers, Figure 2.23)

BMPR DEVICE	Thickness		Characteristic times, Depot		Lag time, barrier		
5 pulse (short)	Depot	Barrier	t_{swell}	$t_{release}$	t_L	$t_{L(exp)}$	% (t_{Lexp}/t_L)
	[μm]	[μm]	[hours]	[hours]	[hours]	[hours]	
Pulse-1	88	122	0.22	0.39	7.5	3.8	50
Pulse-2	90	126	0.23	0.41	8.0	5.3	66
Pulse-3	95	126	0.26	0.45	8.0	3.0	38
Pulse-4	96	127	0.27	0.46	8.1	5.3	65
Pulse-5	98	130	0.28	0.48	8.5	7.5	88
Average	**93**	**126**	**0.25**	**0.44**	**8.0**	**5.0**	**62**

Table 3.2 Analytical prediction of 5-pulse BMPR device (thick barriers, Figure 2.23)

BMPR DEVICE	Thickness		Characteristic times, Depot		Lag time, barrier		
5-pulse (long)	Depot	Barrier	t_{swell}	$t_{release}$	t_L	$t_{L(exp)}$	% (t_{Lexp}/t_L)
	[μm]	[μm]	[hours]	[hours]	[hours]	[hours]	
Pulse-1	97	242	0.27	0.47	29.5	5.5	19
Pulse-2	98	242	0.28	0.48	29.5	15.5	53
Pulse-3	103	248	0.31	0.53	31.0	17.0	55
Pulse-4	103	248	0.31	0.53	31.0	23.0	74
Pulse-5	103	248	0.31	0.53	31.0	30.0	97
Average	**101**	**246**	**0.29**	**0.51**	**30.4**	**18.2**	**60**

Table 3.3 Analytical prediction of 3-pulse BMPR device (short pulses, Figure 2.25)

BMPR DEVICE	Thickness		Characteristic times, Depot		Lag time, barrier		
Bilayer (ZnO Facing Upstream)	Depot	Barrier	t_{swell}	$t_{release}$	t_L	$t_{L(exp)}$	% (t_{Lexp}/t_L)
	[μm]	[μm]	[hours]	[hours]	[hours]	[hours]	
Pulse-1	130	No barrier	0.49	0.85	NA	NA	
Pulse-2	145	227	0.61	1.06	5.3	5.4	103
Pulse-3	153	232	0.68	1.18	5.5	5.6	102

Table 3.4 Analytical prediction of 3-pulse BMPR device (long pulses, Figure 2.25)

BMPR DEVICE	Thickness		Characteristic times, Depot		Lag time, barrier		
Bilayer (ZnO Facing Downstream)	Depot	Barrier	t_{swell}	$t_{release}$	t_L	$t_{L(exp)}$	% (t_{Lexp}/t_L)
	[μm]	[μm]	[hours]	[hours]	[hours]	[hours]	
Pulse-1	130	No barrier	0.49	0.85	NA	NA	
Pulse-2	154	230	0.69	1.19	20.3	20.2	100
Pulse-3	162	235	0.76	1.32	21.2	20.6	97

Table 3.5 Analytical prediction of multi-solute BMPR device (Figure 2.26)

BMPR DEVICE	Thickness		Characteristic times, Depot		Lag time, barrier		
Multi-solute-1	Depot [μm]	Barrier [μm]	t_{swell} [hours]	$t_{release}$ [hours]	t_L [hours]	$t_{L(exp)}$ [hours]	% (t_{Lexp}/t_L)
Pulse-1 (MB)	133	211	0.47	0.89	11.8	11.7	99
Pulse-2 (MO)	125	221	0.43	5.66	13.0	13.2	102
Pulse-3 (MB)	145	224	0.54	1.06	13.3	11.8	88
Pulse-4 (MO)	121	226	0.38	5.31	13.6	12.0	88
Pulse-5 (MB)	138	228	0.53	0.96	13.8	14.4	104
Average	**132**	**222**	**0.47**	**2.77**	**13.1**	**12.6**	**96**

Table 3.6 Analytical prediction of multi-solute BMPR device (Figure 2.27)

BMPR DEVICE	Thickness		Characteristic times, Depot		Lag time, barrier		
Multi-solute-2	Depot [μm]	Barrier [μm]	t_{swell} [hours]	$t_{release}$ [hours]	t_L [hours]	$t_{L(exp)}$ [hours]	% (t_{Lexp}/t_L)
Pulse-1 (MO)	240	No barrier	1.83	20.88	NA	NA	NA
Pulse-2 (MB)	230	202	1.68	2.66	6.4	4.8	75
Pulse-3 (MO)	239	208	1.81	20.71	6.8	5.3	78
Pulse-4 (MB)	200	202	1.27	2.01	6.4	3.7	58
Pulse-5 (MO)	188	207	1.12	12.81	6.7	4.8	71
Average	**219**	**205**	**1.54**	**11.81**	**6.6**	**4.6**	**71**

Table 3.7 Analytical prediction of 10-pulse BMPR device (Figure 2.28)

BMPR DEVICE	Thickness		Characteristic times, Depot		Lag time, barrier		
10-pulse	Depot [μm]	Barrier [μm]	t_{swell} [hours]	$t_{release}$ [hours]	t_L [hours]	$t_{L(exp)}$ [hours]	% (t_{Lexp}/t_L)
Pulse-1	149	150	0.59	1.11	6.1	5.7	94
Pulse-2	159	161	0.67	1.27	7.0	6.5	92
Pulse-3	162	175	0.69	1.32	8.3	4.8	57
Pulse-4	146	173	0.56	1.07	8.1	6.6	81
Pulse-5	176	181	0.82	1.55	8.9	5.8	65
Pulse-6	136	184	0.49	0.93	9.2	6.7	73
Pulse-7	154	181	0.63	1.19	8.9	9.0	101
Pulse-8	150	200	0.59	1.13	10.9	10.9	100
Pulse-9	146	208	0.56	1.07	11.8	11.3	96
Pulse-10	154	203	0.63	1.19	11.2	11.5	102
Average	**153**	**181.6**	**0.62**	**1.18**	**9.0**	**7.9**	**87**

The calculations of characteristic swelling and release times of the depots are based on the assumption that they were allowed to swell freely in isotropic direction in pH 3 buffer. In actual experiments of BMPR trials, these depots swelled in anisotropic direction until they got delaminated and then swelled isotropically. It is difficult to predict analytically when the delamination occurs in the device. However, it was observed that delamination occurred rapidly as soon as the stimulant hit the depot after consuming the barrier, which allowed the gel to detach from the device and to swell isotropically. Thus, the time required to delaminate the depots was significantly lower compared to the overall time required to swell and release the solute completely from the depot. The characteristic times are used to provide a quick estimate of how long the swelling and release takes, and how they scale with each relevant parameter. By comparing these characteristic swelling time analytically for a particular depots used in a particular BMPR devices, it helps predicting the release behavior based on whether the process of depot swelling and release of solute is diffusion limited or not. It was observed that in most of the cases, characteristic time estimates did line up qualitatively well with experimental results in most situations, as depicted in Figure 2.13. When the depot got really thin, the characteristic swelling time becomes no longer decreased with square of the thickness and become insignificant. Although the characteristic release times are comparable, it is important to note that the release starts well before the swelling is complete but cannot end until after swelling is complete. These times impact on the overall release profiles which are now dependent on both swelling and drug diffusion process. The overall release rate and shape of drug containing p(MMA/DMA) depot can vary with change in any of the parameters shown in Eq. 2.1 and 2.2.

3.2 Numerical Modeling

Computational models are very useful for controlled release systems to predict release kinetics before release systems are realized. Although the physical BMPR device provides straightforward and reliable results, computational model can provide faster results at relative ease. As described in Section 3.1, while permeation time for stimulant is relatively easy to calculate analytically, the subsequent release rate is difficult to predict analytically for even the delaminating BMPR system. Solute release does not begin uniformly throughout the film, but rather starts progressively at the outer face of the film and advances to the inner face, depending on the initial conditions (such as amount of scavenger, amount of solute, diffusion and partition coefficients etc.) of the system. As depicted in Section 3.1, these transport rates are often of comparable magnitude. Except under certain extreme conditions, the shape of the pulse of such a system with several different parameters affecting the release, can only be predicted computationally. While there is a limit on manipulating all these parameters experimentally, a computational model allows one to vary all these parameters across a wide range to check their effect for a given BMPR system. For instance, it would be very difficult to change the diffusion coefficient of solute without also changing its saturation concentration even more dramatically. Thus, the model lets the user separately explore those parameters. It also allows rapid exploration on a wide range of parameter space. A computational model can be adapted to accommodate additional complications such as intermediate swelling states, concentration dependent diffusion coefficients, time dependent upstream stimulant concentration, and non-instantaneous swelling or

dissolutions rates. However, these complications are not addressed in the modeling for this thesis.

Besides being a convenient tool for examining the delaminating BMPR system, the computational model becomes very important and useful for multi-layer non-delaminating BMPR systems with a physical situation where layers do not delaminate, but rather are physically bound to keep the device intact throughout its use. In such situation, stimulation of subsequent pulses has additional delay due to stimulant transport resistance by the previously spent layers. This resistance builds up as the process moves towards later and later pulses, affecting not only the timing of the pulses, but also their width. As a result, later pulses becomes wider than earlier pulses, effectively limiting the pulse frequency. This limit changes with each pulse in a manner that is best determined computationally.

The model also allows the measurement of some important parameters that help in model fitting on experimental release data. It provides much cleaner data for quantifying trends which could only be qualitatively measured experimentally, and it allows rapid estimation of parameter values such as film thickness and scavenger loading when designing devices for a specific release profile. Thus, computational model can serve as a guide to calculate the performance of the physical model for both delaminating and non-delaminating BMPR system.

This section primarily discusses the construction and validation computational model for delaminating BMPR system, with a brief insight on how to adapt of this model for non-delaminating BMPR system. Thorough analysis on exploring the model for non-delaminating BMPR system is discussed in Chapter 5.

3.2.1 Model Construction

The model was constructed in FORTRAN for easy access and modifications. FTN 95 Plato IDE compiler was used for building, running and executing the code. Further exploration of models was done using a high performance computing system, called the Helium Cluster (provided by The University of Iowa), which is a 3508 processor comprised of 359 compute nodes and 3 login nodes. This FORTRAN based model was built using centered finite approximations for second order spatial derivatives for barrier calculations, backward finite difference approximations for second order spatial derivatives for depot calculations and explicit Euler method for first order derivatives. All of these approximations are based on Fickian Diffusion for each mobile species through these layers.

The proposed computational model was based on one dimensional (perpendicular to the layer's plane) diffusional characteristics. The layer thickness (for both barriers and depots) was specified from which an array of nodes were generated with a linear node density. Each of these nodes were specified with initial conditions which include concentrations, partition coefficients and diffusion coefficients for all four mobile species (stimulant (acid), scavenger, solid solute and dissolved solute) along with the node distance based on layer thickness and number of nodes. Changes in concentration due to diffusion were applied only for mobile species, *i.e.* dissolved solute and stimulant. Scavenger concentrations change in stoichiometric proportions based on the amount of the stimulant diffusing in the particular node. Diffusion and partition coefficients were kept constant for barrier layers along with node distance. On the contrary, for the depot layers, these coefficients along with the layer distance vary with change in integrated

stimulant flux at corresponding node depending upon the shrunken or swollen condition of that node. Adjacent layers were assumed to be at equilibrium at their interface. The boundary conditions at the top of the device for both BMPR systems were assumed constant. For delaminating BMPR system, when the final node of depot layer switches from shrunken to swollen state, the stimulant boundary conditions were applied to the first node of the next barrier layer, as it would be directly subjected to stimulant at that time. The flux of the solute release from the system was recorded and integrated over time along with the flux of stimulant into the system.

As described earlier, the layers were segmented in an array of nodes with a linear node density. The optimum node density was determined by varying the density and observing the consequent change in release profile to balance computation time vs accuracy, assuming that models with increased node density are more accurate. Similarly, appropriate time steps were also determined for each trial depending upon the increase or

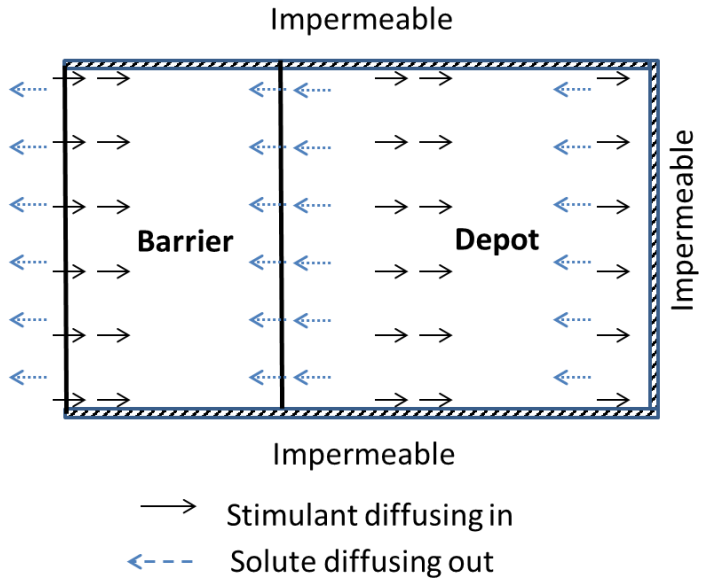

Figure 3.2 Schematic of single pulse computational BMPR model

decrease in node count and we ensured for each trial that both node density and time step were simultaneously optimized with a desired accuracy of model results.

To start with a simplistic case, the model was constructed for a single pulse BMPR system which comprised of one barrier and one depot. An arbitrary one dimensional BMPR system was considered with a single depot protected by a barrier, in

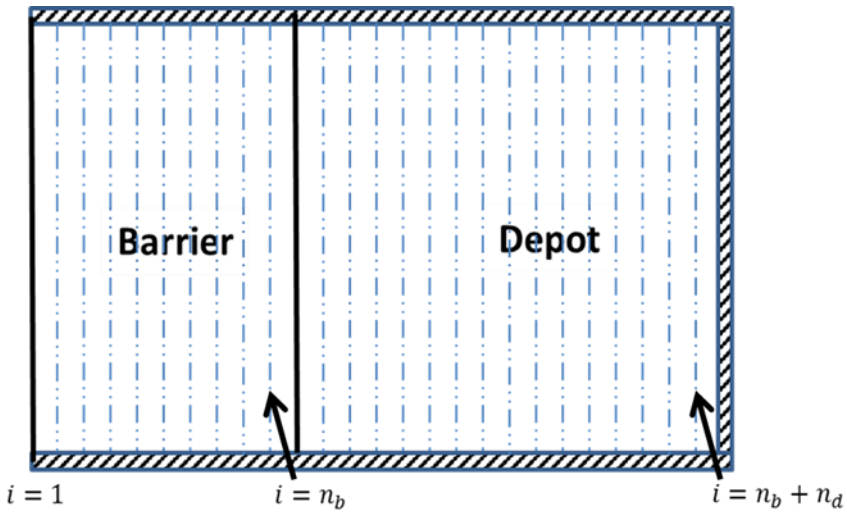

Figure 3.3 Single pulse BMPR model, each layer was divided in to array of nodes.

which the diffusion of the species going in and out of the system in only one direction as shown Figure 3.2. All the other sides of the devices were considered to be impermeable as they are sealed with beeswax in the experimental BMPR device. Each layer in the device was divided into definite number computational segments respectively with a node at each end of each segment, except for the inner most-node of the depot as shown in Figure 3.3. Each barrier was divided into n_b number of computational segments resulting in to same number of nodes in the barrier. The depot was rather divided in to (n_d-1) segments for n_d number of nodes. The inner most node (n_d^{th} node) of the depot has no corresponding segment, as it has the impermeable boundary. Each node of each layer

was assigned with initial conditions for stimulant concentration (G), the solid scavenger concentration (F), the solid solute concentration (B) and dissolved solute concentration (C). At a given node, these initial conditions represent the average parameter values for the segment on its inner side. The local diffusion coefficients of the stimulant (D_g) and of the solute (D_c) were also defined for each node along with their respective partition coefficients of stimulant (H_g) and of solute (H_c). Each node was defined with its segment thickness (h) that represented the distance from particular node to the next innermost node. This segment thickness (h) was defined by dividing the actual thickness of layer and the total numbers of nodes assigned in that layer. For instance, if the actual thickness of layer (barrier or depot) is 200 units and if that layer is divided in to 100 nodes then the thickness for each segment of the barrier is considered to be 2 units. Similar to segment thickness (h), the concentration of solid solute (B) and scavenger (F) was also divided in to the total numbers of segments in each layer. However, the amount of the scavenger in the first node of the barrier was set to zero as the outer most surface of the barrier would be in the direct contact with the upstream stimulant consuming the scavenger instantaneously. As a result, the total amount of scavenger in the barrier was redistributed in the rest of the nodes of the barrier. As the given node of the barrier represents the average amount of scavenger on the inner side of that node, redistributing the scavenger in rest of the nodes kept the center of mass exactly in the middle of barrier. Scavenger in depot nodes was kept unaltered, as the depot is not exposed directly to the external simulant. More importantly, redistribution of scavenger in depot nodes would also require emptying out the first node of depot, which would computationally cause termination of the triggering mechanism in the first node of depot to change from

shrunken to swollen state, leading to erroneous release profile. However, keeping the depot nodes without redistributing scavenger concentration would slightly shift its center of mass, but the effect would be negligible on overall release profile as compared to that in barriers, especially for pulse timings.

After determining the initial conditions for each parameter on each node, the solid species concentrations (B & F) were tracked based on the flux of mobile species arriving at the node. For instance, the scavenger concentration (F) would change when the stimulant arrives at that node. For a given amount of stimulant arriving at the node in a particular time step, the scavenger amount was decreased in stoichiometric proportion. Similarly, solute departing a node was replaced by a corresponding decrease in solid particles (B). We assume here that the reaction is instantaneous in each case. For the nodes with scavenger present in them, the initial stimulant concentrations (G) were fixed at zero.

3.2.2 Flux Calculations for Barriers using Centered Finite Difference

For the barrier layer, stimulant concentration (G) was tracked based on Fick's second law as shown in Eq. 3.6.

$$\frac{dG_i}{dt} = D_{g_i} \frac{d^2 G_i}{dx^2} \tag{3.6}$$

Here, x is the dimension normal to the plane of the barrier layer and D_g is diffusion coefficient of stimulant through barrier. Transport of stimulant at each node was calculated using centered finite difference approximation. The change in concentration of stimulant at particular node was calculated using following equation, where i is the node index, G is the concentration at each node and h is the thickness of corresponding node.

$$\frac{d^2G_i}{dx^2} = \frac{G_{i-1}-2G_i+G_{i+1}}{h^2} \tag{3.7}$$

Similarly, solute concentration (C) in the barrier was also tracked using Fick's 2nd law using the following equation where D_c is the diffusion coefficient of solute through barrier.

$$\frac{dC_i}{dt} = D_{c_i}\frac{d^2C_i}{dx^2} \tag{3.8}$$

Transport of solute through barrier was also calculated using centered finite difference approximation using following equation.

$$\frac{d^2C_i}{dx^2} = \frac{C_{i-1}-2C_i+C_{i+1}}{h^2} \tag{3.9}$$

The error in using the CFD approximation is proportional to the square of the segment thickness (h). By increasing the number of nodes, h can be decreased proportionally and the error would even further decrease with the square of the thickness while using this approximation. However, to determine the flux at boundaries this approximation does not work as it requires the concentrations at the node itself along with the concentrations before and after that node. For instance, at node $i = 1$ we cannot use the CFD approximation as it would require the concentration at node $i = 0$ which does not exist. Instead, we need to use Forward Finite Difference (FFD) approximation as described in following equation for the change in stimulant concentration in which the error is proportional to segment thickness (h) [instead of square of thickness (h^2)].

$$\frac{dG_1}{dx} = \frac{G_2-G_1}{h} \tag{3.10}$$

Similar scenario would also occur at the last node of last layer.

3.2.3 Explicit Euler's Method for Temporal Domains

For a given set of G_i and C_i values at a given time along with corresponding h values, $\frac{d^2G_i}{dx^2}$ and $\frac{d^2C_i}{dx^2}$ can be solved at every node. $\frac{dG_i}{dt}$ and $\frac{dC_i}{dt}$ can be solved at every node using equation 3.8 after knowing the values for D_{g_i}, D_{c_i}, $\frac{d^2G_i}{dx^2}$ and $\frac{d^2C_i}{dx^2}$.

Using explicit Euler's method, $\frac{dG_i}{dt}$ and $\frac{dC_i}{dt}$ can be approximated in its simplistic form as $\frac{dG_i}{dt} = \frac{\Delta G_i}{\Delta t}$, and $\frac{dC_i}{dt} = \frac{\Delta C_i}{\Delta t}$. Combining with Eq. 3.6 & 3.8, ΔG_i and ΔC_i can be calculated as described below.

$$\Delta G_i = D_{g_i} \frac{d^2G_i}{dx^2} \Delta t \tag{3.11}$$

$$\Delta C_i = D_{c_i} \frac{d^2C_i}{dx^2} \Delta t \tag{3.12}$$

Change in concentration at each node at given time step can be defined by following equations.

$$\Delta G_i = G_{i,j+1} - G_{i,j} \tag{3.13}$$

$$\Delta C_i = C_{i,j+1} - C_{i,j} \tag{3.14}$$

Here, j is the time step. So, for instance, if $G_{i,j}$ (or $C_{i,j}$) is known then $G_{i,j+1}$ and $C_{i,j+1}$ can be calculated as,

$$G_{i,j+1} = G_{i,j} + D_{g_i} \frac{d^2G_i}{dx^2} \Delta t \tag{3.15}$$

$$C_{i,j+1} = C_{i,j} + D_{c_i} \frac{d^2C_i}{dx^2} \Delta t \tag{3.16}$$

Thus, values for G and C for can be derived for the next time step and process can be repeated to advance forward in time. The error for the explicit Euler's method is proportional to Δt. Results are more accurate with smaller time steps. There are other more stable implicit methods in which such concentration changes can be calculated in more accurate ways by guessing the concentration in next node and iterating the calculations until the error is minimized. But such implicit methods are more intensive, complicated and require large computation time making them much slower than explicit Euler's method. Thus, it is more convenient here to use explicit Euler's method for the proposed model. However, it also has certain limitations in which smallest possible time step is dependent on the ratio of square of the node thickness and the diffusion coefficient which will be discussed further in section 3.2.7 (Stability limits of the model).

3.2.4 Flux Calculations for Depots using Backward Finite Difference

Flux calculations for depot layers are little more complex as the geometry of the hydrogel changes upon swelling. Diffusion and partition coefficients of stimulant and solute (D_g, D_c, H_g and H_c) for shrunken hydrogels were assumed to be zero. However, a certain amount of stimulant is required to trigger the hydrogel to change its form from shrunken to swollen. We treat the amine groups in the hydrogel as scavenger which reacts instantaneously and irreversibly. When all or a specific portion of the amine groups are protonated by incoming acid at given node, that node can be flipped to swollen condition. At this point, the node will be assigned definite nonzero values of D_g and H_g for swollen condition. As the node is in swollen condition now, the segment thickness h for that node also changes. At the same time when node changes from shrunken to swollen, diffusion coefficient and partition of dissolved solute (D_c and H_c) also changes

to a nonzero value. Water is assumed to be ubiquitous, entering the swollen node of depot instantaneously (*i.e.*, it occurs as soon as the node is triggered). At this point, some of the solid solute particle in that node dissolves, raising its concentration from C_i to C_{sat} and decreasing B by a stoichiometric proportion. The dissolved solute then diffuses out again from the swollen node based on Fick's law.

Flux of species going in and out from the swollen depot were calculated based on Backward Finite Difference (BFD) approximation. The reason for not using the centered finite difference here is due to the swelling mechanism of the depot layer. As soon as the stimulant diffuses in to particular node and consumes the scavenger completely, that node in the depot gets switched from shrunken to swollen state. In Eq. 3.15, G_i can only increase if ($D_{g_i} \frac{d^2 G_i}{dx^2} \Delta t$) is positive. However, for shrunken nodes the diffusion coefficient of acid is still zero and will remain zero until its scavenger is consumed. So CFD approximation cannot be used as in Eq. 3.15; G_i cannot increase if D_{gi} is zero, and that node remains permanently shrunken. Instead, we have to calculate the flux based on the previous nodes to determine how much G_i should increase (until that acid is scavenged), using BFD approximation. It requires the flux from previous node that is already swollen and flux of the current node which has just been triggered. As both of these nodes have already occupied the parameter values (of dissolved solute and stimulant) in swollen conditions, the fluxes $J_{C(i)}$ and $J_{G(i)}$ are first calculated using Eq. 3.17 and 3.18 respectively. Using backward finite difference approximation, the change in concentrations ΔC_i and ΔG_i can then be obtained using Eq. 3.19 and 3.20 with the use of these fluxes.

$$J_{C(i)} = \frac{(D_{c(i-1)}+D_{c(i)})}{2} * \frac{(C_{i-1}-C_i)}{h_i} \quad (3.17)$$

$$J_{G(i)} = \frac{(D_{g(i)}+D_{g(i+1)})}{2} * \frac{(G_i-G_{i+1})}{h_i} \quad (3.18)$$

$$\Delta C_i = \frac{(J_{C(i-1)}-J_{C(i)})*\Delta t}{h_i} \quad (3.19)$$

$$\Delta G_i = \frac{(J_{G(i-1)}-J_{G(i)})*\Delta t}{h_i} \quad (3.20)$$

3.2.5 Parameters for Model

Stimulant concentration (C_{gup}), scavenger concentration in barrier (F_b), scavenger concentration in depot (F_d), solid solute concentration (B) and dissolved concentration of solute (C_{sat}) were independently measured and used in the model as needed.

Table 3.8 Zinc oxide concentrations in barriers

ZnO% in PVA (w/w)	ZnO, (F_b) [M]	Equivalent [H^+] [M]
0	0	0
10	0.793	1.587
20	1.765	3.531
30	2.983	5.967
40	4.555	9.111
50	6.661	13.32
60	9.628	19.26
70	14.12	28.24
80	21.72	43.44

Stimulant concentration (C_{gup}) was set to 0.001 M as the upstream pH was held at constant pH of 3 using 0.01 M citrate buffer. Scavenger concentration in barrier was calculated based on the equivalent molar concentration of ZnO loaded in PVA barriers. Equivalent molar concentration of ZnO in PVA barriers with various ZnO loading (10%

to 80% (w/w)) is reported in Table 3.8. The procedure for confirming scavenger concentration in depot (F_d) was already described in Section 2.2.3 of Chapter 2. Scavenger concentration in p(MMA/DMA) (F_d) is considered to be an equivalent concentration of DMA content (25% (by mole)) which is equal to 2.33 M.

Solid solute concentration (B) was calculated based on the initial loading of 5% (w/w) dye content in p(MMA/DMA) depots. Based on density of methylene blue (1.23 g/cm^3) , methyl orange (1.28 g/cm^3) and equivalent density of 75/25 p(MMA/DMA) (1.13 g/cm^3); equivalent molar concentration of methylene blue and methyl orange in p(MMA/DMA) was found to be 0.145 M and 0.166 M respectively for 5 % (w/w) dye content.

Dissolved solid concentration (C_{sat}) inside the depot matrix was calculated based on saturation concentration of dye. Excess amount of each dye was added in 100 mL of pH 3 buffer with stirring rate of 1200 rpm for 7 days in 125 mL polyethylene beaker for both methylene blue and methyl orange in separate trials. After 7 days, the saturated dye solution was centrifuged in 50 mL centrifuge tubes and measured for saturation concentration. An average saturation concentration of 5.9 mM for methylene blue and 1.1 mM for methyl orange was reported. However, these concentrations were measured by dissolving fresh dye powder in pH 3 buffer. When the dye powder is immobilized in p(MMA/DMA) matrix that swells by only a factor of 4 to 6 g water/g dry gel within relatively short time of 2 to 4 hours, saturation concentrations of these dyes were expected to be considerably lower than that was observed when the dye powder was freely dissolved in pH 3 buffer. In the computational model, C_{sat} was assumed to be 4 times lower than the observed values of saturation concentrations.

The diffusion coefficients and partition coefficients of stimulant and solute through PVA barriers were calculated using diaphragm cell experiments, already described in Section 2.2.3 in Chapter 2. With an average permeability (DH) of 1.47×10^{-5} cm^2/s (±6.8% RSD), and partition coefficient (H_{gb}) of 0.6 PVA barriers, the diffusion coefficient of stimulant (acid) through PVA barriers (D_{gb}) was set to 2.5×10^{-5} cm^2/s. Similarly, with an average permeability of methylene blue to be 3.57×10^{-7} cm^2/s (RSD ± 18.3%) and a partition coefficient (H_{cb}) of 0.6 (based on volume fraction of water), the diffusion coefficient of methylene blue (D_{cb}) was set to 6.0×10^{-7} cm^2/s. Permeability of methyl orange through 88 micron scavenger-free PVA film was found to be 1.8×10^{-8} cm^2/s for a single diaphragm cell trial, which corresponds to diffusion coefficient (D_{cb}) of 3.0×10^{-8} cm^2/s for methyl orange.

The transport properties of stimulant and solute through depots were calculated using diaphragm cell trials and have already been described in Section 2.2.2 of Chapter 2. For swollen depots, diffusion coefficient of stimulant (acid) (D_{gsw}), was set to 5.1×10^{-5} cm^2/s along with its partition coefficient (H_{gd}) to be 1. For simplicity, at pH 7 permeability of acid in depot during shrunken state is negligible. Diffusion coefficient of acid (D_{gsh}) and partition coefficient (H_{gsh}) of shrunken depots were considered to be zero, as permeability of acid through shrunken depot was negligible. Similarly diffusion coefficient of solute (D_{csh}) and partition coefficient of solute (H_{csh}) for shrunken depots was set to zero as there was negligible transport of dye at pH 7. With an average permeability (DH) of 3.4×10^{-7} cm^2/s ((± 7.9%) and the corresponding lag times observed in diaphragm cell trials, diffusion coefficient of methylene blue through swollen depot (D_{csw}) was set to 7.1×10^{-7} cm^2/s with an average partition coefficient (H_c) of 0.43.

The equilibrium partition coefficient of methylene blue in the depot film was determined by swelling dry, solute-free film in a small volume of known dye concentration, then transferring the film to solute-free buffer. The absorbance changes in both the original solute solution and the initially solute-free solution were used to confirm partition coefficients ($C_{film}/C_{solution}$) of 0.48 for methylene blue. Average permeability of methyl orange through swollen depot was found to be 3.0 x 10^{-7} cm^2/s (± 16% RSD) with a partition coefficient of 23.9 (± 35% RSD) using the diaphragm cell. However, equilibrium partition coefficient of methyl orange was found to be 548 when it was determined using a similar procedure described above for methylene blue. Significant variation of the partition coefficient of methyl orange in p(MMA/DMA) hydrogel with different experimental procedure suggested that there is a possibility of reaction between negatively charged methyl orange with protonated hydrogel. Methyl orange is an azo-dye and its reactivity significantly changes with pH. It was difficult to accurately measure the partition coefficient of methyl orange, especially when the methyl orange dye particles are suspended in dry form in a p(MMA/DMA) matrix which simultaneously dissolve and react with protonated hydrogel in a complex pH environment, where the dissolved dye is possibly reacting with both amine groups of p(MMA/DMA) with a pK_a of 7.7 and also outside buffer solution of pH-3 citrate buffer with a pK_a of 3.7. Thus, computational model was validated using accurate and known values of diffusion and partition coefficients of methylene blue. Table 3.9 summarizes all of the above calculated parameters that are incorporated in the computational model.

Table 3.9 Summary of model parameters

Symbol	MODEL PARAMETERS	Input value	Unit
	Physical parameters		
n_b	Number of nodes in PVA barrier	60	-
n_d	Number of nodes in p(MMA/DMA) depot	120	-
t_b	Barrier thickness	100	µm
t_{dsh}	Depot thickness (shrunken)	100	µm
s	Anisotropic swelling factor	2	-
t_{dsw}	Depot thickness (swollen)	200	µm
h_b	Individual node thickness of barrier	1.667	µm
h_{sh}	Individual node thickness of shrunken depot	0.833	µm
h_{sw}	Individual node thickness of swollen depot	1.667	µm
	Scavenger properties		
F_b	Scavenger concentration in barriers with 10 % ZnO (w/w)	0.793	moles/L
F_d	Equivalent Scavenger concentration of DMA in Depot	2.330	moles/L
	Stimulant (acid) properties		
C_{gup}	Upstream stimulant (pH 3 citrate buffer) concentration	0.001	moles/L
D_{gb}	Diffusion coefficient of acid in barrier	2.5×10^{-5}	cm^2/s
D_{gsh}	Diffusion coefficient of acid in shrunken depot	0	cm^2/s
D_{gsw}	Diffusion coefficient of acid in swollen depot	5.1×10^{-5}	cm^2/s
H_{gb}	Partition coefficient of acid in barrier	0.6	-
H_{gsh}	Partition coefficient of acid in shrunken depot	0	-
H_{gd}	Partition coefficient of acid in swollen depot	1.0	-
	Solute (Methylene Blue) properties		
B_d	Solute concentration (solid)	0.145	moles/L
C_{sat}	Dissolved solute concentration	0.0015	moles/L
D_{cb}	Diffusion coefficient of methylene blue in barrier	6.0×10^{-7}	cm^2/s
D_{csh}	Diffusion coefficient of methylene blue in shrunken depot	0	cm^2/s
D_{csw}	Diffusion coefficient of methylene blue in swollen depot	7.1×10^{-7}	cm^2/s
H_{cb}	Partition coefficient of methylene blue in barrier	0.6	-
H_{dsh}	Partition coefficient of methylene blue in shrunken depot	0	-
H_{cd}	Partition coefficient of methylene blue in swollen depot	0.48	-

3.2.6 Node Accuracy for Delaminating BMPR Model

A FORTRAN code was generated in FTN 95 Plato IDE compiler using the methods described in Section 3.2.2 to 3.2.5 and the parameter values shown in the Table 3.9. An example code for delaminating BMPR system is shown in APPENDIX B.

To check the node accuracy the code was compiled for a single pulse delaminating BMPR device with a 100 micron barrier and 100 micron depot. The barrier was divided in various number of nodes (n_b) starting from 5, 10, 20, 40, 60, 80, 100 and

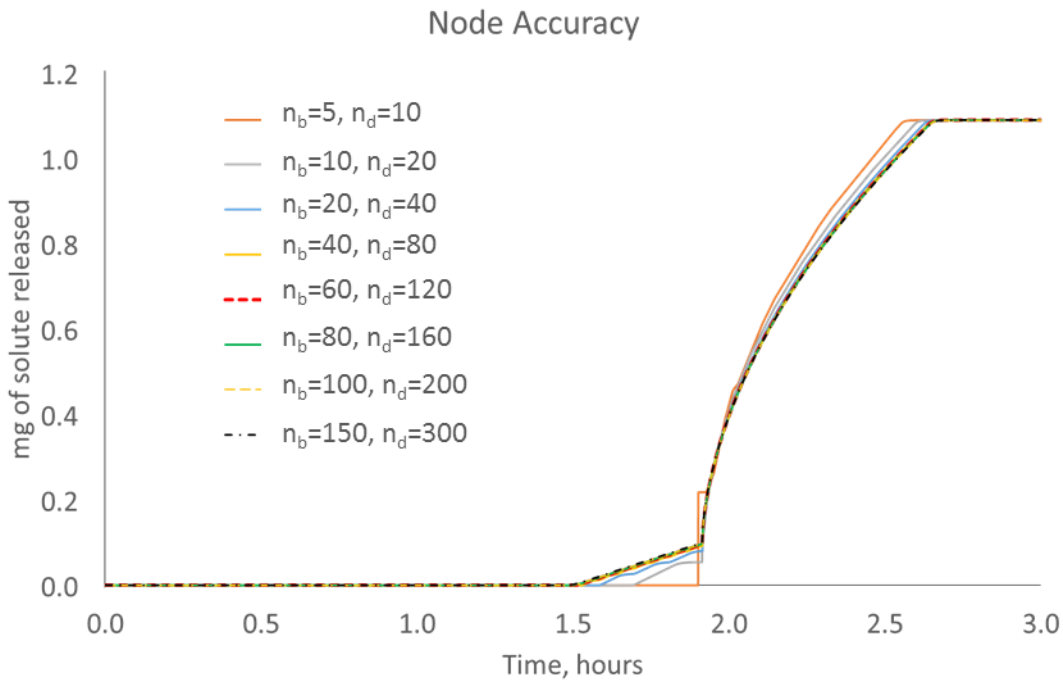

Figure 3.4 Node accuracy for delaminating BMPR model using various number of node size.

150. Similarly, the depot was also divided in to corresponding number of nodes (n_d) starting from 10, 20, 40, 80, 120, 160, 200 and 300. After compiling and executing the model, a plot was generated for the amount of solute released in mg with time for each set of node size, which is shown in Figure 3.4. An accurate amount of solute was released (99.9999993% of the expected total release) for each set of node size. However, as the

node size increased from (n_b, n_d) = (5, 10) to (n_b, n_d) = (150, 300), the pulse time started to decrease. Analytically, the barrier should get consumed after 1.4003 hours. Once the barrier is consumed, the release of the solute should occur as soon as the stimulant hits the depot triggering the first node of depot. Delamination of the depot was arbitrarily set to occur when 10% of the depot thickness gets triggered by the stimulant. After delamination, the diffusion of species was set to occur from the both faces of the layers. As shown in Figure 3.4, maximum node accuracy was observed with the node size of (n_b, n_d) equal to (150, 300). However, for the node size of (n_b, n_d) equal to (60, 120) and above, the release profiles almost overlapped on each other with similar accuracy. Thus, node size was kept at as low as 60 nodes of barrier and 120 nodes of depot for further validation of model.

3.2.7 Stability Limits and Time-step Accuracy for Delaminating BMPR Model

It is very important to keep the model within its stability limits. The parameters that affect the stability of the model are those which are used for determining second derivatives of flux calculations via explicit Euler's method for temporal domains. The model stability is dependent on the combination of the parameters which include value of thickness of individual node (h), the diffusion coefficient (D) and time step (Δt) used for calculating second derivative. Keeping these factors in mind, for a given model run stability limits were defined based on Equation 3.21 and 3.22, where $D_g$and D_c are diffusion coefficients of stimulant and solute, h is a node thickness and Δt is a time step. While running the model with constant diffusion coefficients and preset thickness of individual nodes, time step would be the only parameter than can be altered to keep the model within stability limits. As depicted in Figure 3.5, for a given model run for a

delaminating BMPR, model only remains stable with a maximum time-step of 0.00027 s for the parameters that are shown in Table 3.9. It is important to note that the model produces accurate and identical release profiles for all the time-steps below the maximum

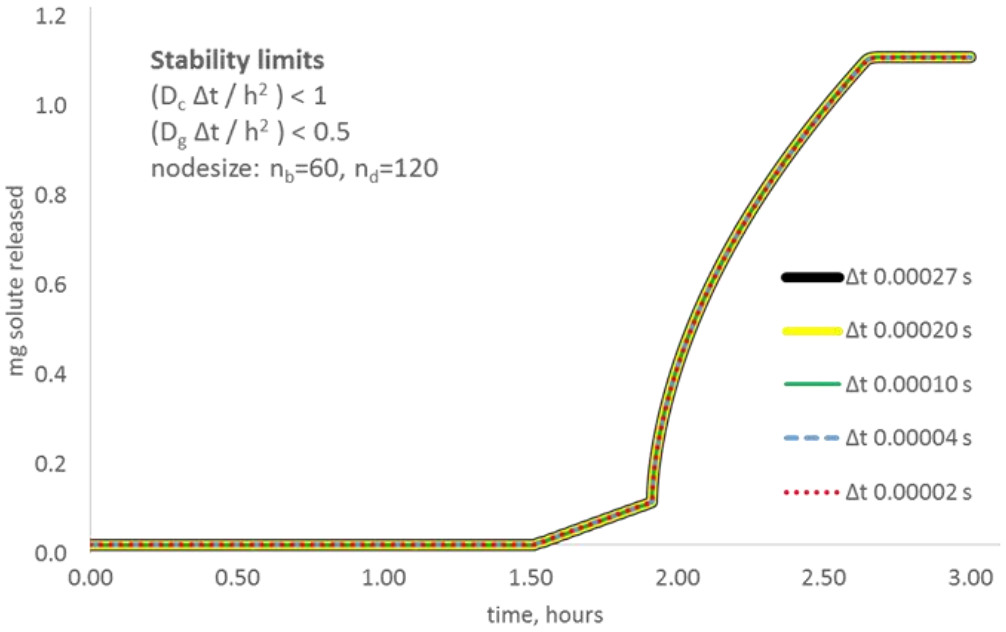

Figure 3.5 Stability limits for delaminating BMPR model.

limit as indicated in Figure 3.5. However, for exploring model on various user-defined conditions where the accuracy of the model is not a primary concern, any of the parameters (h, D or Δt) can be altered in a way that satisfies both the Eq. 3.21 and 3.22.

$$\frac{D_g \Delta t}{h^2} < 0.5 \tag{3.21}$$

$$\frac{D_c \Delta t}{h^2} < 1 \tag{3.22}$$

It was also observed that if the total number of time steps for a given run exceed the value 1×10^9, the code becomes unstable and does not produce output due to machine limitations.

3.2.8 Validation of Computational BMPR Model with Experimental BMPR System

The computer model was validated with experimental delaminating BMPR trials. Each pulse (comprised of single barrier and single depot) of experimental 10-pulse delaminating BMPR trial (Chapter 2, Figure 2.28) was separately run with computational model with their corresponding input parameters (such as thickness, scavenger concentration, diffusion and partition coefficients, solute and stimulant concentrations, etc.). Parameter values used for these runs were already discussed earlier in Section 3.2.5. An example code for the delaminating BMPR system is shown in APPENDIX B. Each model run for every single pulse produced an output where amount of solute release was tracked against time. Time was also tracked when each node got triggered which provided the values for depletion time for barrier, delamination time when 10% of the depot got triggered and also the time when all the nodes depot got completely triggered. Delamination time during each pulse was deliberated as the start time for penetration of the next barrier. Complete release time of each pulse was deliberated as the time when 99.9999% of the solute was released from that particular pulse. After tracking these times (depletion time of each barrier, delamination time of each depot and complete release time from each depot), release data for all the 10 model runs for each pulse was combined together in a single spreadsheet on one chart. The comparison between model results and experimental results for the 10-pulse delaminating BMPR device is shown in Figure 3.6 (right). The model results accurately predict the pulse shape, pulse time and amount of solute released during each pulse. As discussed earlier in Chapter 2, earlier pulses (3-6) showed a premature delamination due to weak adhesion of the beeswax with the periphery of the layers, which resulted in to quicker pulse times than the model

predictions. However, lag times for remaining pulses (pulse 1, 2, 7, 8, 9 and 10) were in a good agreement with model results.

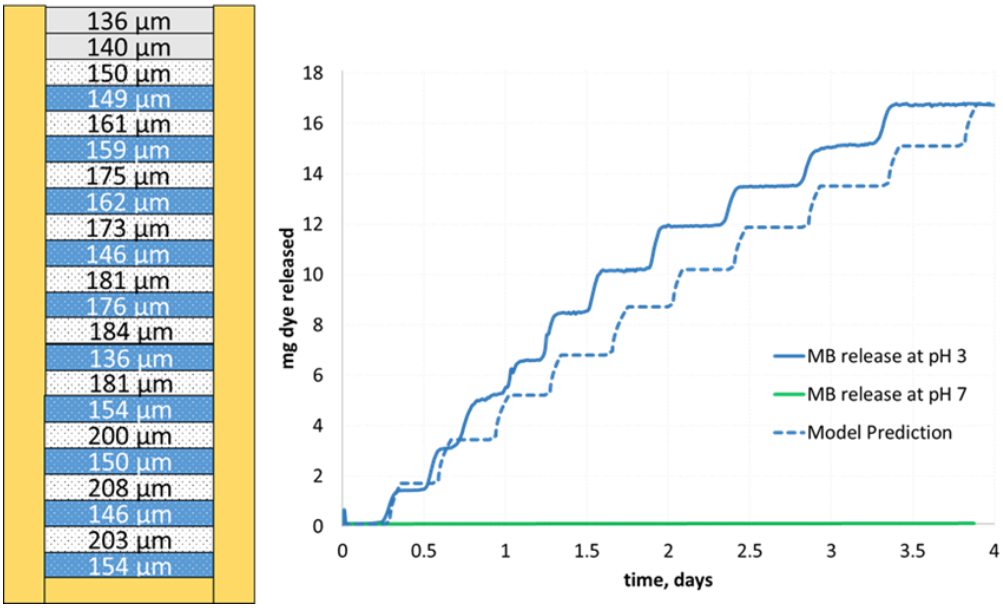

Figure 3.6 Validation of computational model for 10-pulse BMPR device

In similar way as described above for 10-pulse system, model validation was reconfirmed with 3-pulse delaminating BMPR trial (Figure 2.25). The model results are shown in Figure 3.7. Both devices were made using bilayer barriers, with half of the barrier containing no scavenger and remaining half filled with ZnO. The only difference in these two devices (Figure 3.7 (right)) was the orientation of the barrier, which was reversed in the later one. While running the computational model for each pulse of these devices, half of the barrier nodes were initialized with zero values of scavenger (F_b) and the remaining nodes in that particular barrier were initialized with equivalent molar value of ZnO in each node. All other parameters were set to the values that were described earlier in Section 3.2.5. As described for 10-pulse device earlier, the computer model was run for each pulse and solute release was tracked against time. Demo code for each pulse (containing bilayer barrier and depot) is shown in APPENDIX D. Based on depletion

time of barrier, preset delamination time (when 10% of the depot gets triggered), and 99.99999% of release time, output release data was combined in a single spreadsheet on one chart. Model predictions for these trials are shown in Figure 3.7 and compared against experimental results. Pulse timings and amount of solute released form both of these devices are in good agreement with experimental results and further validates the

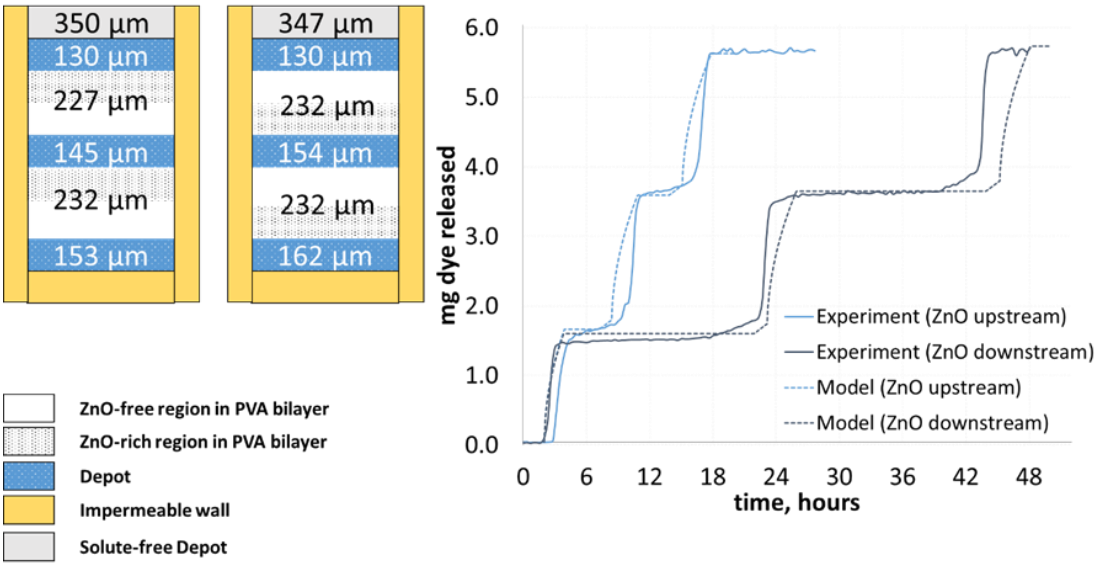

Figure 3.7 Validation of computational model for 3-pulse delaminating BMPR system

computational model. It must be noticed that first depot in both of these devices did not contain any barrier, and rather was protected by a single dye free depot. So the time required for delamination for the first dye-free depot was recorded manually by visual inspection. As soon as the dye-free depot was removed, clock was set to zero and the first pulse was considered for single dye loaded depot (without any barrier). The computational model is capable of predicting the release behavior of single depot without any barrier on top of it. Code for single layer depot is shown in APPENDIX C.

Now as the computational model has been validated, it becomes a good tool for guiding the delaminating BMPR system. More importantly it can also be adapted for predicting

performances of non-delaminating system where layers do not delaminate making the system more complex for the species diffusing in and out of the multilayer laminates. Analytical prediction of such multilayer BMPR systems becomes very tedious and more difficult to calculate. Strategies for experimental non-delaminating BMPR systems are discussed in Chapter 4 for 2-pulse non-delaminating BMPR devices. Further expansion of computational model for non-delaminating system along with its exploration on wide range of parameter space is discussed in Chapter 5.

3.3 Conclusions

Experimental pulse times of delaminating BMPR systems from Chapter 2 were compared against analytical predictions with good agreement. A computational model of the delaminating BMPR system was constructed and appropriate node size and time-step sizes (stability limits) were determined. The model was validated against both analytical predictions and experimental results with good agreement.

This chapter shows that one can quickly and easily predict most of the performance parameters of a delaminating BMPR system analytically. The parameters that cannot be predicted analytically (e.g. shape of the pulse), can be predicted computationally. Moreover, the analytical and computational validation of the model is a critical starting point for the non-delaminating BMPR model, which is currently extremely difficult to validate experimentally as described in the next chapter.

CHAPTER 4 NON-DELAMINATING BMPR SYSTEM

The next aim of the research was to create a BMPR system in which the layers do not leave the stack during release of solute. The removal of spent layers is not desirable in some applications where degradation products cannot be tolerated or the whole device must remain in place for later removal or treatment. The proposed non-delaminating BMPR system can provide pulsed release even in such cases. This approach is also contrasting to surface eroding polymer BMPR system, as it would not rely on a

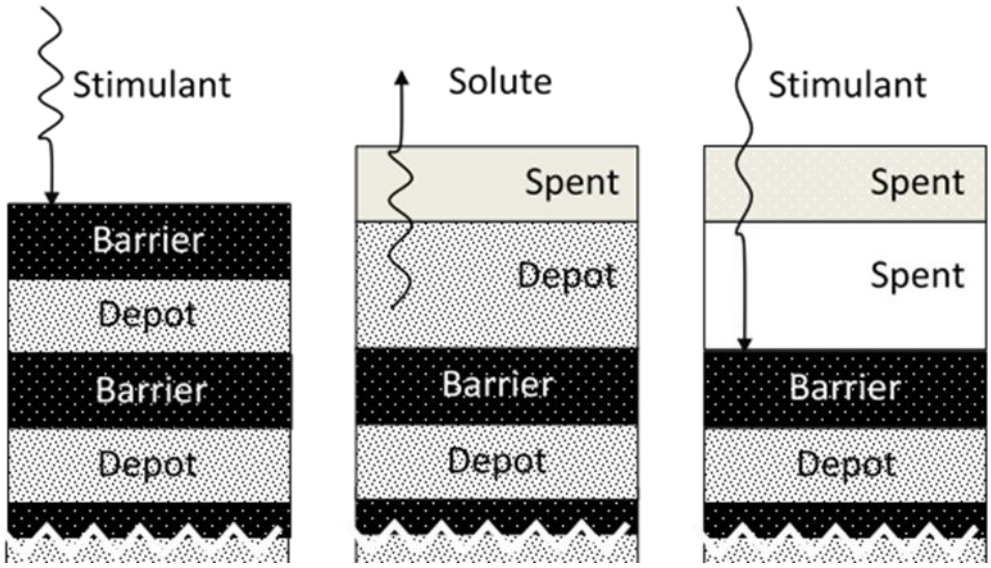

Figure 4.1 Schematic of non-delaminating BMPR system; release of solute occurs due to anisotropic swelling with spent layers remain intact in the device.

degradation or dissolution mechanism for releasing solute. Both depot layers and barriers are fused together which restricts the swelling of depot layer in only one dimension as shown in Figure 4.1. Additional mass transfer resistance caused by spent layers slows down the diffusion of stimulant deeper into the device. Lag time of an active barrier increases due to slower rate of stimulant diffusing into that layer. This also slows down

triggering of the depot. Due to such slower diffusion process, deeper barrier layers require less scavenger than those near the top of the device to provide the same delay interval between corresponding pulses. In a similar way, amassed resistance of spent layers also slows down the rate of solute diffusing out of the device. It increases the delay time of the solute pulse and spreads it out over a longer time, which creates a limit on the minimum periodicity of the pulses. Pulses that are too close together in time can overlap, effectively becoming continuous release due to the longer diffusion process. However, non-delaminating BMPR system can still provide distinct pulses by altering the amount of scavenger in deeper layers with reduced thicknesses compared to the layers near to the surface of the device.

4.1 Materials

The proposed non-delaminating BMPR device uses the same p(MMA/DMA) depots immobilized with model drugs (methylene blue or methyl orange) and ZnO-filled PVA barriers that were used to design delaminating BMPR system descried in Chapter 2. Most of the materials used to design the non-delaminating BMPR system are the same as described in Chapter 2, Section 2.1. Additionally, rubber cement (Elmer's) was used to seal the bottom of the device to provide flexibility for the layers to swell in one direction and simultaneously to avoid any breakage of the device due to developed swelling pressure, preventing any possible release from the bottom of the device.

4.2 Depots

p(MMA/DMA) depots used to design non-delaminating BMPR system, were fabricated in similar way as described in Chapter 2. For the delaminating BMPR system, these depots swelled in all directions upon swelling. This isotropic swelling was not

desirable for non-delaminating BMPR system because it can cause the depot layers to delaminate from adjacent barrier or can break the seal which could allow the stimulant to bypass the underlying barrier and approach the depot from the sides. To avoid this it was necessary to control the swelling in one dimension perpendicular to the plane of the layers. Restricting swelling to only the perpendicular direction had considerable impact on swelling behavior of the depot layer. Figure 2.5 demonstrated isotropic swelling kinetics of depot layers at various pHs, where discs swelled significantly below pH 5 and in each case the swelling behavior was observed to behave in a sigmoidal manner (inset of Figure 2.5), with the rate slowing initially as the front moved deeper into the film before suddenly increasing sharply again and then remaining stable at equilibrium. As the water and stimulant approaches the surface well before the center region (core) of the disk, the surface region swells first. The surface swelling occurs in perpendicular direction from the surface plane as the core of the disk is still in shrunken condition. When swelling fronts from both faces of the disks meet at the core, there is no longer any shrunken polymer to restrain swelling in the lateral dimension and as a result the disk expands very rapidly in lateral directions, with a slight shrinkage in perpendicular dimension. Similar behavior was also observed for depot layers of various thicknesses as shown in Figure 2.9. The initial linear region of swelling (Figure 2.5 & Figure 2.9) represents one-dimensional swelling. To determine the maximum possible one-dimensional swelling before the lateral swelling begins, the p(MMA/DMA) disks were polymerized on microscope slides that were pre-silanized with 2 % solution of 3-(trimethoxysilyl) propyl methacrylate in toluene. Pendant hydroxyl group on glass surface reacted with methoxysilane group and covalently bonded the molecule to the

glass surface. Thus, attached methacrylate pendant groups on the microscope slides participate in polymerization with p(MMA/DMA) hydrogel and covalently bond the hydrogel to the glass surface, which is shown in Figure 4.2 (left). The gels covalently bonded with the glass substrate were then immersed in pH 3 citrate buffer and thickness was measured periodically to study the one dimensional swelling behavior. Figure 4.2 (right) indicates that the swelling of p(MMA/DMA) is still pH sensitive with a swelling ratio of over 3 even when the disks were constrained to a single dimension.

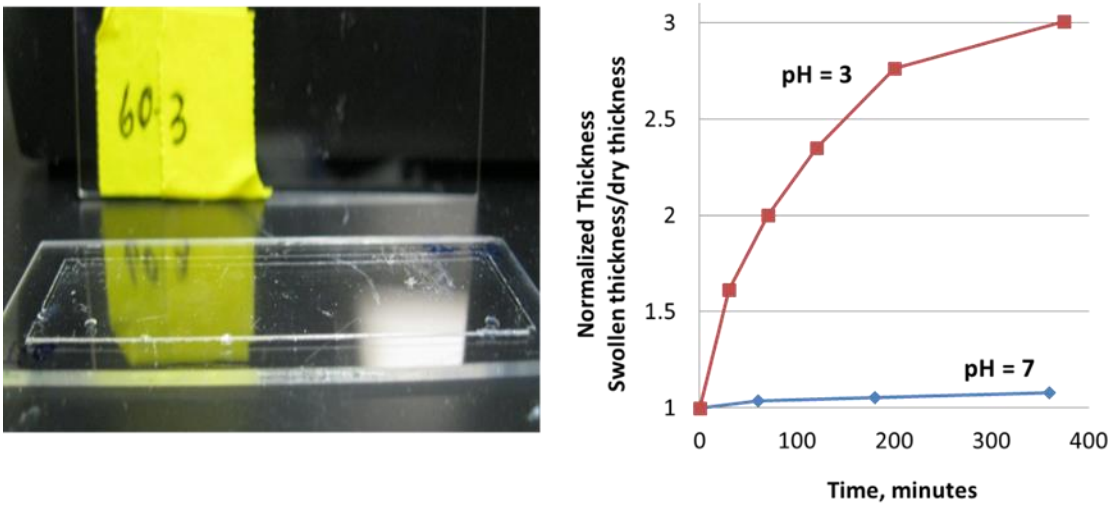

Figure 4.2 Anisotropic swelling of p(MMA/DMA) disk at pH 7 and at pH 3; p(MMA/DMA) disk (240 µm thick) that was covalently adhered to the glass substrate (left).

The swelling pressure of the depot layers can also be reduced by increasing the crosslink density of the p(MMA) matrix. More cross-linking reduces the swelling pressure of the hydrogel and still allows in enough water to dissolve the solute and allow it to diffuse out of the layer. Figure 4.3 depicts the swelling and release rates for three depot layers with molar crosslink densities of 0.1 %, 1.0 and 5.0 %. Depots with 5% cross-linking restricted the swelling ratio to 1 but the release rate of methyl orange was also significantly reduced. Release of methyl orange was almost unchanged with the

increase in crosslinking density from 0.1 to 1.0 % with a 50 % reduction in swelling while maintaining the similar kinetics. Thus, depots with up to 1.0 % crosslinking density restricted swelling ratio of up to 3 (as similar to that was achieved in Figure 4.2, in case of adhered p(MMA/DMA) to the glass substrate), and still produced significant release of solute from the depot matrix.

A similar effect was also visible when 5% methylene blue loaded p(MMA/DMA)

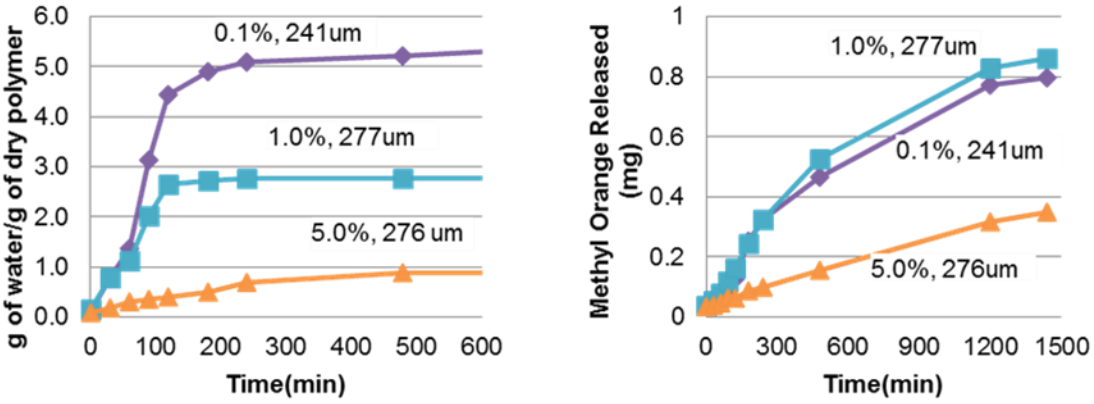

Figure 4.3 Effect of cross linking on swelling and release; p(MMA/DMA) disks with various amount of crosslinker (mole %), along with disk thickness. Release of Methyl Orange (5 wt %) from p(MMA/DMA) disks in pH 3 buffer environment.

disks (75 and 150 µm thick) with different crosslinking density of 0.1 and 1% were subjected to pH 3 buffer. This is indicated in Figure 4.4, where the films showed almost a 50% reduction in equilibrium swelling ratio when cross-linking density was increased from 0.1 to 1% (mole%). However, unlike methyl orange loaded films, release rates of methylene blue were slightly lowered with increase in crosslinking density from 0.1 to 1 %. These release rates were still significant enough to provide complete equilibrium release from the hydrogel.

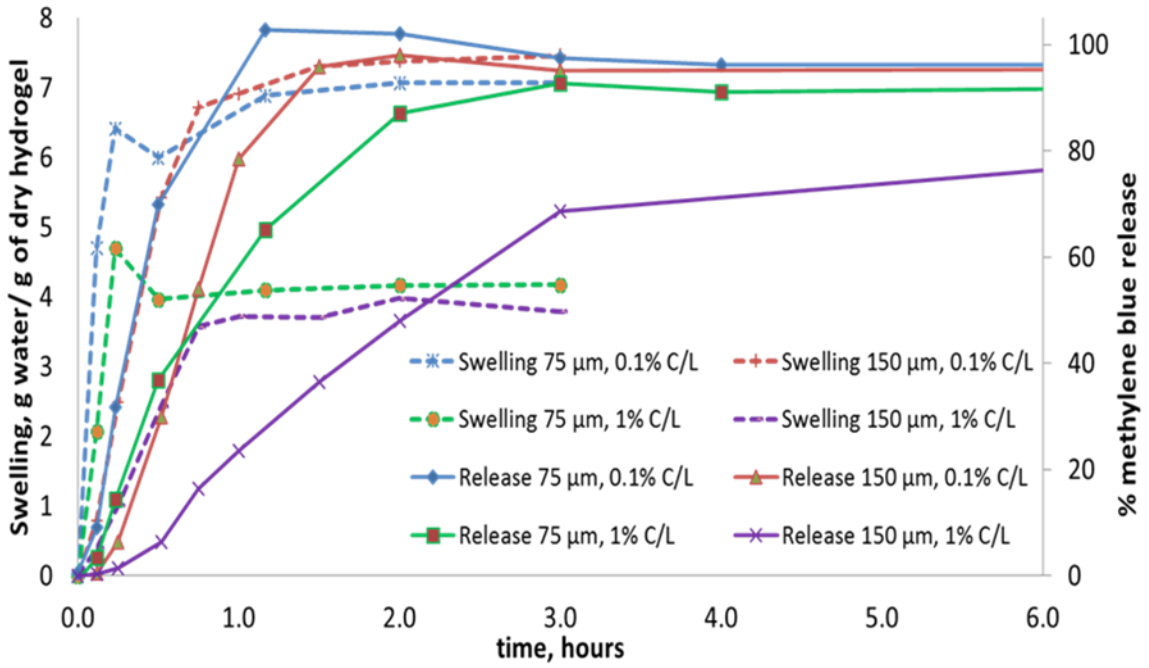

Figure 4.4 Effect of cross-linking on swelling and release of methylene blue loaded depots; 5% methylene blue loaded p(MMA/DMA) disks with 0.1 and 1 (mole %) crosslink-density were studied for swelling and release at pH 3. Swelling and release behavior of these films are represented by same colored "dotted" and "solid" lines respectively. Swelling rate reduces significantly with increase in crosslinks, but complete equilibrium release was observed even with lowered swelling ratio.

4.3 Barriers

PVA barriers used for the non-delaminating BMPR system were fabricated exactly the same way as described in Chapter 2. These barriers were hydrated in water for at least a day before using them in a BMPR device. As the barriers were already pre-swelled in water, no further swelling of these barriers was anticipated either in vertical or in lateral direction when placed in BMPR device. ZnO loading in these barriers were varied from 10 % to 60 % (w/w) in various non-delaminating BMPR trials.

4.4 Strategies for Designing Non-delaminating BMPR Device

The experimental non-delaminating BMPR system was constructed using the same p(MMA/DMA) depots and PVA barriers as described earlier. However, the integration of these layers to create a non-delaminating device was significantly different. If the depot layers swelled isotropically, they would delaminate from the adjacent barrier or laterally push the seal around the perimeter of the device due to lateral swelling, allowing the stimulant to seep around the underlying barrier and hit the depot layers from the side. To avoid this, swelling of the depots needed to be restricted to the dimension perpendicular to the plane of the layers. Several strategies were pursued to restrict the swelling in a single dimension keeping the device intact. One key design point was to keep the aspect ratio of the layers greater than 100, by using the layers of approximately 1 cm width but only 50-100 microns thickness. This facilitates swelling in the perpendicular direction rather than in lateral direction. However, coupling of the layers (barriers and depots) was essential to guarantee the swelling only in perpendicular direction. Various strategies were explored to create a working non-delaminating BMPR device which includes plasma bonding, chemical bonding using NIPAm, heat bonding and mechanical clamping to integrate the layers together. However, these techniques could not provide a robust non-delaminating BMPR design. Finally, to create a working BMPR device, the stack was held together with a metal mesh at the top of the device and a sidewall of beeswax to physically restrict the lateral swelling. To accommodate the swelling pressure from the deeper depots, the bottom of the stack could move downward along with the wax sidewall, pushing out a PTFE plug sealed across the bottom with rubber cement. All of

the above mentioned strategies are explained below along with their impact on design and performance.

4.4.1 Strategy 1: Chemical Bonding

Plasma bonding was briefly studied for integrating faces of p(MMA/DMA) depots with their adjacent PVA barriers. During plasma bonding, the surface of the polymer is bombarded with reactive ions (such as oxygen), populating the surface with sites to which covalent bonds can be formed. Earlier it was reported that plasma bonding was successfully used to graft poly(ethylene glycol) chains to p(MMA)[63] and to bond p(MMA) layers to other p(MMA)[64] layers as well as poly(dimethylsilioxane) (PDMS)[65]. To check the effect of plasma bonding between PVA and p(MMA/DMA), thin dry discs (100 µm) of dye-free p(MMA/DMA) and ZnO-free PVA were placed in oxygen plasma etcher (OXFORD INSTRUMENTS, RIE NGP80, University of Iowa Microfabrication Facility) with their adjoining faces aimed upwards. A mild oxygen plasma was generated in the reactive ion etcher at room temperature and the oxygen atoms were bombarded on these polymer surfaces for 1 min. The films were instantly removed from the etcher, and the etched faces were attached and pressed together and kept pressed for 24 hours. However, these films did not bond with each other. As soon as the plasma bonded stack of single barrier and depot was kept in water, the PVA started to swell and instantly got detached from p(MMA/DMA) due to very weak adherence of PVA with p(MMA/DMA). Thus, plasma bonding was not considered as a good approach to design non-delaminating BMPR device.

Few attempts were made for gluing p(MMA/DMA) with a different polymer other than PVA as barriers, such as polyacrylamide (PA) and n-isopropylacrylamide

(NIPAm). During these trials, p(MMA/DMA) was polymerized in between earlier polymerized sheets of either PA or P(NIPAm). Both PA and NIPAm got attached to the p(MMA/DMA) network up to certain extent during gluing process in their separate trials. However, in both cases, when the glued layers of PA-p(MMA/DMA)-PA and p(NIPAm)-p(MMA/DMA)-p(NIPAm) were immersed in pH 3 buffer, PA and p(NIPAm) layers got instantly detached from the p(MMA/DMA) layer due to their temperature sensitive swelling behavior. PA and P(NIPAm) swelled instantaneously with water upon hydration causing rapid delamination of these layers from p(MMA/DMA) layer. However, p(MMA/DMA) swelled gradually with water to a much higher equilibrium swelling ratio (5 g water/ g dry gel) compared to PA or p(NIPAm). This approach of using PA or P(NIPAm) as an alternate barrier, did not work either to create non-delaminating BMPR system.

4.4.2 Strategy 2: Heat Bonding

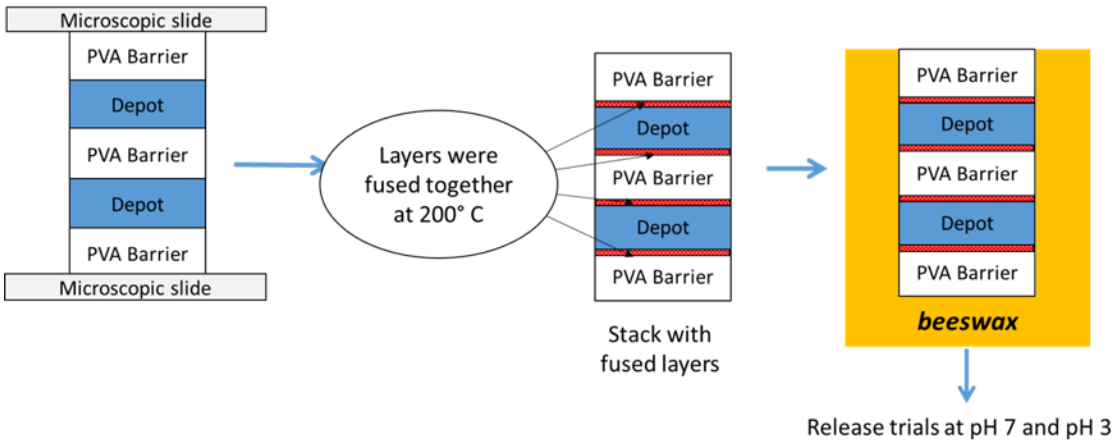

Figure 4.5 Non-delaminating BMPR device by heat bonding mechanism; the barriers and depots were fused together at 200° C. Sidewalls of the fused stack were then sealed using beeswax.

In this strategy, dry discs of PVA barriers and dye loaded p(MMA/DMA) depots were first stacked alternatively and clamped between two glass microslides as shown in

Figure 4.5. The clamped stack was then placed in an oven at 200°C for 30 min at 1 atmosphere pressure. The glass microscopic slides were removed later, and the layers were found fused together. The sidewalls and bottom of this stack was later sealed by pouring melted beeswax in a PTFE mold followed by instant freezing as described in Chapter 2. The stack was further subjected to pH 7 and then to pH 3 to for release studies.

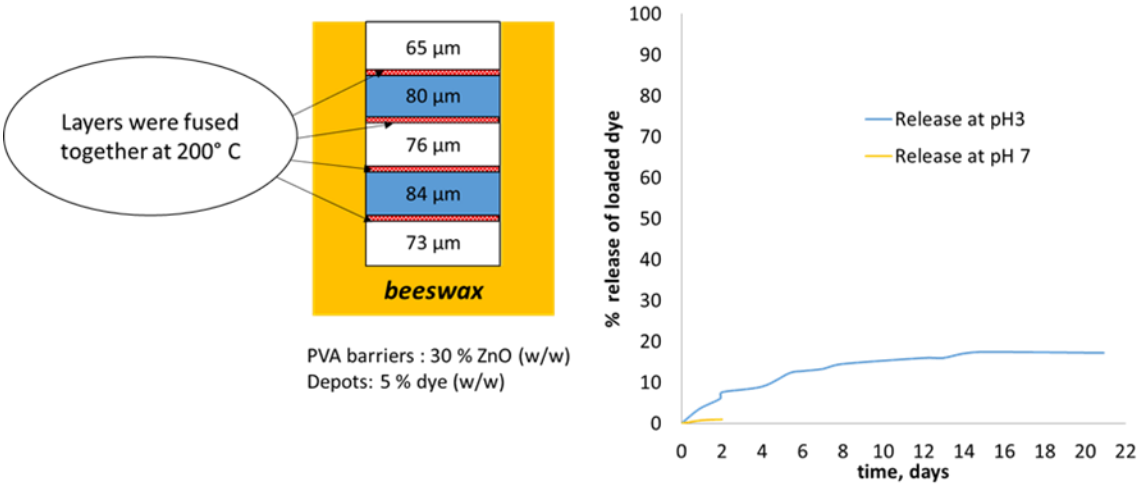

Figure 4.6 Performance of heat-bonded non-delaminating BMPR device; layers did not delaminate from the device when subjected to pH 3, but the release of solute was less than 20% (w/w) during 3 week period due to possible decomposition of drug during heat treatment.

Figure 4.6 shows a configuration (left) of a similar device with its release profile (right) in which two depots (1% cross-linking) with 5% methylene blue loading (w/w) were layered alternatively between 30% ZnO loaded (w/w) PVA barriers. All the layers were fused together at 200°C as described above. Negligible release was observed at pH 7 up to 48 hours. At pH 3, the device remained intact for more than three weeks without any delamination of the layers, but the release rate of the drug was found significantly low. The release of methylene blue started after the first barrier layer (65 µm) got consumed within less than 4 hours (visual observation). Less than 20% (w/w) of the loaded solute was released, and at a significantly lower rate requiring more than three

weeks. The decomposition temperature of methylene blue is 190°C. The incomplete release of the drug was mostly due to its decomposition while the stack was under the heat treatment at 200°C. Melting point of p(MMA) is 160°C. It is possible that p(MMA/DMA) produced significantly more cross-links in the depot itself during heat treatment at 200°C, which reduced the permeability of the solute to diffuse out from the depot. Thus, heat-bonding was not considered suitable approach for designing the non-delaminating BMPR device due to decomposition of the drug at high temperature and also possible reduction in permeability through the depot matrix. Similar heat bonding trials were conducted at lower temperatures of 100°C and also at 150°C. However, the layers did not fuse together at neither of these temperatures and got delaminated when depots got triggered with swelling.

4.4.3 Strategy 3: Mechanical Clamping

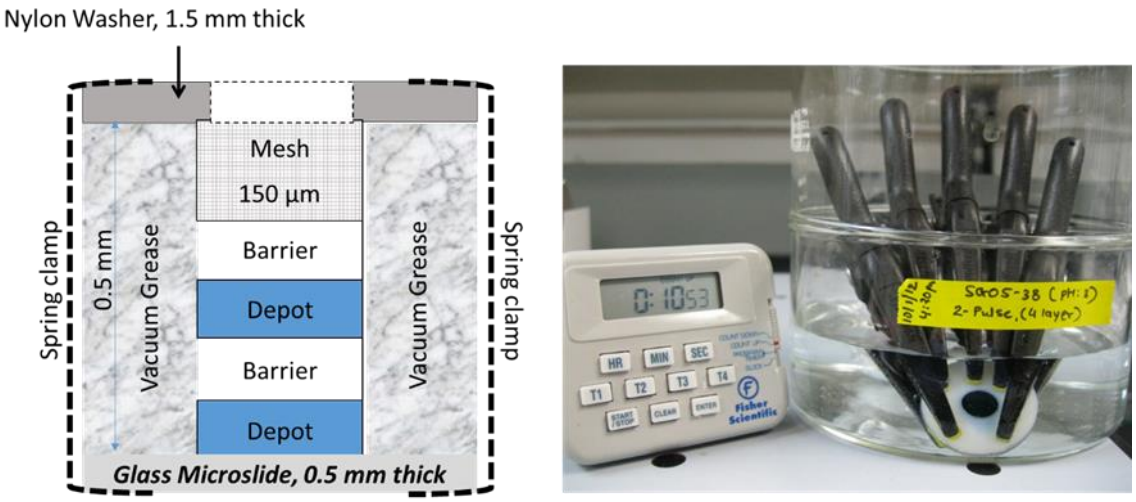

Figure 4.7 Mechanical clamping of layers to restrict lateral swelling; schematic (left), actual device (right) immersed in pH 3 buffer.

Another approach to restrict the lateral swelling was to clamp the device mechanically. As shown in Figure 4.7, 2-pulse non-delaminating BMPR device was

constructed in which a metal mesh (150 µm) was placed on top of the stack of alternatingly layered barriers and depots which was initially placed on a glass microslide. A nylon washer was placed above the metal mesh filter and the entire assembly was mechanically held in place by using polycarbonate spring clamps. Sides of the stack were sealed using vacuum grease before clamping. The device was immersed in pH 3 to check the release behavior.

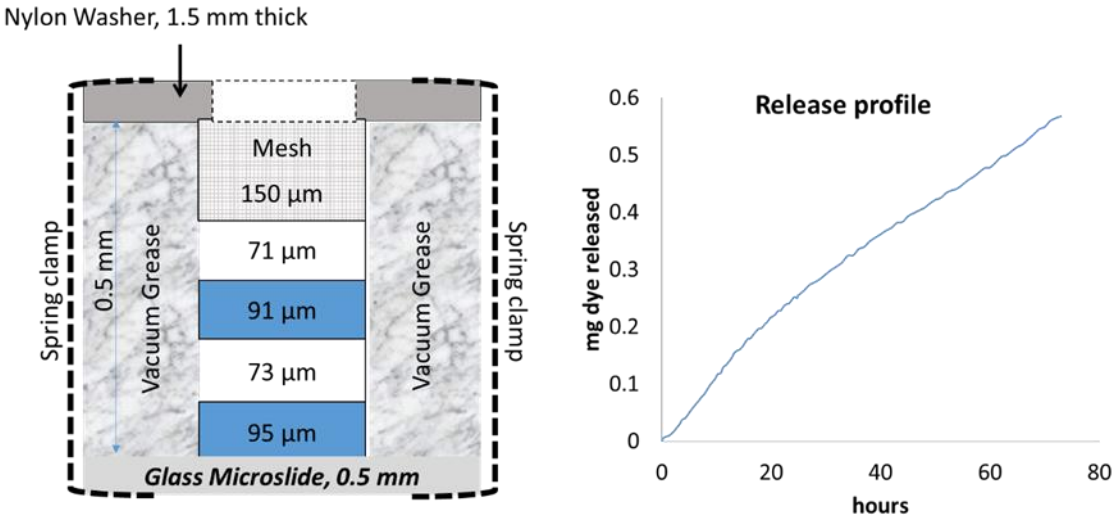

Figure 4.8 Premature penetration of stimulant through the sidewalls, stimulant penetrated through the periphery of the layers due to improper sealing and solute released from the sides of the device; swollen hydrogel was found broken in pieces from the periphery of the device due to relatively high clamping pressure.

Figure 4.8 shows a configuration and release profile of such device. The barriers used in this trial contained 10% ZnO (w/w). The depots were loaded with 5% methylene blue by weight and had 1% (w/w) crosslinking. The release of dye started within less than one hour of lag time and then continued at almost constant rate. It was also visually observed during the trial the solute was leaking from the sides of the device after couple of hours of the trial. The leakage from the sidewalls gradually increased as the gels swelled and the trial was stopped after 73 hours of continuous release. Later, when the device was opened, the hydrogel was found broken in to pieces from the periphery where

they were clamped, which had allowed premature permeation of both stimulant and solute from the sides of the device. All the layers were also found sticky with vacuum grease that was used to seal the side walls. This approach of mechanical clamping also did not work effectively to build a robust non-delaminating BMPR device.

4.4.4 Strategy 4: Modified Design using Metal Mesh, Beeswax and Flexible Coating of Rubber Cement

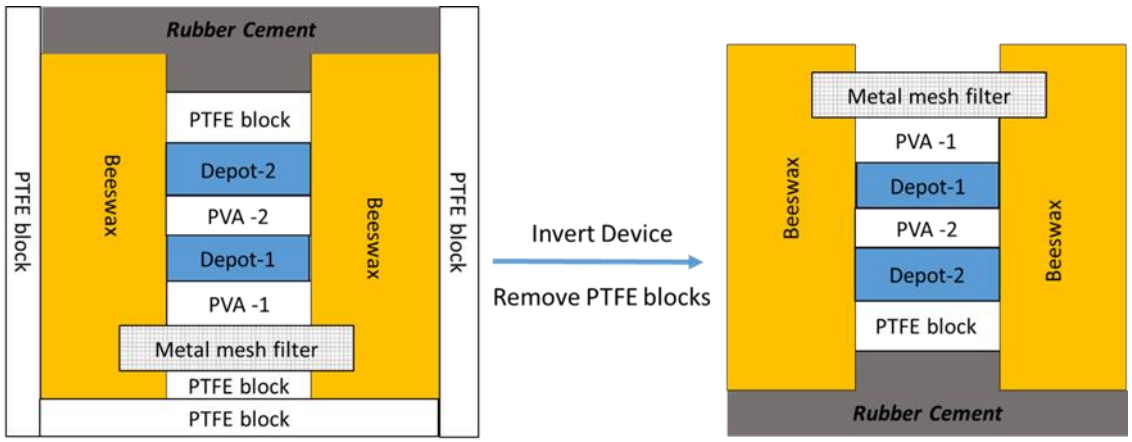

Figure 4.9 Fabrication of working non-delaminating BMPR device; metal mesh at top and bees wax at sides restrict the delamination. Thin layer of rubber cement at the bottom allows the layers to swell in only perpendicular direction.

Results of previous strategy of mechanical clamping suggested that a better system was needed for holding the mesh in place than a washer-clamp system since that had damaged the film. It was also necessary to have some mechanism that could accommodate the remaining swelling pressure to prevent the breaking of the device. To achieve this, non-delaminating BMPR device was constructed in similar way described for delaminating BMPR systems described in Chapter 2 with slight modification in design, using the same p(MMA/DMA) depot layers and PVA barriers. The integration of layers was significantly different to provide a non-delaminating system in which all the layers remained intact in the system without any delamination and provided a solute

release upon anisotropic swelling of depot layers through the spent layers. A schematic of 2-pulse non-delaminating BMPR device is shown in Figure 4.9. p(MMA/DMA) depots (1 cm in diameter) with 1% cross-linking density and up to 5 % solute loading (w/w) were alternately layered between hydrated PVA barriers (1.2 cm diameter) immobilized with varying ZnO loading (10 to 60 weight %). This layered stack was placed on a 200 micron mesh filter (24 mm wide) that was placed on PTFE block as shown in Figure 4.9. Another 3 mm thick PTFE block (1 cm wide) was placed on top to hold the stack. Melted beeswax was then poured in the mold-space (4 cm wide) and instantly refrigerated for 15 minutes. A thin layer of rubber cement was applied as shown in Figure 4.9 and the device was then refrigerated for 24 hours while the rubber cement cured completely. Later, the PTFE mold was removed from the sides and bottom. The device was then inverted, allowing the metal mesh to face upstream. The device was immersed in 0.5 L of 0.01 M phosphate buffer of pH 7 (ionic strength, 0.1 M) for at least 24 hours. The device was later transferred to 0.5 L of 0.01 M citrate buffer of pH 3 (ionic strength 0.1 M) for further release studies. Due to presence of the metal mesh-filter on top, and relatively solid sidewalls of beeswax, the lateral swelling of the depots were restricted in the device and thus, any possible delamination of the layers due to swelling pressure was avoided. As the layers were not swelling in lateral direction, they swelled in anisotropic direction, towards the bottom of the device moving the PTFE block in the bottom direction. The flexible thin layer of rubber cement at the bottom allowed the PTFE block to move without breaching the seal at the bottom of the device. There was no significant release observed at pH 7, except in few cases where first PVA barrier was loosely attached to the beeswax due to which a small amount of premature release was observed from the

surface of the underneath depot. Later, this was avoided by placing a dry-free p(MMA/DMA) in between the metal mesh and first PVA barrier. At pH 3, the barriers were sequentially consumed as the acid penetrated through the layers and triggered the anisotropic swelling of depots underneath. The solute of the depot got dissolved and diffused through the spent layers above it and released from the top of the device through metal mesh-filter. This strategy for designing non-delaminating BMPR device was found relatively robust compared to the strategies described previously in this section. Release trials from such non-delaminating BMPR devices are discussed in following section.

4.5 Release Trials and Comparison with Model Results

As shown in Figure 4.10 (right), a non-delaminating BMPR device containing two depots with methylene blue, showed robustness while studied for release in both pH 3

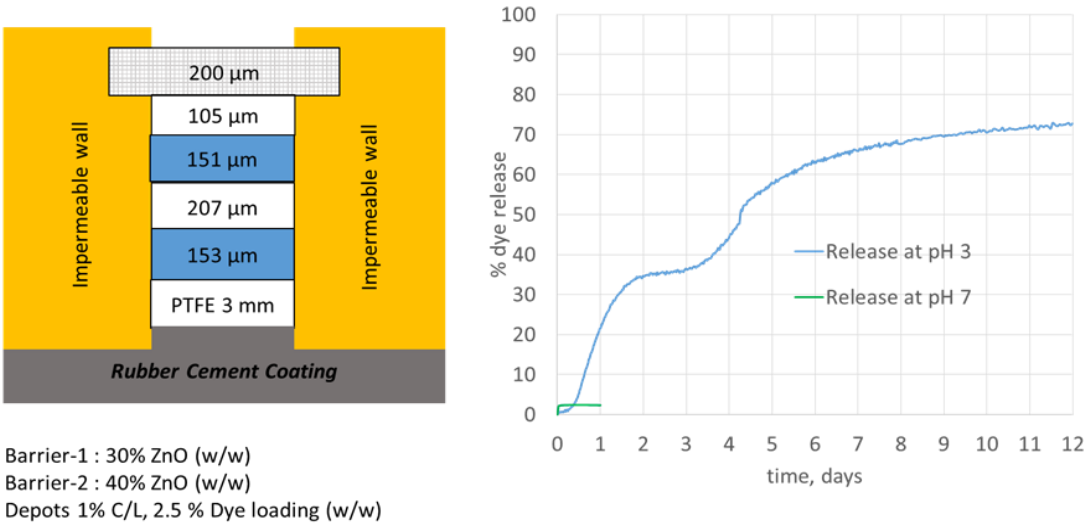

Figure 4.10 Non-delaminating BMPR device with two distinct pulses

and pH 7 environment. The device showed no leakage or release of methylene blue at pH 7 for 24 hours. Upon transferring the device in pH 3, the acid from citrate buffer started

to diffuse in to the device from metal mesh filter, and as soon as the first barrier (containing 30% (w/w) ZnO), was depleted, the first pulse of methylene blue started within half a day and kept releasing for almost two days with a steady slope as depicted in Figure 4.10, before leveling off. The second pulse from the device started to release at around 3.5 days, leveling off a few days later. Thus, this non-delaminating BMPR device produced two distinct pulses of methylene blue. After 12 days of release, device was taken out from the pH 3 buffer, and all the layers were manually removed. There was no leakage observed during this 12 day trial. However, the bottom PTFE block was found pushed towards rubber cement due to anisotropic swelling of depots. Upon opening the device, the bottom depot was found squeezed through the periphery of the PTFE block, with some broken pieces stuck in between PTFE block and rubber cement. However, a significant amount of dye (in the dissolved form) was observed in between the layers inside the device. Based on the 5% dye loading in depots, it was observed that only 73 % of loaded dye was released at pH 3, almost 2 % dye was released at pH 7, and the remaining 25% of dye had not released from the device.

This trial was repeated with similar layers as shown in Figure 4.11. This trial also showed similar results with two distinct pulses. First pulse started exactly after half day after putting the device in pH 3 and continued until 3rd day similar to previous trial. Also similarly, the second pulse started at 3.5 days, before leveling off few days later. There was a little bit of discrepancy in the release rate of second pulse between these two trails shown in Figure 4.10 and Figure 4.11, but it could be the outcome of how much of the depots inside the device swelled in anisotropic direction to push the PTFE block downwards. This device was also opened after release rate stopped increasing further on

day 8. The device looked intact without any kind of leakage from the bottom. However, there was still a significant amount of dye in between the layers inside the device. Mass balance suggested that, 77% of the loaded dye was released at pH 3, 6% of the dye was released at pH 7 and almost 17% of dye remained inside the device.

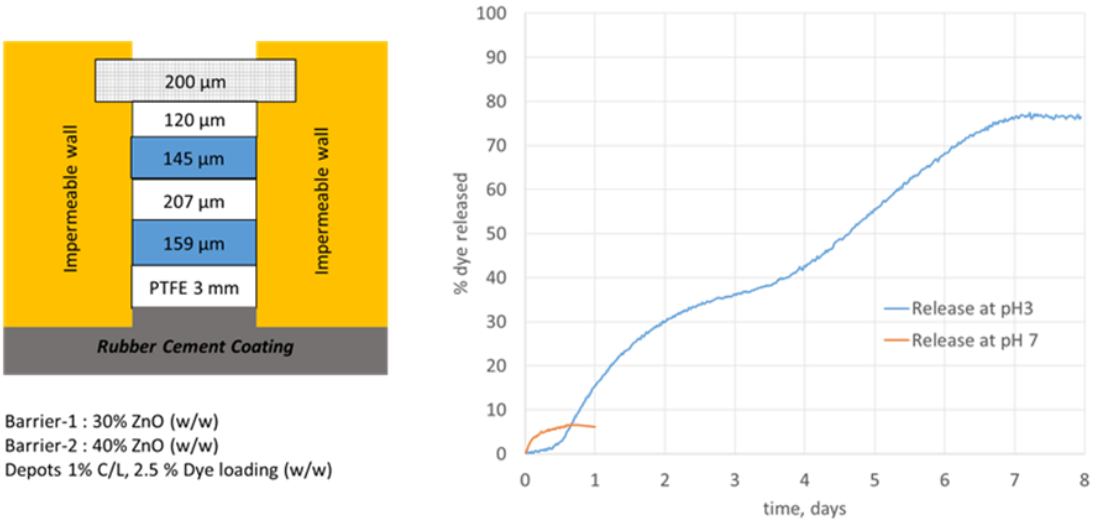

Figure 4.11 Replicate of 2-pulse non-delaminating device shown in Figure 4.10.

Although these two devices (shown in Figure 4.10 and 4.11), successfully produced two distinct pulses, it is difficult to analytically predict these release behavior as the device contained multiple layers squeezed together with an unknown swelling pressure due to the design of device itself, with a metal mesh on top, PTFE block in the center supported by flexible rubber cement. However, the experimental results of Figure 4.11 were compared with a computational model designed for 2-pulse non-delaminating device. The code for this model run is shown in APPENDIX E. This code was a further modification of a delaminating BMPR code. Details for the modeling for non-delaminating system are discussed in Chapter 5. However, it is important to note that the numerical model mentioned in APPENDIX E does not account for resistance provided by

metal mesh filter. Model parameters (such as diffusion coefficients, partition coefficients etc.) were taken from Table 3.9 from a delaminating BMPR model. It also assumes the definite anisotropic swelling factor of 2, which can be manipulated to different number.

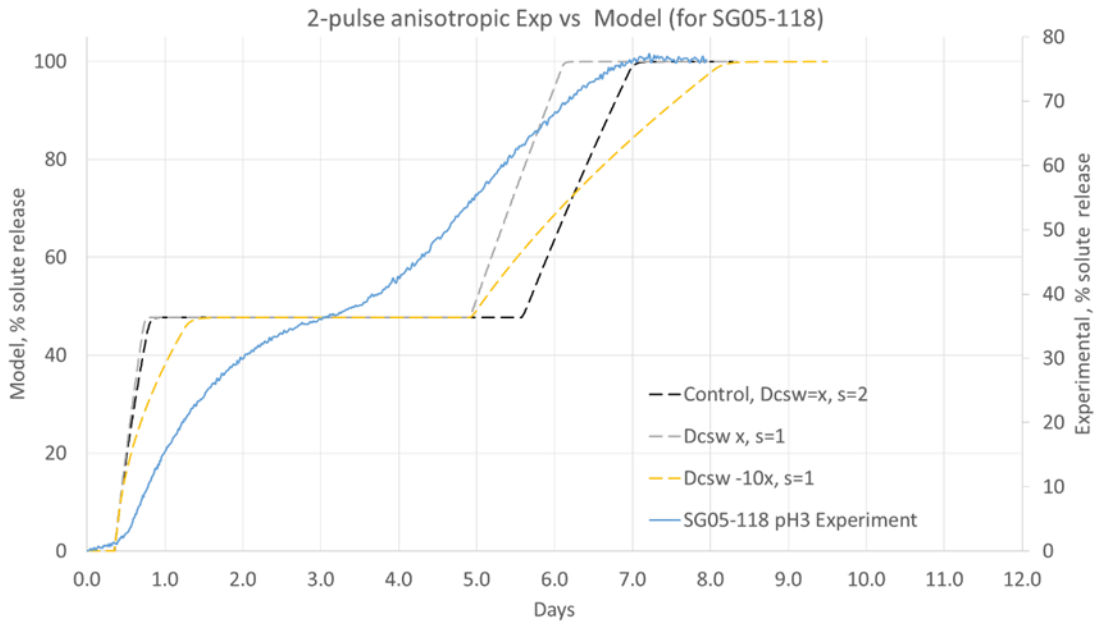

Figure 4.12 Comparison of 2-pulse non-delaminating device with model results

Comparison of experimental trial (shown in Figure 4.11) with model results are depicted in Figure 4.12. As depicted in Figure 4.12, model results for the control profile (swelling factor 2) shows that the lag time observed for the first pulse was comparable to experimental results, but for the second pulse, model predicted significantly higher lag time. Keeping the swelling factor of 2 for the depot in the model, increases the overall path length for the stimulant to travel, especially for consuming the 2nd barrier. Reducing the swelling factor from 2 to 1, decreased a lag time for second pulse by almost a half day. However, it was still predicted much higher than that was observed in experimental results, by almost 36 hours. The discrepancy in lag time between model results and experimental results could be due to the difference between the relative diameter of

barriers and depots used in the experimental device. Both barriers were of 1.2 cm in diameter, while the depots were of 1 cm in diameter, which indicates that the periphery of both the barriers (0.2 mm wide) could have affected the experimental lag time. As the hydrated barrier are rubbery and flexible in nature, both the barriers might have been in contact with each other due to mechanical pressure created for the non-delaminating design of the device (as the layers get squeezed a little bit in between metal mesh filter, and PTFE block). Now as this 0.2 mm periphery is exposed from the beginning of the trial, second barrier might have started depleting from the beginning. If we assume that these two barriers were in contact with each other in periphery area and stimulant is bypassing the first depot in the peripheral area, then the periphery of these two bilayer can be considered as just one bilayer barrier of 307 microns (102 microns (30% ZnO) and 207 micron (40% ZnO). Analytical lag time for such a single bilayer was calculated, which was found to be 83.9 hours (3.5 days) and 92 hours (3.8 days) for the experimental trials shown in Figure 4.10 and Figure 4.11. These lag times line up with the experimental pulse timings for second pulse. However, it is important to note that once the first depot swells, it would occupy this peripheral space between the barriers and increase the pulse timings as the path length would increase for stimulant diffusion. There is also a possibility if this peripheral space of barriers was squeezed from the beginning, and stimulant is bypassing from the sidewall of the beeswax, which resulted in to quicker depletion of second barrier.

Model results also showed a significantly higher release rate for a control run, where the diffusion coefficient of solute was taken from delaminating BMPR model, which was calculated for 0.1 % cross-linked depot. Depots used in non-delaminating

BMPR system contained 1% cross-linking, which is 10 times higher. Due to extra crosslinking, further model run was done with 10 time slower diffusion coefficients with a swelling factor of 1. With this lower diffusion coefficient, the slope of the pulses in experimental and model results are quite comparable as depicted in Figure 4.12 (right) with a dotted yellow line.

Thus, experimental non-delaminating BMPR system could provide distinct pulses, but it requires significant number of different strategies along with unpredictable pulse timings and release behavior due to multilayer configuration with no straightforward analytical means of predicting the performance. As a result, it demands a numerical model that can be explored on a wide scale of parameters for non-delaminating BMPR system and can guide the physical system. Numerical model for up to 5-pulse non-delaminating BMPR system is discussed in Chapter 5 with extensive analysis.

4.6 Conclusions

Several approaches to constructing non-delaminating BMPR systems were explored. Mechanical constriction using a metal mesh top and expandable bottom within rigid side walls proved to be the best. Covalently-bound depot membranes swelled in one dimension by a factor of three, rather than five. Increased cross-linking (ten times higher) also decreased the swelling of a depot to a factor of three (not five) with no impact on release. Additional cross-linking further decreased swelling, but inhibited the release of a drug. Two-pulse non-delaminating BMPR systems were demonstrated.

However, currently it is difficult to develop a non-delaminating experimental system that yields data clean enough to establish predictive correlations. Experimental strategies for non-delaminating BMPR devices still require a lot of optimization which

will be very material specific (*e.g.*, figuring out how to fuse specific materials using plasma bonding). Such optimization is only worthwhile if one can predict the performance of a device in advance to show that it can actually deliver the desired release profile for a target application. The only way to know that in advance is to develop a computational model, which is discussed in next chapter.

.

CHAPTER 5
PARAMETER LIMITS: NON-DELAMINATING BMPR SYSTEM

5.1 Importance of a Computational Model for Non-Delaminating BMPR System

As discussed in Section 3.1, performance of delaminating BMPR systems can be predicted analytically to large extent as every pulse (of single depot and single barrier) can be treated individually due to its delaminating nature. In contrast, non-delaminating

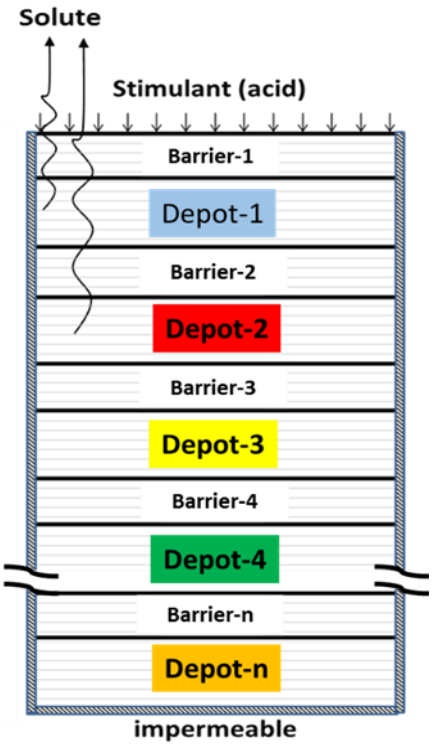

Figure 5.1 Schematic of non-delaminating BMPR system with n pulses each containing different solute.

BMPR systems are comprised of multiple depots and barriers (with no limits of number of layers or type of solute) as shown in Figure 5.1 which remain fused together throughout the release. In such physical situations, the layers do not delaminate, but rather are physically bound to keep the device intact throughout its use. As a result, the

stimulation of subsequent pulses has an additional delay due to stimulant transport resistance by the previous spent layers. This resistance accumulates as one moves towards later pulses, which affects not only the timing of the pulses but also their width. With species (stimulant and solute) diffusing in and out of such a multilayered system with each layer having its own characteristic parameters, performances of such complex system become very intricate to predict analytically. Using the computational model discussed in Section 3.2 which was validated by the analytical and experimental results of the delaminating BMPR system, we now extend this model for non-delaminating BMPR systems whose performance cannot be predicted analytically. With such a model, the feasibility of a system can be evaluated before doing the physical trials for the target application.

A computational model for non-delaminating BMPR systems can be used as a screening tool to determine whether a proposed application would even be feasible, assuming all the fabrication details could be worked out. For a given set of parameter values (diffusion & partition coefficients, film thickness, scavenger and stimulant concentration, solubility of each solute loaded in individual depot, *etc*.), there is a limit to how many pulses can be delivered at a desired frequency from a given system. Subsequent pulses may become so broad that they would no longer act as pulses. Such limits can be quickly realized with an appropriate computational model for any given set of parameter values. More importantly, by using the model across wide range of parameter space, some basic correlations can be developed for estimating such limits without having to return the computations for every film thickness explored. In this way

an unfeasible application can quickly be realized without massive experimental development efforts as discussed in Chapter 4.

Another advantage of computationally modeling the non-delaminating BMPR system is to explore the parameters that cannot be easily manipulated experimentally. One can easily vary such parameters across wide range to check their effects using the model. For instance, it would be hard to alter the diffusion coefficients of particular solute without also changing its saturation concentration even more dramatically. As another example, it would be difficult to incorporate enormously large amount of scavenger in a barrier or solute in depot experimentally beyond certain limits. The model would allow such flexibility to separately change and explore any particular parameter to check its effect without any scaling limitations. Along with a computational model developed for delaminating BMPR discussed in Section 3.2, the model was concurrently modified and extended for non-delaminating BMPR systems. This Chapter primarily discusses how the numerical non-delaminating BMPR model was constructed by adapting it from delaminating BMPR mode, and then explored with various parameter space limits. This model was used to discern analytical guidelines for the design and feasibility of a given non-delaminating BMPR systems.

5.2 Construction of multilayered non-delaminating BMPR model

As with the delaminating model discussed in Section 3.2, the non-delaminating model was developed in FORTRAN using the FTN 95 Plate IDE compiler, then deployed

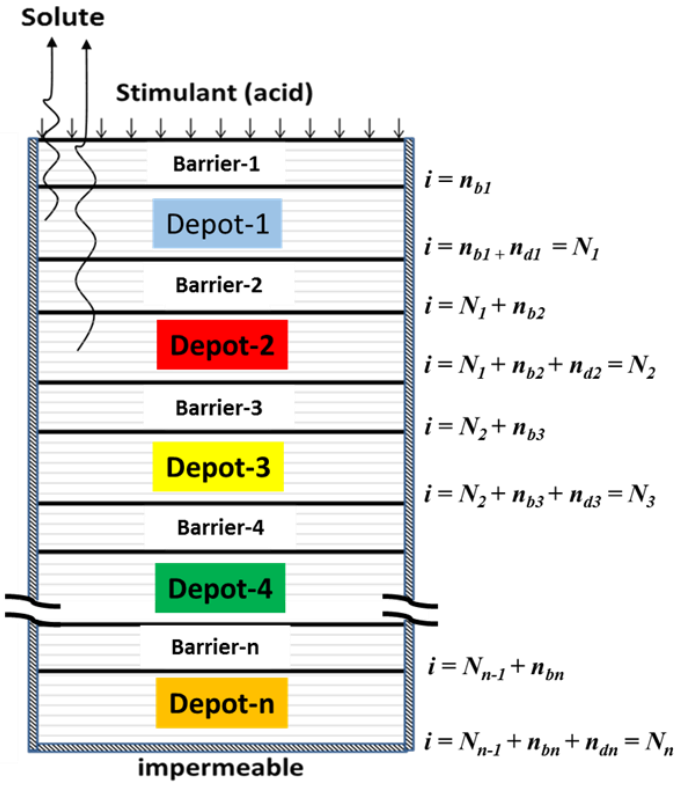

Figure 5.2 Schematic of 1-D computational model for multi-pulse non-delaminating BMPR system along with node distribution of each layer

on the Helium Cluster. 1-D non-delaminating BMPR model was also built using centered finite approximation for second order spatial derivative and explicit Euler method for temporal derivatives similar to that described for delaminating BMPR model. While the delaminating BMPR model considered only an individual pulse, non-delaminating BMPR model was designed for multiple pulses. While the model explained in this thesis calculated the performance of five pulse devices, in principle, there is no limit to the

number of pulses, given sufficient computing power. An example code for the five pulse non-delaminating BMPR system is shown in APPENDIX F.

Consider a non-delaminating BMPR system with multiple barriers and depots (each depot with a different solute) alternatively layered as shown in Figure 5.2. Diffusion of species (solute and stimulant) occurs in only one dimension and all other sides are assumed to be impermeable. Each barrier and depot are now divided to their own definite number of segments respectively with a node at each end of each segment. For example, the first barrier and the first depot were divided in to n_{b1} and n_{d1} computational segments resulting in n_{b1} and n_{d1} nodes respectively. Node distribution was done in similar way for all subsequent barriers and depots as shown in Figure 5.2. The number of segments remains the same as the number of nodes for every layer except the last layer in the device, with each node representing the segment on its downstream side. The inner-most node of the last layer has no corresponding segment. Each node was defined with its segment thickness (h), defined by dividing the layer thickness by the total number of segments assigned in that layer. Each node of every layer was assigned with initial conditions (such as concentration of solute (B, C_{sat}), concentration of stimulant (G) and scavenger (F), diffusion coefficients of stimulant and solutes (D_g and D_c respectively) and partition coefficients of solute and stimulant (H_c and H_g respectively). At a given node, these input values represent the average parameter values for the segment on its inner side. The first node of the first barrier was set to zero scavenger concentration as it would be in direct contact with the stimulant getting consumed instantaneously. So, the total amount scavenger in first barrier was redistributed in rest of the nodes which also shifts the center of mass of the first barrier back to the center of layer, as discussed earlier in

Section 3.2. Although rest of the barriers in the device were not exposed directly to the stimulant, the scavenger concentration in the first node of each subsequent barrier was also set to zero and the amount of scavenger in each barrier was also redistributed in rest of the nodes of the corresponding barrier to keep the scavenger center of mass of back at the center of the layer. Scavenger concentration in depot nodes were kept unaltered, as it is necessary to have a finite amount of scavenger in each node (including the first node of each depot) to initiate the triggering mechanism from shrunken to swollen node when the scavenger gets consumed by stimulant. Additionally, the effect of slight shift in center of mass in depot would be very negligible on release profiles as mentioned in Section 3.2.

Once the initial conditions are defined, all the mobile species of each layer (C & G) were tracked based on flux of mobile species entering and existing the node. Scavenger concentration would change at each node upon arrival of stimulant in stoichiometric proportion as described in Section 3.2.1. Similarly solute departing each node was replaced by corresponding decrease in solid particles (B). It is important to note that each depot contained its own type of solute as shown in Figure 5.2. So, solute for each pulse was separately tracked in the device throughout the release.

Flux calculations for each barrier were calculated using centered finite difference approximation similar to that was described in Section 3.2.2. Similarly, flux calculations for each depot were done using backward finite difference approximation as described in Section 3.2.4. As shown in APPENDIX F, the code for five pulse non-delaminating BMPR system illustrates these calculations for each barrier and depot in to their own individual loop for ease of understanding the code. The fluxes of species (both stimulant and solute) at the interface of each barrier and its subsequent depot were calculated

similar to that described in Section 3.2. In a delaminating BMPR model involving only single barrier and single depot, diffusion of species were terminated after the last node of depot. However, multilayer non-delaminating BMPR model required some modifications in flux calculations which can account for the diffusion of mobile species from a particular depot into the next barrier, except from the last depot. In this modification, the flux of the stimulant coming from the last node of a particular depot was linked with the flux of stimulant diffusing into the first node of its subsequent barrier. As dissolved solute can diffuse in both directions in the device, flux of a solute coming from the last node of a particular depot was also linked with the flux of solute diffusing into the first node of subsequent barrier. Linking these fluxes at the interfaces is critical to maintaining a closed mass balance between regions using different diffusional calculation methods. These modifications are addressed in the demo code shown in APPENDIX F.

5.2.1 Parameters for the Non-delaminating BMPR Model

Since the goal is to explore the parameter space for a non-delaminating BMPR model, convenient values near those determined in Section 3.2 were used, and subsequently varied by orders of magnitude. For instance, base value for thickness of each barrier (t_b) and depot (t_d) was set to 100 microns with t_b/t_d being 1. Swelling ratio (s) of each depot was set to 2. Stimulant concentration was set to 0.01 M (C_{gup}), scavenger concentration (F_b) was set to 0.3 M for every barrier. Ratio of scavenger concentration of barrier to that of depot (F_b / F_d) was arbitrarily set to 5. Base values for solid solute concentration (B) and saturation concentration of solute were set to 0.1 M and 0.01 M respectively for each depot. Base values for all the diffusion coefficients of both solute and stimulant were set to 10^{-5} cm^2/s for all the layers. Partition coefficients of stimulant

and all the solutes were set to 1 for all the layers. Once the model was set with its base parameter values, it was checked for node accuracy and its stability limits before beginning to investigate the effects of each parameter. Stability limits and node accuracy were checked for both continuous and pulsatile release profiles, which are discussed in Section 5.2.2 and Section 5.2.3 respectively.

5.2.2 Node Accuracy for Non-delaminating BMPR Model

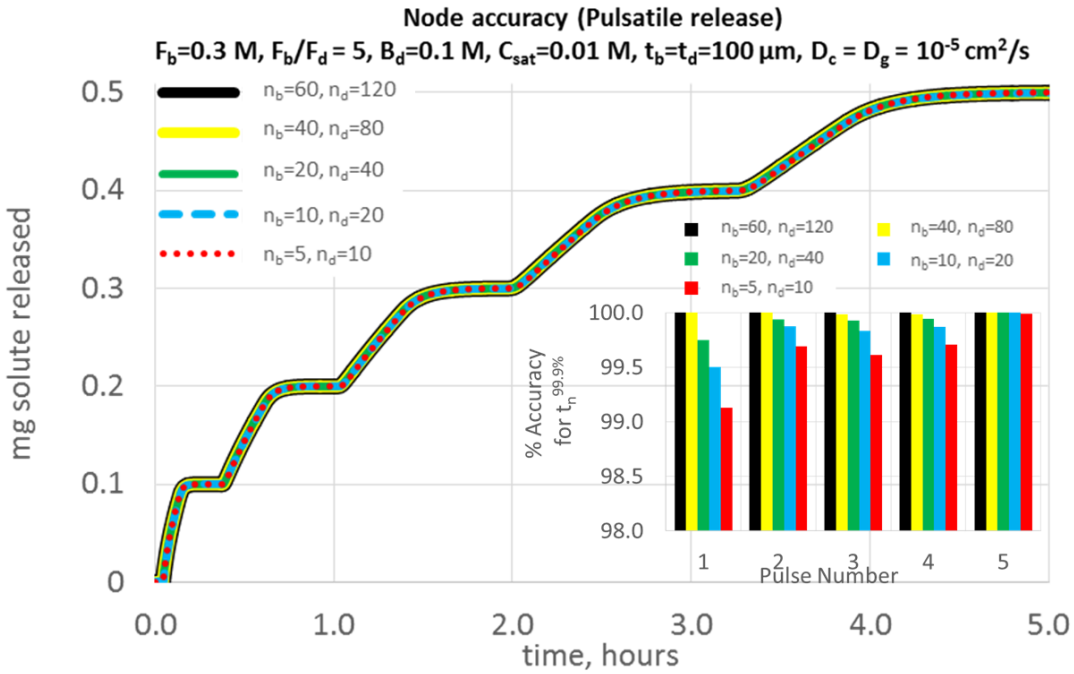

Figure 5.3 Node accuracy for non-delaminating BMPR (pulsatile release); results for nodesize (n_b=20, n_d=40) are within 99.9% (average) of the results observed for the nodesize (n_b=60, n_d=120), with significantly less computational time.

Based on the parameter values discussed in section 5.2.1, the model was checked for the effect of various node size on a release profile. All the barriers and depots (each 100 micron thick) were divided into various number nodes, ($n_b = n_{bN}$, $n_d = n_{dN}$). First set of nodes were tried with 60 barrier nodes and 120 depot nodes (n_b, n_d = 60, 120), and then decreased the barrier nodes to 40, 20, 10 and 5, each time reducing the depot nodes proportionally. As the anisotropic swelling factor for depots was set to a factor of two,

number of nodes in the depot was kept twice then the number of nodes in the barrier to keep the node thickness uniform for all the layers in the device (*i.e.* for barriers and swollen depots). For all these set of nodes (n_b, n_d), code was compiled and executed using Helium Cluster.

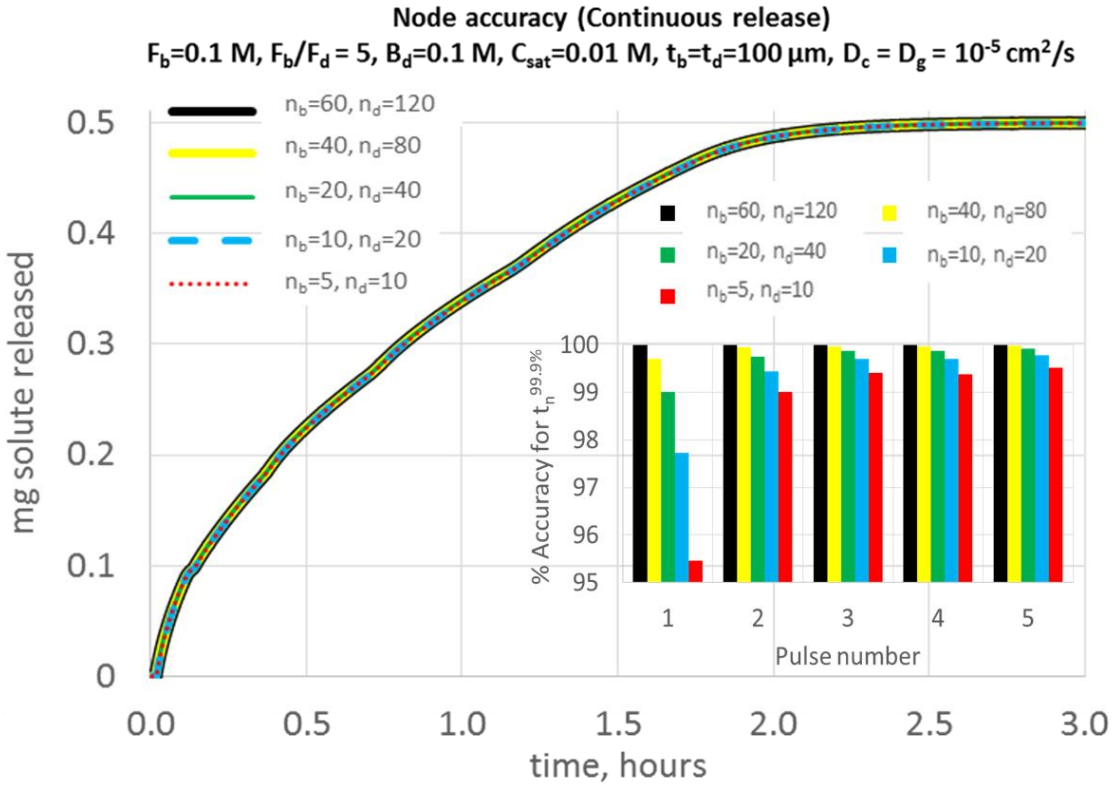

Figure 5.4 Node accuracy for non-delaminating model (continuous release); results for nodesize (n_b=20, n_d=40) are within 99.7% (average) as compared to the results for node size (n_b=60, n_d=120), with significantly less computational time.

As depicted in Figure 5.3, release plot was generated for the total amount of solute released in mg with time for each set of node size, showing five distinct pulses released periodically. Total amount of solute released from each pulse was within 99.999996% of initiallly assigned value of solid solute (B) in each depot. However, accuracy for the time required to release 99.9% of the solute ($t_n^{99.9\%}$) from each pulse increased with the increase in node size as shown in insert Figure 5.3. For instance, percentage accuracy for time required to release 99.9% at node size [(n_b, n_d) = (5, 10)] for

first pulse was found to be 99.1% as compared to the time was obsrved at maximum node size of [(n_b, n_d) = (60, 120)]. However, average accuracy for all five pulses at node size [(n_b, n_d) = (5, 10)] was 99.6% compared to that of maximum node size. This accuracy was above 99.9% for the node size ≥ (n_b=20, n_d=40). Changing the value of any of the base parameters could change the shape of the release profile. When the scavenger amount in all the barriers was reduced by a factor of 3, acid penetrates almost 3 times faster in the device and the release becomes rather continous as shown in Figure 5.4. The insert of this figure indicates the accuracy for different nodesize. Even in this case total amount of solute released was accurate up to 99.99996 % than predicted values. However, percentage accuracy for time required to release 99.9% of the solute for first pulse was found to be 95% at node size [(n_b, n_d) = (5, 10)] compared to that of at maximum node size of [(n_b, n_d) = (60, 120)]. This accuracy was increased with the node size (insert Figure 5.4). For the node size of [(n_b, n_d) = (20, 40)] and above, average node accuracy of five pulses was found to be higher than 99.7% for pulsatile release (Figure 5.3) and 99.9% for continuous release (Figure 5.4), as compared to those observed at maximum node size of [(n_b, n_d) = (60, 120)]. Further exploration of model done with node size [(n_b, n_d) = (20, 40)].

5.2.3 Stability Limits for Non-delaminating BMPR Model

As this model also uses the explicit Euler's method for determining second derivatives of flux calculations for temporal domains, it needs be run within its stability limits (similar to that described for delaminating BMPR model in Section 3.2.7). Stability limits still remain the same based on Equation 3.21 and 3.22 as discussed earlier and depends on the combinations of thickness of the node (h), diffusion coefficients (D) and

the time-step (Δt). This 5-pulse non-delaminating model [node size (n_b, n_d) = (20, 40)] was checked for these stability limits for both pulsatile and continuous release as depicted in Figure 5.5 and 5.6. Both figures predicted the correct amount of solute released with an accuracy of 99.99996% at all time-steps within stability limits.

As depicted in Figure 5.5, for $\Delta t \leq 0.005$ s, all the profiles remain identical and accuracy for releasing 99.9 % solute from each pulse remained 100% as compared to that was observed at minimum time-step of 0.0001 s. However, for time-step of $\Delta t \geq 0.0055$ s

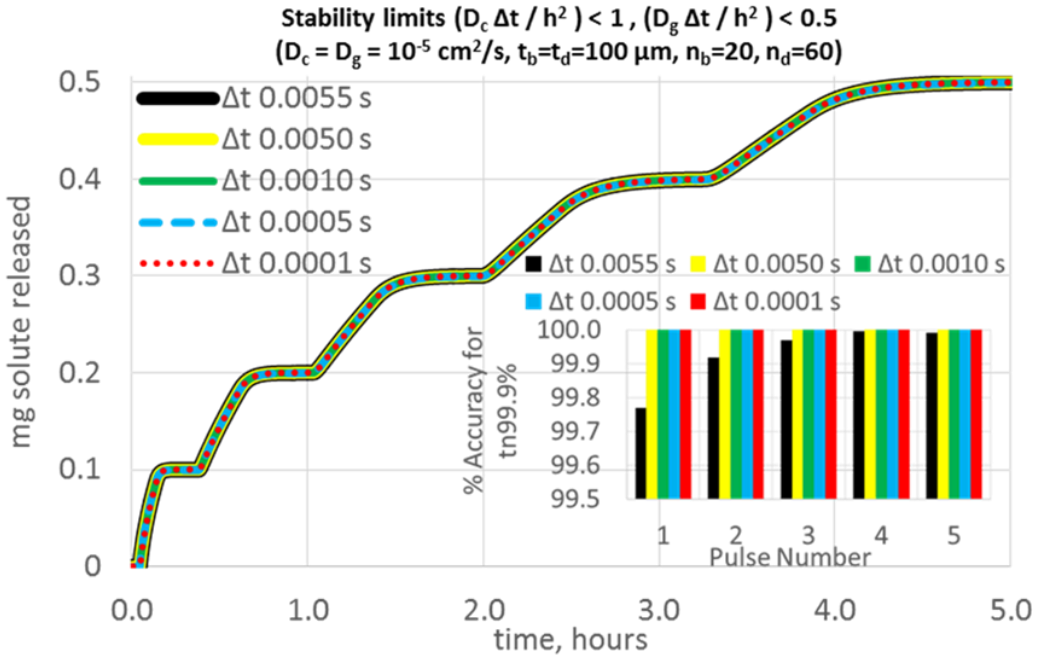

Figure 5.5 Stability limits for non-delaminating BMPR system (pulsatile release)

(above stability limits), this accuracy started to decrease as depicted in insert of Figure 5.5. Further increase in Δt makes the model unstable and produces null output data.

Similar effects were found when diffusion coefficients of solutes (D_c) in all the layers in the device were reduced by a factor of 10, resulting in continuous release as depicted in Figure 5.6. For $\Delta t \leq 0.005$ continuous release profiles remained identical and

lied on top of each other and accuracy for releasing 99.9% solute from each pulse remained 100% as compared to what was observed for minimum time-step of 0.0001 s.

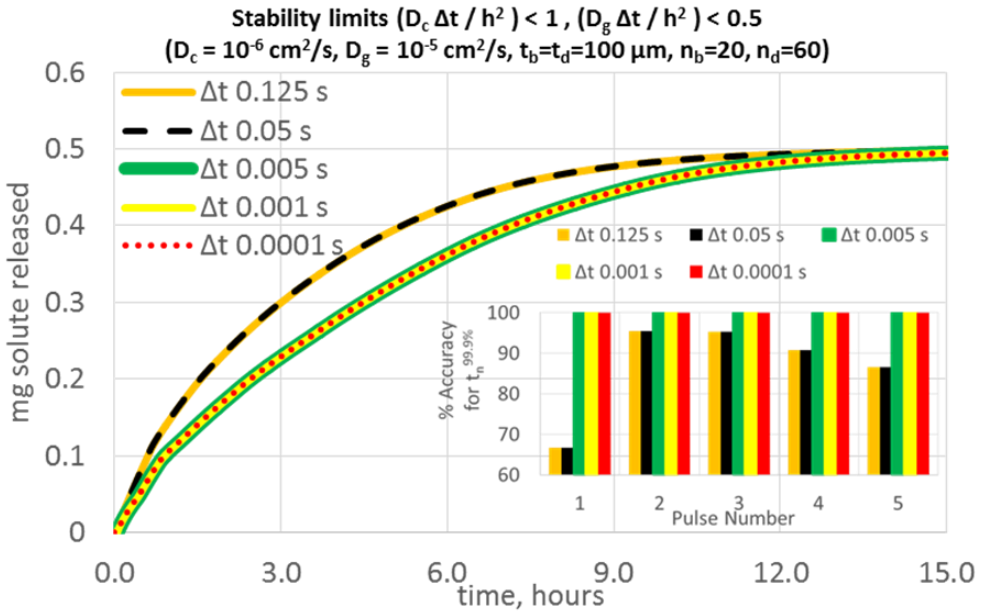

Figure 5.6 Stability limits for non-delaminating BMPR system (continuous release)

However, the stability effects were even more pronounced as depicted in Figure 5.6 for $\Delta t \geq 0.05$ where the accuracy for time required to release the 99.9% solute from first pulse significantly decreased to 67%, and average accuracy for all the pulses reduced to 87% compared to that was observed at Δt=0.0001s. Further increase in time-step ($\Delta t >$ 0.125 s) makes the model unstable and produces null output data. Based on Figure 5.5 and 5.6, further exploration of model was done with a time-step (Δt) of 0.005 s, provided that the diffusion coefficients (D) and node thickness (h) also remain within stability limits given by Eq. 3.21 and 3.22.

5.3 Defining Pulsatile Release Mode for a BMPR System

As discussed in Section 5.2, based on the set of parameter values, the release profile can be pulsatile or continuous. Since one cannot get truly "all" the solute out, the model has to be set to an arbitrary threshold value for what counts as "all" the solute,

which can define the release mode to be pulsatile or not. If we set the released percentage too low, there may still be a lot of overlap between pulses, so they won't be distinct. If we set the released percentage too high, it will be dictated by transport of solute that has a much smaller concentration gradient driving its diffusion. For this model, we chose to define pulsatile delivery by having 99% of solute from one depot released from the device before 1% from the next depot is released.

In short, for a given non-delaminating BMPR system with n pulses, if the time at which 99% of the solute from a depot is released before the time when 1% of the solute from the subsequent depot is released ($t_n^{1\%} - t_{n-1}^{99\%} > 0$, for n pulses), then the shape of the release is categorized as pulsatile. Conversely, if any of the pulses do not follow the definition of pulsatile release (*i.e.* if $t_n^{1\%} - t_{n-1}^{99\%} \leq 0$, for n pulses), then the system is termed as continuous as some of the pulses start to overlap on each other.

It is important to note that by this definition ($t_n^{1\%} - t_{n-1}^{99\%} > 0$ or $t_n^{1\%} - t_{n-1}^{99\%} \leq 0$), one part of the release profile could be pulsatile, while the other part could remain continuous. Since later pulses will invariably be wider than earlier pulses, one might expect the early part of the release profile to be pulsatile while the later part is continuous, effectively demonstrating a limit to how many discrete pulses can be delivered from a particular BMPR device. While it is useful to evaluate whether the given profile is pulsatile or continuous based on the time difference ($t_n^{1\%} - t_{n-1}^{99\%}$) of the release data for subsequent pulses, it is more important if one can quickly estimate how much one or more of the parameter values would need to change in order to switch from one release mode to the other, as discussed in next section.

5.4 Derivation of Dimensionless Parameter Φ (Pulsatility Factor)

There are so many independent variables in even a 5-pulse system that even with a computational model it is not feasible in this thesis to explore the entire parameter space, and so the model was explored with some restrictions. Since there can be an infinite number of different depots, we assume that every depot is identical. Each depot has the same thickness. Each depot has the same amount of solute with the same saturation concentration and diffusion coefficient. Each depot has the same amount of scavenger and conducts stimulant at the same rate. Similarly, we assume that every barrier is the same. Each one has the same thickness and scavenger loading. Their stimulant diffusivity and partition coefficients are all the same, and their solute diffusivities and partition coefficients are all the same. Many of these parameters act in similar way, and those can be combined in a single correlation.

As shown in Chapter 2, the swelling of a depot node is limited by the transport rate of stimulant (rather than polymer relaxation limit), and the release rate of solute from the device is limited (if not only by the swelling rate) by the transport rate of the solute (rather than a dissolution limit). Both of these processes can affect the shape of release profile. If the time required to stimulate and swell a depot node is longer than the time required for the solute in that node to exit the device, then it is assured that the solute will release from the depot as quickly as the swelling front crosses it, and that all the solute from that depot will have exited the device before solute from the next depot can; *i.e.*, the release will be pulsatile. If, on the other hand, the solute release is the rate-limiting step, then the swelling front may sweep through the depot and start releasing solute from the

next pulse before the solute from the previous pulse has exited, making the release mode to be continuous.

We hypothesize that if the solute can escape from a given position in the membrane faster than the stimulant can penetrate that position in the membrane, then the solute will come out in discrete pulses, while if the stimulant can penetrate and expose solute faster than the solute can escape the device, the pulses will overlap and continuous release will be observed. Since both of these processes are transport limited, we can compare their transport rates to see which rate is faster. The ratio of the stimulant transport rate vs. the solute transport rate can determine whether the release is pulsatile or continuous, and the model can be used to quickly correlate that ratio to the release mode.

Based on above assumptions, such ratio can be determined in the form of dimensionless number (Φ). Following key points were considered to derive this relationship.

i. All of the solute diffusion coefficients can be represented by a single D_c. Similarly, all the stimulant diffusion coefficients can be represented by a single D_g. Although both D_c and D_g are different in the barrier than the depot, they are still at a fixed ratio. Thus, the user must keep track of only one diffusion coefficient of solute (D_c) and one diffusion coefficient (D_g) for stimulant.

ii. As the scavenger concentrations in the barriers and depots are fixed, all the scavenger loadings can be represented by a single F. The user must keep track of only one scavenger concentration either (F_b) or (F_d) by keeping the F_b/F_d ratio constant for a given system.

iii. All the depot solute loadings are represented by a single B and $C_{sat,}$ where B is the solid solute concentration and C_{sat} is the saturation concentration of a dissolved solute. Both B and C_{sat} are also fixed and can easily be tracked by the user.

iv. The characteristic time required for the solute to leave a node is proportional to the ratio of amount of solute in that node (B) and its flux (J_c) as shown in Eq. 5.1

$$t_{solute} \propto \frac{B}{J_c} \tag{5.1}$$

This flux (J_c) is proportional to the saturated solute concentration C_{sat} and diffusion coefficient (D_c), as well as inversely proportional to the node's distance from outer surface (L), which is shown in Eq. 5.2.

$$J_c \propto \frac{D_c C_{sat}}{L} \tag{5.2}$$

Combining Equations 5.1 and 5.2, characteristic time required for the solute to escape the devices (t_{solute}) is given by Eq. 5.3.

$$t_{solute} \propto \frac{B L}{D_c C_{sat}} \tag{5.3}$$

v. Similarly, we can say that characteristic time required to trigger a given stimulant node ($t_{stimulant}$) is proportional to the ratio of scavenger concentration (F) and the stimulant flux (J_g) as shown in Eq. 5.4.

$$t_{stimulant} \propto \frac{F}{J_g} \tag{5.4}$$

Now, the stimulant flux (J_g) is proportional to the upstream stimulant concentration (C_{gup}) and stimulant diffusion coefficient (D_g), as well as inversely proportional to the node's distance from outer surface (L), which is shown in Eq. 5.5.

$$J_g \propto \frac{D_g\, C_{gup}}{L} \tag{5.5}$$

Combining Eq. 5.4 in Eq. 5.5, characteristic time required to trigger the stimulant node is now given by Eq. 5.6.

$$t_{stimulant} \propto \frac{F\ L}{D_g\, C_{gup}} \tag{5.6}$$

vi. When stimulant transport is compared against solute transport, the distance to the device surface (L) at a given time for both processes remain essentially the same. So, the ratio of time for acid to trigger a given node vs the time for solute to escape the node can be given by combining Eq. 5.3 and 5.6. This dimensionless ratio can be termed as a pulsatility factor (Φ) as shown in Eq. 5.7.

$$\Phi = \frac{t_{stimulant}}{t_{solute}} = \frac{F\, D_c\, C_{sat}}{B\, D_g\, C_{gup}} \tag{5.7}$$

One can determine the Φ for a given BMPR system from the six input parameters of Eq. 5.7 then check the release mode. At this particular value of Φ, one can check the time difference ($t_n^{1\%}$ - $t_{n-1}^{99\%}$) of the release data for subsequent pulses the for n pulses as discussed earlier, and determine whether the given system is stimulant-limited or solute limited, in other words, pulsatile or continuous. For example, if we use the input parameters of release profile shown for Figure 5.3 and Figure 5.5 in Eq. 5.7, the value of Φ comes out to be 3. For this Φ=3, pulse times for 99% solute release from 1st, 2nd, 3rd and 4th pulses were 10.9, 46.2, 104.5 and 186 minutes respectively, and pulse times for 1% release from 2nd, 3rd, 4th and 5th pulses were 23.1, 62.5, 120.6 and 197.6 minutes respectively. Thus, time difference for first four pulses ($t_n^{1\%}$ - $t_{n-1}^{99\%}$) is found to be

greater than zero (12.2, 16.3, 16.1 and 11.6 minutes respectively) suggesting the stimulant transport is rate limiting and so release mode is pulsatile which is visible in the shape of the release profiles in Figure 5.3 and 5.5. Similarly, when we use the input parameters of Fig. 5.4 in Eq. 5.7, where scavenger loading F was reduced by a factor of 3, we get the value of Φ to be 1, where pulse times for 99% solute release for first four pulses were 9.7, 39.0, 78.5 and 120.4 minutes respectively, and 1% solute release from their subsequent pulses were 8.3, 22.5, 43.4 and 71.1 minutes respectively. Thus, time difference ($t_n^{1\%} - t_{n-1}^{99\%}$) for first four pulses in Figure 5.4, was found to be less than zero (-1.4, -16.5, -35.1 and -49.4 minutes respectively), suggesting that the solute transport is rate limiting, making the release mode continuous. For Φ = 0.3 (Fig. 5.6), where the diffusion coefficient of solute was reduced by a factor of 10 as compared to Φ = 3 (Fig. 5.3), pulse times for 99% solute release for first four pulses were 4.9, 10.2, 13.1 and 15.4 hours respectively, and 1% solute release from their subsequent pulses were 0.4, 1.1, 2.2 and 3.6 hours respectively. Thus, time difference ($t_n^{1\%} - t_{n-1}^{99\%}$) was found to be negative for first four pulses (-4.5, -9.1, -11.0 and -11.9 hours respectively), confirming the clear overlapping of the pulses, resulting in to continuous release.

Φ can be varied or kept constant by changing any of the six parameters of Eq. 5.7 which could determine the release mode. The results in above paragraph support this hypothesis of parameter interchangeability, but this must be investigated in more depth. A variety of codes with different values of Φ were executed to understand the release behavior of non-delaminating BMPR system which is discussed in next Section 5.5.

5.5 Explore Φ limits

5.5.1 Scaling Φ on a Wide Range

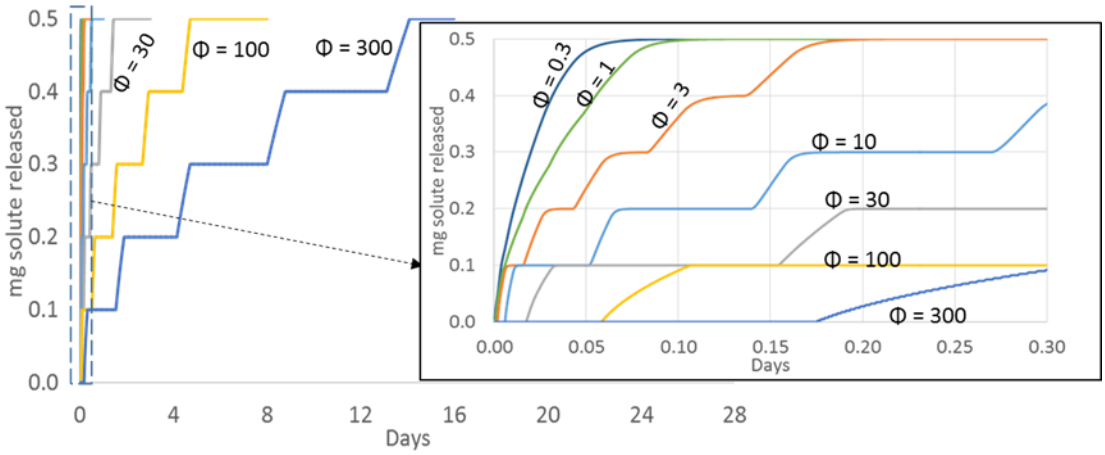

Figure 5.7 Release behavior of 5-pulse non-delaminating systems at various values of Φ, thickness ratio (t_b/t_d=1) and scavenger ratio (F_b/F_d =5) were constant. Φ was varied by varying scavenger concentration in barrier (F_b) in all cases.

To check this effect various model runs were executed at different values of Φ ranging from 0.3 to 300 as shown in Figure 5.7. The value of Φ was varied by changing the scavenger concentration in barrier (F_b) and depot (F_d). All other parameters were kept constant as described in Section 5.2.1. Initial thicknesses of all the layers were kept constant at 100 microns making t_b/t_d ratio constant at 1. Similarly the scavenger ratio of barriers to depots was kept constant at 5 for all these runs. Diffusion coefficients of solutes and stimulants were (D_c and D_g) were kept constant to 10^{-5} cm^2/s. Solid solute loading in each depot was assigned to be 0.1 M with a saturation concentration of solute to be 0.01 M keeping the ratio (B_d/C_{sat}) ratio constant at 10. Upstream acid concentration (C_{gup}) was held constant at 0.01 M.

As depicted in Figure 5.7 (insert), it is clear that the for the Φ values of 0.3 and 1, release was found to be continuous in both cases due to relatively less amount of

scavenger in the barriers (0.03 and 0.1 M respectively). The continuous mode of the release was confirmed by calculating the ($t_n^{1\%}$ - $t_{n-1}^{99\%}$) for first four pulses starting from pulse-2, indicating that they overlap each other. With increase in Φ value by increasing the amount of scavenger in barrier, acid took more time to deplete the barriers before triggering each depot and as a result lag time for each pulse increased proportionally. As a result, the release mode became pulsatile. For all the runs with (Φ = 3, 10, 30, 100 and 300), 99% solute from each depot was released well before 1% of solute started to release from next depot, following the definition of pulsatile release (($t_n^{1\%}$ - $t_{n-1}^{99\%}$) >0) as described earlier. As a result all of the runs with Φ > 3 provided five distinct pulses as depicted in Figure 5.7. In all these runs at a given Φ, the slope of each pulse decreased with increase in pulse number due to increased resistance of spent layers as solute had to travel more distance from the depots located deeper in the device. As Φ was increased by increasing F_b, it also increased the amount scavenger in depot to keep the F_b/F_d constant and as a result acid took more time to trigger the depot accordingly, decreasing the slope of each pulse with increase in Φ.

5.5.2 Effect of Individual Parameters of a Φ Correlation

Of all the six parameters that define Φ in Eq. 5.7, only F was varied for all the model runs discussed in the previous section with Φ ranging from 0.3 to 300. Figure 5.7 (insert), transition from continuous to pulsatile release occurs in between Φ = 1 and Φ = 3. These two values of Φ were used to explore the other parameters of Eq. 5.7, such as diffusion coefficients of stimulant (D_g), upstream stimulant concentration (C_{gup}), diffusion coefficient of solute (D_c), solid solute concentration in depot (B_d) and dissolved solute concentration (C_{sat}).

To check the effect of these parameters, each of the six parameters was altered individually on various scales, keeping Φ constant by correspondingly altering F_b. As shown in Figure 5.8, five distinct profiles were plotted for percentage solute release from

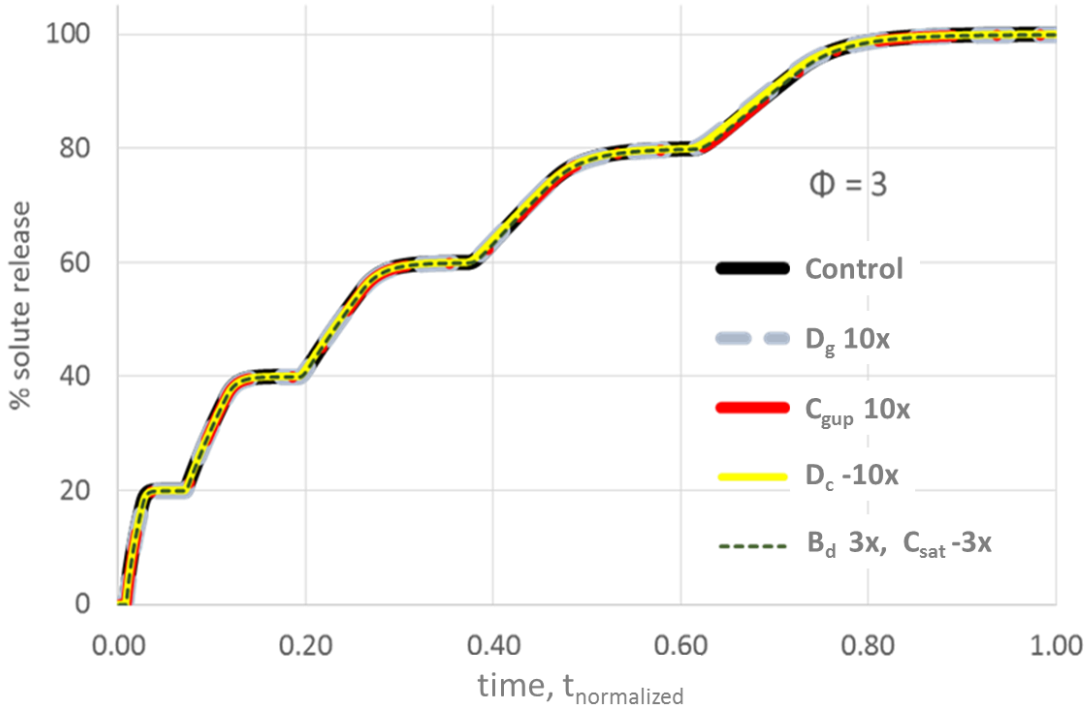

Figure 5.8 Identical pulsatile release profiles at Φ =3 regardless of change in parameters that defines Φ.

the device against the normalized time. Time on x-axis was normalized by dividing the actual release time by the time required to release 99.9% of the total solute from the device (*i.e.*, $t_{normalized} = (t_{actual}/t_{99.9\%})$). As depicted in the figure, for all these various combinations of parameters giving the same value of (Φ=3) give identical release profiles, normalized for time. For instance, when diffusion coefficient of stimulant (D_g) was increased by a factor of 10, with a corresponding increase in amount of scavenger in barrier to keep the same Φ, the release behavior was identical. Same effect was observed when C_{gup} was increased by a factor of 10 instead of D_g as shown in Figure 5.8.

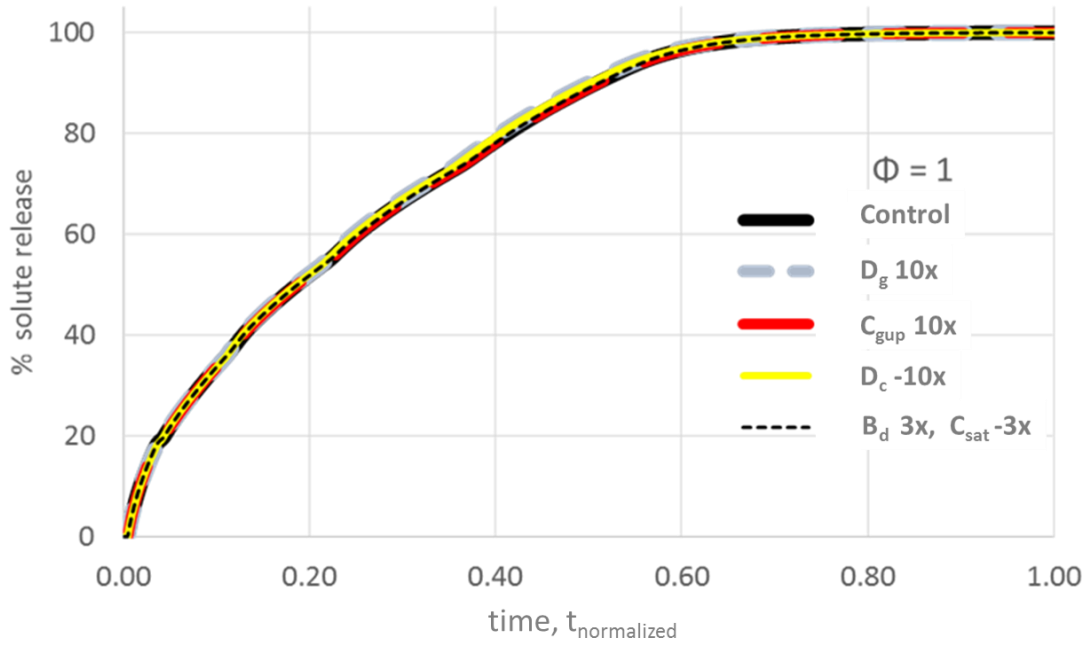

Figure 5.9 Identical release profiles at Φ =1 where the release mode is continuous regardless of change in parameters that defines Φ.

Similarly, when diffusion coefficient of solute (D_c) was reduced by a factor of 10, amount of scavenger was increased by a factor of 10 to keep the same Φ. However, while doing this, overall release time for this run was increased significantly (almost by a factor of 10), but with normalized time ($t_{actual}/t_{99.9\%}$), the shape of the release curve remained identical to that of control release profile shown in Figure 5.8.

The last two parameters, B_d and C_{sat} were increased simultaneously by a factor of 3, keeping the B_d/C_{sat} ratio constant (10) which by itself kept the value of Φ = 3, constant. As the solute was increased by a factor of 3 in each depot, overall solute released was 3 times higher compared to that of a control release profile shown Figure 5.8, but while the release is plotted as a percentage of total solute release against normalized time, the shape of the profile still remain identical. Similar effects were observed for Φ =1, where release is rather continuous as depicted in Figure 5.9. Here also, various combinations of Φ

parameters still provide the identical release profiles when plotted for percentage solute release vs normalized time. When the solute release is plotted against the square root of normalized time, the shape of each pulse becomes identical which is shown in Figure 5.10 (B) as compared to the one that is shown in Figure 5.10 (A). This indicates that the

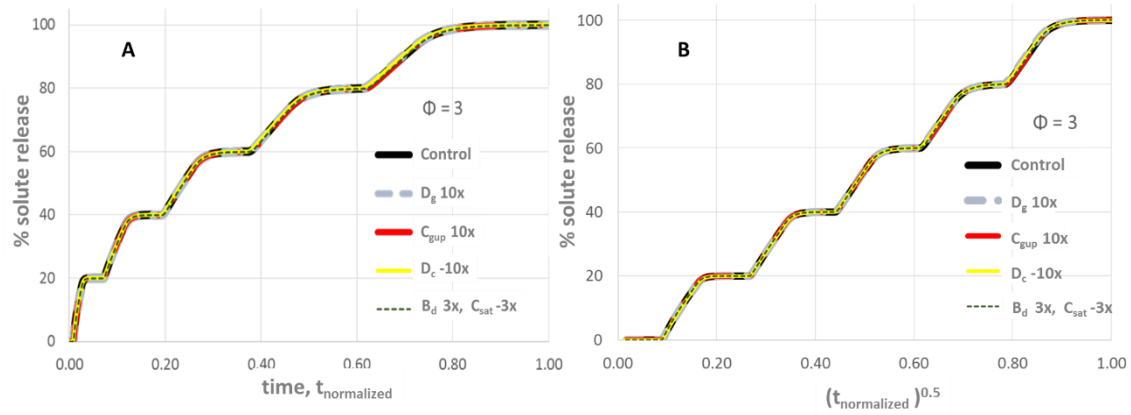

Figure 5.10 Identical release profiles at Φ =3; pulses become evenly shaped (B) when solute release was plotted vs $(t_{normalized})^{0.5}$ as compared to the one that was plotted vs $t_{normalized}$ (A).

diffusion of stimulant and solute in the device varies with square root of the distance that each species has to travel in the device. Similar effect is shown in Figure 5.11, which

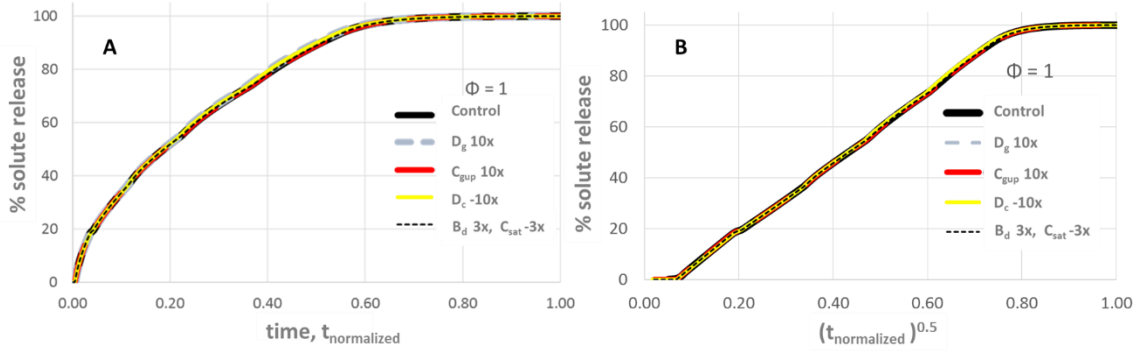

Figure 5.11 Identical release profiles at Φ =1 with continuous release; slope is constant when solute release was plotted vs $(t_{normalized})^{0.5}$ as compared to the one that was plotted vs $t_{normalized}$ (A).

confirms the continuous release at Φ =1.

All the profiles in Figure 5.8 to Figure 5.11 lay on top of each other regardless of which of the parameter in Φ definition is changed. All the results indicated in Figure 5.8

and 5.9, confirm that regardless of which parameter is changed in the definition of Φ provided by Equation 5.7, shape of the profile remains identical at a given value of Φ. However, in all of these trials, F/C_{gup} and B_d/C_{sat} ratios were kept large enough (>> 1) to provide reasonable concentration gradient. If these ratios are small, the shape of the profile can change even at same Φ value. These effects are discussed in next section.

5.5.3 Effect of F/C_{gup} and B_d/C_{sat} on Release Profile

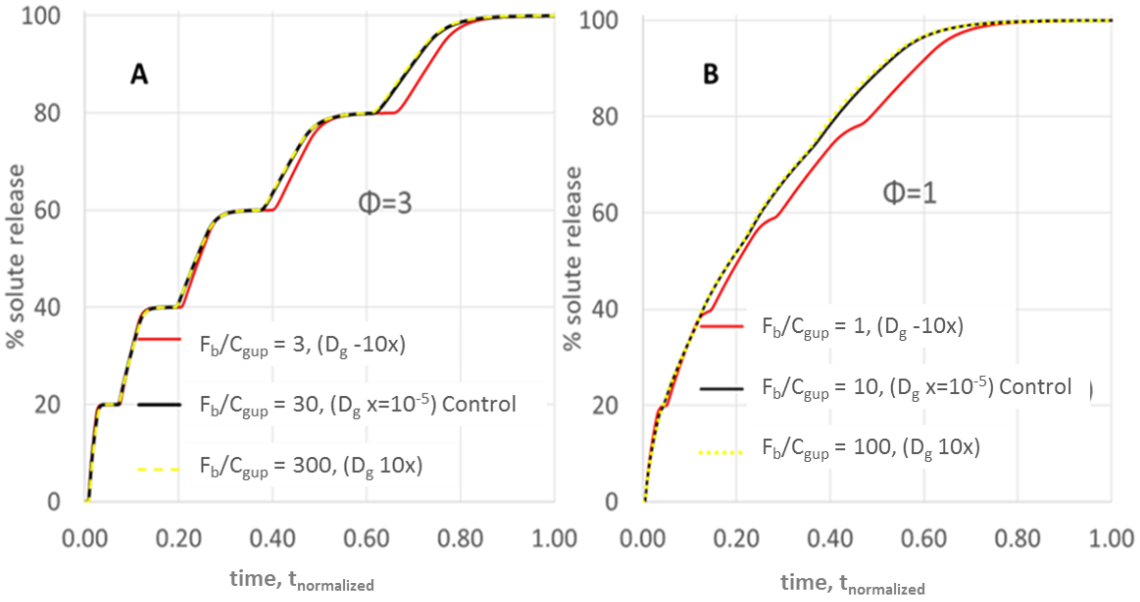

Figure 5.12 Effect of F/C_{gup} along with D_g on a release profile: (A) Φ= 3, (B) Φ = 1; F/C_{gup} ratio must be large enough (> > 1).

Amount of scavenger (F) relative to that of upstream stimulant concentration (C_{gup}) can affect the shape of release profiles. As shown in Figure 5.12, diffusion coefficient of stimulant (D_g) was varied by a factor of 10 in either direction for both Φ =3 and Φ =1, by varying the corresponding F/C_{gup} ratio. In both cases, when D_g was increased by a factor of 10, F/C_{gup} was increased from 30 to 300 to keep the same value of Φ, and the shape of the release profile was found identical when plotted for percentage solute release vs. normalized time. However, when D_g was decreased by a factor of 10,

the shape of the release profiles started to deviate from the control release profile as shown in Figure 5.12 (A) (red line), as F/C_{gup} ratio was significantly reduced from 30 to 3 for Φ =3. This effect increases further when F/C_{gup} ratio was further decreased to 1 for Φ =1 as depicted in Figure 5.12 (B). This confirms the assumption in Φ derivation, that F/C_{gup} ratio must be large enough so that the amount of acid needed to develop the concentration profile remains negligible compared to the amount needed to consume the

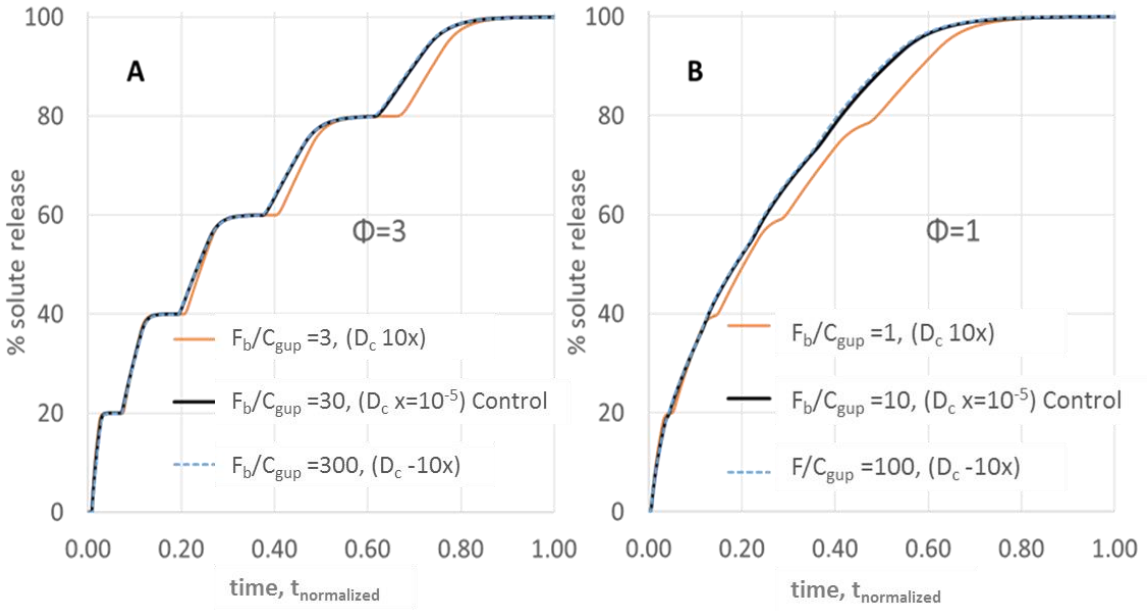

Figure 5.13 Effect of F/C_{gup} along with D_c on a release profile: (A) Φ = 3, (B) Φ = 1; F/C_{gup} ratio must be large enough (> > 1).

scavenger. When F/C_{gup} is small, the time for stimulant to penetrate a node is no longer strictly proportional to F, because stimulant is required just to establish the concentration profile, and this amount is not negligible if F is small.

Same effects were observed when diffusion coefficient of solute (D_c) was altered instead of D_g for various F/C_{gup} ratio as depicted in Figure 5.13, reconfirming that F/C_{gup} ratio must be large enough for Φ to remain significant. Similarly, ratio of solid solute (B_d) to that of dissolved solute (C_{sat}) can also affect the shape of the curve depending on solute

loading in the depot. Upstream dissolved solute concentration remains constant at C_{sat} for a given solute until all of the solid particles have dissolved. Then the upstream solute concentraion decreases, decreasing the concentraion gradient driving solute diffusion out of the device. This effect is depicted in Figure 5.14 where B_d/C_{sat} ratio was varied on various order of magnitude, and the release was plotted as percentatge solute release vs. time for both Φ =3 and Φ =1. When B_d/C_{sat} ratio was kept greater or equal to 10, the shape of the profiles remain identical and they lie on top of each other in both cases, but

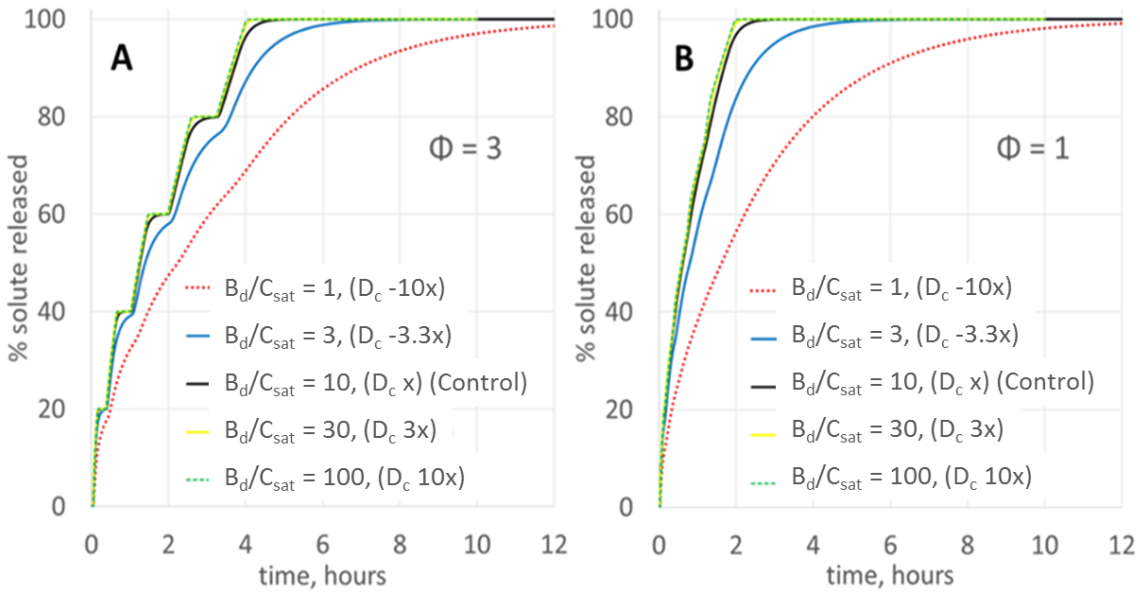

Figure 5.14 Effect B_d/C_{sat} on a release profile: (A) Φ = 3, and (B) Φ =1; solid to dissolved solute ratio (B_d/C_{sat}) must be large enough (>>10)

when the solute laoding was decreased by a factor of 3 (B_d/C_{sat} = 3), the shape of the curve started to deviate from the standard profile, with even more deviation when B_d/C_{sat} is further lowered to 1. These results confirm the assumption used in Φ derivationa that the ratio of B_d/C_{sat} must be kept large enough (>> 10. If solute loading in depot is is too low ($B_d \leq C_{sat}$), then the release could no longer remain pulsatile even at larger Φ values.

5.5.4 *Defining Critical Φ ($Φ_c$) for Transition from Continuous to Pulsatile Release*

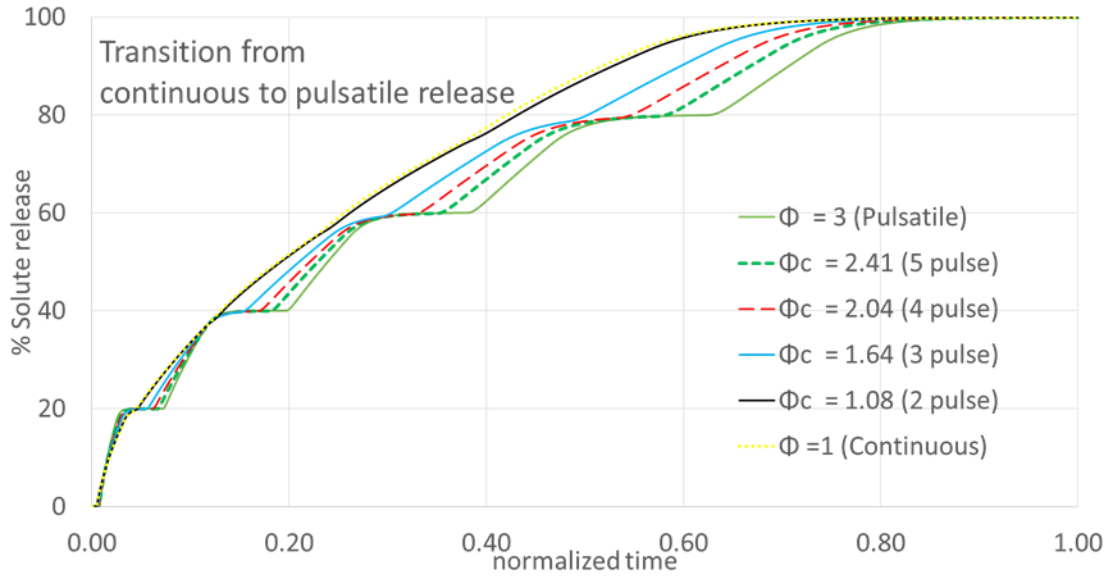

Figure 5.15 Transition from continuous to pulsatile release at $Φ_c$ for a given pulse

In most of the above trials discussed earlier section, where F/C_{gup} ratio and B/C_{sat} ratio was large enough, it was clear that the release mode of a given BMPR system was continuous at Φ =1 and pulsatile at Φ =3 based on time difference between subsequent pulses ($t_n^{1\%} - t_{n-1}^{99\%}$). In other words, at Φ=1, ($t_n^{1\%} - t_{n-1}^{99\%}$) < 0 for all the first four pulses starting from pulse-2, while at Φ =3, ($t_n^{1\%} - t_{n-1}^{99\%}$) was greater than zero for all the first four pulses. It is important to note that this time difference was not constant for each pulse. For instance, this time difference for first four pulses at Φ=1, was -0.8, -14.9, -32.4 and -47.4 minutes for first, second, third and fourth pulse respectively. It indicates that when transition occurs from Φ =1 to Φ =3, earlier depots meet the definition of pulsatile release more strongly than the depots that are placed in the deeper in the device.

A series of model runs were executed in between Φ =1 and Φ = 3 in 0.01 intervals, and the time difference ($t_n^{1\%} - t_{n-1}^{99\%}$) was tracked for each subsequent pulse for first four

pulses starting from pulse-2. For a given value of Φ, whenever this time difference ($t_n^{1\%} - t_{n-1}^{99\%}$) became greater than zero, that Φ value was considered as a critical Φ value (Φ_c) , where release mode changes from continuous to pulsatile for n number of pulses. Figure 5.15 shows this effect. When Φ is increased from 1 to 3, at each Φ_c value,

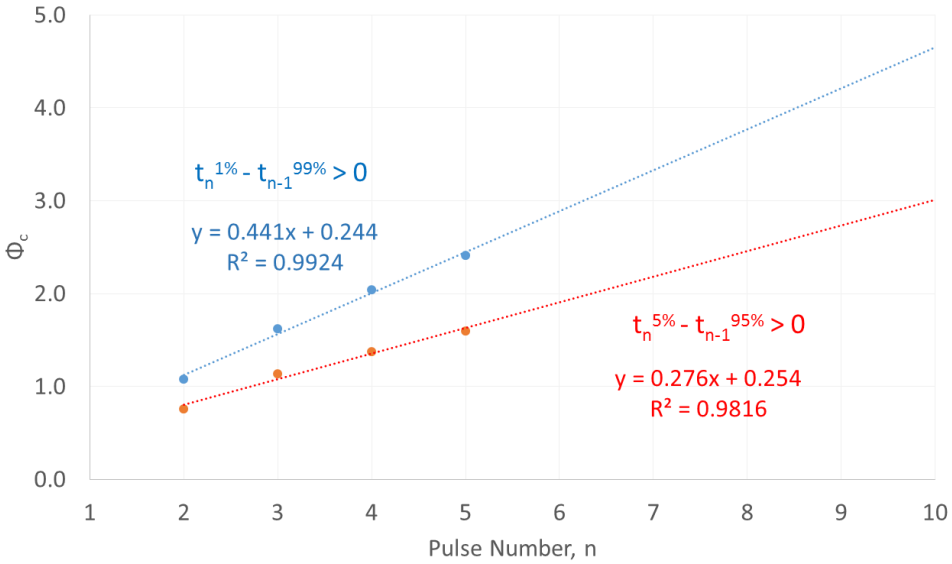

Figure 5.16 Relationship between critical Φ and pulse number for the release to be pulsatile for n-pulse BMPR system with F_b/F_d = 5, t_b/t_d =1.

subsequent depots turn pulsatile in a gradual order from depot 1 to depot 2, depot 2 to depot 3, and so on. The time difference ($t_n^{1\%} - t_{n-1}^{99\%}$) just turns positive from negative at these Φ_c values for a given set of subsequent pulses. At Φ_c = 2.41, the last depot in the device started to release 1% solute after fourth depot had just finished releasing 99% of solute, meaning all the 5 pulses become pulsatile. Similarly, at Φ_c < 1.08, all the depots show continuous release mode (for, ($t_n^{1\%} - t_{n-1}^{99\%}$) < 1). Thus, Φ_c value matters the most where one can identify how many pulses in a given BMPR system are clearly pulsatile or continuous. For a given F_b/F_d =5, t_b/t_d=1, these Φ_c values were plotted against pulse number as shown in Figure 5.16, which also indicates the data if pulsatile release was defined based on ($t_n^{5\%} - t_{n-1}^{95\%}$) combination instead of ($t_n^{1\%} - t_{n-1}^{99\%}$) combination for the

release from subsequent depots. One could use the relationship between Φ_c and pulse number for a given BMPR system with constant F_b/F_d and t_b/t_d ratio, and can design the system for number of pulses. However, it is important to note that in all these runs, F_b/F_d and t_b/t_d ratio was kept constant at 5 and 1 respectively. If any of these ratio changes, then Φ_c will also change. In other words, even if the Φ_c value was kept the same, but t_b/t_d was altered keeping F_b/F_d constant; then all pulses can become pulsatile/continuous based on increase/decrease in ratio. Similarly, at the same Φ_c value, if F_b/F_d ratio was altered keeping t_b/t_d constant, then all the pulses can become either pulsatile/continuous based on increase or decrease in ratio. Effect of relative thickness of barrier to depot (t_b/t_d) and effect of relative scavenger concentration of barrier to depot (F_b/F_d) on Φ_c value is discussed in next section by running numerous number of model runs using Helium.

5.6 Effect of Thickness and Scavenger Loading on Φ Limits

The thickness ratio (t_b/t_d) and scavenger ratio F_b/F_d ratio was assumed to be constant in the derivation of Φ. These ratios, however, can vary for various BMPR systems. For instance F_b/F_d can change, since the scavenger in barrier can be manipulated much more readily than the scavenger in depot. Similarly, t_b/t_d can also change if the either of the layer thickness is altered. Even if the depot nodes can be stimulated faster than their solute can exit (as in case of Φ=1 (Fig. 5.4) and Φ=0.3 (Fig. 5.6)), it doesn't necessarily mean the release can be continuous in all cases at similar Φ values, because if the stimulant takes long time to penetrate in next barrier for a given BMPR system (either due to increased amount of scavenger or increased thickness of barrier), then all the solute may still get to exit before the first node of next depot is triggered, and release can become pulsatile at the same Φ values. In other words, the release mode of a particular

BMPR system at a given value of Φ depends on the relative thickness of the layers (t_b/t_d) and the relative scavenger content of the layers (F_b/F_d), which are discussed in following subsections.

5.6.1 Effect of Thickness on Φ_c Limits

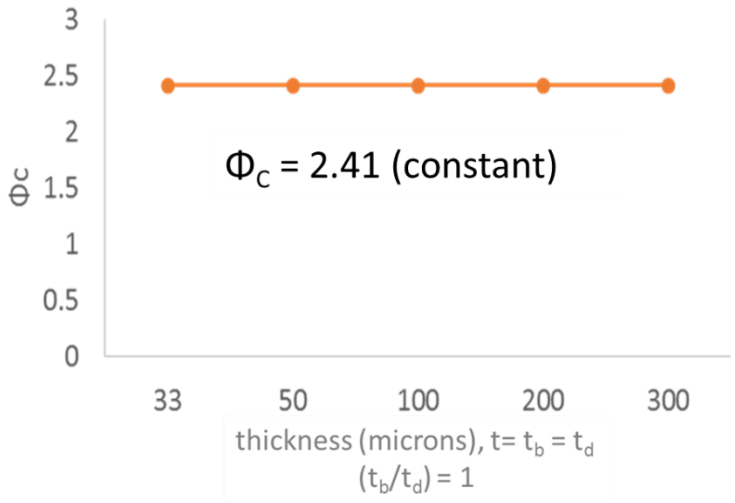

Figure 5.17 Φ_c remains same at a constant t_b/t_d regardless of absolute thickness. F_b/F_d was also kept constant at 5 in all cases.

For a constant thickness ratio of barrier to depot (t_b/t_d), Φ_c value remains the same regardless of absolute thickness of the layer. This effect is show in in Figure 5.17. This indicates that, at any given thickness of layers, as far as the value of Φ is kept constant then the shape of the profile would remain consistent. Absolute thickness was varied from 33, 50, 100, 200 and microns for both barrier and depots keeping t_b/t_d equal to 1. Φ_c remained constant at 2.41 in all case. Next set of trials was done with various t_b/t_d ratios of 0.1, 0.2, 0.5, 1, 2, 5 and 10 at a constant F_b/F_d ratio of 5. Barrier thickness was altered to change this ratio keeping the depot thickness constant at 100 microns. At each t_b/t_d ration, number of model runs were executed on various ranges of Φ to determine Φ_c based on the time difference of release data for subsequent depots satisfying the condition

$t_n^{1\%} - t_{n-1}^{99\%} > 0$. As the stimulant penetration and the solute release, both processes, are transport limited, their characteristic times vary with the square of film thickness. Now for example, if t_b/t_d increases by a factor of 3, then to keep the acid penetration and solute release times comparable, the ratio of the remaining transport parameters in Φ definition (based on Equations 5.3, 5.6 and 5.7) must decrease by $3^{0.5}$. This is confirmed by the

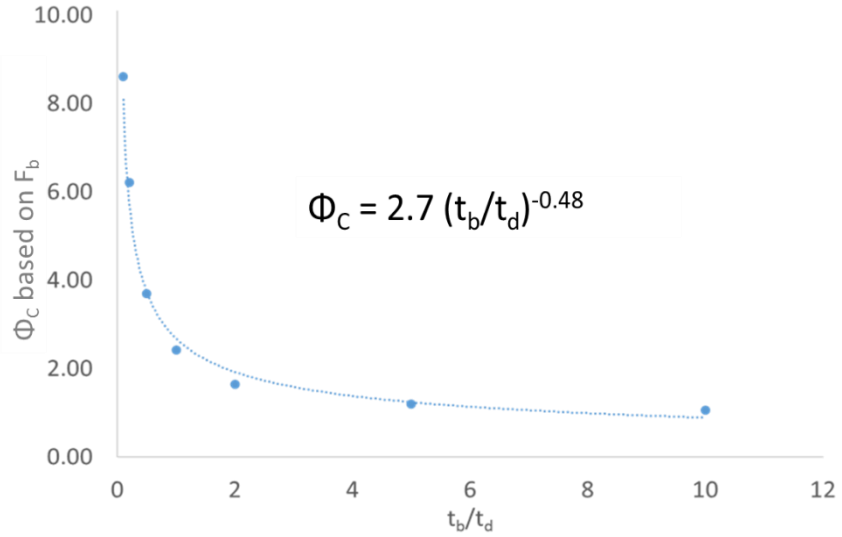

Figure 5.18 Effect of t_b/t_d on Φ_c; Φ_c varies inversely with a square root of thickness ratio (t_b/t_d)

square root dependency in Figure 5.18 where Φ_c varies inversely with a square root of thickness ratio (t_b/t_d). It also indicates that, for a given t_b/t_d ratio, release will be pulsatile for all the values of Φ above critical value Φ_c for a given 5-pulse BMPR system. It also indicates that for a given value of Φ_c, the release mode can change its shape from pulsatile to continuous if t_b/t_d ratio is reduced from the ratio that was kept at Φ_c. If all the values of Φ_c for every set of subsequent pulses for a 5-pulse BMPR system are plotted against its corresponding t_b/t_d ratio on log scale, then an analytical relationship can be developed based on pulse number, t_b/t_d ratio and Φ_c as depicted in Figure 5.19.

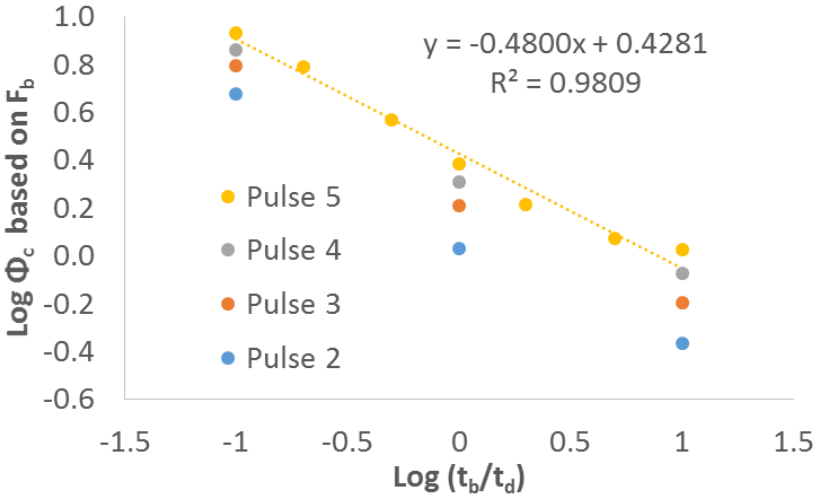

Figure 5.19 Analytical relationship between Φ_c and pulse number at various t_b/t_d ratios; F_b/F_d ratio was kept constant at 5.

As described earlier in Figure 5.16, Φ_c was also checked for each pulse and plotted against all these values of t_b/t_d ratio which is depicted in Figure 5.20. It shows that Φ_c can be extrapolated for more number of pulses (>5) for a given of t_b/t_d ratio.

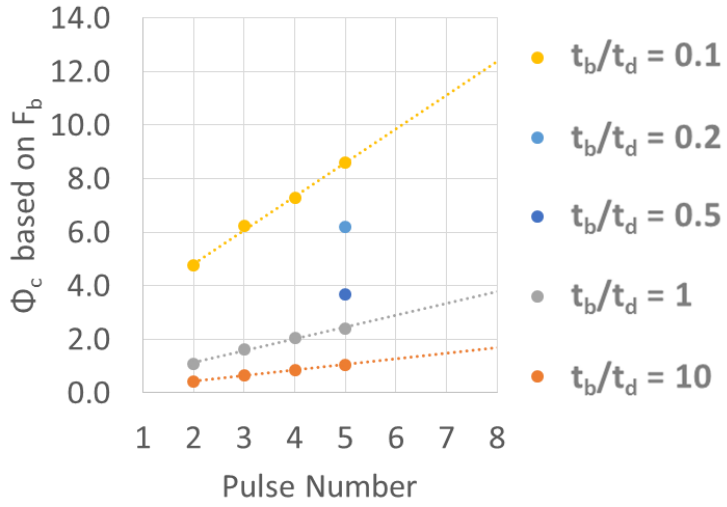

Figure 5.20 Relationship between pulse number, t_b/t_d and Φ_c. Φ_c can be extrapolated as it increases linearly with pulse number for a given t_b/t_d ratio. F_b/F_d was kept constant at 5.

5.6.2 *Effect of Scavenger on Φ_c Limits*

To check the effect of relative concentration of scavenger in the barrier to that in the depot on Φ_c value, F_b/F_d was varied from 0.1, 0.2, 0.5, 1, 2 and 10 for a constant t_b/t_d

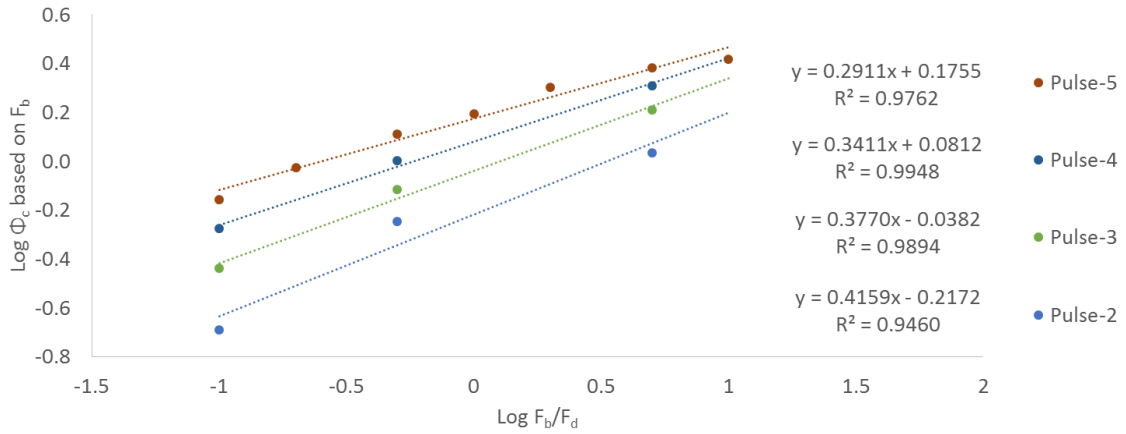

Figure 5.21 Relationship between Φ_c based on F_b, pulse number and F_b/F_d ratio for a 5-pulse non-delaminating BMPR.

ratio of 1. A series of model runs were executed to find out the critical of Φ where the release becomes pulsatile based on the time difference of release data for subsequent

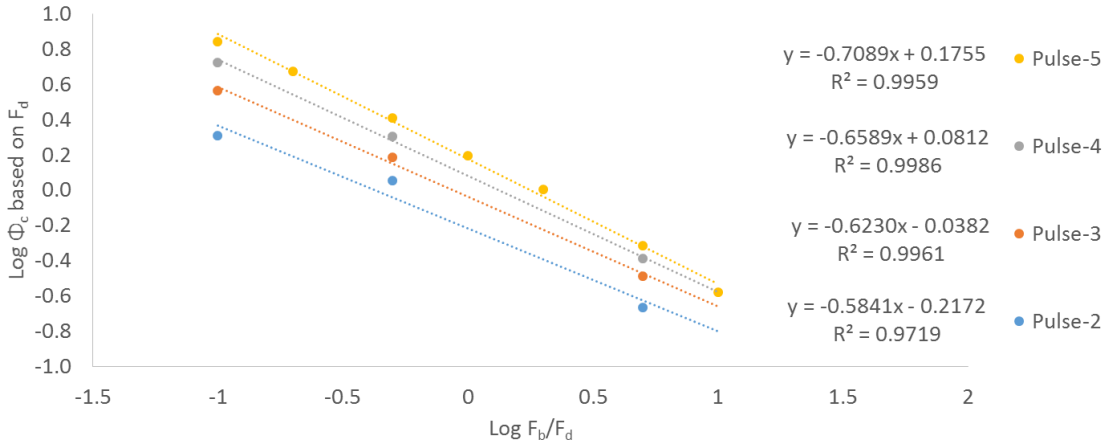

Figure 5.22 Relationship between Φ_c based on F_d, pulse number and F_b/F_d ratio for a 5-pulse non-delaminating BMPR system.

depots satisfying the condition, $t_n^{1\%} - t_{n-1}^{99\%} > 0$, for a given five pulse BMPR system. Each pulse was checked for Φ_c as described earlier. Once all the values of Φ_c were

determined for each pulse for various F_b/F_d ratio, the analytical relationship between pulse number, Φ_c and F_b/F_d ratio was generated as depicted in Figure 5.21 and 5.22.

As the Φ_c was compared against F_b/F_d ratio, Φ value was calculated based on both F_b and F_d, separately. Figure 5.21 predicts the analytical relationship between pulse number, F_b/F_d ratio and Φ_c based on F_b. Figure 5.22 shows the same chart for Φ_c based on F_d. Both the figures show the analytical relationship for each pulse as a linear equation on this plot. The slope of these lines are the factors by which Φ_c is dependent on F_b/F_d ratio. If one compares these slopes (*i.e.* factors) for each pulse in both the figures, the

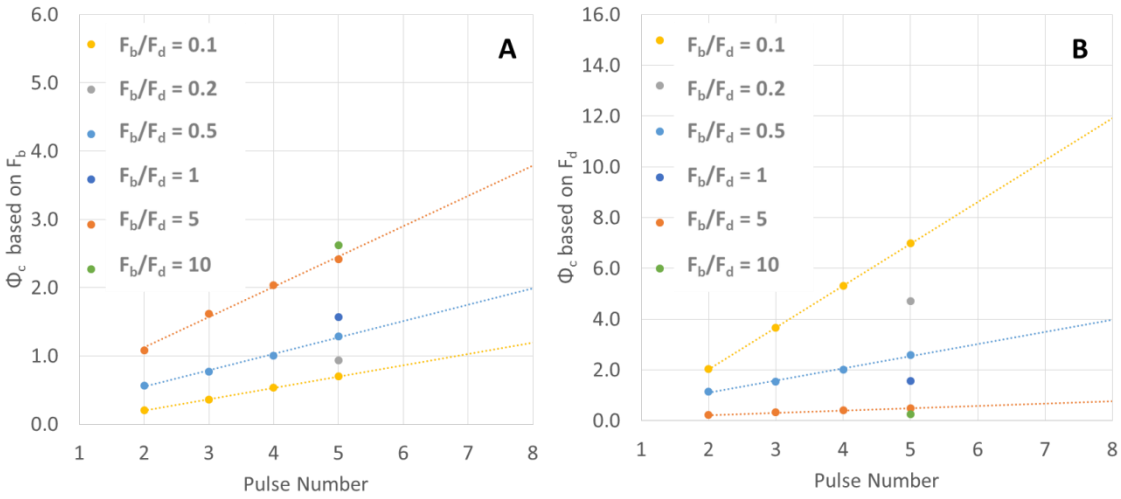

Figure 5.23 Relationship between Φ_c, pulse number (n) at various F_b/F_d ratios. t_b/t_d ratio was kept constant at 1 in each case. (A) Φ_c based on F_b, (B) Φ_c based on F_d.

difference between these factors becomes exactly to unity (*i.e.* equal to 1) up to four decimal points. For instance, for pulse four Φ_c (based on F_b) is proportional to $(F_b/F_d)^{0.2911}$ (considering all four depots to be pulsatile). At the same time Φ_c (based on F_d) is proportional to $(F_b/F_d)^{-0.7089}$ for all four depots to be pulsatile. This indicates that Φ_c is dependent on scavenger loading in both depot and barrier. As the difference in these power factors (or slopes of the lines in Figure 5.21 and 5.22) adds up to 1, it effectively indicates that the Φ value varies linearly with the amount of scavenger with a combined

equivalent content of scavenger of barrier and depot. As shown in Figure 5.23, one can use the relationship between Φ_c and F_b/F_d ratio for a given BMPR system for definite number of pulses and can extrapolate for more number of pulses to check their release behavior.

5.7 Conclusions

The computational model for delaminating BMPR system from Chapter 3 was adapted to non-delaminating BMPR system. The model was explored extensively to understand various release modes of a given BMPR system on wide range of parameter values. A definition of pulsatile release was created for a fixed number of pulses in a given BMPR system. Dimensionless parameter Φ (pulsatility factor) was derived to combine the effects of six different variables on the release mode of the system. Correlation between Φ and pulsatile release was demonstrated computationally. The pulsatility factor at the pulsatile/continuous transition (Φ_c) was correlated to pulse number. These correlations remain valid only when the scavenger loading is large enough than the upstream stimulant concentration (*i.e.* $F/C_{gup} >> 10$), and the solid solute loading is large enough than its saturation concentration (*i.e.* $B/C_{sat} \geq 10$). Overall membrane thickness had no effect on this correlation. However, the thickness ratio between barrier and depot did affect the Φ_c correlation with a $(t_b/t_d)^{-0.5}$ dependence. The scavenger ratio between barrier and depot (F_b/F_d) did affect the Φ_c correlation with $(F_b/F_d)^{-1}$ dependence. The pulsatility factor Φ can guide the design of physical BMPR systems for desired number of pulses with a targeted release profile.

This non-delaminating computational model is very useful for estimating the feasibility of the system before investing the resources into developing actual physical

systems. The model allows the flexibility to tweak any of the parameters to check their effects on a release profile of a given system. The correlations developed between the pulsatility factor and the pulse number with respect to thickness of the layers and their scavenger loadings, are even more useful in extrapolating the performances of systems with any given number of doses. For instance, if an application needs 25 pulses, large computational resources would be required to predict the performance with every slight variation in parameters. The correlations developed in this chapter allow the user to quickly narrow down the range of possible parameter values even before running the model.

CHAPTER 6 SUMMARY & NEW DIRECTIONS

6.1 Summary

BMPR technology offers an elegant material-based alternative for pulsatile delivery using stimuli-sensitive depots protected by reactive barriers and shows a clear advantage over current methods of pulsatile delivery based on polymer degradation. This is the first time that a non-degrading device has ever been constructed for BMPR delivery. This approach of BMPR system is more beneficial as it has been decoupled from polymer degradation and instead linked to sacrificial scavenging of the external stimulant. These systems allow the delay time between pulses to be scaled across orders of magnitude with only minor changes in barrier properties (such as thickness, scavenger loading and scavenger location) and open the BMPR approach to variety of stimulants. There are no electronic or mechanical components, nor power supply or circuitry, greatly reducing the cost and possible failure modes of the device.

Synthesis of pH-sensitive depots of p(MMA/DMA) loaded with model drugs (methylene blue or methyl orange) was demonstrated. These hydrogels confirmed the complete immobilization of the drug at pH 7. In acidic environment, depots swelled significantly and completely released the model drugs. Experiments on swelling and solute release kinetics showed that both processes are usually transport limited. Characteristic swelling and characteristic release times of these depots were comparable, which can also be analytically predicted and manipulated. To protect the acid stimulant for these depots, ZnO-loaded barrier films were synthesized and demonstrated. The lag time of the barrier varies with the square of the thickness of the barrier and linearly with its scavenger loading. The lag time also depends on the location of the scavenger in the

barrier in a precisely quantifiable fashion. Characteristics of both depots and barriers were independently investigated. Diffusion and partition coefficients were experimentally determined for weak acid stimulant and model drugs in both depot and barrier membranes. Acid appears to have little interaction with polymer, diffusing through absorbed water as through bulk water. Model drug diffusion is hindered by polymer network; however, the drug diffuses out as the hydrogel swells and is completely released at equilibrium. Various multi-pulse delaminating BMPR devices were designed by integrating depots and barriers together using beeswax. No solute was released at pH 7, but sharp pulses of drug were observed from the device at regular time intervals at pH 3. These BMPR devices were demonstrated for variety of pulse periodicity where pulse times varied with the square of the thicknesses and also with the location of the scavenger in the barriers. Sequential release of multiple solutes was achieved from a single device. The number of pulses assimilated in to a single device is limited only by the art of making them. Up to ten distinct pulses were demonstrated at regular time intervals from a single delaminating BMPR device.

These experimental delaminating BMPR devices produced release profiles which were in good agreement with analytical predictions. A computational model of the delaminating BMPR system was also constructed and appropriate node size and time-step sizes were determined. The model was validated against both analytical predictions and experimental results with good agreement.

Several approaches to constructing non-delaminating BMPR systems were explored. Mechanical constriction using a metal mesh top and expandable bottom within rigid side walls proved to be the best. Covalently-bound depot membranes swelled in one

dimension by a factor of three, rather than five. Increased cross-linking (ten times higher) also decreased the swelling of a depot to a factor of three (not five) with no impact on release. Additional cross-linking further decreased swelling, but inhibited the release of a drug. Two-pulse experimental non-delaminating BMPR systems were demonstrated.

However, it is still currently difficult to develop a non-delaminating experimental system yielding results clean enough to establish predictive correlations, so the computational model for delaminating BMPR systems was adapted to non-delaminating BMPR systems. The model was explored extensively to understand various release modes of a given BMPR system on wide range of parameter values. A definition of pulsatile release was created for a fixed number of pulses in a given BMPR system. Dimensionless parameter Φ (pulsatility factor) was derived to combine the effects of six different variables on the release mode of the system. Correlation between Φ and pulsatile release was demonstrated computationally. The pulsatility factor at the pulsatile/continuous transition (Φ_c) was correlated to pulse number. These correlations remain valid only when the scavenger loading is large enough than the upstream stimulant concentration (*i.e.* $F/C_{gup} >> 10$), and the solid solute loading is large enough than its saturation concentration (*i.e.* $B/C_{sat} \geq 10$). Overall membrane thickness had no effect on this correlation. However, the thickness ratio between barrier and depot did affect the Φ_c correlation with a $(t_b/t_d)^{-0.5}$ dependence. The scavenger ratio between barrier and depot (F_b/F_d) did affect the Φ_c correlation with $(F_b/F_d)^{-1}$ dependence. The pulsatility factor Φ can guide the design of physical BMPR systems for desired number of pulses with a targeted release profile.

This non-delaminating computational model is very useful for estimating the feasibility of the system before investing the resources into developing actual physical systems. The model allows the flexibility to tweak any of the parameters to check their effects on a release profile of a given system. The correlations developed between the pulsatility factor and the pulse number with respect to thickness of the layers and their scavenger loadings, are even more useful in extrapolating the performances of the systems with any given number of doses. These correlations allow the user to quickly narrow down the range of possible parameter values even before running the model.

6.2 New Directions

BMPR technology sets the foundation for a new field of drug delivery. Existing BMPR systems in this research relied upon acid as a stimulant. For practical implementations of drug delivery, it would require a physiologically relevant stimulant, glucose being a prime example. To demonstrate the feasibility of this next step, preliminary trials using glucose as a stimulant are reported below.

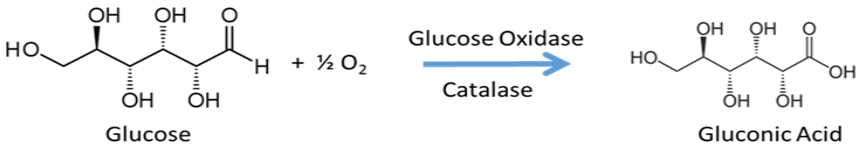

Figure 6.1 Glucose can be converted to gluconic acid in presence of glucose oxidase/catalase enzyme; this acid can work as a stimulant for BMPR system.

As shown in Figure 6.1 glucose can be converted to gluconic acid with glucose oxidase and catalase. This acid can serve as a local stimulant source if created inside the barrier matrix. To further investigate the effect of enzyme in PVA barriers films, glucose oxidase and catalase were immobilized as shown in Figure 6.2.

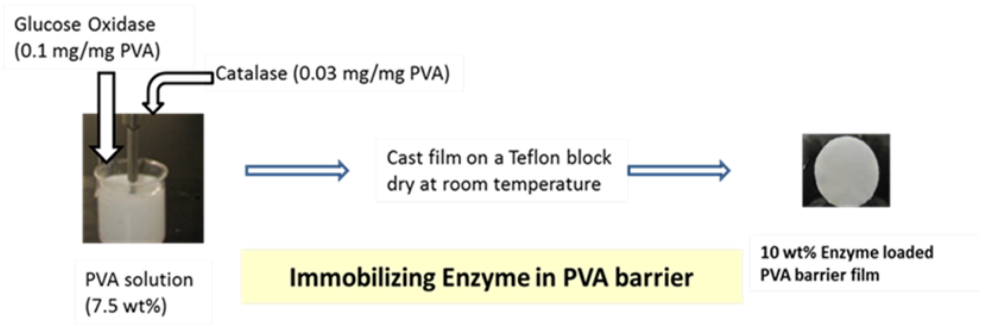

Figure 6.2 Immobilization of enzyme in PVA barrier

Resulting PVA barriers with 10% enzyme loading were further investigated to see if they can produce enough acid to drive the BMPR system. Enzyme loaded barrier films were immersed in a known solution of saline and then spiked with a small amount of

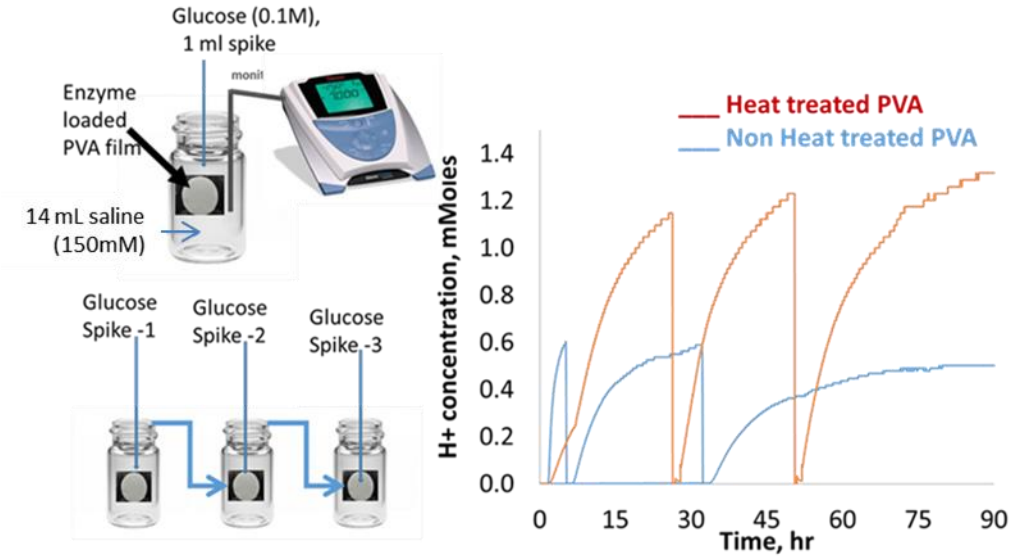

Figure 6.3 Organic acid can be produced from glucose due to presence of active enzyme in the barrier; this acid can drive a BMPR system**.**

glucose as shown in Figure 6.3. The solution was continuously monitored with a pH meter. Figure 6.3 (right) shows that as soon as the glucose was added, it started diffusing in the barrier films, reacted with enzyme and produced acid. Films were taken out of the

solution periodically and transferred to a fresh saline solution where small amount of fresh glucose was spiked. Enzyme remained active throughout this 3-stage trial and kept producing acid. Results were even more encouraging with heat treated barrier films with enzyme still producing acid despite a 150ºC heat treatment and also remaining safely immobilized within the cross-linked membrane.

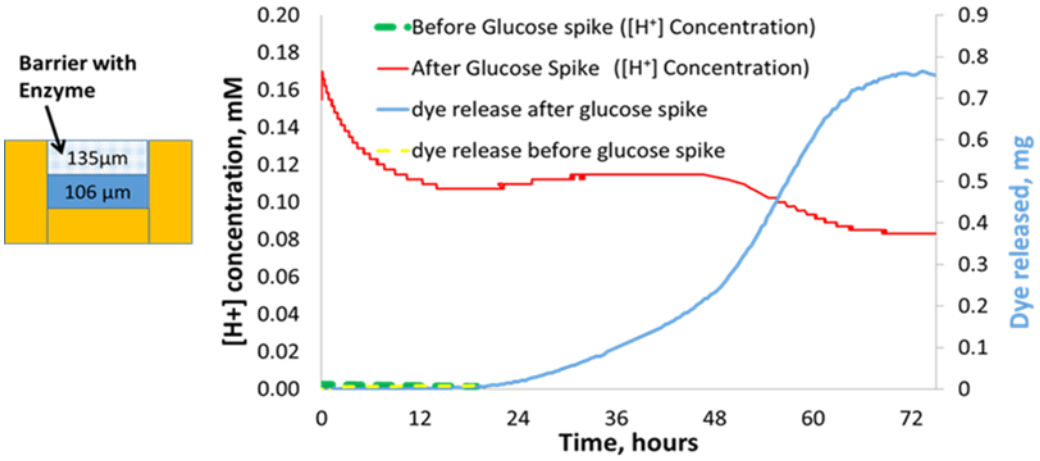

Figure 6.4 Single pulse BMPR system with glucose as a stimulant; zinc oxide loaded barrier (10% by weight) was immobilized with glucose oxidase/catalase.

Using such enzyme loaded barrier films, a 1-pulse BMPR system was evaluated with glucose as a stimulant. As shown in Figure 6.4, a single depot loaded with methylene blue was protected by an enzyme filled PVA barrier containing 10% ZnO. Upon immersing this device in a saline solution at neutral pH, no release was observed for 24 hours as no acid was generated without glucose. As soon as the saline solution was spiked with 0.1 M glucose, that glucose started to diffuse in the PVA barrier for almost 24 hours generating acid inside the PVA matrix. This acid gradually depleted the ZnO scavenger in the barrier and diffused inside the depot. As the pH started to decrease, acid

triggered the depot and methylene blue started to release as depicted in Figure 6.4. However, the release rate was slow compared to that observed with citrate buffer at pH 3, and equilibrium swelling of the depot was not as dramatic as observed with the delaminating BMPR systems. As a result all the release occurred through the spent PVA matrix without any delamination.

These preliminary results of glucose-based systems demonstrate the feasibility of physiologically relevant stimulants for BMPR technology. Many challenges remain, however, such as determining the optimum placement of the enzyme within the stack. If enzyme is near the external interface of the device, the resulting acid may simply diffuse back out of the device rather than down into the underlying depot membrane. Determining the appropriate depth at which the enzyme should be loaded is a prime example of the importance of the computational model. A third mobile species, glucose, can easily be added to the model, along with a third immobile species, the enzyme. A second reaction rule can be added to the barrier nodes, where coexistence of enzyme and glucose results in a decrease of glucose and an increase of gluconic acid. The transport parameters for glucose and gluconic acid in the membranes can be independently determined by diaphragm cell experiments and the reaction parameters can be independently determined by a set of reaction trials varying enzyme and glucose concentrations separately and monitoring pH. One could then use the model to guide the development of this more complicated physical system. This is one of several new directions this technology may take.

APPENDICES

APPENDIX A PERMEABILITY OF ACID THROUGH BARRIERS

ACID PERMEABILITY DATA THROUGH ZnO free PVA BARRIERS

				Upstream Cell			Downstream Cell						
Sr. No	Reference Lab book No.	PVA barrier type	thickness [µm]	Starting pH	Average pH	NaCl [mM]	Max pH at slope	Min pH at slope	Average pH	NaCl [mM]	DS Cell Volume, [mL]	Slope [moles/min]	DH [cm^2/s]
1	MG01-33	ZnO-free	106	2.14	2.13	150	4.92	2.94	3.24	150	22	1.41E-04	1.56E-05
2	MG01-34	ZnO-free	94	2.13	2.13	150	3.38	2.63	2.86	150	22	1.66E-04	1.85E-05
3	MG01-35	ZnO-free	72	2.16	2.13	150	4.06	3.22	3.46	150	22	1.45E-04	1.06E-05
4	MG01-43	ZnO-free	83	2.12	2.12	150	5.26	3.13	3.43	150	22	1.37E-04	1.14E-05
5	MG01-46	ZnO-free	156	2.23	2.23	150	4.5	3.65	3.89	150	22	5.98E-05	1.17E-05
6	MG01-47	ZnO-free	182	2.27	2.27	150	3.86	3.31	3.50	150	21	5.94E-05	1.48E-05
7	MG01-48	ZnO-free	129	2.23	2.23	150	4.12	3.34	3.57	150	22	9.19E-05	1.53E-05
8	MG01-49	ZnO-free	151	2.24	2.24	150	4.08	3.52	3.72	150	21	6.74E-05	1.26E-05
9	MG01-116	ZnO-free	110	2.90	2.90	95	3.86	3.53	3.66	95	22	1.87E-05	1.43E-05
10	SG03-142	Spent single layer (10% ZnO)	130	2.98	2.98	100	3.75	3.54	3.63	100	23	1.14E-05	1.38E-05
11	SG03-153	Spent 3-layers (10% ZnO)	520	2.90	2.90	100	4.03	3.87	3.94	100	23	4.69E-06	1.61E-05

Overall Average Permeability [cm^2/s]	1.41E-05	Average Permeability [cm^2/s]	1.38E-05	Average Permeability [cm^2/s]	1.47E-05
%RSD (n=11, trials 1-11)	15.9	%RSD (n=8, trial 1 to 8)	18.1	%RSD (n=3, trial 9 to 11)	6.8

APPENDIX B CODE FOR DELAMINATING BMPR SYSTEM

Example code for individual pulse for delaminating BMPR system containing single barrier and single depot

```
! Code for Delaminating BMPR Validation!
!PULSE-1 of 10-Pulse BMPR!
Program Main
Integer i,j,m,th,tmax,nb,nd
Real*8 Cgup, Ccsat(500),t,delt,Qc,Fb,B1,Bd,Fd,tb,
tdsh,tdsw, d, A,Qc1,x2,x3,x4,s,Hgb,Hgd,Hcb,Hcd !Qg
Real*8 B(500), C(500), Dc(500), Dg(500), F(500),G(500),
Dcsw,Dgsw, Dcsh, Dgsh,hb,hsh,hsw, Dcb,Dgb
Real*8 h(500), Hc(500),
Hg(500),jc(500),jg(500),delc(500),delg(500)
Real*8 d2cdx2(500),d2gdx2(500),Cdiff(500)
Open (3,File='tQ.txt')
Open (4,File='CBi.txt')
Open (5,File='GFi.txt')
Open (6,File='node_t.txt')
Open (7,File='x2 x3 x4.txt')

!$$$$$$ Input Time, Timesteps and Total Number of Timesteps
th=  12 ! hours
tmax = th*60*60! seconds
delt = 0.0005! seconds
m = tmax/delt

!$$$$$$ Input Physical Parameters
d=1.6 !cm
A=3.14/4*d*d

!$$$$$$ Define node number and node thicknesses for barrier
and depot
nb=60!barrier nodes
nd=120!depot nodes
!!!!!!!   10-Pulse Validation ! PULSE-1!!!!!!!!!!!!!!!!!!
tb=150!microns barrier thickness
tdsh=149!microns depot thickness shrunken
s=2!swelling ratio of depot in 1D
tdsw=tdsh*s    !microns depot thickness swollen
hb = tb*0.0001/nb     !cm thickness of each node in barrier
hsh = tdsh*0.0001/nd  !cm thickness of each node in depot
hsw = tdsw*0.0001/nd  !cm thickness of each node in swollen
depot
```

```
!$$$$$$ Input scavenger concentrations in barrier and depot
Fb = 3.531*(nb)/(nb-1) !Equivalent molar concentration of
[H+] required to consume X% ZnO PVA,!ZnO + 2HCl= H20+ZnCl2
!X%(w/w)ZnO (Fb, equivalent molar [H+]):
!10%(1.587), 20%(3.531), 30%(5.967),40% (9.111),
50%(13.322), 60%(19.255),70%(28.239),80% (43.44)

Fd = 2.33 ! Equivalent scavenger concentration of DMA in
Depot, R3N + HCl -----> [(R3NH)+Cl-],
!28% DMA in 72/28 pMMA/DMA is equal to  2.735 M,
!(85% consumption based on titratoin, = 2.735* 0.85 = 2.33
M)

!$$$$$    Input Partition Coefficient
Hgb=0.6 ! Partition coefficient of acid in PVA
Hgd=1     ! Partition coefficient of acid in p(MMA/DMA)
Hcb=0.6 ! Partition coefficient of dissolved solute (dye)
in PVA
Hcd=0.4 ! Partition coefficient of dissolved solute (dye)
in p(MMA/DMA)

!$$$$$$ Input stimulant concentrations and diffusion
coefficient in barrier and depot
Cgup = 0.0012023   ! M, upstream pH = 2.92
Dgb= 0.000025 ! DH = 1.47*10-5, diffusion of acid through
PVA,  D =2.5E-5 cm2/s, as H=0.6
Dgsh = 0!cm2/s Diffusion Coefficient of acid in shrunken
hydrogel
Dgsw = 0.000051!DH= 5.1*10-5, Diffusion coefficient of acid
in swollen hydrogel, Dgsw =5.1E-05 cm2/s as H=1
!based on pH3-pH4 diaphragm cell trial, DH=5.09E-5,
assuming H=1

!$$$$$$ Input solute concentrations and diffusion
coefficients in barrier and depot
B1 = 0.145 ! solid solute M, actual dye concentration in
dry p(MMA/DMA)
!Concentration of 5% Methylene Blue in 72/28 MMA/DMA 0.145
M
!Concentration of 5% Methyl Orange in 72/28 MMA/DMA 0.166 M
Bd = B1/s ! solid solute M, Equivalent solute distributed
in swollen hydrogel
Csh = 0 ! Saturation concentration of solute (dye) in
shrunken state (zero)
Csw = 0.0059/4 ! Saturation concentration of dissolved
solute M, MB (0.0059), MO (0.0011)
```

```
Dcb= 0.0000006 ! DH=3.57*10-7, diffusion coeff of solute
through PVA, Dcb=6.0E-07 cm2/s,,H=0.6
Dcsh = 0!cm2/s Diffusion Coeff of Solute in Shrunken
hydrogel
Dcsw = 0.000009 !DH=3.76*10-7, Diffusion coefficient of
solute from swollen hydrogel, Dcsw=9 E-07 cm2/s,as H=0.43

!$$$$$$ Define Initial conditions in barrier
Do i = 1, nb

B(i) = 0    ! M
C(i) = 0    ! M
Dc(i) =   Dcb ! cm2/s
Dg(i) =   Dgb ! cm2/s
F(i) = Fb
G(i) = 0   ! M
h(i) = hb    ! cm
Hc(i) = Hcb
Hg(i) = Hgb
Ccsat(i)=Csh
End Do
!$$$$$$ Define Initial conditions in depot
Do i = nb+1, nb+nd

B(i) = Bd
C(i) = 0    ! M
Ccsat(i)= Csh
Dc(i) = Dcsh   ! cm2/s
Dg(i) = Dgsh   ! cm2/s
F(i) = Fd
G(i) = 0    ! M
h(i) = hsh    ! cm
Hc(i) = Hcd
Hg(i) = Hgd
End Do
!$$$$$$ Define Initial conditions at boundaries after last
node
B(nb+nd+1) = 0    ! M
C(nb+nd+1) = 0    ! M
Dc(nb+nd+1) = 0    ! cm2/s
Dg(nb+nd+1) = 0    ! cm2/s
F(nb+nd+1) = 0    ! M
G(nb+nd+1) = 0    ! M
h(nb+nd+1) = hsh    ! cm
Hc(nb+nd+1) = Hcd
Hg(nb+nd+1) = Hgd
!$$$$$$ Initialize t, Qc, x2,x3,x4,Qc1,Qg to zero
```

```
t = 0
Qc = 0 ! mg
x2=0
x3=0
x4=0
Qc1=0
!Qg =0
!$$$$$$ Define initial conditions at 1st node
B(1) = 0    ! M
C(1) = 0    ! M
Dc(1) = Dcb    ! cm2/s
Dg(1) = Dgb    ! cm2/s
Hc(1) = 0.6
Hg(1) = 0.6
F(1) = 0    ! M
G(1) = Cgup*Hg(1)    ! M
h(1) = hb    ! cm

Do j = 1,m !j=1,m Main timestep loop starts here

! ACID & SOLUTE in BARRIER! Calculate mass transport in
barrier layer using centered finite difference
approximation
Do i = 2, nb-1 !From node 2 to 2nd last node of 1st
barrier!
!Acid!
d2gdx2(i)=(G(i-1) - 2*G(i) + G(i+1))/(h(i)*h(i))
delg(i)= Dg(i)* d2gdx2(i)*delt
!Solute!
d2cdx2(i)=(C(i-1)- 2*C(i)+ C(i+1))/(h(i)*h(i))
delc(i)= Dc(i)*d2cdx2(i)*delt
End Do

!ACID and SOLUTE in last node of barrier and first node of
depot

d2gdx2(nb)=(G(nb-1)-
2*G(nb)+(Hg(nb)/Hg(nb+1))*G(nb+1))/(h(nb)*h(nb+1))
delg(nb)= Dg(nb)*d2gdx2(nb)*delt
jg(nb-1) = Dg(nb-1)*(G(nb-1)-G(nb))/h(nb-1)
jg(nb)=jg(nb-1)-delg(nb)*h(nb)/delt

d2cdx2(nb)=(C(nb-1)-
2*C(nb)+(Hc(nb)/Hc(nb+1))*C(nb+1))/(h(nb)*h(nb+1))
delc(nb)= Dc(nb)*d2cdx2(nb)*delt
jc(nb)= Dc(nb)*(C(nb-1)-C(nb))/h(nb)
jc(nb+1) = jc(nb)-delc(nb)*h(nb)/delt
```

```
! ACID! Calculate mass transport of acid in depot layer by
first calculating flux from i to i+1
Do i = nb+1,nb+nd  ! Note that flux from last barrier layer
is also needed
jg(i) = ((Dg(i)+Dg(i+1))/2)*(G(i)-G(i+1))/h(i)
End Do

! ACID! Once all fluxes are calculated, determine change in
node concentration using Backward finite difference
approximation
Do i = nb+1, nb+nd  ! Note that change in concentrations
has already been calculated for last barrier node
delg(i) = (jg(i-1)-jg(i))*delt/h(i)
End Do

! SOLUTE ! Calculate mass transport in depot layer by first
calculating flux from i to i+1
Do i = nb+2,nb+nd  ! Note that flux from last barrier layer
is also needed
jc(i) = ((Dc(i-1)+Dc(i))/2)*(C(i-1)-C(i))/h(i)
End Do
jc(nb+nd+1)=0

! SOLUTE ! Once all fluxes are calculated, determine change
in node concentration using Backward finite difference
approximation
Do i = nb+1, nb+nd  ! Note that change in concentrations
has already been calculated for last barrier node
delc(i) = (jc(i)-jc(i+1))*delt/h(i)
End Do

! Change node concentrations in barrier layer
Do i = 2, nb
G(i) = G(i) + delg(i)
C(i) = C(i) + delc(i)

! Consume scavenger
If (F(i).gt.0) then
If (G(i).gt.F(i)) then
G(i) = G(i)-F(i)
write(6,*)'i F(i) t(h) ',i,F(i),j*delt/3600
F(i) = 0
Elseif (G(i).gt.0) then
F(i) = F(i)-G(i)
G(i) = 0
End If
```

```
End If
End Do

! Change node concentrations in depot layer
Do i  = nb+1, nb+nd
G(i) = G(i) + delg(i)
C(i) = C(i) + delc(i)


! Consume scavenger before dissolving solute, in case this
changes Csat of a node
If (F(i).gt.0) then
If (G(i).gt.F(i)) then
G(i) = G(i)-F(i)
write(6,*)'i F(i) t(h) ',i,F(i),j*delt/3600
F(i) = 0
Ccsat(i) = Csw
B(i)=B(i)-Ccsat(i)+C(i)/s
C(i)=Ccsat(i)
Dc(i) = Dcsw
Dg(i) = Dgsw
h(i) = hsw
Elseif (G(i).gt.0) then
F(i)=F(i)-G(i)
G(i) = 0
End If
End If

!Dissolve solid
Cdiff(i) = Ccsat(i) - C(i)
If (B(i).gt.0) then
If (Cdiff(i).gt.0) then
If (B(i).gt.Cdiff(i)) then
B(i) = B(i)-Cdiff(i)
C(i) = Ccsat(i)
Else
C(i) = Ccsat(i) - Cdiff(i) + B(i)
B(i) = 0
End If
End If
End If
End Do

!Maintain impermeable boundary condition on inner boundary
C(nb+nd+1) = C(nb+nd)
G(nb+nd+1) = G(nb+nd)
```

```
!!! IF DELAMINATION OCCURS
If (F(nb + nd/10).le.0)then
G(nb+1)=Cgup*Hg(nb+1)
G(nb+nd)=Cgup*Hg(nb+nd)
F(nb+1)=0
F(nb+nd)=0
Dg(nb+1)=Dgsw
Dg(nb+nd)=Dgsw
Dc(nb+1)=Dcsw
Dc(nb+nd)=Dcsw
h(nb+1)=hsw
h(nb+nd)=hsw
Dg(nb+nd+1)=Dgsw
Dc(nb+nd+1)=Dcsw

x2=(C(nb)+B(nb))*A*h(nb)*373.9 !solute left in node nb
x3=(C(nb+1)+B(nb+1))*A*h(nb+1)*373.9!solute left in node
nb+1
x4=(C(nb+nd)+B(nb+nd))*A*h(nb+nd)*373.9 !solute left in
node nb+nd

C(nb)=0
C(nb+1)=0
C(nb+nd)=0
B(nb)=0
B(nb+1)=0
B(nb+nd)=0
Endif

!Cumulative Release of solute at node 1!
Qc1= Dc(1)*(C(2)-C(1))*delt/h(1) *373.9*A ! release at node
1 before delamination and after delamination
Qc = Qc + Qc1 + x2+x3+x4 ! Cumulative release including
combined solute release before and after delamination
!Calculate cumulative influx of acid
!Qg = Qg + Dg(1)*(G(1)-G(2))*delt/h(1)!
t=t+delt

!$$$$$$ Write results for cumulative solute release Qc vs
time
if(Mod(j,12000).lt.0.001)then
write(3,*)'t(h) Qc ',t/3600,Qc
write(7,*)'x2 x3 x4 t(h) ',x2,x3,x4,t/3600
EndIf

End Do !! j=1,m Main loop ends here
```

```
!$$$$$$ Write C,B,G,F, Dc,Dg at each node at the end of m
number of timesteps!
Do i=1,nb+nd+1

write(4,*)'i,C,B,Dc',i,C(i),B(i),Dc(i)
write(5,*)'i,G,F,Dg',i,G(i),F(i),Dg(i)
EndDo
End
```

APPENDIX C CODE FOR SINGLE LAYER DEPOT

Example code for release from single layer depot for delaminating BMPR system

```
!DELAMINATING BMPR CODE FOR SINGLE LAYER DEPOT WITH NO
BARRIER
Program Main
Integer i,j,m,tmax,nd
Real*8 Cgup, Ccsat(500),t,delt,Qc,B1,Bd,Fd,tdsh,tdsw, d,
A,Qc1,x3,x4,s,Hgd!,Hcd
Real*8 B(500), C(500), Dc(500), Dg(500), F(500),G(500),
Dcsw,Dgsw, Dcsh, Dgsh,hsh,hsw
Real*8 h(500),
Hg(500),jc(500),jg(500),delc(500),delg(500)!, Hc(500)
Real*8 Cdiff(500)!d2cdx2(500),d2gdx2(500)
Open (3,File='tQ.txt')
Open (4,File='CBi.txt')
Open (5,File='GFi.txt')
Open (6,File='node_t.txt')
Open (7,File='x3 x4.txt')

!!! DELAMINATING BMPR CODE FOR SINGLE LAYER DEPOT !!
!!! Trial : SG05-86 Bilayer, Pulse_1, 130 micron depot !!!
!$$$$$$ Input Time, Timesteps and Total Number of Timesteps
tmax = 3*60*60! seconds
delt = 0.0004! seconds
m = tmax/delt
!$$$$$$ Input Physical Parameters
d=1.41 !cm
A=3.14/4*d*d

!$$$$$$ Define node number and node thicknesses for barrier
and depot
nd=120!depot nodes
tdsh=130!microns depot thickness shrunken
s=2!swelling ratio of depot in 1D
tdsw=tdsh*s    !microns depot thickness swollen
hsh = tdsh*0.0001/nd  !cm thickness of each node in depot
hsw = tdsw*0.0001/nd  !cm thickness of each node in swollen
depot

!$$$$$$ Input scavenger concentrations in depot
Fd = 2.33*nd/(nd-1) ! Equivalent scavenger concentration of
DMA in Depot, R3N + HCl -----> [(R3NH)+Cl-],
!28% DMA in 72/28 pMMA/DMA is equal to  2.735 M,
!(85% consumption based on titratoin, = 2.735* 0.85 = 2.33
M)
```

```
!$$$$$    Input Partition Coefficient
Hgd=1     ! Partition coefficient of acid in p(MMA/DMA)
!Hcd=0.4 ! Partition coefficient of dissolved solute (dye)
in p(MMA/DMA)

!$$$$$$ Input stimulant concentrations and diffusion
coefficeint in barrier and depot
Cgup = 0.0010965   ! M, upstream pH = 2.96
Dgsh = 0!cm2/s Diffusion Coeff of acid in shrunken hydrogel
Dgsw = 0.000051!DH= 5.1*10-5, Diffusion coeff of acid in
swollen hydrogel, Dgsw =5.1E-05 cm2/s as H=1
!based on pH3-pH4 diaphragm cell trial, DH=5.09E-5,
assuming H=1

!$$$$$$ Input solute concentrations and diffusion
coefficients in barrier and depot
B1 = 0.214*nd/(nd-1) ! solid solute M, actual dye
concentration in dry p(MMA/DMA)
!Concentration of 5% Methylene Blue in 72/28 MMA/DMA 0.145
M
!Concentration of 5% Methyl Orange in 72/28 MMA/DMA 0.166 M
Bd = B1/s ! solid solute M, Equivalent solute distributed
in swollen hydrogel
Csh = 0 ! Saturation concentration of solute (dye) in
shrunken state (zero)
Csw = 0.0059/4 ! Saturation concetration of dissolved
solute M, MB (0.0059), MO (0.0011)
Dcsh = 0!cm2/s Diffusion Coeff of Solute in Shrunken
hydrogel
Dcsw = 0.0000009 !DH=3.76*10-7, Diffusion coefficient of
solute from swollen hydrogel, Dcsw=9.0E-07 cm2/s,as H=0.42

!$$$$$$ Define Initial conditions in depot
Do i = 1, nd
B(i) = Bd
C(i) = 0    ! M
Ccsat(i)= Csh
Dc(i) = Dcsh   ! cm2/s
Dg(i) = Dgsh   ! cm2/s
F(i) = Fd
G(i) = 0    ! M
h(i) = hsh    ! cm
!Hc(i) = Hcd
Hg(i) = Hgd
End Do
```

```
!$$$$$$ Define Initial conditions at boundaries after last
node
B(nd+1) = 0     ! M
C(nd+1) = 0     ! M
Dc(nd+1) = 0     ! cm2/s
Dg(nd+1) = 0     ! cm2/s
F(nd+1) = 0     ! M
G(nd+1) = 0     ! M
h(nd+1) = hsh     ! cm
!Hc(nd+1) = Hcd
Hg(nd+1) = Hgd
!$$$$$$ Initialize t, Qc, x2,x3,x4,Qc1,Qg to zero
t = 0
Qc = 0 ! mg
x3=0
x4=0
Qc1=0
!Qg =0
!$$$$$$ Define initial conditions at 1st node
B(1) = 0     ! M
C(1) = 0     ! M
Dc(1) = Dcsw     ! cm2/s
Dg(1) = Dgsw     ! cm2/s
!Hc(1) = Hcd
Hg(1) = Hgd
F(1) = 0     ! M
G(1) = Cgup*Hg(1)     ! M
h(1) = hsw     ! cm

Do j = 1,m !j=1,m Main timestep loop starts here


! ACID! Calculate mass transport of acid in depot layer by
first calculating flux from i to i+1
Do i = 1,nd  ! Note that flux from last barrier layer is
also needed
jg(i) = ((Dg(i)+Dg(i+1))/2)*(G(i)-G(i+1))/h(i)
End Do

! ACID! Once all fluxes are calculated,determine change in
node concentration using Backward finite difference
approximation
Do i = 2, nd  ! Note that change in concentrations has
already been calculated for last barrier node
delg(i) = (jg(i-1)-jg(i))*delt/h(i)
End Do
```

```
! SOLUTE ! Calculate mass transport in depot layer by first
calculating flux from i to i+1
Do i = 2,nd  ! Note that flux from last barrier layer is
also needed
jc(i) = ((Dc(i-1)+Dc(i))/2)*(C(i-1)-C(i))/h(i)
End Do
jc(nd+1)=0

! SOLUTE ! Once all fluxes are calculated,determine change
in node concentration using Backward finite difference
approximation
Do i = 2, nd  ! Note that change in concentrations has
already been calculated for last barrier node
delc(i) = (jc(i)-jc(i+1))*delt/h(i)
End Do


! Change node concentrations in depot layer
Do i  = 2, nd
G(i) = G(i) + delg(i)
C(i) = C(i) + delc(i)


! Consume scavenger before dissolving solute, in case this
changes Csat of a node
If (F(i).gt.0) then
If (G(i).gt.F(i)) then
G(i) = G(i)-F(i)
write(6,*)'i F(i) t(h) ',i,F(i),j*delt/3600
F(i) = 0
Ccsat(i) = Csw
B(i)=B(i)-Ccsat(i)+C(i)/s
C(i)=Ccsat(i)
Dc(i) = Dcsw
Dg(i) = Dgsw
h(i) = hsw
Elseif (G(i).gt.0) then
F(i)=F(i)-G(i)
G(i) = 0
End If
End If

!Dissolve solid
Cdiff(i) = Ccsat(i) - C(i)
If (B(i).gt.0) then
If (Cdiff(i).gt.0) then
If (B(i).gt.Cdiff(i)) then
```

```
B(i) = B(i)-Cdiff(i)
C(i) = Ccsat(i)
Else
C(i) = Ccsat(i) - Cdiff(i) + B(i)
B(i) = 0
End If
End If
End If
End Do

!Maintain impermeable boundary condition on inner boundary
C(nd+1) = C(nd)
G(nd+1) = G(nd)

!!! IF DELAMINATION OCCURS
If (F(nd/10).le.0)then
G(nd)=Cgup*Hg(nd)
F(nd)=0
Dg(nd)=Dgsw
Dc(nd)=Dcsw
h(nd)=hsw
Dg(nd+1)=Dgsw
Dc(nd+1)=Dcsw
x3=(C(1)+B(1))*A*h(1)*373.9!solute left in node nb+1
x4=(C(nd)+B(nd))*A*h(nd)*373.9 !solute left in node nb+nd
C(1)=0
C(nd)=0
B(1)=0
B(nd)=0
Endif

!Cumulative Release of solute at node 1!
Qc1= Dc(1)*(C(2)-C(1))*delt/h(1) *373.9*A ! release at node
1 before delamination and after delamination
Qc = Qc + Qc1 +x3+x4 ! Cumulative release including
combined solute release before and after delamination
t=t+delt

!$$$$$$ Write results for cumulative solute release Qc vs
time
if(Mod(j,15000).lt.0.001)then
write(3,*)'t(h) Qc ',t/3600,Qc
write(7,*)'x3 x4 t(h) ',x3,x4,t/3600
EndIf

End Do !! j=1,m Main loop ends here
```

```
!$$$$$$ Write C,B,G,F, Dc,Dg at each node at the end of m
number of timesteps!
Do i=1,nd+1

write(4,*)'i,C,B,Dc',i,C(i),B(i),Dc(i)
write(5,*)'i,G,F,Dg',i,G(i),F(i),Dg(i)
EndDo
End
```

APPENDIX D CODE FOR DELAMAINATING BMPR SYSTEM WITH BILAYER BARRIERS

Example code for delaminating BMPR system containing bilayer barriers

```
!Demo Code for SG05-86 Bilayer, Pulse_2
Program Main
Integer i,j,m,tmax,nb,nd
Real*8 Cgup, Ccsat(500),t,delt,Qc,Fb,B1,Bd,Fd,tb,
tdsh,tdsw, d, A,Qc1,x2,x3,x4,s,Hgb,Hgd,Hcb,Hcd !Qg
Real*8 B(500), C(500), Dc(500), Dg(500), F(500),G(500),
Dcsw,Dgsw, Dcsh, Dgsh,hb,hsh,hsw, Dcb,Dgb
Real*8 h(500), Hc(500),
Hg(500),jc(500),jg(500),delc(500),delg(500)
Real*8 d2cdx2(500),d2gdx2(500),Cdiff(500)
Open (3,File='tQ.txt')
Open (4,File='CBi.txt')
Open (5,File='GFi.txt')
Open (6,File='node_t.txt')
Open (7,File='x2 x3 x4.txt')

!!! Trial : SG05-86 Bilayer, Pulse_2!!!
!$$$$$$ Input Time, Timesteps and Total Number of Timesteps
tmax = 12*60*60! seconds
delt = 0.0004! seconds
m = tmax/delt


!$$$$$$ Input Physical Parameters
d=1.41 !cm
A=3.14/4*d*d

!$$$$$$ Define node number and node thicknesses for barrier
and depot
nb=60!barrier nodes
nd=120!depot nodes
tb=227!microns barrier thickness
tdsh=145!microns depot thickness shrunken
s=2!swelling ratio of depot in 1D
tdsw=tdsh*s    !microns depot thickness swollen
hb = tb*0.0001/nb     !cm thickness of each node in barrier
hsh = tdsh*0.0001/nd  !cm thickness of each node in depot
hsw = tdsw*0.0001/nd  !cm thickness of each node in swollen
depot
```

```
!$$$$$$ Input scavenger concentrations in barrier and depot
Fb = 2*3.344 !Equivalen molar concentration of [H+]
required to consume X% ZnO PVA,!ZnO + 2HCl= H20+ZnCl2
!X%(w/w)ZnO (Fb, equivalent molar [H+]):
!10%(1.587), 20%(3.531), 30%(5.967),40% (9.111),
50%(13.322), 60%(19.255),70%(28.239),80% (43.44)

Fd = 2.33 ! Equivalent scavenger concentration of DMA in
Depot, R3N + HCl -----> [(R3NH)+Cl-],
!28% DMA in 72/28 pMMA/DMA is equal to  2.735 M,
!(85% consumption based on titratoin, = 2.735* 0.85 = 2.33
M)

!$$$$$    Input Partition Coefficient
Hgb=0.6 ! Partition coefficient of acid in PVA
Hgd=1     ! Partition coefficient of acid in p(MMA/DMA)
Hcb=0.6 ! Partition coefficient of dissolved solute (dye)
in PVA
Hcd=0.4 ! Partition coefficient of dissolved solute (dye)
in p(MMA/DMA)

!$$$$$$ Input stimulant concentrations and diffusion
coefficeint in barrier and depot
Cgup = 0.0010965   ! M, upstream pH = 2.96
Dgb= 0.000025 ! DH = 1.51*10-5, diffusion of acid through
PVA,  D =2.5E-5 cm2/s, as H=0.6
Dgsh = 0!cm2/s Diffusion Coeff of acid in shrunken hydrogel
Dgsw = 0.000051!DH= 5.1*10-5, Diffusion coeff of acid in
swollen hydrogel, Dgsw =5.1E-05 cm2/s as H=1
!based on pH3-pH4 diaphragm cell trial, DH=5.09E-5,
assuming H=1

!$$$$$$ Input solute concentrations and diffusion
coefficients in barrier and depot
B1 = 0.228 ! solid solute M, actual dye concentration in
dry p(MMA/DMA)
!Concentration of 5% Methylene Blue in 72/28 MMA/DMA 0.145
M
!Concentration of 5% Methyl Orange in 72/28 MMA/DMA 0.166 M
Bd = B1/s ! solid solute M, Equivalent solute distributed
in swollen hydrogel
Csh = 0 ! Saturation concentration of solute (dye) in
shrunken state (zero)
Csw = 0.0059/4 ! Saturation concetration of dissolved
solute M, MB (0.0059), MO (0.0011)
Dcb= 0.0000006 ! DH=3.57*10-7, diffusion coeff of solute
through PVA, Dcb=6.0E-07 cm2/s,,H=0.6
```

```
Dcsh = 0!cm2/s Diffusion Coeff of Solute in Shrunken
hydrogel
Dcsw = 0.0000009 !DH=3.76*10-7, Diffusion coefficient of
solute from swollen hydrogel, Dcsw=9.0E-07 cm2/s,as H=0.42

!$$$$$$ Define Initial conditions in barrier
Do i = 1, nb

B(i) = 0    ! M
C(i) = 0    ! M
Dc(i) =   Dcb ! cm2/s
Dg(i) =   Dgb ! cm2/s
!F(i) = Fb separate loop for bilayer
G(i) = 0   ! M
h(i) = hb    ! cm
Hc(i) = Hcb
Hg(i) = Hgb
Ccsat(i)=Csh
End Do

Do i= 2, 25
F(i)= Fb*25/24
End do
Do i=26,nb
F(i)=0
End do

!$$$$$$ Define Initial conditions in depot
Do i = nb+1, nb+nd

B(i) = Bd
C(i) = 0    ! M
Ccsat(i)= Csh
Dc(i) = Dcsh   ! cm2/s
Dg(i) = Dgsh   ! cm2/s
F(i) = Fd
G(i) = 0    ! M
h(i) = hsh    ! cm
Hc(i) = Hcd
Hg(i) = Hgd
End Do
!$$$$$$ Define Initial conditions at boundaries after last
node
B(nb+nd+1) = 0    ! M
C(nb+nd+1) = 0    ! M
Dc(nb+nd+1) = 0    ! cm2/s
Dg(nb+nd+1) = 0    ! cm2/s
```

```
F(nb+nd+1) = 0    ! M
G(nb+nd+1) = 0    ! M
h(nb+nd+1) = hsh    ! cm
Hc(nb+nd+1) = Hcd
Hg(nb+nd+1) = Hgd
!$$$$$$ Initialize t, Qc, x2,x3,x4,Qc1,Qg to zero
t = 0
Qc = 0 ! mg
x2=0
x3=0
x4=0
Qc1=0
!Qg =0
!$$$$$$ Define initial conditions at 1st node
B(1) = 0    ! M
C(1) = 0    ! M
Dc(1) = Dcb    ! cm2/s
Dg(1) = Dgb    ! cm2/s
Hc(1) = Hcb
Hg(1) = Hgb
F(1) = 0    ! M
G(1) = Cgup*Hg(1)    ! M
h(1) = hb    ! cm

Do j = 1,m !j=1,m Main timestep loop starts here

! ACID & SOLUTE in BARRIER! Calculate mass transport in
barrier layer using centered finite difference
approximation
Do i = 2, nb-1 !From node 2 to 2nd last node of 1st
barrier!
!Acid!
d2gdx2(i)=(G(i-1) - 2*G(i) + G(i+1))/(h(i)*h(i))
delg(i)= Dg(i)* d2gdx2(i)*delt
!Solute!
d2cdx2(i)=(C(i-1)- 2*C(i)+ C(i+1))/(h(i)*h(i))
delc(i)= Dc(i)*d2cdx2(i)*delt
End Do

!ACID and SOLUTE in last node of barrier and first node of
depot

d2gdx2(nb)=(G(nb-1)-
2*G(nb)+(Hg(nb)/Hg(nb+1))*G(nb+1))/(h(nb)*h(nb+1))
delg(nb)= Dg(nb)*d2gdx2(nb)*delt
jg(nb-1) = Dg(nb-1)*(G(nb-1)-G(nb))/h(nb-1)
jg(nb)=jg(nb-1)-delg(nb)*h(nb)/delt
```

```
d2cdx2(nb)=(C(nb-1)-
2*C(nb)+(Hc(nb)/Hc(nb+1))*C(nb+1))/(h(nb)*h(nb+1))
delc(nb)= Dc(nb)*d2cdx2(nb)*delt
jc(nb)= Dc(nb)*(C(nb-1)-C(nb))/h(nb)
jc(nb+1) = jc(nb)-delc(nb)*h(nb)/delt

! ACID! Calculate mass transport of acid in depot layer by
first calculating flux from i to i+1
Do i = nb+1,nb+nd  ! Note that flux from last barrier layer
is also needed
jg(i) = ((Dg(i)+Dg(i+1))/2)*(G(i)-G(i+1))/h(i)
End Do

! ACID! Once all fluxes are calculated,determine change in
node concentration using Backward finite difference
approximation
Do i = nb+1, nb+nd  ! Note that change in concentrations
has already been calculated for last barrier node
delg(i) = (jg(i-1)-jg(i))*delt/h(i)
End Do

! SOLUTE ! Calculate mass transport in depot layer by first
calculating flux from i to i+1
Do i = nb+2,nb+nd  ! Note that flux from last barrier layer
is also needed
jc(i) = ((Dc(i-1)+Dc(i))/2)*(C(i-1)-C(i))/h(i)
End Do
jc(nb+nd+1)=0

! SOLUTE ! Once all fluxes are calculated,determine change
in node concentration using Backward finite difference
approximation
Do i = nb+1, nb+nd  ! Note that change in concentrations
has already been calculated for last barrier node
delc(i) = (jc(i)-jc(i+1))*delt/h(i)
End Do

! Change node concentrations in barrier layer
Do i = 2, nb
G(i) = G(i) + delg(i)
C(i) = C(i) + delc(i)

! Consume scavenger
If (F(i).gt.0) then
If (G(i).gt.F(i)) then
G(i) = G(i)-F(i)
```

```
write(6,*)'i F(i) t(h) ',i,F(i),j*delt/3600
F(i) = 0
Elseif (G(i).gt.0) then
F(i) = F(i)-G(i)
G(i) = 0
End If
End If
End Do

! Change node concentrations in depot layer
Do i  = nb+1, nb+nd
G(i) = G(i) + delg(i)
C(i) = C(i) + delc(i)

! Consume scavenger before dissolving solute, in case this
changes Csat of a node
If (F(i).gt.0) then
If (G(i).gt.F(i)) then
G(i) = G(i)-F(i)
write(6,*)'i F(i) t(h) ',i,F(i),j*delt/3600
F(i) = 0
Ccsat(i) = Csw
B(i)=B(i)-Ccsat(i)+C(i)/s
C(i)=Ccsat(i)
Dc(i) = Dcsw
Dg(i) = Dgsw
h(i) = hsw
Elseif (G(i).gt.0) then
F(i)=F(i)-G(i)
G(i) = 0
End If
End If

!Dissolve solid
Cdiff(i) = Ccsat(i) - C(i)
If (B(i).gt.0) then
If (Cdiff(i).gt.0) then
If (B(i).gt.Cdiff(i)) then
B(i) = B(i)-Cdiff(i)
C(i) = Ccsat(i)
Else
C(i) = Ccsat(i) - Cdiff(i) + B(i)
B(i) = 0
End If
End If
End If
End Do
```

```
!Maintain impermeable boundary condition on inner boundary
C(nb+nd+1) = C(nb+nd)
G(nb+nd+1) = G(nb+nd)

!!! IF DELAMINATION OCCURS
If (F(nb+ nd/10).le.0)then
G(nb+1)=Cgup*Hg(nb+1)
G(nb+nd)=Cgup*Hg(nb+nd)
F(nb+1)=0
F(nb+nd)=0
Dg(nb+1)=Dgsw
Dg(nb+nd)=Dgsw
Dc(nb+1)=Dcsw
Dc(nb+nd)=Dcsw
h(nb+1)=hsw
h(nb+nd)=hsw
Dg(nb+nd+1)=Dgsw
Dc(nb+nd+1)=Dcsw

x2=(C(nb)+B(nb))*A*h(nb)*373.9 !solute left in node nb
x3=(C(nb+1)+B(nb+1))*A*h(nb+1)*373.9!solute left in node
nb+1
x4=(C(nb+nd)+B(nb+nd))*A*h(nb+nd)*373.9 !solute left in
node nb+nd

C(nb)=0
C(nb+1)=0
C(nb+nd)=0
B(nb)=0
B(nb+1)=0
B(nb+nd)=0
Endif

!Cumulative Release of solute at node 1!
Qc1= Dc(1)*(C(2)-C(1))*delt/h(1) *373.9*A ! release at node
1 before delamination and after delamination
Qc = Qc + Qc1 + x2+x3+x4 ! Cumulative release including
combined solute release before and after delamination
!Calculate cumulative influx of acid
!Qg = Qg + Dg(1)*(G(1)-G(2))*delt/h(1)!
t=t+delt

!$$$$$$ Write results for cumulative solute release Qc vs
time
if(Mod(j,15000).lt.0.001)then
write(3,*)'t(h) Qc ',t/3600,Qc
write(7,*)'x2 x3 x4 t(h) ',x2,x3,x4,t/3600
```

```
EndIf

End Do !! j=1,m Main loop ends here

!$$$$$$ Write C,B,G,F, Dc,Dg at each node at the end of m
number of timesteps!
Do i=1,nb+nd+1

write(4,*)'i,C,B,Dc',i,C(i),B(i),Dc(i)
write(5,*)'i,G,F,Dg',i,G(i),F(i),Dg(i)
EndDo
End
```

APPENDIX E CODE FOR 2-PULSE NON-DELAMINATING BMPR SYSTEM

Example code for 2-pulse non-delaminating BMPR system

```
Program Main
Integer i,j,m,tmax
Integer nb,nd,nb2,nd2,N1,N1b,N2
Real*8    tb,tdsh,tdsw,tb2,tdsh2,tdsw2
Real*8 Cgup, Ccsat(1000),t,delt,Qc,Qg,Fb,Fb2,Bd,Fd, d,
A,Qc1,s,s2
Real*8 B(1000), C(1000), Dc(1000), Dg(1000),
F(1000),G(1000), Dcsw,Dgsw, Dcsh, Dgsh,hb,hsh,hsw, Dcb,Dgb
Real*8 h(1000), Hc(1000),
Hg(1000),jc(1000),jg(1000),delc(1000),delg(1000)
Real*8 d2cdx2(1000),d2gdx2(1000),Cdiff(1000)
Open (3,File='tQ.txt')
Open (4,File='CBi.txt')
Open (5,File='GFi.txt')
Open (8,File='node_t.txt')

!$$$$$$ Input Time, Timesteps and Total Number of Timesteps
tmax = 48*60*60! seconds
delt = 0.001 ! seconds
m = tmax/delt

!$$$$$$ Input Physical Parameters
s=2!swelling ratio of depot-1 in 1D
s2=s ! swelling ratio of depot-2 in 1D
d=1 !cm
A=3.14/4*d*d

!$$$$$$ Define node number and node thicknesses for 1st
barrier and 1st depot
nb=20!barrier nodes
nd=40!depot nodes
tb=72!microns barrier thickness
tdsh=75!microns depot thickness shrunken
tdsw=tdsh*s    !microns depot thickness swollen
hb = tb*0.0001/nb     !cm thickness of each node in barrier
hsh = tdsh*0.0001/nd  !cm thickness of each node in depot
hsw = tdsw*0.0001/nd  !cm thickness of each node in swollen
depot
```

```
!$$$$$$ Define node number and node thicknesses for 2nd
barrier and 2nd depot
nb2=20!barrier nodes
nd2=40!depot nodes
tb2=66!microns barrier thickness
tdsh2=73!microns depot thickness shrunken
tdsw2=tdsh2*s2 !microns depot thickness swollen
hb2 = tb2*0.0001/nb2     !cm thickness of each node in
barrier
hsh2 = tdsh2*0.0001/nd2  !cm thickness of each node in
depot
hsw2 = tdsw2*0.0001/nd2  !cm thickness of each node in
swollen depot

!! Ease of node-numbering for multilayer combination
N1=nb+nd
N1b=N1+nb2
N2=N1+nb2+nd2

!$$$$$$ Input scavenger concentrations in barrier and depot
!Fb= Equivalen molar concentration of [H+] required to
consume X% ZnO PVA,!ZnO + 2HCl= H20+ZnCl2
!X%(w/w)ZnO (Fb, equivalent molar [H+]): !10%(1.587),
20%(3.531), 30%(5.967),40% (9.111), 50%(13.322),
60%(19.255),70%(28.239),80% (43.44)
Fb = 1.587 !
Fb = Fb*nb/(nb-1) ! molar concentration of ZnO in 1st
barrier divided in rest of the nodes except 1st node

Fb2= 1.587 !molar concentration of X% ZnO in hydrated
Barrier-2
Fb2= Fb2*nb2/(nb2-1)

Fd = 2.33 !28% DMA, 2.33 M, (85% consumption based on
titratoin,assume delamination occurs at when 15% DMA is
consumed), 2.33 M

!$$$$$    Input Partition Coefficient
Hgb=0.6 ! Partition coefficient of acid in PVA
Hgd=1     ! Partition coefficient of acid in p(MMA/DMA)
Hcb=0.6 ! Partition coefficient of dissolved solute (dye)
in PVA
Hcd=0.4 ! Partition coefficient of dissolved solute (dye)
in p(MMA/DMA)

!$$$$$$ Input stimulant concentrations and diffusion
coefficient in barrier and depot
```

```
Cgup = 0.001   ! M (0.001 for pH 3)
Dgb= 0.000025 ! 2.5*10-5 cm2/s diffusion of acid through
PVA, DH=1.5E-5 cm2/s, Hcb=0.6
Dgsh = 0!cm2/s Diffusion Coeff of acid in shrunken hydrogel
Dgsw = 0.000051!5.1*10-5 cm2/s Diffusion coeff of acid in
swollen hydrogel, DH=5.1E-5, Hgd=1

!$$$$$$ Input solute concentrations and diffusion
coefficients in barrier and depot
Bd = 0.145 !Solid solute M, Concentration of 5% MB in 72/28
MMA/DMA is 0.145, Redistribute in shrunken depot nodes as
B(i)= Bd/s while initilazing depot nodes
Csh = 0 ! Dissolved solute in shrunken depot is zero M
Csw = 0.0059/4 ! Dissolved solute M,Experimental MB
saturation concentration = 0.0059, assumed to be 4 times
lower when immobilized in depot
Dcb= 0.0000006 ! 6*10-7 cm2/s diffusion coeff of solute
through PVA, DH=3.6E-7. H=0.6
Dcsh = 0!cm2/s Diffusion Coeff of Solute in Shrunken
hydrogel
Dcsw = 0.0000009 !9*10-7 cm2/s Diffusion coeff of solute
from swollen hydrogel, DH=3.76E-7, H=0.4

!$$$$$$ Define Initial conditions in 1st barrier
Do i = 1, nb
B(i) = 0    ! M
C(i) = 0    ! M
Dc(i) =  Dcb ! cm2/s
Dg(i) =  Dgb ! cm2/s
F(i) = Fb
G(i) = 0   ! M
h(i) = hb    ! cm
Hc(i) = Hcb
Hg(i) = Hgb
Ccsat(i)=Csh
End Do

!$$$$$$ Define Initial conditions in 2nd barrier
Do i = N1+1, N1+nb2

B(i) = 0    ! M
C(i) = 0    ! M
Dc(i) =   Dcb ! cm2/s
Dg(i) =   Dgb ! cm2/s
F(i) = Fb2
G(i) = 0   ! M
h(i) = hb2    ! cm
```

```
Hc(i) = Hcb
Hg(i) = Hgb
Ccsat(i)=Csh
End Do
!$$$$$$ Define Initial conditions in 1st Depot
Do i = nb+1, N1

B(i) = Bd/s ! redistributing the total solid solute in
shrunken depot-1 with corresponding swelling factor
C(i) = 0    ! M
Ccsat(i)= Csh
Dc(i) = Dcsh   ! cm2/s
Dg(i) = Dgsh   ! cm2/s
F(i) = Fd
G(i) = 0    ! M
h(i) = hsh    ! cm
Hc(i) = Hcd
Hg(i) = Hgd
End Do

!$$$$$$ Define Initial conditions in 2nd Depot
Do i = N1b+1, N2

B(i) = Bd/s2 !redistributing the total solid solute in
shrunken depot-2 with corresponding swelling factor
C(i) = 0    ! M
Ccsat(i)= Csh
Dc(i) = Dcsh   ! cm2/s
Dg(i) = Dgsh   ! cm2/s
F(i) = Fd
G(i) = 0    ! M
h(i) = hsh2    ! cm
Hc(i) = Hcd
Hg(i) = Hgd
End Do

!$$$$$$ Initialize t, Qc,Qg to zero
t = 0
Qc = 0
Qg =0

!$$$$$$ Define initial conditions at 1st node of 1st
barrier
B(1) = 0    ! M
C(1) = 0    ! M
Dc(1) = Dcb    ! cm2/s
Dg(1) = Dgb    ! cm2/s
```

```
Hc(1) = Hcb
Hg(1) = Hgb
F(1) = 0    ! M
G(1) = Cgup*Hg(1)    ! M
h(1) = hb    ! cm

!$$$$$$ Intialize 1st node of all the barriers to zero to
Divide scavenger evenly corresponding barrier
F(N1+1)=0

!$$$$$$ Define Initial conditions at boundaries after last
node
B(N2+1) = 0    ! M
C(N2+1) = 0    ! M
Dc(N2+1) = 0    ! cm2/s
Dg(N2+1) = 0    ! cm2/s
F(N2+1) = 0    ! M
G(N2+1) = 0    ! M
h(N2+1) = hsh2    ! cm
Hc(N2+1) = Hcd
Hg(N2+1) = Hgd

!$$$$ MAIN LOOP $$$$$
Do j = 1,m

!Barrier-1, Acid & Solid-solute transport using Centered
Finte Difference(CFD)
Do i = 2, nb-1 !From node 2 to 2nd last node of 1st
barrier!
!Acid!
d2gdx2(i)=(G(i-1) - 2*G(i) + G(i+1))/(h(i)*h(i))
delg(i)= Dg(i)* d2gdx2(i)*delt
!Solute!
d2cdx2(i)=(C(i-1)- 2*C(i)+ C(i+1))/(h(i)*h(i))
delc(i)= Dc(i)*d2cdx2(i)*delt
End Do
!Acid in last node of Barrier-1
d2gdx2(nb)=(G(nb-1)-
2*G(nb)+(Hg(nb)/Hg(nb+1))*G(nb+1))/(h(nb)*h(nb+1))
delg(nb)= Dg(nb)*d2gdx2(nb)*delt

!Solute in last node of Barrier-1
d2cdx2(nb)=(C(nb-1)-
2*C(nb)+(Hc(nb)/Hc(nb+1))*C(nb+1))/(h(nb)*h(nb+1))
delc(nb)= Dc(nb)*d2cdx2(nb)*delt

!BARRIER-2, Acid & Solid-solute transport using CFD
```

```
!ACID IN 1ST node of Barrier-2
d2gdx2(N1+1)=(G(N1)*(Hg(N1+1)/Hg(N1))-
2*G(N1+1)+G(N1+2))/(h(N1)*h(N1+1))
delg(N1+1)= Dg(N1+1)*d2gdx2(N1+1)*delt
jg(N1+1)=Dg(N1+1)*(G(N1+1)-G(N1+2))/h(N1+1)!This flux will
be needed to link flux between Depot-1 and Barrier-2

!SOLUTE IN 1ST node Barrier-2
d2cdx2(N1+1)=(C(N1)*(Hc(N1+1)/Hc(N1))-
2*C(N1+1)+C(N1+2))/(h(N1)*h(N1+1))
delc(N1+1)= Dc(N1+1)*d2cdx2(N1+1)*delt
jc(N1+2)=Dc(N1+2)*(C(N1+1)-C(N1+2))/h(N1+2)!!This flux will
be needed to link flux between Depot-1 and Barrier-2

!Acid & solute transport from 2nd node to second last node
of Barrier-2
Do i = N1+2, N1b-1 !From node 2 to 2nd last node of 1st
barrier!
!Acid!
d2gdx2(i)=(G(i-1) - 2*G(i) + G(i+1))/(h(i)*h(i))
delg(i)= Dg(i)* d2gdx2(i)*delt
!Solute!
d2cdx2(i)=(C(i-1)- 2*C(i)+ C(i+1))/(h(i)*h(i))
delc(i)= Dc(i)*d2cdx2(i)*delt
End Do
!Acid transport in last node of Barrier-2
d2gdx2(N1b)=(G(N1b-1)-
2*G(N1b)+(Hg(N1b)/Hg(N1b+1))*G(N1b+1))/(h(N1b)*h(N1b+1))
delg(N1b)= Dg(N1b)*d2gdx2(N1b)*delt

!Solute transport in last node of Barrier-2
d2cdx2(N1b)=(C(N1b-1)-
2*C(N1b)+(Hc(N1b)/Hc(N1b+1))*C(N1b+1))/(h(N1b)*h(N1b+1))
delc(N1b)= Dc(N1b)*d2cdx2(N1b)*delt

!DEPOT-1, ACID & SOLUTE TRANSPORT

!Acid transport using Fick's First law to calcualte flux
and Backward-Finite Diffrence to calcualate delg
!Acid fluxes from barrier-1 will be needed to link with
Depot-1, to calculate delg(i) in depot nodes
jg(nb-1) = Dg(nb-1)*(G(nb-1)-G(nb))/h(nb-1)
jg(nb)=jg(nb-1)-delg(nb)*h(nb)/delt ! This flux is linked
from Barrier-1 to Depot-1

! ACID! Calculate fluxes in Depot-1 using Fick's First law
```

```
Do i = nb+1,N1-1
jg(i) = ((Dg(i)+Dg(i+1))/2)*(G(i)-G(i+1))/h(i)
End Do
jg(N1)= delg(N1+1)*h(N1+1)/delt + jg(N1+1)
!This flux from the last node of  Depot-1 is linked with
Barrier-2 to calcualte delg(N1)

! ACID! Once all fluxes are calculated,determine change in
node concentration using Backward-Finite difference
Do i = nb+1, N1  ! Note that change in concentrations has
already been calculated for last barrier node
delg(i) = (jg(i-1)-jg(i))*delt/h(i)
End Do

!Solute transport using Fick's First law & Forward-Finite
Difference to caclulate delc
!Flux coming from last node of barrier-1 is linked to the
1st node of depot-1
!solute fluxes from Barrier-1 will be needed to link the
flux from Depot-1 to Barrier-1
jc(nb)= Dc(nb)*(C(nb-1)-C(nb))/h(nb)
jc(nb+1) = jc(nb)-delc(nb)*h(nb)/delt !This flux is linked
between Barrier-1 and Depot-1

! SOLUTE! Calculate flux in rest of the nodes in depot-1
layer using Fick's First Law
Do i = nb+2,N1
jc(i) = ((Dc(i-1)+Dc(i))/2)*(C(i-1)-C(i))/h(i)
End Do
jc(N1+1)= delc(N1+1)*h(N1+1)/delt + jc(N1+2)
!This Flux from last node of the Depot-1 layer is linked
with Barrier-2 and will be used to calculate delc(N1)

! SOLUTE ! Once all fluxes are calculated,determine change
in node concentration using Forward-Finite difference
Do i = nb+1, N1  ! Note that change in concentrations has
already been calculated for last barrier node
delc(i) = (jc(i)-jc(i+1))*delt/h(i)
End Do

!DEPOT-2, ACID & SOLUTE CALCULATIONS (LAST DEOPOT in this
case, as 2-pulse code)
!ACID
!Acid fluxes from barrier-2, that will be needed to link
with Depot-2
jg(N1b-1) = Dg(N1b-1)*(G(N1b-1)-G(N1b))/h(N1b-1)
```

```
jg(N1b)=jg(N1b-1)-delg(N1b)*h(N1b)/delt ! This flux is
linked between barrier-2 and depot-2

! ACID! Calculate flux in depot-2 layer using Fick's First
law
Do i = N1b+1,N2
jg(i) = ((Dg(i)+Dg(i+1))/2)*(G(i)-G(i+1))/h(i)
End Do
! ACID! Once all fluxes are calculated,determine change in
node concentration using Backward finite difference
approximation
Do i = N1b+1, N2  ! Note that change in concentrations has
already been calculated for last barrier node
delg(i) = (jg(i-1)-jg(i))*delt/h(i)
End Do

!SOLUTE CALCULATIONS
!solute flux from barrier barrier to depot
jc(N1b)= Dc(N1b)*(C(N1b-1)-C(N1b))/h(N1b)
jc(N1b+1) = jc(N1b)-delc(N1b)*h(N1b)/delt ! Note that flux
from last barrier layer is also needed
! SOLUTE ! Calculate mass transport in depot layer
Do i = N1b+2,N2
jc(i) = ((Dc(i-1)+Dc(i))/2)*(C(i-1)-C(i))/h(i)
End Do
jc(N2+1)=0
! SOLUTE ! Once all fluxes are calculated,determine change
in node concentration using Backward finite difference
approximation
Do i = N1b+1, N2  ! Note that change in concentrations has
already been calculated for last barrier node
delc(i) = (jc(i)-jc(i+1))*delt/h(i)
End Do

!!CHANGE IN CONCENCTRATIONS!!
Do i = 2, N2
G(i) = G(i) + delg(i)
C(i) = C(i) + delc(i)
End Do

!@@@@@@@@@@@@@@@@@@@@-----PULSE-1---@@@@@@@@@@@@@@@@@@@@

!Barrier-1
Do i = 2, nb
! Consume scavenger
If (F(i).gt.0) then
If (G(i).gt.F(i)) then
```

```
G(i) = G(i)-F(i)
write(8,*)'i F(i) t(h) ',i,F(i),j*delt/3600
F(i) = 0
Elseif (G(i).gt.0) then
F(i) = F(i)-G(i)
G(i) = 0
End If
End If
End Do

!Depot-1
Do i  = nb+1, nb+nd
! Consume scavenger before dissolving solute, in case this
changes Csat of a node
If (F(i).gt.0) then
If (G(i).gt.F(i)) then
G(i) = G(i)-F(i)
write(8,*)'i F(i) t(h) ',i,F(i),j*delt/3600
F(i) = 0
Ccsat(i) = Csw
B(i)=B(i)-Ccsat(i)+C(i)/s
C(i)=Ccsat(i)
Dc(i) = Dcsw
Dg(i) = Dgsw
h(i) = hsw
Elseif (G(i).gt.0) then
F(i)=F(i)-G(i)
G(i) = 0
End If
End If

!Dissolve solid
Cdiff(i) = Ccsat(i) - C(i)
If (B(i).gt.0) then
If (Cdiff(i).gt.0) then
If (B(i).gt.Cdiff(i)) then
B(i) = B(i)-Cdiff(i)
C(i) = Ccsat(i)
Else
C(i) = Ccsat(i) - Cdiff(i) + B(i)
B(i) = 0
End If
End If
End If
End Do

!@@@@@@@@@@---PULSE-1 LOOP END----@@@@@@@@@@@@@@@@@@@@@@
```

```
!@@@@@@@@@@@@@@@@@@@@----PULSE-2-------@@@@@@@@@@@@@@@@@@@@

!Barrier-2
Do i = N1+1, N1b
! Consume scavenger
If (F(i).gt.0) then
If (G(i).gt.F(i)) then
G(i) = G(i)-F(i)
write(8,*)'i F(i) t(h) ',i,F(i),j*delt/3600
F(i) = 0
Elseif (G(i).gt.0) then
F(i) = F(i)-G(i)
G(i) = 0
End If
End If
End Do


!Depot-2
Do i  = N1b+1, N2
! Consume scavenger before dissolving solute, in case this
changes Csat of a node
If (F(i).gt.0) then
If (G(i).gt.F(i)) then
G(i) = G(i)-F(i)
write(8,*)'i F(i) t(h) ',i,F(i),j*delt/3600
F(i) = 0
Ccsat(i) = Csw
B(i)=B(i)-Ccsat(i)+C(i)/s2
C(i)=Ccsat(i)
Dc(i) = Dcsw
Dg(i) = Dgsw
h(i) = hsw2
Elseif (G(i).gt.0) then
F(i)=F(i)-G(i)
G(i) = 0
End If
End If

!Dissolve solid
Cdiff(i) = Ccsat(i) - C(i)
If (B(i).gt.0) then
If (Cdiff(i).gt.0) then
If (B(i).gt.Cdiff(i)) then
B(i) = B(i)-Cdiff(i)
```

```
C(i) = Ccsat(i)
Else
C(i) = Ccsat(i) - Cdiff(i) + B(i)
B(i) = 0
End If
End If
End If
End Do

!@@@@@@@@@@@@@@@@@@---PULSE-2 LOOP END---@@@@@@@@@@@@@@@@@@

!Maintain impermeable boundary condition on inner boundary
C(N2+1) = C(N2)
G(N2+1) = G(N2)

!Cumulative Release of solute at node 1!
Qc1= Dc(1)*(C(2)-C(1))*delt/h(1) *373.9*A ! release at node
1 before delamination and after delamination
Qc = Qc + Qc1
!Calculate cumulative influx of acid
Qg = Qg + Dg(1)*(G(1)-G(2))*delt/h(1)!
t=t+delt

!$$$$$$ Write results for cumulative solute release Qc and
cumulative influx Qg vs time
if(Mod(j,10000).lt.0.001)then
write(3,*)'t(h) Qc Qg',t/3600,Qc,Qg
EndIf
End Do

!$$$$$$ Write C,B,G,F, Dc,Dg at each node at the end of m
number of timesteps!
Do i=1,N2

write(4,*)'i,C,B,Dc',i,C(i),B(i),Dc(i)
write(5,*)'i,G,F,Dg',i,G(i),F(i),Dg(i)
EndDo
End
```

APPENDIX F CODE FOR 5-PULSE NON-DELAMINATING BMPR SYSTEM

Example code for 5-pulse non-delaminating BMPR system

```
Program Main
Integer i,j,m,tmax
Integer nb,nb2,nb3,nb4,nb5    ! Initialize Barrier Nodes
for each pulse
Integer nd,nd2,nd3,nd4,nd5    ! Initialize Depot Nodes for
each pulse
Integer N1,N2,N3,N4,N5        ! Initialize the total number
of barrier+depot nodes, For eg. nb+nd=N1
Integer N1b,N2b,N3b,N4b !Initialize Intermediate nodes as
combination of B+D+B. For eg. nb+nd+nb1=N1+nb1=N1b
Real*8    tb,tb2,tb3,tb4,tb5 ! Initialize barrier thickness
of each pulse
Real*8    hb,hb2,hb3,hb4,hb5  !Initialize each barrier node
thickness
Real*8    tdsh,tdsh2, tdsh3, tdsh4, tdsh5 ! Initialize
Depot thickness of each pulse in shrunken state
Real*8    hsh,hsh2,hsh3,hsh4,hsh5 ! Initialize each
shrunken depot node thickness
Real*8    s,s2,s3,s4,s5 ! Initialize swelling factor for
each depot
Real*8    tdsw,tdsw2, tdsw3, tdsw4, tdsw5    !  Initialize
Depot thickness of each pulse in swollen state
Real*8    hsw,hsw2,hsw3,hsw4,hsw5 ! Initialize each swollen
depot node thickness
Real*8    Cgup  ! Initialize upstream stimulant
concentration
Real*8    Fb,Fb2,Fb3,Fb4,Fb5 ! Initialize Scavenger
Concentration in each barrier
Real*8    Fd! Initialize Scavenger in Depot
Real*8    Bd,Bd2, Bd3, Bd4, Bd5,
Ccsat(1000),Ccsat2(1000),Ccsat3(1000),Ccsat4(1000),Ccsat5(1
000)
Real*8  M1,M2,M3,M4,M5 ! Molecular weight of each solute
g/mole
Real*8    t,delt,Qc,Qg,A,Qc1,Qc2,Qc3,Qc4,Qc5 ! Other
parameters, delt(timestep), t(time),Qc(cumulative solute
release),Qg(Cumulative acid),d(diameter),A(area)
Real*8    Dcb,Dgb,Dcsh,Dgsh,Dcsw,Dgsw ! Initialize
Diffusion Coefficients of stimulant and solute through
barrier and depot, C(solute), G(acid)
```

```
!Initialize Array Numbers () for each parameter that is
being used in transport calculations
Real*8 B(1000),B2(1000),B3(1000),B4(1000),B5(1000)
Real*8 C(1000),C2(1000),C3(1000),C4(1000),C5(1000)
Real*8 Dc(1000), Dg(1000), F(1000),G(1000)
Real*8 h(1000), Hc(1000),
Hg(1000),jc(1000),jg(1000),delc(1000),delg(1000)
Real*8 d2cdx2(1000),d2gdx2(1000),Cdiff(1000)
Real*8
d2c2dx2(1000),d2c3dx2(1000),d2c4dx2(1000),d2c5dx2(1000)
Real*8 Cdiff2(1000),Cdiff3(1000),Cdiff4(1000),Cdiff5(1000)
Real*8 delc2(1000),delc3(1000),delc4(1000),delc5(1000)
Real*8 jc2(1000),jc3(1000),jc4(1000),jc5(1000)

Open (3,File='tQ.txt')
Open (8,File='node_t.txt')
Open (4,File='GFi.txt')
Open (5,File='CBi.txt')
Open (6,File='C2B2i.txt')
Open (7,File='C3B3i.txt')
Open (9,File='C4B4i.txt')
Open (10,File='C5B5i.txt')



!$$$$$$ Input Time, Time-steps and Total Number of Time-
steps
tmax = 8*60*60! seconds
delt = 0.005 ! seconds
m = tmax/delt

!$$$$$$ Input Physical Parameters
s=2!swelling ratio of depot-1 in 1D
s2=s! swelling ratio of depot-2 in 1D
s3=s! swelling ratio of depot-3 in 1D
s4=s! swelling ratio of depot-4 in 1D
s5=s! swelling ratio of depot-5 in 1D

!d=1 !cm
A=1 ! cm2 unit area
M1=100! Molecular weight of solute1
M2=100! Molecular weight of solute2
M3=100! Molecular weight of solute3
M4=100! Molecular weight of solute4
M5=100! Molecular weight of solute5
```

```
!$$$$$$ Define node number and node thicknesses for 1st
barrier and 1st depot
nb=20!barrier nodes
nd=40!depot nodes
tb=100!microns barrier thickness
tdsh=100!microns depot thickness shrunken
tdsw=tdsh*s    !microns depot thickness swollen
hb = tb*0.0001/nb     !cm thickness of each node in barrier
hsh = tdsh*0.0001/nd  !cm thickness of each node in depot
hsw = tdsw*0.0001/nd  !cm thickness of each node in swollen
depot


!$$$$$$ Define node number and node thicknesses for 2nd
barrier and 2nd depot
nb2=20!barrier nodes
nd2=40!depot nodes
tb2=100!microns barrier thickness
tdsh2=100!microns depot thickness shrunken
tdsw2=tdsh2*s2 !microns depot thickness swollen
hb2 = tb2*0.0001/nb2     !cm thickness of each node in
barrier
hsh2 = tdsh2*0.0001/nd2  !cm thickness of each node in
depot
hsw2 = tdsw2*0.0001/nd2  !cm thickness of each node in
swollen depot

!$$$$$$ Define node number and node thicknesses for 3rd
barrier and 3rd depot
nb3=20!barrier nodes
nd3=40!depot nodes
tb3=100!microns barrier thickness
tdsh3=100!microns depot thickness shrunken
tdsw3=tdsh3*s3 !microns depot thickness swollen
hb3 = tb3*0.0001/nb3     !cm thickness of each node in
barrier
hsh3 = tdsh3*0.0001/nd3  !cm thickness of each node in
depot
hsw3 = tdsw3*0.0001/nd3  !cm thickness of each node in
swollen depot

!$$$$$$ Define node number and node thicknesses for 4th
barrier and 4th depot
nb4=20!barrier nodes
nd4=40!depot nodes
tb4=100!microns barrier thickness
```

```
tdsh4=100!microns depot thickness shrunken
tdsw4=tdsh4*s4 !microns depot thickness swollen
hb4 = tb4*0.0001/nb4     !cm thickness of each node in
barrier
hsh4 = tdsh4*0.0001/nd4  !cm thickness of each node in
depot
hsw4 = tdsw4*0.0001/nd4  !cm thickness of each node in
swollen depot

!$$$$$$ Define node number and node thicknesses for 2nd
barrier and 2nd depot
nb5=20!barrier nodes
nd5=40!depot nodes
tb5=100!microns barrier thickness
tdsh5=100!microns depot thickness shrunken
tdsw5=tdsh5*s5 !microns depot thickness swollen
hb5 = tb5*0.0001/nb5     !cm thickness of each node in
barrier
hsh5 = tdsh5*0.0001/nd5  !cm thickness of each node in
depot
hsw5 = tdsw5*0.0001/nd5  !cm thickness of each node in
swollen depot

!! Ease of node-numbering for multilayer combination
N1=nb+nd
N1b=N1+nb2
N2=N1+nb2+nd2
N2b=N2+nb3
N3=N2+nb3+nd3
N3b=N3+nb4
N4=N3+nb4+nd4
N4b=N4+nb5
N5=N4+nb5+nd5


!$$$$$$ Input scavenger concentrations in barrier and depot
!Fb= Equivalent molar concentration of [H+] required to
consume X% ZnO PVA,!ZnO + 2HCl= H20+ZnCl2
!X%(w/w)ZnO (Fb, equivalent molar [H+]):
!10%(1.587), 20%(3.531),30%(5.967), 40% (9.111)
!50%(13.322),60%(19.255), 70%(28.239),80% (43.44)

Fb = 0.3 !Molar concentration of equivalent [H+] based on
X% ZnO in hydrated Barrier-1
Fb = Fb*nb/(nb-1) ! Fb re-divided into rest of the nodes
except 1st node of barrier
```

```
Fb2= 0.3 !Molar concentration of equivalent [H+] based on
X% ZnO in hydrated Barrier-2
Fb2= Fb2*nb2/(nb2-1)

Fb3= 0.3 !Molar concentration of equivalent [H+] based on
X% ZnO in hydrated Barrier-3
Fb3= Fb3*nb3/(nb3-1)

Fb4= 0.3 !Molar concentration of equivalent [H+] based on
X% ZnO in hydrated Barrier-4
Fb4= Fb4*nb4/(nb4-1)

Fb5= 0.3 !Molar concentration of equivalent [H+] based on
X% ZnO in hydrated Barrier-5
Fb5= Fb5*nb5/(nb5-1)

Fd = 0.06 !28% DMA, 2.33 M, (based on 85% consumption based
on titration data)

!$$$$$    Input Partition Coefficient
Hgb=1!0.6 ! Partition coefficient of acid in PVA
Hgd=1!1   ! Partition coefficient of acid in p(MMA/DMA)
Hcb=1!0.6 ! Partition coefficient of dissolved solute (dye)
in PVA
Hcd=1!0.4 ! Partition coefficient of dissolved solute (dye)
in p(MMA/DMA)

!$$$$$$ Input stimulant concentrations and diffusion
coefficient in barrier and depot
Cgup = 0.01   ! M (0.001 for pH 3)
Dgb= 0.00001 ! 2.5*10-5 cm2/s diffusion of acid through
PVA, DH=1.5E-5 cm2/s, Hcb=0.6
Dgsh = 0!cm2/s Diffusion Coeff of acid in shrunken hydrogel
Dgsw = 0.00001!5.1*10-5 cm2/s Diffusion coeff of acid in
swollen hydrogel, DH=5.1E-5, Hgd=1

!$$$$$$ Input solute concentrations and diffusion
coefficients in barrier and depot
Bd = 0.1!0.145 !Solid solute M, Concentration of 5% MB in
72/28 MMA/DMA is 0.145, Redistribute in shrunken depot
nodes as B(i)= Bd/s while initializing depot nodes
Bd2=0.1
Bd3=0.1
Bd4=0.1
Bd5=0.1

Csh = 0 ! Dissolved solute in shrunken depot is zero M
```

```
Csw = 0.1*Bd/s!0.0059/4 ! Dissolved solute M, Experimental
MB saturation concentration = 0.0059, assumed to be 4 times
lower when immobilized in depot
Csw2 =Csw !0.9*Bd2/s
Csw3 = Csw!0.9*Bd3/s
Csw4 = Csw!0.9*Bd4/s
Csw5 = Csw!0.9*Bd5/s

Dcb= 0.00001 ! 6*10-7 cm2/s diffusion coeff of solute
through PVA, DH=3.6E-7. H=0.6
Dcsh = 0!cm2/s Diffusion Coeff of Solute in Shrunken
hydrogel
Dcsw = 0.00001 !7.9*10-7 cm2/s Diffusion coeff of solute
from swollen hydrogel, DH=3.4E-7, H=0.43


!$$$$$$ Define Initial conditions in 1st barrier
Do i = 1, nb
B(i) = 0    ! M
B2(i) = 0
B3(i) = 0
B4(i) = 0
B5(i) = 0

C(i) = 0    ! M
C2(i) = 0
C3(i) = 0
C4(i) = 0
C5(i) = 0


Ccsat(i)=Csh
Ccsat2(i)=Csh
Ccsat3(i)=Csh
Ccsat4(i)=Csh
Ccsat5(i)=Csh

Dc(i) =  Dcb ! cm2/s
Dg(i) =  Dgb ! cm2/s
F(i) = Fb
G(i) = 0   ! M
h(i) = hb    ! cm
Hc(i) = Hcb
Hg(i) = Hgb
End Do

!$$$$$$ Define Initial conditions in 2nd barrier
```

```
Do i = N1+1, N1+nb2

B(i) = 0    ! M
B2(i) = 0
B3(i) = 0
B4(i) = 0
B5(i) = 0

C(i) = 0    ! M
C2(i) = 0
C3(i) = 0
C4(i) = 0
C5(i) = 0


Ccsat(i)=Csh
Ccsat2(i)=Csh
Ccsat3(i)=Csh
Ccsat4(i)=Csh
Ccsat5(i)=Csh

Dc(i) =   Dcb ! cm2/s
Dg(i) =   Dgb ! cm2/s
F(i) = Fb2
G(i) = 0   ! M
h(i) = hb2    ! cm
Hc(i) = Hcb
Hg(i) = Hgb

End Do

!$$$$$$ Define Initial conditions in 3rd barrier
Do i = N2+1, N2+nb3

B(i) = 0    ! M
B2(i) = 0
B3(i) = 0
B4(i) = 0
B5(i) = 0

C(i) = 0    ! M
C2(i) = 0
C3(i) = 0
C4(i) = 0
C5(i) = 0
```

```
Ccsat(i)=Csh
Ccsat2(i)=Csh
Ccsat3(i)=Csh
Ccsat4(i)=Csh
Ccsat5(i)=Csh

Dc(i) =   Dcb ! cm2/s
Dg(i) =   Dgb ! cm2/s
F(i) = Fb3
G(i) = 0   ! M
h(i) = hb3    ! cm
Hc(i) = Hcb
Hg(i) = Hgb

End Do

!$$$$$$ Define Initial conditions in 4th barrier
Do i = N3+1, N3+nb4

B(i) = 0    ! M
B2(i) = 0
B3(i) = 0
B4(i) = 0
B5(i) = 0

C(i) = 0    ! M
C2(i) = 0
C3(i) = 0
C4(i) = 0
C5(i) = 0

Ccsat(i)=Csh
Ccsat2(i)=Csh
Ccsat3(i)=Csh
Ccsat4(i)=Csh
Ccsat5(i)=Csh

Dc(i) =   Dcb ! cm2/s
Dg(i) =   Dgb ! cm2/s
F(i) = Fb4
G(i) = 0   ! M
h(i) = hb4    ! cm
Hc(i) = Hcb
Hg(i) = Hgb

End Do
```

```
!$$$$$$ Define Initial conditions in 5th barrier
Do i = N4+1, N4+nb5

B(i) = 0    ! M
B2(i) = 0
B3(i) = 0
B4(i) = 0
B5(i) = 0

C(i) = 0    ! M
C2(i) = 0
C3(i) = 0
C4(i) = 0
C5(i) = 0


Ccsat(i)=Csh
Ccsat2(i)=Csh
Ccsat3(i)=Csh
Ccsat4(i)=Csh
Ccsat5(i)=Csh

Dc(i) =   Dcb ! cm2/s
Dg(i) =   Dgb ! cm2/s
F(i) = Fb5
G(i) = 0   ! M
h(i) = hb5    ! cm
Hc(i) = Hcb
Hg(i) = Hgb

End Do


!$$$$$$ Define Initial conditions in Depot-1
Do i = nb+1, N1

B(i) =  Bd/s ! Redistributing the total solid solute in
shrunken depot-1 with corresponding swelling factor
B2(i) = 0
B3(i) = 0
B4(i) = 0
B5(i) = 0

C(i) = 0    ! M
C2(i) = 0
C3(i) = 0
C4(i) = 0
```

```
C5(i) = 0


Ccsat(i)=Csh
Ccsat2(i)=Csh
Ccsat3(i)=Csh
Ccsat4(i)=Csh
Ccsat5(i)=Csh

Dc(i) = Dcsh    ! cm2/s
Dg(i) = Dgsh    ! cm2/s
F(i) = Fd
G(i) = 0     ! M
h(i) = hsh     ! cm
Hc(i) = Hcd
Hg(i) = Hgd
End Do

!$$$$$$ Define Initial conditions in Depot-2
Do i = N1b+1, N2

B(i) =  0
B2(i) = Bd2/s2 ! Redistributing the total solid solute in
shrunken depot-2 with corresponding swelling factor
B3(i) = 0
B4(i) = 0
B5(i) = 0

C(i) = 0     ! M
C2(i) = 0
C3(i) = 0
C4(i) = 0
C5(i) = 0

Ccsat(i)=Csh
Ccsat2(i)=Csh
Ccsat3(i)=Csh
Ccsat4(i)=Csh
Ccsat5(i)=Csh

Dc(i) = Dcsh    ! cm2/s
Dg(i) = Dgsh    ! cm2/s
F(i) = Fd
G(i) = 0     ! M
h(i) = hsh2     ! cm
Hc(i) = Hcd
Hg(i) = Hgd
```

```
End Do
!$$$$$$ Define Initial conditions in Depot-3
Do i = N2b+1, N3

B(i) =  0
B2(i) = 0
B3(i) = Bd3/s3 ! Redistributing the total solid solute in
shrunken depot-3 with corresponding swelling factor
B4(i) = 0
B5(i) = 0

C(i) = 0    ! M
C2(i) = 0
C3(i) = 0
C4(i) = 0
C5(i) = 0

Ccsat(i)=Csh
Ccsat2(i)=Csh
Ccsat3(i)=Csh
Ccsat4(i)=Csh
Ccsat5(i)=Csh


Dc(i) = Dcsh   ! cm2/s
Dg(i) = Dgsh   ! cm2/s
F(i) = Fd
G(i) = 0    ! M
h(i) = hsh3    ! cm
Hc(i) = Hcd
Hg(i) = Hgd
End Do
!$$$$$$ Define Initial conditions in Depot-4
Do i = N3b+1, N4

B(i) =  0
B2(i) = 0
B3(i) = 0
B4(i) = Bd4/s4 ! Redistributing the total solid solute in
shrunken depot-4 with corresponding swelling factor
B5(i) = 0

C(i) = 0    ! M
C2(i) = 0
C3(i) = 0
C4(i) = 0
C5(i) = 0
```

```
Ccsat(i)=Csh
Ccsat2(i)=Csh
Ccsat3(i)=Csh
Ccsat4(i)=Csh
Ccsat5(i)=Csh

Dc(i) = Dcsh    ! cm2/s
Dg(i) = Dgsh    ! cm2/s
F(i) = Fd
G(i) = 0     ! M
h(i) = hsh4     ! cm
Hc(i) = Hcd
Hg(i) = Hgd
End Do
!$$$$$$ Define Initial conditions in Depot-5
Do i = N4b+1, N5

B(i) =  0
B2(i) = 0
B3(i) = 0
B4(i) = 0
B5(i) = Bd5/s5 ! Redistributing the total solid solute in
shrunken depot-5 with corresponding swelling factor

C(i) = 0     ! M
C2(i) = 0
C3(i) = 0
C4(i) = 0
C5(i) = 0

Ccsat(i)=Csh
Ccsat2(i)=Csh
Ccsat3(i)=Csh
Ccsat4(i)=Csh
Ccsat5(i)=Csh
Dc(i) = Dcsh    ! cm2/s
Dg(i) = Dgsh    ! cm2/s
F(i) = Fd
G(i) = 0     ! M
h(i) = hsh5     ! cm
Hc(i) = Hcd
Hg(i) = Hgd
End Do
```

```
!$$$$$$ Initialize t, Qc,Qg to zero
t = 0
Qc1=0
Qc2=0
Qc3=0
Qc4=0
Qc5=0
Qc= 0
Qg =0

!$$$$$$ Define initial conditions at 1st node of 1st
barrier
B(1) = 0    ! M
B2(1) = 0
B3(1) = 0
B4(1) = 0
B5(1) = 0

C(1) = 0    ! M
C2(1) = 0
C3(1) = 0
C4(1) = 0
C5(1) = 0

Dc(1) = Dcb    ! cm2/s
Dg(1) = Dgb    ! cm2/s
Hc(1) = Hcb
Hg(1) = Hgb
F(1) = 0    ! M
G(1) = Cgup*Hg(1)    ! M
h(1) = hb    ! cm

!$$$$$$ Initialize 1st node of all the barriers to zero to
Divide scavenger evenly corresponding barrier
F(N1+1)=0
F(N2+1)=0
F(N3+1)=0
F(N4+1)=0

!$$$$$$ Define Initial conditions at BOUNDARIES after LAST
NODE of the Device
B(N5+1) = 0    ! M
B2(N5+1) = 0
B3(N5+1) = 0
B4(N5+1) = 0
B5(N5+1) = 0
```

```
C(N5+1) = 0     ! M
C2(N5+1) = 0
C3(N5+1) = 0
C4(N5+1) = 0
C5(N5+1) = 0

Dc(N5+1) = 0     ! cm2/s
Dg(N5+1) = 0     ! cm2/s

F(N5+1) = 0     ! M
G(N5+1) = 0     ! M
h(N5+1) = hsh5     ! cm
Hc(N5+1) = Hcd
Hg(N5+1) = Hgd


!$$$$ MAIN LOOP $$$$$
Do j = 1,m

!BARRIER-1, Acid & Solid-solute transport using Centered
Finite Difference(CFD)
Do i = 2, nb-1 !From node 2 to 2nd last node of 1st
barrier!
!Acid!
d2gdx2(i)=(G(i-1) - 2*G(i) + G(i+1))/(h(i)*h(i))
delg(i)= Dg(i)* d2gdx2(i)*delt
!Solute!
d2cdx2(i)=(C(i-1)- 2*C(i)+ C(i+1))/(h(i)*h(i))
delc(i)= Dc(i)*d2cdx2(i)*delt

d2c2dx2(i)=(C2(i-1)- 2*C2(i)+ C2(i+1))/(h(i)*h(i))
delc2(i)= Dc(i)*d2c2dx2(i)*delt

d2c3dx2(i)=(C3(i-1)- 2*C3(i)+ C3(i+1))/(h(i)*h(i))
delc3(i)= Dc(i)*d2c3dx2(i)*delt

d2c4dx2(i)=(C4(i-1)- 2*C4(i)+ C4(i+1))/(h(i)*h(i))
delc4(i)= Dc(i)*d2c4dx2(i)*delt

d2c5dx2(i)=(C5(i-1)- 2*C5(i)+ C5(i+1))/(h(i)*h(i))
delc5(i)= Dc(i)*d2c5dx2(i)*delt
End Do


!Acid in last node of Barrier-1
d2gdx2(nb)=(G(nb-1)-
2*G(nb)+(Hg(nb)/Hg(nb+1))*G(nb+1))/(h(nb)*h(nb+1))
```

```
delg(nb)= Dg(nb)*d2gdx2(nb)*delt

!Solute in last node of Barrier-1
d2cdx2(nb)=(C(nb-1)-
2*C(nb)+(Hc(nb)/Hc(nb+1))*C(nb+1))/(h(nb)*h(nb+1))
delc(nb)= Dc(nb)*d2cdx2(nb)*delt

d2c2dx2(nb)=(C2(nb-1)-
2*C2(nb)+(Hc(nb)/Hc(nb+1))*C2(nb+1))/(h(nb)*h(nb+1))
delc2(nb)= Dc(nb)*d2c2dx2(nb)*delt

d2c3dx2(nb)=(C3(nb-1)-
2*C3(nb)+(Hc(nb)/Hc(nb+1))*C3(nb+1))/(h(nb)*h(nb+1))
delc3(nb)= Dc(nb)*d2c3dx2(nb)*delt

d2c4dx2(nb)=(C4(nb-1)-
2*C4(nb)+(Hc(nb)/Hc(nb+1))*C4(nb+1))/(h(nb)*h(nb+1))
delc4(nb)= Dc(nb)*d2c4dx2(nb)*delt

d2c5dx2(nb)=(C5(nb-1)-
2*C5(nb)+(Hc(nb)/Hc(nb+1))*C5(nb+1))/(h(nb)*h(nb+1))
delc5(nb)= Dc(nb)*d2c5dx2(nb)*delt

!BARRIER-2, Acid & Solid-solute transport using CFD

!ACID IN 1ST node of Barrier-2
d2gdx2(N1+1)=(G(N1)*(Hg(N1+1)/Hg(N1))-
2*G(N1+1)+G(N1+2))/(h(N1)*h(N1+1))
delg(N1+1)= Dg(N1+1)*d2gdx2(N1+1)*delt
jg(N1+1)=Dg(N1+1)*(G(N1+1)-G(N1+2))/h(N1+1)!This flux will
be needed to link flux between Depot-1 and Barrier-2

!SOLUTE IN 1ST node Barrier-2
d2cdx2(N1+1)=(C(N1)*(Hc(N1+1)/Hc(N1))-
2*C(N1+1)+C(N1+2))/(h(N1)*h(N1+1))
d2c2dx2(N1+1)=(C2(N1)*(Hc(N1+1)/Hc(N1))-
2*C2(N1+1)+C2(N1+2))/(h(N1)*h(N1+1))
d2c3dx2(N1+1)=(C3(N1)*(Hc(N1+1)/Hc(N1))-
2*C3(N1+1)+C3(N1+2))/(h(N1)*h(N1+1))
d2c4dx2(N1+1)=(C4(N1)*(Hc(N1+1)/Hc(N1))-
2*C4(N1+1)+C4(N1+2))/(h(N1)*h(N1+1))
d2c5dx2(N1+1)=(C5(N1)*(Hc(N1+1)/Hc(N1))-
2*C5(N1+1)+C5(N1+2))/(h(N1)*h(N1+1))

delc(N1+1)= Dc(N1+1)*d2cdx2(N1+1)*delt
delc2(N1+1)= Dc(N1+1)*d2c2dx2(N1+1)*delt
delc3(N1+1)= Dc(N1+1)*d2c3dx2(N1+1)*delt
```

```
delc4(N1+1)= Dc(N1+1)*d2c4dx2(N1+1)*delt
delc5(N1+1)= Dc(N1+1)*d2c5dx2(N1+1)*delt

jc(N1+2)=Dc(N1+2)*(C(N1+1)-C(N1+2))/h(N1+2)!!This flux will
be needed to link flux between Depot-1 and Barrier-2
jc2(N1+2)=Dc(N1+2)*(C2(N1+1)-C2(N1+2))/h(N1+2)
jc3(N1+2)=Dc(N1+2)*(C3(N1+1)-C3(N1+2))/h(N1+2)
jc4(N1+2)=Dc(N1+2)*(C4(N1+1)-C4(N1+2))/h(N1+2)
jc5(N1+2)=Dc(N1+2)*(C5(N1+1)-C5(N1+2))/h(N1+2)

!Acid & solute transport from 2nd node to second last node
of Barrier-2
Do i = N1+2, N1b-1 !From node 2 to 2nd last node of 2nd
barrier!
!Acid!
d2gdx2(i)=(G(i-1) - 2*G(i) + G(i+1))/(h(i)*h(i))
delg(i)= Dg(i)* d2gdx2(i)*delt
!Solute!
d2cdx2(i)=(C(i-1)- 2*C(i)+ C(i+1))/(h(i)*h(i))
d2c2dx2(i)=(C2(i-1)- 2*C2(i)+ C2(i+1))/(h(i)*h(i))
d2c3dx2(i)=(C3(i-1)- 2*C3(i)+ C3(i+1))/(h(i)*h(i))
d2c4dx2(i)=(C4(i-1)- 2*C4(i)+ C4(i+1))/(h(i)*h(i))
d2c5dx2(i)=(C5(i-1)- 2*C5(i)+ C5(i+1))/(h(i)*h(i))

delc(i)= Dc(i)*d2cdx2(i)*delt
delc2(i)= Dc(i)*d2c2dx2(i)*delt
delc3(i)= Dc(i)*d2c3dx2(i)*delt
delc4(i)= Dc(i)*d2c4dx2(i)*delt
delc5(i)= Dc(i)*d2c5dx2(i)*delt

End Do
!Acid transport in last node of Barrier-2
d2gdx2(N1b)=(G(N1b-1)-
2*G(N1b)+(Hg(N1b)/Hg(N1b+1))*G(N1b+1))/(h(N1b)*h(N1b+1))
delg(N1b)= Dg(N1b)*d2gdx2(N1b)*delt

!Solute transport in last node of Barrier-2
d2cdx2(N1b)=(C(N1b-1)-
2*C(N1b)+(Hc(N1b)/Hc(N1b+1))*C(N1b+1))/(h(N1b)*h(N1b+1))
d2c2dx2(N1b)=(C2(N1b-1)-
2*C2(N1b)+(Hc(N1b)/Hc(N1b+1))*C2(N1b+1))/(h(N1b)*h(N1b+1))
d2c3dx2(N1b)=(C3(N1b-1)-
2*C3(N1b)+(Hc(N1b)/Hc(N1b+1))*C3(N1b+1))/(h(N1b)*h(N1b+1))
d2c4dx2(N1b)=(C4(N1b-1)-
2*C4(N1b)+(Hc(N1b)/Hc(N1b+1))*C4(N1b+1))/(h(N1b)*h(N1b+1))
d2c5dx2(N1b)=(C5(N1b-1)-
2*C5(N1b)+(Hc(N1b)/Hc(N1b+1))*C5(N1b+1))/(h(N1b)*h(N1b+1))
```

```
delc(N1b)= Dc(N1b)*d2cdx2(N1b)*delt
delc2(N1b)= Dc(N1b)*d2c2dx2(N1b)*delt
delc3(N1b)= Dc(N1b)*d2c3dx2(N1b)*delt
delc4(N1b)= Dc(N1b)*d2c4dx2(N1b)*delt
delc5(N1b)= Dc(N1b)*d2c5dx2(N1b)*delt

!BARRIER-3, Acid & Solid-solute transport using CFD

!ACID IN 1ST node of Barrier-3
d2gdx2(N2+1)=(G(N2)*(Hg(N2+1)/Hg(N2))-
2*G(N2+1)+G(N2+2))/(h(N2)*h(N2+1))
delg(N2+1)= Dg(N2+1)*d2gdx2(N2+1)*delt
jg(N2+1)=Dg(N2+1)*(G(N2+1)-G(N2+2))/h(N2+1)!This flux will
be needed to link flux between Depot-2 and Barrier-3

!SOLUTE IN 1ST node Barrier-3
d2cdx2(N2+1)=(C(N2)*(Hc(N2+1)/Hc(N2))-
2*C(N2+1)+C(N2+2))/(h(N2)*h(N2+1))
d2c2dx2(N2+1)=(C2(N2)*(Hc(N2+1)/Hc(N2))-
2*C2(N2+1)+C2(N2+2))/(h(N2)*h(N2+1))
d2c3dx2(N2+1)=(C3(N2)*(Hc(N2+1)/Hc(N2))-
2*C3(N2+1)+C3(N2+2))/(h(N2)*h(N2+1))
d2c4dx2(N2+1)=(C4(N2)*(Hc(N2+1)/Hc(N2))-
2*C4(N2+1)+C4(N2+2))/(h(N2)*h(N2+1))
d2c5dx2(N2+1)=(C5(N2)*(Hc(N2+1)/Hc(N2))-
2*C5(N2+1)+C5(N2+2))/(h(N2)*h(N2+1))

delc(N2+1)= Dc(N2+1)*d2cdx2(N2+1)*delt
delc2(N2+1)= Dc(N2+1)*d2c2dx2(N2+1)*delt
delc3(N2+1)= Dc(N2+1)*d2c3dx2(N2+1)*delt
delc4(N2+1)= Dc(N2+1)*d2c4dx2(N2+1)*delt
delc5(N2+1)= Dc(N2+1)*d2c5dx2(N2+1)*delt

jc(N2+2)=Dc(N2+2)*(C(N2+1)-C(N2+2))/h(N2+2)!!This flux will
be needed to link flux between Depot-2 and Barrier-3
jc2(N2+2)=Dc(N2+2)*(C2(N2+1)-C2(N2+2))/h(N2+2)
jc3(N2+2)=Dc(N2+2)*(C3(N2+1)-C3(N2+2))/h(N2+2)
jc4(N2+2)=Dc(N2+2)*(C4(N2+1)-C4(N2+2))/h(N2+2)
jc5(N2+2)=Dc(N2+2)*(C5(N2+1)-C5(N2+2))/h(N2+2)

!Acid & solute transport from 2nd node to second last node
of Barrier-3
Do i = N2+2, N2b-1 !From node 2 to 2nd last node of 3rd
barrier!
!Acid!
d2gdx2(i)=(G(i-1) - 2*G(i) + G(i+1))/(h(i)*h(i))
```

```
delg(i)= Dg(i)* d2gdx2(i)*delt
!Solute!
d2cdx2(i)=(C(i-1)- 2*C(i)+ C(i+1))/(h(i)*h(i))
d2c2dx2(i)=(C2(i-1)- 2*C2(i)+ C2(i+1))/(h(i)*h(i))
d2c3dx2(i)=(C3(i-1)- 2*C3(i)+ C3(i+1))/(h(i)*h(i))
d2c4dx2(i)=(C4(i-1)- 2*C4(i)+ C4(i+1))/(h(i)*h(i))
d2c5dx2(i)=(C5(i-1)- 2*C5(i)+ C5(i+1))/(h(i)*h(i))

delc(i)= Dc(i)*d2cdx2(i)*delt
delc2(i)= Dc(i)*d2c2dx2(i)*delt
delc3(i)= Dc(i)*d2c3dx2(i)*delt
delc4(i)= Dc(i)*d2c4dx2(i)*delt
delc5(i)= Dc(i)*d2c5dx2(i)*delt
End Do
!Acid transport in last node of Barrier-3
d2gdx2(N2b)=(G(N2b-1)-
2*G(N2b)+(Hg(N2b)/Hg(N2b+1))*G(N2b+1))/(h(N2b)*h(N2b+1))
delg(N2b)= Dg(N2b)*d2gdx2(N2b)*delt

!Solute transport in last node of Barrier-3
d2cdx2(N2b)=(C(N2b-1)-
2*C(N2b)+(Hc(N2b)/Hc(N2b+1))*C(N2b+1))/(h(N2b)*h(N2b+1))
d2c2dx2(N2b)=(C2(N2b-1)-
2*C2(N2b)+(Hc(N2b)/Hc(N2b+1))*C2(N2b+1))/(h(N2b)*h(N2b+1))
d2c3dx2(N2b)=(C3(N2b-1)-
2*C3(N2b)+(Hc(N2b)/Hc(N2b+1))*C3(N2b+1))/(h(N2b)*h(N2b+1))
d2c4dx2(N2b)=(C4(N2b-1)-
2*C4(N2b)+(Hc(N2b)/Hc(N2b+1))*C4(N2b+1))/(h(N2b)*h(N2b+1))
d2c5dx2(N2b)=(C5(N2b-1)-
2*C5(N2b)+(Hc(N2b)/Hc(N2b+1))*C5(N2b+1))/(h(N2b)*h(N2b+1))

delc(N2b)= Dc(N2b)*d2cdx2(N2b)*delt
delc2(N2b)= Dc(N2b)*d2c2dx2(N2b)*delt
delc3(N2b)= Dc(N2b)*d2c3dx2(N2b)*delt
delc4(N2b)= Dc(N2b)*d2c4dx2(N2b)*delt
delc5(N2b)= Dc(N2b)*d2c5dx2(N2b)*delt


!BARRIER-4, Acid & Solid-solute transport using CFD

!ACID IN 1ST node of Barrier-4
d2gdx2(N3+1)=(G(N3)*(Hg(N3+1)/Hg(N3))-
2*G(N3+1)+G(N3+2))/(h(N3)*h(N3+1))
delg(N3+1)= Dg(N3+1)*d2gdx2(N3+1)*delt
jg(N3+1)=Dg(N3+1)*(G(N3+1)-G(N3+2))/h(N3+1)!This flux will
be needed to link flux between Depot-3 and Barrier-4
```

```
!SOLUTE IN 1ST node Barrier-4
d2cdx2(N3+1)=(C(N3)*(Hc(N3+1)/Hc(N3))-
2*C(N3+1)+C(N3+2))/(h(N3)*h(N3+1))
d2c2dx2(N3+1)=(C2(N3)*(Hc(N3+1)/Hc(N3))-
2*C2(N3+1)+C2(N3+2))/(h(N3)*h(N3+1))
d2c3dx2(N3+1)=(C3(N3)*(Hc(N3+1)/Hc(N3))-
2*C3(N3+1)+C3(N3+2))/(h(N3)*h(N3+1))
d2c4dx2(N3+1)=(C4(N3)*(Hc(N3+1)/Hc(N3))-
2*C4(N3+1)+C4(N3+2))/(h(N3)*h(N3+1))
d2c5dx2(N3+1)=(C5(N3)*(Hc(N3+1)/Hc(N3))-
2*C5(N3+1)+C5(N3+2))/(h(N3)*h(N3+1))

delc(N3+1)= Dc(N3+1)*d2cdx2(N3+1)*delt
delc2(N3+1)= Dc(N3+1)*d2c2dx2(N3+1)*delt
delc3(N3+1)= Dc(N3+1)*d2c3dx2(N3+1)*delt
delc4(N3+1)= Dc(N3+1)*d2c4dx2(N3+1)*delt
delc5(N3+1)= Dc(N3+1)*d2c5dx2(N3+1)*delt

jc(N3+2)=Dc(N3+2)*(C(N3+1)-C(N3+2))/h(N3+2)!!This flux will
be needed to link flux between Depot-3 and Barrier-4
jc2(N3+2)=Dc(N3+2)*(C2(N3+1)-C2(N3+2))/h(N3+2)
jc3(N3+2)=Dc(N3+2)*(C3(N3+1)-C3(N3+2))/h(N3+2)
jc4(N3+2)=Dc(N3+2)*(C4(N3+1)-C4(N3+2))/h(N3+2)
jc5(N3+2)=Dc(N3+2)*(C5(N3+1)-C5(N3+2))/h(N3+2)

!Acid & solute transport from 2nd node to second last node
of Barrier-4
Do i = N3+2, N3b-1 !From node 2 to 2nd last node of 4th
barrier!
!Acid!
d2gdx2(i)=(G(i-1) - 2*G(i) + G(i+1))/(h(i)*h(i))
delg(i)= Dg(i)* d2gdx2(i)*delt
!Solute!
d2cdx2(i)=(C(i-1)- 2*C(i)+ C(i+1))/(h(i)*h(i))
d2c2dx2(i)=(C2(i-1)- 2*C2(i)+ C2(i+1))/(h(i)*h(i))
d2c3dx2(i)=(C3(i-1)- 2*C3(i)+ C3(i+1))/(h(i)*h(i))
d2c4dx2(i)=(C4(i-1)- 2*C4(i)+ C4(i+1))/(h(i)*h(i))
d2c5dx2(i)=(C5(i-1)- 2*C5(i)+ C5(i+1))/(h(i)*h(i))

delc(i)= Dc(i)*d2cdx2(i)*delt
delc2(i)= Dc(i)*d2c2dx2(i)*delt
delc3(i)= Dc(i)*d2c3dx2(i)*delt
delc4(i)= Dc(i)*d2c4dx2(i)*delt
delc5(i)= Dc(i)*d2c5dx2(i)*delt

End Do
!Acid transport in last node of Barrier-4
```

```
d2gdx2(N3b)=(G(N3b-1)-
2*G(N3b)+(Hg(N3b)/Hg(N3b+1))*G(N3b+1))/(h(N3b)*h(N3b+1))
delg(N3b)= Dg(N3b)*d2gdx2(N3b)*delt

!Solute transport in last node of Barrier-4
d2cdx2(N3b)=(C(N3b-1)-
2*C(N3b)+(Hc(N3b)/Hc(N3b+1))*C(N3b+1))/(h(N3b)*h(N3b+1))
d2c2dx2(N3b)=(C2(N3b-1)-
2*C2(N3b)+(Hc(N3b)/Hc(N3b+1))*C2(N3b+1))/(h(N3b)*h(N3b+1))
d2c3dx2(N3b)=(C3(N3b-1)-
2*C3(N3b)+(Hc(N3b)/Hc(N3b+1))*C3(N3b+1))/(h(N3b)*h(N3b+1))
d2c4dx2(N3b)=(C4(N3b-1)-
2*C4(N3b)+(Hc(N3b)/Hc(N3b+1))*C4(N3b+1))/(h(N3b)*h(N3b+1))
d2c5dx2(N3b)=(C5(N3b-1)-
2*C5(N3b)+(Hc(N3b)/Hc(N3b+1))*C5(N3b+1))/(h(N3b)*h(N3b+1))

delc(N3b)= Dc(N3b)*d2cdx2(N3b)*delt
delc2(N3b)= Dc(N3b)*d2c2dx2(N3b)*delt
delc3(N3b)= Dc(N3b)*d2c3dx2(N3b)*delt
delc4(N3b)= Dc(N3b)*d2c4dx2(N3b)*delt
delc5(N3b)= Dc(N3b)*d2c5dx2(N3b)*delt


!BARRIER-5, Acid & Solid-solute transport using CFD

!ACID IN 1ST node of Barrier-5
d2gdx2(N4+1)=(G(N4)*(Hg(N4+1)/Hg(N4))-
2*G(N4+1)+G(N4+2))/(h(N4)*h(N4+1))
delg(N4+1)= Dg(N4+1)*d2gdx2(N4+1)*delt
jg(N4+1)=Dg(N4+1)*(G(N4+1)-G(N4+2))/h(N4+1)!This flux will
be needed to link flux between Depot-4 and Barrier-5

!SOLUTE IN 1ST node Barrier-5
d2cdx2(N4+1)=(C(N4)*(Hc(N4+1)/Hc(N4))-
2*C(N4+1)+C(N4+2))/(h(N4)*h(N4+1))
d2c2dx2(N4+1)=(C2(N4)*(Hc(N4+1)/Hc(N4))-
2*C2(N4+1)+C2(N4+2))/(h(N4)*h(N4+1))
d2c3dx2(N4+1)=(C3(N4)*(Hc(N4+1)/Hc(N4))-
2*C3(N4+1)+C3(N4+2))/(h(N4)*h(N4+1))
d2c4dx2(N4+1)=(C4(N4)*(Hc(N4+1)/Hc(N4))-
2*C4(N4+1)+C4(N4+2))/(h(N4)*h(N4+1))
d2c5dx2(N4+1)=(C5(N4)*(Hc(N4+1)/Hc(N4))-
2*C5(N4+1)+C5(N4+2))/(h(N4)*h(N4+1))

delc(N4+1)= Dc(N4+1)*d2cdx2(N4+1)*delt
delc2(N4+1)= Dc(N4+1)*d2c2dx2(N4+1)*delt
delc3(N4+1)= Dc(N4+1)*d2c3dx2(N4+1)*delt
```

```
delc4(N4+1)= Dc(N4+1)*d2c4dx2(N4+1)*delt
delc5(N4+1)= Dc(N4+1)*d2c5dx2(N4+1)*delt

jc(N4+2)=Dc(N4+2)*(C(N4+1)-C(N4+2))/h(N4+2)!!This flux will
be needed to link flux between Depot-4 and Barrier-5
jc2(N4+2)=Dc(N4+2)*(C2(N4+1)-C2(N4+2))/h(N4+2)
jc3(N4+2)=Dc(N4+2)*(C3(N4+1)-C3(N4+2))/h(N4+2)
jc4(N4+2)=Dc(N4+2)*(C4(N4+1)-C4(N4+2))/h(N4+2)
jc5(N4+2)=Dc(N4+2)*(C5(N4+1)-C5(N4+2))/h(N4+2)

!Acid & solute transport from 2nd node to second last node
of Barrier-5
Do i = N4+2, N4b-1 !From node 2 to 2nd last node of 5th
barrier!
!Acid!
d2gdx2(i)=(G(i-1) - 2*G(i) + G(i+1))/(h(i)*h(i))
delg(i)= Dg(i)* d2gdx2(i)*delt
!Solute!
d2cdx2(i)=(C(i-1)- 2*C(i)+ C(i+1))/(h(i)*h(i))
d2c2dx2(i)=(C2(i-1)- 2*C2(i)+ C2(i+1))/(h(i)*h(i))
d2c3dx2(i)=(C3(i-1)- 2*C3(i)+ C3(i+1))/(h(i)*h(i))
d2c4dx2(i)=(C4(i-1)- 2*C4(i)+ C4(i+1))/(h(i)*h(i))
d2c5dx2(i)=(C5(i-1)- 2*C5(i)+ C5(i+1))/(h(i)*h(i))

delc(i)= Dc(i)*d2cdx2(i)*delt
delc2(i)= Dc(i)*d2c2dx2(i)*delt
delc3(i)= Dc(i)*d2c3dx2(i)*delt
delc4(i)= Dc(i)*d2c4dx2(i)*delt
delc5(i)= Dc(i)*d2c5dx2(i)*delt
End Do
!Acid transport in last node of Barrier-5
d2gdx2(N4b)=(G(N4b-1)-
2*G(N4b)+(Hg(N4b)/Hg(N4b+1))*G(N4b+1))/(h(N4b)*h(N4b+1))
delg(N4b)= Dg(N4b)*d2gdx2(N4b)*delt

!Solute transport in last node of Barrier-5
d2cdx2(N4b)=(C(N4b-1)-
2*C(N4b)+(Hc(N4b)/Hc(N4b+1))*C(N4b+1))/(h(N4b)*h(N4b+1))
d2c2dx2(N4b)=(C2(N4b-1)-
2*C2(N4b)+(Hc(N4b)/Hc(N4b+1))*C2(N4b+1))/(h(N4b)*h(N4b+1))
d2c3dx2(N4b)=(C3(N4b-1)-
2*C3(N4b)+(Hc(N4b)/Hc(N4b+1))*C3(N4b+1))/(h(N4b)*h(N4b+1))
d2c4dx2(N4b)=(C4(N4b-1)-
2*C4(N4b)+(Hc(N4b)/Hc(N4b+1))*C4(N4b+1))/(h(N4b)*h(N4b+1))
d2c5dx2(N4b)=(C5(N4b-1)-
2*C5(N4b)+(Hc(N4b)/Hc(N4b+1))*C5(N4b+1))/(h(N4b)*h(N4b+1))
```

```
delc(N4b)= Dc(N4b)*d2cdx2(N4b)*delt
delc2(N4b)= Dc(N4b)*d2c2dx2(N4b)*delt
delc3(N4b)= Dc(N4b)*d2c3dx2(N4b)*delt
delc4(N4b)= Dc(N4b)*d2c4dx2(N4b)*delt
delc5(N4b)= Dc(N4b)*d2c5dx2(N4b)*delt

!DEPOT-1, ACID & SOLUTE TRANSPORT

!Acid transport using Fick's First law to Calculate flux
and Backward-Finite Difference to calculate delg
!Acid fluxes from barrier-1 will be needed to link with
Depot-1, to calculate delg(i) in depot nodes
jg(nb-1) = Dg(nb-1)*(G(nb-1)-G(nb))/h(nb-1)
jg(nb)=jg(nb-1)-delg(nb)*h(nb)/delt ! This flux is linked
from Barrier-1 to Depot-1

! ACID! Calculate fluxes in Depot-1 using Fick's First law
Do i = nb+1,N1-1
jg(i) = ((Dg(i)+Dg(i+1))/2)*(G(i)-G(i+1))/h(i)
End Do
jg(N1)= delg(N1+1)*h(N1+1)/delt + jg(N1+1)
!This flux from the last node of  Depot-1 is linked with
Barrier-2 to Calculate delg(N1)

! ACID! Once all fluxes are calculated, determine change in
node concentration using Backward-Finite difference
Do i = nb+1, N1  ! Note that change in concentrations has
already been calculated for last barrier node
delg(i) = (jg(i-1)-jg(i))*delt/h(i)
End Do

!Solute transport using Fick's First law & Forward-Finite
Difference to calculate delc
!Flux coming from last node of barrier-1 is linked to the
1st node of depot-1
!solute fluxes from Barrier-1 will be needed to link the
flux from Depot-1 to Barrier-1
jc(nb)= Dc(nb)*(C(nb-1)-C(nb))/h(nb)
jc2(nb)= Dc(nb)*(C2(nb-1)-C2(nb))/h(nb)
jc3(nb)= Dc(nb)*(C3(nb-1)-C3(nb))/h(nb)
jc4(nb)= Dc(nb)*(C4(nb-1)-C4(nb))/h(nb)
jc5(nb)= Dc(nb)*(C5(nb-1)-C5(nb))/h(nb)

jc(nb+1) = jc(nb)-delc(nb)*h(nb)/delt !This flux is linked
between Barrier-1 and Depot-1
jc2(nb+1) = jc2(nb)-delc2(nb)*h(nb)/delt
jc3(nb+1) = jc3(nb)-delc3(nb)*h(nb)/delt
```

```
jc4(nb+1) = jc4(nb)-delc4(nb)*h(nb)/delt
jc5(nb+1) = jc5(nb)-delc5(nb)*h(nb)/delt

! SOLUTE! Calculate flux in rest of the nodes in depot-1
layer using Fick's First Law
Do i = nb+2,N1
jc(i) = ((Dc(i-1)+Dc(i))/2)*(C(i-1)-C(i))/h(i)
jc2(i) = ((Dc(i-1)+Dc(i))/2)*(C2(i-1)-C2(i))/h(i)
jc3(i) = ((Dc(i-1)+Dc(i))/2)*(C3(i-1)-C3(i))/h(i)
jc4(i) = ((Dc(i-1)+Dc(i))/2)*(C4(i-1)-C4(i))/h(i)
jc5(i) = ((Dc(i-1)+Dc(i))/2)*(C5(i-1)-C5(i))/h(i)
End Do
jc(N1+1)=  delc(N1+1)*h(N1+1)/delt + jc(N1+2)
jc2(N1+1)= delc2(N1+1)*h(N1+1)/delt + jc2(N1+2)
jc3(N1+1)= delc3(N1+1)*h(N1+1)/delt + jc3(N1+2)
jc4(N1+1)= delc4(N1+1)*h(N1+1)/delt + jc4(N1+2)
jc5(N1+1)= delc5(N1+1)*h(N1+1)/delt + jc5(N1+2)
!This Flux from last node of the Depot-1 layer is linked
with Barrier-2 and will be used to calculate delc(N1)

! SOLUTE ! Once all fluxes are calculated, determine change
in node concentration using Forward-Finite difference
Do i = nb+1, N1  ! Note that change in concentrations has
already been calculated for last barrier node
delc(i) = (jc(i)-jc(i+1))*delt/h(i)
delc2(i) = (jc2(i)-jc2(i+1))*delt/h(i)
delc3(i) = (jc3(i)-jc3(i+1))*delt/h(i)
delc4(i) = (jc4(i)-jc4(i+1))*delt/h(i)
delc5(i) = (jc5(i)-jc5(i+1))*delt/h(i)
End Do

!DEPOT-2, ACID & SOLUTE TRANSPORT

!Acid transport using Fick's First law to Calculate flux
and Backward-Finite Difference to calculate delg
!Acid fluxes from BARRIER-2 will be needed to link with
DEPOT-2, to calculate delg(i) in depot nodes
jg(N1b-1) = Dg(N1b-1)*(G(N1b-1)-G(N1b))/h(N1b-1)
jg(N1b)=jg(N1b-1)-delg(N1b)*h(N1b)/delt ! This flux is
linked from BARRIER-2 to DEPOT-2

! ACID! Calculate fluxes in DEPOT-2 using Fick's First law
Do i = N1b+1,N2-1
jg(i) = ((Dg(i)+Dg(i+1))/2)*(G(i)-G(i+1))/h(i)
End Do
jg(N2)= delg(N2+1)*h(N2+1)/delt + jg(N2+1)
```

```
!This flux from the last node of  DEPOT-2 is linked with
BARRIER-3 to Calculate delg(N2)

! ACID! Once all fluxes are calculated, determine change in
node concentration using Backward-Finite difference
Do i = N1b+1, N2  ! Note that change in concentrations has
already been calculated for last barrier node
delg(i) = (jg(i-1)-jg(i))*delt/h(i)
End Do

!Solute transport using Fick's First law & Forward-Finite
Difference to calculate delc
!Flux coming from last node of BARRIER-2 is linked to the
1st node of DEPOT-2
!solute fluxes from BARRIER-2 will be needed to link the
flux from DEPOT-2 to BARRIER-2
jc(N1b)= Dc(N1b)*(C(N1b-1)-C(N1b))/h(N1b)
jc2(N1b)= Dc(N1b)*(C2(N1b-1)-C2(N1b))/h(N1b)
jc3(N1b)= Dc(N1b)*(C3(N1b-1)-C3(N1b))/h(N1b)
jc4(N1b)= Dc(N1b)*(C4(N1b-1)-C4(N1b))/h(N1b)
jc5(N1b)= Dc(N1b)*(C5(N1b-1)-C5(N1b))/h(N1b)

jc(N1b+1) = jc(N1b)-delc(N1b)*h(N1b)/delt !This flux is
linked between BARRIER-2 and DEPOT-2
jc2(N1b+1) = jc2(N1b)-delc2(N1b)*h(N1b)/delt
jc3(N1b+1) = jc3(N1b)-delc3(N1b)*h(N1b)/delt
jc4(N1b+1) = jc4(N1b)-delc4(N1b)*h(N1b)/delt
jc5(N1b+1) = jc5(N1b)-delc5(N1b)*h(N1b)/delt

! SOLUTE! Calculate flux in rest of the nodes in DEPOT-2
layer using Fick's First Law
Do i = N1b+2,N2
jc(i) = ((Dc(i-1)+Dc(i))/2)*(C(i-1)-C(i))/h(i)
jc2(i) = ((Dc(i-1)+Dc(i))/2)*(C2(i-1)-C2(i))/h(i)
jc3(i) = ((Dc(i-1)+Dc(i))/2)*(C3(i-1)-C3(i))/h(i)
jc4(i) = ((Dc(i-1)+Dc(i))/2)*(C4(i-1)-C4(i))/h(i)
jc5(i) = ((Dc(i-1)+Dc(i))/2)*(C5(i-1)-C5(i))/h(i)
End Do

jc(N2+1)=  delc(N2+1)*h(N2+1)/delt + jc(N2+2)
jc2(N2+1)= delc2(N2+1)*h(N2+1)/delt + jc2(N2+2)
jc3(N2+1)= delc3(N2+1)*h(N2+1)/delt + jc3(N2+2)
jc4(N2+1)= delc4(N2+1)*h(N2+1)/delt + jc4(N2+2)
jc5(N2+1)= delc5(N2+1)*h(N2+1)/delt + jc5(N2+2)

!This Flux from last node of the DEPOT-2 layer is linked
with BARRIER-3 and will be used to calculate delc(N2)
```

```
! SOLUTE ! Once all fluxes are calculated, determine change
in node concentration using Forward-Finite difference
Do i = N1b+1, N2  ! Note that change in concentrations has
already been calculated for last barrier node
delc(i) =  (jc(i)-jc(i+1))*delt/h(i)
delc2(i) = (jc2(i)-jc2(i+1))*delt/h(i)
delc3(i) = (jc3(i)-jc3(i+1))*delt/h(i)
delc4(i) = (jc4(i)-jc4(i+1))*delt/h(i)
delc5(i) = (jc5(i)-jc5(i+1))*delt/h(i)
End Do

!DEPOT-3, ACID & SOLUTE TRANSPORT

!Acid transport using Fick's First law to Calculate flux
and Backward-Finite Difference to calculate delg
!Acid fluxes from BARRIER-3 will be needed to link with
DEPOT-3, to calculate delg(i) in depot nodes
jg(N2b-1) = Dg(N2b-1)*(G(N2b-1)-G(N2b))/h(N2b-1)
jg(N2b)=jg(N2b-1)-delg(N2b)*h(N2b)/delt ! This flux is
linked from BARRIER-3 to DEPOT-3

! ACID! Calculate fluxes in DEPOT-3 using Fick's First law
Do i = N2b+1,N3-1
jg(i) = ((Dg(i)+Dg(i+1))/2)*(G(i)-G(i+1))/h(i)
End Do
jg(N3)= delg(N3+1)*h(N3+1)/delt + jg(N3+1)
!This flux from the last node of  DEPOT-3 is linked with
BARRIER-4 to Calculate delg(N3)

! ACID! Once all fluxes are calculated, determine change in
node concentration using Backward-Finite difference
Do i = N2b+1, N3  ! Note that change in concentrations has
already been calculated for last barrier node
delg(i) = (jg(i-1)-jg(i))*delt/h(i)
End Do

!Solute transport using Fick's First law & Forward-Finite
Difference to calculate delc
!Flux coming from last node of BARRIER-3 is linked to the
1st node of DEPOT-3
!solute fluxes from BARRIER-3 will be needed to link the
flux from DEPOT-3 to BARRIER-3
jc(N2b)= Dc(N2b)*(C(N2b-1)-C(N2b))/h(N2b)
jc2(N2b)= Dc(N2b)*(C2(N2b-1)-C2(N2b))/h(N2b)
jc3(N2b)= Dc(N2b)*(C3(N2b-1)-C3(N2b))/h(N2b)
jc4(N2b)= Dc(N2b)*(C4(N2b-1)-C4(N2b))/h(N2b)
```

```
jc5(N2b)= Dc(N2b)*(C5(N2b-1)-C5(N2b))/h(N2b)

jc(N2b+1) = jc(N2b)-delc(N2b)*h(N2b)/delt !This flux is
linked between BARRIER-3 and DEPOT-3
jc2(N2b+1) = jc2(N2b)-delc2(N2b)*h(N2b)/delt
jc3(N2b+1) = jc3(N2b)-delc3(N2b)*h(N2b)/delt
jc4(N2b+1) = jc4(N2b)-delc4(N2b)*h(N2b)/delt
jc5(N2b+1) = jc5(N2b)-delc5(N2b)*h(N2b)/delt

! SOLUTE! Calculate flux in rest of the nodes in DEPOT-3
layer using Fick's First Law
Do i = N2b+2,N3
jc(i) = ((Dc(i-1)+Dc(i))/2)*(C(i-1)-C(i))/h(i)
jc2(i) = ((Dc(i-1)+Dc(i))/2)*(C2(i-1)-C2(i))/h(i)
jc3(i) = ((Dc(i-1)+Dc(i))/2)*(C3(i-1)-C3(i))/h(i)
jc4(i) = ((Dc(i-1)+Dc(i))/2)*(C4(i-1)-C4(i))/h(i)
jc5(i) = ((Dc(i-1)+Dc(i))/2)*(C5(i-1)-C5(i))/h(i)
End Do
jc(N3+1)=  delc(N3+1)*h(N3+1)/delt + jc(N3+2)
jc2(N3+1)= delc2(N3+1)*h(N3+1)/delt + jc2(N3+2)
jc3(N3+1)= delc3(N3+1)*h(N3+1)/delt + jc3(N3+2)
jc4(N3+1)= delc4(N3+1)*h(N3+1)/delt + jc4(N3+2)
jc5(N3+1)= delc5(N3+1)*h(N3+1)/delt + jc5(N3+2)

!This Flux from last node of the DEPOT-3 layer is linked
with BARRIER-4 and will be used to calculate delc(N3)

! SOLUTE ! Once all fluxes are calculated, determine change
in node concentration using Forward-Finite difference
Do i = N2b+1, N3  ! Note that change in concentrations has
already been calculated for last barrier node
delc(i) =  (jc(i)-jc(i+1))*delt/h(i)
delc2(i) = (jc2(i)-jc2(i+1))*delt/h(i)
delc3(i) = (jc3(i)-jc3(i+1))*delt/h(i)
delc4(i) = (jc4(i)-jc4(i+1))*delt/h(i)
delc5(i) = (jc5(i)-jc5(i+1))*delt/h(i)
End Do

!DEPOT-4, ACID & SOLUTE TRANSPORT

!Acid transport using Fick's First law to Calculate flux
and Backward-Finite Difference to calculate delg
!Acid fluxes from BARRIER-4 will be needed to link with
DEPOT-4, to calculate delg(i) in depot nodes
jg(N3b-1) = Dg(N3b-1)*(G(N3b-1)-G(N3b))/h(N3b-1)
jg(N3b)=jg(N3b-1)-delg(N3b)*h(N3b)/delt ! This flux is
linked from BARRIER-4 to DEPOT-4
```

```
! ACID! Calculate fluxes in DEPOT-4 using Fick's First law
Do i = N3b+1,N4-1
jg(i) = ((Dg(i)+Dg(i+1))/2)*(G(i)-G(i+1))/h(i)
End Do
jg(N4)= delg(N4+1)*h(N4+1)/delt + jg(N4+1)
!This flux from the last node of  DEPOT-4 is linked with
BARRIER-5 to Calculate delg(N4)

! ACID! Once all fluxes are calculated, determine change in
node concentration using Backward-Finite difference
Do i = N3b+1, N4  ! Note that change in concentrations has
already been calculated for last barrier node
delg(i) = (jg(i-1)-jg(i))*delt/h(i)
End Do

!Solute transport using Fick's First law & Forward-Finite
Difference to calculate delc
!Flux coming from last node of BARRIER-4 is linked to the
1st node of DEPOT-4
!solute fluxes from BARRIER-4 will be needed to link the
flux from DEPOT-4 to BARRIER-4
jc(N3b)= Dc(N3b)*(C(N3b-1)-C(N3b))/h(N3b)
jc2(N3b)= Dc(N3b)*(C2(N3b-1)-C2(N3b))/h(N3b)
jc3(N3b)= Dc(N3b)*(C3(N3b-1)-C3(N3b))/h(N3b)
jc4(N3b)= Dc(N3b)*(C4(N3b-1)-C4(N3b))/h(N3b)
jc5(N3b)= Dc(N3b)*(C5(N3b-1)-C5(N3b))/h(N3b)

jc(N3b+1) = jc(N3b)-delc(N3b)*h(N3b)/delt !This flux is
linked between BARRIER-3 and DEPOT-3
jc2(N3b+1) = jc2(N3b)-delc2(N3b)*h(N3b)/delt
jc3(N3b+1) = jc3(N3b)-delc3(N3b)*h(N3b)/delt
jc4(N3b+1) = jc4(N3b)-delc4(N3b)*h(N3b)/delt
jc5(N3b+1) = jc5(N3b)-delc5(N3b)*h(N3b)/delt

! SOLUTE! Calculate flux in rest of the nodes in DEPOT-4
layer using Fick's First Law
Do i = N3b+2,N4
jc(i) = ((Dc(i-1)+Dc(i))/2)*(C(i-1)-C(i))/h(i)
jc2(i) = ((Dc(i-1)+Dc(i))/2)*(C2(i-1)-C2(i))/h(i)
jc3(i) = ((Dc(i-1)+Dc(i))/2)*(C3(i-1)-C3(i))/h(i)
jc4(i) = ((Dc(i-1)+Dc(i))/2)*(C4(i-1)-C4(i))/h(i)
jc5(i) = ((Dc(i-1)+Dc(i))/2)*(C5(i-1)-C5(i))/h(i)
End Do
jc(N4+1)=  delc(N4+1)*h(N4+1)/delt + jc(N4+2)
jc2(N4+1)= delc2(N4+1)*h(N4+1)/delt + jc2(N4+2)
jc3(N4+1)= delc3(N4+1)*h(N4+1)/delt + jc3(N4+2)
```

```
jc4(N4+1)= delc4(N4+1)*h(N4+1)/delt + jc4(N4+2)
jc5(N4+1)= delc5(N4+1)*h(N4+1)/delt + jc5(N4+2)
!This Flux from last node of the DEPOT-4 layer is linked
with BARRIER-5 and will be used to calculate delc(N4)

! SOLUTE ! Once all fluxes are calculated, determine change
in node concentration using Forward-Finite difference
Do i = N3b+1, N4  ! Note that change in concentrations has
already been calculated for last barrier node
delc(i) = (jc(i)-jc(i+1))*delt/h(i)
delc2(i) = (jc2(i)-jc2(i+1))*delt/h(i)
delc3(i) = (jc3(i)-jc3(i+1))*delt/h(i)
delc4(i) = (jc4(i)-jc4(i+1))*delt/h(i)
delc5(i) = (jc5(i)-jc5(i+1))*delt/h(i)
End Do


!DEPOT-5, ACID & SOLUTE CALCULATIONS (LAST DEOPOT in this
case, as 5-pulse code)
!ACID
!Acid fluxes from barrier-5, that will be needed to link
with Depot-5
jg(N4b-1) = Dg(N4b-1)*(G(N4b-1)-G(N4b))/h(N4b-1)
jg(N4b)=jg(N4b-1)-delg(N4b)*h(N4b)/delt ! This flux is
linked between barrier-5 and depot-5

! ACID! Calculate flux in depot-5 layer using Fick's First
law
Do i = N4b+1,N5
jg(i) = ((Dg(i)+Dg(i+1))/2)*(G(i)-G(i+1))/h(i)
End Do
! ACID! Once all fluxes are calculated, determine change in
node concentration using Backward finite difference
approximation
Do i = N4b+1, N5  ! Note that change in concentrations has
already been calculated for last barrier node
delg(i) = (jg(i-1)-jg(i))*delt/h(i)
End Do

!SOLUTE CALCULATIONS
!solute flux from barrier to depot
jc(N4b)= Dc(N4b)*(C(N4b-1)-C(N4b))/h(N4b)
jc2(N4b)= Dc(N4b)*(C2(N4b-1)-C2(N4b))/h(N4b)
jc3(N4b)= Dc(N4b)*(C3(N4b-1)-C3(N4b))/h(N4b)
jc4(N4b)= Dc(N4b)*(C4(N4b-1)-C4(N4b))/h(N4b)
jc5(N4b)= Dc(N4b)*(C5(N4b-1)-C5(N4b))/h(N4b)
```

```
jc(N4b+1) = jc(N4b)-delc(N4b)*h(N4b)/delt ! Note that flux
from last barrier layer is also needed
jc2(N4b+1) = jc2(N4b)-delc2(N4b)*h(N4b)/delt
jc3(N4b+1) = jc3(N4b)-delc3(N4b)*h(N4b)/delt
jc4(N4b+1) = jc4(N4b)-delc4(N4b)*h(N4b)/delt
jc5(N4b+1) = jc5(N4b)-delc5(N4b)*h(N4b)/delt
! SOLUTE ! Calculate mass transport in depot layer
Do i = N4b+2,N5
jc(i) = ((Dc(i-1)+Dc(i))/2)*(C(i-1)-C(i))/h(i)
jc2(i) = ((Dc(i-1)+Dc(i))/2)*(C2(i-1)-C2(i))/h(i)
jc3(i) = ((Dc(i-1)+Dc(i))/2)*(C3(i-1)-C3(i))/h(i)
jc4(i) = ((Dc(i-1)+Dc(i))/2)*(C4(i-1)-C4(i))/h(i)
jc5(i) = ((Dc(i-1)+Dc(i))/2)*(C5(i-1)-C5(i))/h(i)
End Do
jc(N5+1)=0
jc2(N5+1)=0
jc3(N5+1)=0
jc4(N5+1)=0
jc5(N5+1)=0
! SOLUTE ! Once all fluxes are calculated, determine change
in node concentration using Backward finite difference
approximation
Do i = N4b+1, N5  ! Note that change in concentrations has
already been calculated for last barrier node
delc(i) =  (jc(i)-jc(i+1))*delt/h(i)
delc2(i) = (jc2(i)-jc2(i+1))*delt/h(i)
delc3(i) = (jc3(i)-jc3(i+1))*delt/h(i)
delc4(i) = (jc4(i)-jc4(i+1))*delt/h(i)
delc5(i) = (jc5(i)-jc5(i+1))*delt/h(i)
End Do

!!CHANGE IN CONCENCTRATIONS!!
Do i = 2, N5
G(i) = G(i) + delg(i)
C(i) = C(i) + delc(i)
C2(i) = C2(i) + delc2(i)
C3(i) = C3(i) + delc3(i)
C4(i) = C4(i) + delc4(i)
C5(i) = C5(i) + delc5(i)
End Do


!@@@@@@@@@@@@@@@@@@@@---PULSE-1---@@@@@@@@@@@@@@@@@@@@

!Barrier-1
Do i = 2, nb
! Consume scavenger
```

```
If (F(i).gt.0) then
If (G(i).gt.F(i)) then
G(i) = G(i)-F(i)
write(8,*)'i F(i) t(h) ',i,F(i),j*delt/3600
F(i) = 0
Elseif (G(i).gt.0) then
F(i) = F(i)-G(i)
G(i) = 0
End If
End If
End Do


!Depot-1
Do i  = nb+1, nb+nd
! Consume scavenger before dissolving solute, in case this
changes Csat of a node
If (F(i).gt.0) then
If (G(i).gt.F(i)) then
G(i) = G(i)-F(i)
write(8,*)'i F(i) t(h) ',i,F(i),j*delt/3600
F(i) = 0
Ccsat(i) = Csw
B(i)=B(i)-Ccsat(i)+C(i)/s

C(i)=Ccsat(i)
C2(i)=C2(i)/s
C3(i)=C3(i)/s
C4(i)=C4(i)/s
C5(i)=C5(i)/s

Dc(i) = Dcsw
Dg(i) = Dgsw
h(i) = hsw
Elseif (G(i).gt.0) then
F(i)=F(i)-G(i)
G(i) = 0
End If
End If

!Dissolve solid:Depot-1
Cdiff(i) = Ccsat(i) - C(i)
If (B(i).gt.0) then
If (Cdiff(i).gt.0) then
If (B(i).gt.Cdiff(i)) then
B(i) = B(i)-Cdiff(i)
C(i) = Ccsat(i)
```

```
Else
C(i) = Ccsat(i) - Cdiff(i) + B(i)
B(i) = 0
End If
End If
End If
End Do

!@@@@@@@@@@@@@@@@@@---PULSE-1 LOOP END---@@@@@@@@@@@@@@@@@@


!@@@@@@@@@@@@@@@@@@---PULSE-2-------@@@@@@@@@@@@@@@@@@

!Barrier-2
Do i = N1+1, N1b
! Consume scavenger
If (F(i).gt.0) then
If (G(i).gt.F(i)) then
G(i) = G(i)-F(i)
write(8,*)'i F(i) t(h) ',i,F(i),j*delt/3600
F(i) = 0
Elseif (G(i).gt.0) then
F(i) = F(i)-G(i)
G(i) = 0
End If
End If
End Do


!Depot-2
Do i  = N1b+1, N2
! Consume scavenger before dissolving solute, in case this
changes Csat of a node
If (F(i).gt.0) then
If (G(i).gt.F(i)) then
G(i) = G(i)-F(i)
write(8,*)'i F(i) t(h) ',i,F(i),j*delt/3600
F(i) = 0

Ccsat2(i) = Csw2
B2(i)=B2(i)-Ccsat2(i)+C2(i)/s2

C(i)=C(i)/s2 ! This is required, as solute from 1st depot
needs to be redefined based on new swollen thickness of
nodes in swollen depot-2
C2(i)=Ccsat2(i)
C3(i)=C3(i)/s2
```

```
C4(i)=C4(i)/s2
C5(i)=C5(i)/s2

Dc(i) = Dcsw
Dg(i) = Dgsw
h(i) = hsw2
Elseif (G(i).gt.0) then
F(i)=F(i)-G(i)
G(i) = 0
End If
End If

!Dissolve solid:Depot-2
Cdiff2(i) = Ccsat2(i) - C2(i)
If (B2(i).gt.0) then
If (Cdiff2(i).gt.0) then
If (B2(i).gt.Cdiff2(i)) then
B2(i) = B2(i)-Cdiff2(i)
C2(i) = Ccsat2(i)
Else
C2(i) = Ccsat2(i) - Cdiff2(i) + B2(i)
B2(i) = 0
End If
End If
End If
End Do

!@@@@@@@@@@@@@@@@@@@@@@@@---PULSE-2 LOOP END---@@@@@@@@@@


!@@@@@@@@@@@@@@@@@@@@---PULSE-3---@@@@@@@@@@@@@@@@@@

!Barrier-3
Do i = N2+1, N2b
! Consume scavenger
If (F(i).gt.0) then
If (G(i).gt.F(i)) then
G(i) = G(i)-F(i)
write(8,*)'i F(i) t(h) ',i,F(i),j*delt/3600
F(i) = 0
Elseif (G(i).gt.0) then
F(i) = F(i)-G(i)
G(i) = 0
End If
End If
End Do
```

```
!Depot-3
Do i  = N2b+1, N3
! Consume scavenger before dissolving solute, in case this
changes Csat of a node
If (F(i).gt.0) then
If (G(i).gt.F(i)) then
G(i) = G(i)-F(i)
write(8,*)'i F(i) t(h) ',i,F(i),j*delt/3600
F(i) = 0

Ccsat3(i) = Csw3
B3(i)=B3(i)-Ccsat3(i)+C3(i)/s3

C(i)=C(i)/s3
C2(i)=C2(i)/s3
C3(i)=Ccsat3(i)
C4(i)=C4(i)/s4
C5(i)=C5(i)/s4

Dc(i) = Dcsw
Dg(i) = Dgsw
h(i) = hsw3
Elseif (G(i).gt.0) then
F(i)=F(i)-G(i)
G(i) = 0
End If
End If

!Dissolve solid:Depot-3
Cdiff3(i) = Ccsat3(i) - C3(i)
If (B3(i).gt.0) then
If (Cdiff3(i).gt.0) then
If (B3(i).gt.Cdiff3(i)) then
B3(i) = B3(i)-Cdiff3(i)
C3(i) = Ccsat3(i)
Else
C3(i) = Ccsat3(i) - Cdiff3(i) + B3(i)
B3(i) = 0
End If
End If
End If
End Do

!@@@@@@@@@@@@@@@@@@@@@@@@@---PULSE-3 LOOP END---@@@@@@@@@@@
```

```
!@@@@@@@@@@@@@@@@@@@@---PULSE-4---@@@@@@@@@@@@@@@@

!Barrier-4
Do i = N3+1, N3b
! Consume scavenger
If (F(i).gt.0) then
If (G(i).gt.F(i)) then
G(i) = G(i)-F(i)
write(8,*)'i F(i) t(h) ',i,F(i),j*delt/3600
F(i) = 0
Elseif (G(i).gt.0) then
F(i) = F(i)-G(i)
G(i) = 0
End If
End If
End Do


!Depot-4
Do i  = N3b+1, N4
! Consume scavenger before dissolving solute, in case this
changes Csat of a node
If (F(i).gt.0) then
If (G(i).gt.F(i)) then
G(i) = G(i)-F(i)
write(8,*)'i F(i) t(h) ',i,F(i),j*delt/3600
F(i) = 0

Ccsat4(i) = Csw4
B4(i)=B4(i)-Ccsat4(i)+C4(i)/s4

C(i)=C(i)/s4
C2(i)=C2(i)/s4
C3(i)=C3(i)/s4
C4(i)=Ccsat4(i)
C5(i)=C5(i)/s4

Dc(i) = Dcsw
Dg(i) = Dgsw
h(i) = hsw4
Elseif (G(i).gt.0) then
F(i)=F(i)-G(i)
G(i) = 0
End If
End If

!Dissolve solid:Depot-4
```

```
Cdiff4(i) = Ccsat4(i) - C4(i)
If (B4(i).gt.0) then
If (Cdiff4(i).gt.0) then
If (B4(i).gt.Cdiff4(i)) then
B4(i) = B4(i)-Cdiff4(i)
C4(i) = Ccsat4(i)
Else
C4(i) = Ccsat4(i) - Cdiff4(i) + B4(i)
B4(i) = 0
End If
End If
End If
End Do

!@@@@@@@@@@@@@@@@@@@@@@@---PULSE-4 LOOP END---@@@@@@@@@@

!@@@@@@@@@@@@@@@@@@@---PULSE-5---@@@@@@@@@@@@@@@@@

!Barrier-5
Do i = N4+1, N4b
! Consume scavenger
If (F(i).gt.0) then
If (G(i).gt.F(i)) then
G(i) = G(i)-F(i)
write(8,*)'i F(i) t(h) ',i,F(i),j*delt/3600
F(i) = 0
Elseif (G(i).gt.0) then
F(i) = F(i)-G(i)
G(i) = 0
End If
End If
End Do


!Depot-5
Do i  = N4b+1, N5
! Consume scavenger before dissolving solute, in case this
changes Csat of a node
If (F(i).gt.0) then
If (G(i).gt.F(i)) then
G(i) = G(i)-F(i)
write(8,*)'i F(i) t(h) ',i,F(i),j*delt/3600
F(i) = 0


Ccsat5(i) = Csw5
B5(i)=B5(i)-Ccsat5(i)+C5(i)/s5
```

```
C(i)=C(i)/s5
C2(i)=C2(i)/s5
C3(i)=C3(i)/s5
C4(i)=C4(i)/s5
C5(i)=Ccsat5(i)

Dc(i) = Dcsw
Dg(i) = Dgsw
h(i) = hsw5
Elseif (G(i).gt.0) then
F(i)=F(i)-G(i)
G(i) = 0
End If
End If

!Dissolve solid:Depot-5
Cdiff5(i) = Ccsat5(i) - C5(i)
If (B5(i).gt.0) then
If (Cdiff5(i).gt.0) then
If (B5(i).gt.Cdiff5(i)) then
B5(i) = B5(i)-Cdiff5(i)
C5(i) = Ccsat5(i)
Else
C5(i) = Ccsat5(i) - Cdiff5(i) + B5(i)
B5(i) = 0
End If
End If
End If

End Do

!@@@@@@@@@@@@@@@@@@@@@@@@@---PULSE-5 LOOP END---@@@@@@@@@@@

!Maintain impermeable boundary condition on inner boundary
C(N5+1) = C(N5)
C2(N5+1) = C2(N5)
C3(N5+1) = C3(N5)
C4(N5+1) = C4(N5)
C5(N5+1) = C5(N5)

G(N5+1) = G(N5)

!Cumulative Release of solute at node 1!
Qc1= Qc1+Dc(1)*(C(2)-C(1))*delt/h(1) *M1*A ! release at
node 1 before delamination and after delamination
Qc2= Qc2+Dc(1)*(C2(2)-C2(1))*delt/h(1)*M2*A
```

```
Qc3= Qc3+Dc(1)*(C3(2)-C3(1))*delt/h(1)*M3*A
Qc4= Qc4+Dc(1)*(C4(2)-C4(1))*delt/h(1)*M4*A
Qc5= Qc5+Dc(1)*(C5(2)-C5(1))*delt/h(1)*M5*A

Qc = Qc1+Qc2+Qc3+Qc4+Qc5
!Calculate cumulative influx of acid
Qg = Qg + Dg(1)*(G(1)-G(2))*delt/h(1)!

t=t+delt

!$$$$$$ Write results for cumulative solute release Qc and
cumulative influx Qg vs time
if(Mod(j,1000).lt.0.001)then
write(3,*)'m h d
Qc,Qc1,Qc2,Qc3,Qc4,Qc5',t/60,t/3600,t/(3600*24),Qc,Qc1,Qc2,
Qc3,Qc4,Qc5

EndIf
End Do

!$$$$$$ Write C,B,G,F, Dc,Dg at each node at the end of m
number of timesteps!
Do i=1,N5

write(4,*)'i,G,F,Dg',i,G(i),F(i),Dg(i)
write(5,*)'i,C,B,Dc',i,C(i),B(i),Dc(i)
write(6,*)'i,C2,B2,Dc',i,C2(i),B2(i),Dc(i)
write(7,*)'i,C3,B3,Dc',i,C3(i),B3(i),Dc(i)
write(9,*)'i,C4,B4,Dc',i,C4(i),B4(i),Dc(i)
write(10,*)'i,C5,B5,Dc',i,C5(i),B5(i),Dc(i)

EndDo
End
```

APPENDIX G SCRIPT FOR RUNNING FORTRAN JOBS ON HELIUM CLUSTER

Example script for running FORTRAN jobs on Helium Cluster is described below.

array_script.txt

```
#$ -t 1-25
#$ -M user-email@uiowa.edu
#$ -m be
#$ -j y
#$ -cwd
#$ -o /dev/null
cd 150131_SG${SGE_TASK_ID}
gfortran -o 150131_${SGE_TASK_ID}.bin
150131_${SGE_TASK_ID}.f95./150131_${SGE_TASK_ID}.bin
```

To run a particular set of FORTRAN codes on high computing software "Helium Cluster" provided by University of Iowa, the user needs to be logged in to helium.hpc.uiowa.edu using SecureCRT software. It requires SSH port 40 (or 22) depending upon on-campus (or off-campus) internet connection through VPN provided by University of Iowa. Now, let's say user needs to run 25 different codes (maximum allowed jobs in a single array) on Helium. Put each code in 25 different folders with folder name (for example "150131_SG1, 150131_SG2,…and 150131_SG25"). Each folder contains its own .f95 code ("150131_1.f95, 150131_2.f95,..,and 150131_25.f95 respectively). First put all these folders along with the array_script.txt file (as described above) in a single parent folder "JOB_XYZ". Transfer the folder "JOB_XYZ" to remote computer on Helium Cluster from user's local computer using SecureCRT in SFTP

session. Once the jobs are transferred, open the folder "JOB_XYZ". Type "qsub array_script.txt" command on login shell which will submit, compile and execute all the 25 jobs on remote computer. User can check the status of the jobs by running "qstat –u username" command. Once the jobs are done, each code will spit out the output files in its respective folder. Transfer all the files back to local computer using "get –r JOB_XYZ" command in SFTP session.

APPENDIX H MACRO-SCRIPT FOR SCANNING RELEASE DATA

```
Sub TimeScanner()
'Note:  Time must be in Column A, % release for each depot
in Columns K, L, M, N, and O.
'Output will be written in Columns R, S, T, U, and V.
Dim pr(12) As Double
'Declare %'s at which times will be recorded
pr(1) = 0.1
pr(2) = 1
pr(3) = 2
pr(4) = 5
pr(5) = 10
pr(6) = 50
pr(7) = 90
pr(8) = 95
pr(9) = 98
pr(10) = 99
pr(11) = 99.9
pr(12) = 101
'pr(12) is just dummy value for code, must be > 100.

'Label output table
Cells(1, 17) = "% Released"
Cells(1, 18) = "Times (minutes)"
Cells(2, 18) = "Depot 1"
Cells(2, 19) = "Depot 2"
Cells(2, 20) = "Depot 3"
Cells(2, 21) = "Depot 4"
Cells(2, 22) = "Depot 5"
For j = 1 To 11
Cells(j + 2, 17) = pr(j)
Next j

'Scan for times, record on table
For i = 11 To 15
k = 1
For j = 2 To 28000
If Cells(j, i) > pr(k) Then
Cells(k + 2, i + 7) = Cells(j, 1)
k = k + 1
End If
Next j
Next i

End Sub
```

BIBLIOGRAPHY

References

1. Santini, J. T.,Jr. Introduction to Drug Delivery Technology. *Chem. Eng. Prog.* **2013**, *109*, 19-23.

2. Blumenthal, P. D.; Gemzell-Danielsson, K.; Marintcheva-Petrova, M. Tolerability and Clinical Safety of Implanon (R). *Eur. J. Contracept. Reprod. Health Care* **2008**, *13*, 29-36.

3. Fiore, M.; Smith, S.; Jorenby, D.; Baker, T. The Effectiveness of the Nicotine Patch for Smoking Cessation - a Metaanalysis. *J. Am. Med. Assoc.* **1994**, *271*, 1940-1947.

4. Nasrallah, H. A.; Gopal, S.; Gassmann-Mayer, C.; Quiroz, J. A.; Lim, P.; Eerdekens, M.; Yuen, E.; Hough, D. A Controlled, Evidence-Based Trial of Paliperidone Palmitate, A Long-Acting Injectable Antipsychotic, in Schizophrenia. *Neuropsychopharmacol.* **2010**, *35*, 2072-2082.

5. Sierra, C.; Coca, A. The Action Study: Nifedipine in Patients with Symptomatic Stable Angina and Hypertension. *Expert Rev. Cardiovasc. Ther.* **2008**, *6*, 1055-1062.

6. Liu, X.; Pettway, G. J.; McCauley, L. K.; Ma, P. X. Pulsatile Release of Parathyroid Hormone from an Implantable Delivery System. *Biomaterials* **2007**, *28*, 4124-4131.

7. Jeon, J. H.; Puleo, D. A. Formulations for Intermittent Release of Parathyroid Hormone (1-34) and Local Enhancement of Osteoblast Activities. *Pharm. Dev. Technol.* **2008**, *13*, 505-512.

8. Hellman, B. Pulsatility of Insulin Release - A Clinically Important Phenomenon. *Ups. J. Med. Sci.* **2009**, *114*, 193-205.

9. Lin, S.; Kawashima, Y. Current Status and Approaches to Developing Press-coated Chronodelivery Drug Systems. *J. Controlled Release* **2012**, *157*, 331-353.

10. Zhang, J. S.; Lazar, M. A. The Mechanism of Action of Thyroid Hormones. *Annu. Rev. Physiol.* **2000**, *62*, 439-466.

11. Veldhuis, J. D.; Keenan, D. M.; Pincus, S. M. Motivations and Methods for Analyzing Pulsatile Hormone Secretion. *Endocr. Rev.* **2008**, *29*, 823-864.

12. Earhart, M. Types of Opiate Drugs. *http://www.livestrong.com/article/75425-types-opiate-drugs/* (accessed March 8, 2011).

13. Anonymous. Centers for Disease Control and Prevention: Rabies Vaccine What You Need to Know. *http://www.cdc.gov/vaccines/hcp/vis/vis-statements/rabies.html* (accessed October 6, 2009).

14. Matsuo, K.; Hirobe, S.; Okada, N.; Nakagawa, S. Frontiers of Transcutaneous Vaccination Systems: Novel Technologies and Devices for Vaccine Delivery. *Vaccine* **2013**, *31*, 2403-2415.

15. Cox, L.; Esch, R. E.; Corbett, M.; Hankin, C.; Nelson, M.; Plunkett, G. Allergen Immunotherapy Practice in the United States: Guidelines, Measures, and Outcomes. *Ann. Allergy Asthma Immunol.* **2011**, *107*, 289-300.

16. Santini, J. T.; Richards, A. C.; Scheidt, R.; Cima, M. J.; Langer, R. Microchips as Controlled Drug-Delivery Devices. *Angew. Chem. -Int. Edit.* **2000**, *39*, 2397-2407.

17. Maloney, J.; Uhland, S.; Polito, B.; Sheppard, N.; Pelta, C.; Santini, J. Electrothermally Activated Microchips for Implantable Drug Delivery and Biosensing. *J. Controlled Release* **2005**, *109*, 244-255.

18. Ma, P. X.; Liu, X.; McCauley, L. K. Delivery Device and Method for Forming the Same. *US Patent 20080254095* **2008**.

19. Gazzaniga, A.; Palugan, L.; Foppoli, A.; Sangalli, M. E. Oral Pulsatile Delivery Systems based on Swellable Hydrophilic Polymers. *Eur. J. Pharm. Biopharm.* **2008**, *68*, 11-18.

20. Stubbe, B. G.; De Smedt, S. C.; Demeester, J. "Programmed Polymeric Devices" for Pulsed Drug Delivery. *Pharm. Res.* **2004**, *21*, 1732-1740.

21. Niwa, K.; Takaya, T.; Morimoto, T.; Takada, K. Preparation and Evaluation of a Time-Controlled Release Capsule made of Ethylcellulose for Colon Delivery of Drugs. *J. Drug Target.* **1995**, *3*, 83-89.

22. Cleland, J. L.; Powell, M. F.; Lim, A.; Barron, L.; Berman, P. W.; Eastman, D. J.; Nunberg, J. H.; Wrin, T.; Vennari, J. C. Development of a Single-Shot Subunit Vaccine for HIV-1. *AIDS Res. Hum. Retroviruses* **1994**, *10*, S21-S26.

23. Jimoh, A. G.; Wise, D. L.; Gresser, J. D.; Trantolo, D. J. Pulsed FSH Release from an Implantable Capsule System. *J. Controlled Release* **1995**, *34*, 87-95.

24. Manoharan, C.; Singh, J. Evaluation of Poly (1, 6-bis-(p-carboxyphenoxy) Hexane-co-sebacic Acid Microspheres for Controlled Basal Insulin Delivery. *Pharm. Res.* **2013**, *30*, 627-640.

25. Yamaguchi, Y.; Takenaga, M.; Kitagawa, A.; Ogawa, Y.; Mizushima, Y.; Igarashi, R. Insulin-loaded Biodegradable PLGA Microcapsules: Initial Burst Release Controlled by Hydrophilic Additives. *J. Controlled Release* **2002**, *81*, 235-249.

26. Cleland, J. L.; Johnson, O. L.; Putney, S.; Jones, A. J. S. Recombinant Human Growth Hormone Poly(lactic-co-glycolic acid) Microsphere Formulation Development. *Adv. Drug Deliv. Rev.* **1997**, *28*, 71-84.

27. Tamada, J.; Langer, R. The Development of Polyanhydrides for Drug Delivery Applications. *J. Biomater. Sci. -Polym. Ed.* **1992**, *3*, 315-353.

28. Langer, R. New Methods of Drug Delivery. *Science* **1990**, *249*, 1527-1533.

29. Zhang, J.; Saltzman, W. M. Engineering Biodegradable Nanoparticles for Drug and Gene Delivery. *Chem. Eng. Prog.* **2013**, *109*, 25-30.

30. Kumar, N.; Langer, R. S.; Domb, A. J. Polyanhydrides: an Overview. *Adv. Drug Deliv. Rev.* **2002**, *54*, 889-910.

31. Peppas, N.; Langer, R. New Challenges in Biomaterials. *Science* **1994**, *263*, 1715-1720.

32. Gopferich, A. Bioerodible Implants with Programmable Drug Release. *J. Controlled Release* **1997**, *44*, 271-281.

33. Jain, J. P.; Chitkara, D.; Kumar, N. Polyanhydrides as Localized Drug Delivery Carrier: an Update. *Expert Opin. Drug Deliv.* **2008**, *5*, 889-907.

34. Fujioka, K.; Sato, S.; Takada, Y.; Sasaki, Y.; Tamura, N. 5011692, 1986.

35. Moriyama, K.; Ooya, T.; Yui, N. Pulsatile Peptide Release from Multi-layered Hydrogel Formulations Consisting of Poly(ethylene glycol)-grafted and Ungrafted Dextrans. *J. Biomater. Sci. Polym. Ed.* **1999**, *10*, 1251-1264.

36. Jiang, H. L.; Zhu, K. J. Pulsatile Protein Release from a Laminated Device Comprising of Polyanhydrides and pH-Sensitive Complexes. *Int. J. Pharm.* **2000**, *194*, 51-60.

37. Jeon, J. H.; Thomas, M. V.; Puleo, D. A. Bioerodible Devices for Intermittent Release of Simvastatin Acid. *Int. J. Pharm.* **2007**, *340*, 6-12.

38. Jeon, J. H.; Puleo, D. A. Alternating Release of Different Bioactive Molecules from a Complexation Polymer System. *Biomaterials* **2008**, *29*, 3591-3598.

39. Burkersroda, F. V.; Göpferich, A. M. An Approach to Classify Degradable Polymers. **1999**, *550*, 17-22.

40. Siegel, R. A.; Firestone, B. A. pH-dependent Equilibrium Swelling Properties of Hydrophobic Polyelectrolyte Copolymer Gels. *Macromolecules* **1988**, *21*, 3254-3254-3259.

41. Tokuyama, H.; Kato, Y. Preparation of Poly(N-isopropylacrylamide) Emulsion Gels and their Drug Release Behaviors. *Colloids Surf. , B* **2008**, *67*, 92-98.

42. Seto, Y.; Aoki, T.; Kunugi, S. Temperature- and Pressure-Responsive Properties of L- and DL-forms of Poly(N-(1-hydroxymethyl)propylmethacrylamide) in Aqueous Solutions. *Colloid Polym. Sci.* **2005**, *283*, 1137-1142.

43. Sumaru, K.; Kameda, M.; Kanamori, T.; Shinbo, T. Characteristic Phase Transition of Aqueous Solution of Poly(N-isopropylacrylamide) Functionalized with Spirobenzopyran. *Macromolecules* **2004**, *37*, 4949-4955.

44. Sershen, S.; West, J. Implantable, Polymeric Systems for Modulated Drug Delivery. *Adv. Drug Deliv. Rev.* **2002**, *54*, 1225-1235.

45. Miyata, T.; Asami, N.; Uragami, T. A Reversibly Antigen-responsive Hydrogel. *Nature* **1999**, *399*, 766-769.

46. Yang, C. F.; Nuxoll, E. E.; Cussler, E. L. Reactive Barrier Films. *AIChE J.* **2001**, *47*, 295-302.

47. Nuxoll, E. E.; Siegel, R. A.; Cussler, E. L. Layered Reactive Barrier Films. *J. Membr. Sci.* **2005**, *252*, 29-36.

48. Siegel, R. A.; Falamarzian, M.; Firestone, B. A.; Moxley, B. C. pH-controlled Release from Hydrophobic/polyelectrolyte Copolymer Hydrogels. *J. Controlled Release* **1988**, *8*, 179-182.

49. Firestone, B. A.; Siegel, R. A. Dynamic pH-dependent Swelling Properties of a Hydrophobic Polyelectrolyte Gel. *Polym. Comm.* **1988**, *29*, 204-208.

50. Siegel, R. A.; Johannes, I.; Hunt, C. A.; Firestone, B. A. Buffer Effects on Swelling Kinetics in Polybasic Gels. *Pharm. Res.* **1992**, *9*, 76-81.

51. Dhanarajan, A. P.; Misra, G. P.; Siegel, R. A. Autonomous Chemomechanical Oscillations in a Hydrogel/enzyme System Driven by Glucose. *J. Phys. Chem. A.* **2002**, *106*, 8835-8838.

52. Das, N. K.; Mandal, B. M. Methylene-Blue as a Retarder of Free-Radical Polymerization .1. Polymerization of Acrylonitrile, Methyl-Methacrylate and Styrene. *Polymer* **1982**, *23*, 1653-1658.

53. Van de Wetering, P.; Zuidam, N. J.; Van Steenbergen, M. J.; Van der Houwen, O. A. G. J.; Underberg, W. J. M.; Hennink, W. E. A Mechanistic Study of the Hydrolytic Stability of Poly(2-(dimethylamino)ethyl methacrylate). *Macromolecules* **1998**, *31*, 8063-8068.

54. Muller, G. T. A.; Stokes, R. H. The Mobility of the Undissociated Citric Acid Molecule in Aqueous Solution. *Trans. Faraday Soc.* **1957**, *53*, 642-645.

55. Southard, M. Z.; Dias, L. J.; Himmelstein, K. J.; Stella, V. J. Experimental Determinations of Diffusion-Coefficients in Dilute Aqueous-Solution using the Method of Hydrodynamic Stability. *Pharm. Res.* **1991**, *8*, 1489-1494.

56. Harpst, J. A.; Holt, E.; Lyons, P. A. Diffusion in Dilute Hydrochloric Acid-Water Solutions. *J. Phys. Chem.* **1965**, *69*, 2333-&.

57. Leaist, D. G. The Effects of Aggregation, Counterion Binding, and Added NaCl on Diffusion of Aqueous Methylene-Blue. *CAN. J. CHEM.* **1988**, *66*, 2452-2457.

58. Siegel, R. A.; Cussler, E. L. Reactive Barrier Membranes: Some Theoretical Observations Regarding the Time Lag and Breakthrough Curves. *J. Membr. Sci.* **2004**, *229*, 33-41.

59. Daynes, H. The Process of Diffusion through a Rubber Membrane. *Proc. R. soc. Lond. Ser. A-Contain. Pap. Math. Phys. Character* **1920**, *97*, 286-306.

60. Barrer, R. M. In *"Diffusion In and Through Solids", Cambridge University Press, London, England;* 1941; pp 13-19.

61. Finger, K. F.; Lemberger, A. P.; Wurster, D. E.; Higuchi, T. Investigation and Development of Protective Ointments .3. Adsorption Characteristics of Sarin from Solutions. *J. Am. Pharm. Assoc.* **1960**, *49*, 565-568.

62. Silva, A. M. N.; Kong, X.; Parkin, M. C.; Cammack, R.; Hider, R. C. Iron(III) citrate speciation in aqueous solution. *Dalton Trans.* **2009**, 8616-8625.

63. Wei, Y.; Wang, X.; Gao, J.; Chen, Y. Plasma-Induced Graft Polymerization of Poly(ethylene glycol) on Poly(methyl methacrylate) Surfaces for Improving Antistatic Property. *J Appl Polym Sci* **2010**, *118*, 943-949.

64. Shinohara, H.; Mizuno, J.; Shoji, S. Low-temperature Direct Bonding of Poly(methyl methacrylate) for Polymer Microchips. *IEEJ Trans. Electr. Electron. Eng.* **2007**, *2*, 301-306.

65. Kim, S. H.; Cui, Y.; Lee, M. J.; Nam, S.; Oh, D.; Kang, S. H.; Kim, Y. S.; Park, S. Simple Fabrication of Hydrophilic Nanochannels Using the Chemical Bonding between Activated Ultrathin PDMS Layer and Cover Glass by Oxygen Plasma. *Lab Chip* **2011**, *11*, 348-353.